

# **PEM Fuel Cell Multi-Phase System**

**Kevin Hard, BEng**

**Thesis submitted to the University of Nottingham  
for the degree of Doctor of Philosophy**

**Sept 2005**



## **Contents**

<b>Abstract</b>	vii
<b>Acknowledgement</b>	viii
<b>List of Figures</b>	ix
<b>List of Tables</b>	xiii
<b>Nomenclature</b>	xiv

### **Chapter 1: Introduction**

<b>1.0 Introduction</b>	1
<b>1.1 Research Overview</b>	1
<b>1.2 Fuel Cells</b>	2
<b>1.3 The Hydrogen Economy</b>	3
<b>1.4 Fuel Cell and Hydrogen Challenges</b>	4
<b>1.5 Functionally Thermal Fluids</b>	4
<b>1.6 Summary of Research Aims</b>	5

### **Chapter 2: The PEM Fuel Cell**

<b>2.0 Introduction</b>	7
<b>2.1 Fuel Cell Fundamentals</b>	7
2.1.1 What is a Fuel Cell?	7
2.1.2 How does a Fuel Cell Work?	8
2.1.3 Types of Fuel Cell	9
2.1.4 Inherent Strengths of Fuel Cells	11
2.1.5 Fuel Cell Technology Challenges	11
2.1.6 Are Fuel Cells the Future?	12
<b>2.2 Proton Exchange Membrane (PEM) Fuel Cell</b>	14
2.2.1 PEM Stack Overview	15
2.2.2 PEM Materials and Manufacturing	16
2.2.3 Fuel Cell Design Issues	17
2.2.4 PEM Performance and Operating Conditions	17
<b>2.3 PEM Stack Experimentation</b>	18
2.3.1 PEM Stack Description	18
2.3.2 PEM Stack Specifications	19
2.3.3 PEM Stack Testing	20
2.3.4 Operational Fuel Cell Voltage	22
2.3.5 Stack Thermal Evaluation	24

2.3.5.1	<i>Stack Coolant Temperature</i>	24
2.3.5.2	<i>Temperature Difference Across Stack</i>	24
<b>2.4</b>	<b>The PEMFC Thermal Energy System</b>	<b>26</b>
2.4.1	System Overview	26
2.4.2	Fuel Cell Heat Recovery System	28
2.4.3	Thermal Storage Overview	28
2.4.4	Thermal Energy Storage Experimentation	29
2.4.5	Thermal Energy Storage Evaluation	31
2.4.5.1	<i>Conventional Store Sensible Heat Storage</i>	31
2.4.5.2	<i>Alternate Storage Strategies</i>	33
2.4.5.3	<i>Combi-Store Sensible Heat Storage</i>	34
2.4.6	Fuel Cell TES Summary	37
<b>2.5</b>	<b>FC Stack and Thermal Store Design Conditions Summary</b>	<b>37</b>
<b>2.6</b>	<b>Concluding Remarks</b>	<b>38</b>
<b><u>Chapter 3:</u></b>	<b><u>Functionally Thermal Fluids</u></b>	<b>39</b>
<b>3.0</b>	<b>Introduction</b>	<b>39</b>
<b>3.1</b>	<b>Functionally Thermal Fluids</b>	<b>39</b>
<b>3.2</b>	<b>Phase Change Material</b>	<b>42</b>
3.2.1	Overview	42
3.2.2	Paraffin Wax	43
3.2.3	Thermodynamics for Latent Heat Storage	45
3.2.4	Nucleation and Supercooling	48
3.2.5	Stratification+ Agglomeration	49
3.2.6	Requirements of the PCM for the Fuel Cell	50
<b>3.3</b>	<b>Phase Change Slurries</b>	<b>51</b>
<b>3.4</b>	<b>Micro-encapsulation of PCMs</b>	<b>52</b>
3.4.1	Overview	52
3.4.2	Description	53
3.4.3	History	54
3.4.4	Experimentation	55
3.4.5	MicroPCM Applications	57
3.4.5.1	<i>Clothing</i>	57
3.4.5.2	<i>DaimlerChrysler Multiphase Suspension Coolant</i>	59
<b>3.5</b>	<b>Concluding Remarks</b>	<b>60</b>

<b><u>Chapter 4: Thermal Properties Investigation of MicroPCM Slurries</u></b>	61
<b>4.0 Introduction</b>	61
<b>4.1 MicroPCMs Investigated</b>	62
<b>4.2 MicroPCM Slurry Thermal + Physical Evaluation</b>	63
4.2.1 Overview	63
4.2.1 Carrier Fluid	63
4.2.2 Initial Observations	63
<b>4.3 Surface Morphology</b>	65
4.3.1 Aim	65
4.3.2 Background	65
4.3.3 Methodology	66
4.3.4 Evaluation of Result	66
4.3.5 ESEM Summary	69
<b>4.4 Latent Heat of Fusion</b>	69
4.4.1 Aim	69
4.4.2 Background	69
<b>4.5 Differential Scanning Calorimetry</b>	70
4.5.1 Aim	70
4.5.2 Background	70
4.5.3 Methodology	73
4.5.4 Sample Preparation (DSC)	73
4.5.5 Calibration	75
4.5.6 Evaluation of DSC Results	75
4.5.7 Summary of DSC Thermograms	77
4.5.8 Evaluation of DSC Results	79
4.5.9 DSC Summary	80
<b>4.6 Thermal Analysis (TA)</b>	81
4.6.1 Aim	81
4.6.2 Background	81
4.6.3 Sample Preparation	81
4.6.4 Methodology	81
4.6.5 TA Experimental Observations	83
4.6.6 TA Summary	86
<b>4.7 MicroPCM Rheology</b>	86
4.7.1 Aim	86
4.7.2 Background	86
4.7.3 Methodology	87

4.7.4	Evaluation of Rheology Results	87
4.7.5	Rheology Summary	89
<b>4.8</b>	<b>Concluding Remarks</b>	<b>90</b>
 <b><u>Chapter 5: MicroPCM Slurry in a Closed Thermal System</u></b>		<b>92</b>
<b>5.0</b>	<b>Introduction</b>	<b>92</b>
<b>5.1</b>	<b>Experimental Aim</b>	<b>92</b>
<b>5.2</b>	<b>Slurry Performance</b>	<b>93</b>
<b>5.3</b>	<b>Review of Previous MicroPCM Slurry Experimental Work</b>	<b>94</b>
<b>5.4</b>	<b>Experimental Investigation of a Closed Loop System</b>	<b>96</b>
5.4.1	Microcapsules and Slurry Physical Properties	96
5.4.2	Apparatus and Methodology	97
5.4.2.1	<i>Heater Test Section</i>	99
5.4.2.2	<i>Pump</i>	99
5.4.2.3	<i>Other Components</i>	100
5.4.2.4	<i>Data Acquisition</i>	100
5.4.3	Slurry Tuning	101
5.4.4	Equipment Calibration and Experimental Uncertainties	102
<b>5.5</b>	<b>Slurry Test Rig Verification with Dittus+Boelter</b>	<b>104</b>
5.5.1	Dittus & Boelter Evaluation	106
5.5.2	MicroPCM Slurry Preparation and Charging	107
5.5.3	Practical Slurry Issues	107
<b>5.6</b>	<b>Evaluation of Slurry Performance Data</b>	<b>108</b>
5.6.1	Slurry Temperature Difference	108
5.6.2	Thermal Input	109
5.6.3	Pumping Power	111
<b>5.7</b>	<b>Operational Challenges</b>	<b>112</b>
<b>5.8</b>	<b>Concluding Remarks</b>	<b>113</b>
 <b><u>Chapter 6: MicroPCM Slurry in a Closed Thermal System</u></b>		<b>115</b>
<b>6.0</b>	<b>Introduction</b>	<b>115</b>
<b>6.1</b>	<b>MicroPCM Development Process</b>	<b>115</b>
<b>6.2</b>	<b>Fuel Cell Slurry Criteria</b>	<b>116</b>
<b>6.3</b>	<b>Phase Change Material Design</b>	<b>117</b>
<b>6.4</b>	<b>Encapsulation Processes</b>	<b>118</b>
6.4.1	In-Situ Microencapsulation	118

6.4.2	Acrylic Encapsulation	119
6.4.3	Summary of Encapsulation Process's	120
<b>6.5</b>	<b>Methodology and Apparatus</b>	<b>121</b>
6.5.1	Particle Size Analysis (PA)	121
6.5.1.1	<i>Overview</i>	121
6.5.1.2	<i>Methodology</i>	122
6.5.2	Thermal Gravimetric Analysis (TGA)	122
6.5.2.1	<i>Overview</i>	122
6.5.2.2	<i>Basic Principal</i>	123
6.5.2.3	<i>Methodology</i>	123
6.5.3	Preliminary Testing	125
<b>6.6</b>	<b>Myristic Acid</b>	<b>127</b>
6.6.1	Development	127
6.6.2	DSC	127
6.6.3	PA	129
6.6.4	TGA	130
6.6.5	Myristic Acid Summary	130
<b>6.7</b>	<b>Octadecanol</b>	<b>131</b>
6.7.1	Development	131
6.7.2	DSC	131
6.7.3	PA	133
6.7.4	TGA	134
6.7.5	Rheological Behaviour	134
6.7.5.1	<i>Separation Observations</i>	134
6.7.5.2	<i>Viscosity Assessment</i>	135
6.7.6	Summary - Octadecanol	136
<b>6.8</b>	<b>French Paraffin</b>	<b>137</b>
6.8.1	Development	137
6.8.2	DSC	137
6.8.3	PA	139
6.8.4	TGA	139
6.8.5	Rheological Observations	140
6.8.5.1	<i>Separation Observations</i>	140
6.8.5.2	<i>Viscosity Assessment</i>	141
6.8.6	Summary - French Paraffin	142
<b>6.9</b>	<b>Summary of Investigated PCM</b>	<b>143</b>
<b>6.10</b>	<b>Concluding Remarks</b>	<b>143</b>

<b><u>Chapter 7: Fuel Cell Slurry</u></b>	144
<b>7.0 Introduction</b>	144
<b>7.1 Experimental Background</b>	144
<b>7.2 Experimental System Design</b>	147
7.2.1 Fuel Cell Simulator	147
7.2.2 Slurry Pump	149
7.2.3 Data Acquisition	149
<b>7.3 Experimental System Description</b>	151
<b>7.4 Operational Challenges</b>	153
<b>7.5 Pressure Drop Measurement</b>	155
7.5.1 Pump	155
<b>7.6 Thermal Characteristics</b>	158
7.6.1 Fuel Cell Operation	158
7.6.2 Tuning the Fuel Cell and Slurry	160
7.6.3 Parasitic Pumping Analysis	162
<b>7.7 Operational Challenges</b>	163
<b>7.8 Economic Analysis</b>	163
<b>7.8 Concluding Remarks</b>	164
<b><u>Chapter 8: Conclusions</u></b>	165
<b>8.0 Conclusions</b>	165
<b>8.1 Further Work</b>	167
<b>References</b>	R
<b>Appendix</b>	A

## **Abstract:**

This thesis presents an experimental investigation into the feasibility of using a functionally thermal fluid to enhance the performance of a Proton Exchange Membrane (PEM) Fuel Cell. Specifically, a fluid was developed that utilised a liquid-solid phase change to enhance heat transport within the fuel cell. Increasing the convective heat transfer coefficient could permit the use of smaller volumetric flow rates and reduce pumping power.

The objective of the thermal fluid was to create isothermal conditions across a fuel cell and to reduce parasitic loadings from pumps and other components to enhance the overall system performance. Additionally, the fluid could reduce the system size and component cost, and stabilise temperature fluctuations within the system.

The thermal fluid that was developed constituted a mix of fine, Micro-encapsulated Phase Change Material (MicroPCM) particles suspended in a single-phase working fluid. For successful integration with the fuel cell, the microPCMs thermal and fluid properties, and their effectiveness in transferring heat, had to be fully characterised and understood.

Research consisted of experimental investigations of the fuel cell, followed by microPCM development. Experimentation on the fuel cell stack revealed a requirement for thermal stability and reduction in parasitic load from the pumps. Quantitative characterisation and development of the microPCM properties involved state of the art equipment to measure the latent heat of fusion, melting and freezing points, surface morphology and viscosity of the microPCM slurry. The effects of repeated use of solid to liquid phase change particles upon melting and solidification were studied. This led to the further development of microPCM particles and experimentally examined in a fuel cell system.

The use of MicroPCM developed in this study balanced the improvement in thermal capacity of the fluid with the increase in pumping load, when compared to the use of water alone. The study suggested that with further development of the microPCM slurry, it has the potential to significantly increase the thermal capacity of the fluid and stabilise temperatures across the fuel cell, which in turn would result in improved stack performance and electrical conversion efficiency.

## **Acknowledgements:**

I would like to express my thanks and gratitude to Professor S.Riffat for his invaluable support and backing over the years. I would extend my sincere thanks to Dr R.Wilson whom guided, advised and encouraged me throughout this research.

Further thanks are due to my work colleagues and the technicians who have made working at ISET a truly pleasurable experience. To my research mentors and friends, Dr S.Redshaw and Dr M.Gillott.

Thank you to the Baxi Group Ltd, CIBASC and the EPSRC, for their support behind my research. In particular, Ian Stares and David Goddard of Baxi. Many thanks to Guido Gummert of European Fuel Cell, for my time spent in Germany and his support with the invaluable Fuel Cell testing. To Martin Butters and Ian Biggins of CIBASC, for their assistance and specialist knowledge in material development.

I am further grateful to my parents and Katrina who encouraged and supported me throughout this research.

## **List of Figures:**

Figure 1.1a	Fuel Cell Mobile Phone	2
Figure 1.1b	Toyota's Fine-N Hybrid Fuel Cell Car	2
Figure 1.2	The EU Hydrogen Deployment Strategy (EU20719 EN)	4
Figure 2.1	Single Fuel Cell (Image from UTC Fuel Cells)	8
Figure 2.2	Fuel Cell Flow Diagram (Texas Fuel Cells)	9
Figure 2.3	Fuel Cell Stack Durability and Cost (Ballard)	12
Figure 2.4	EFC GmbH - PEMFC Small Scale Stationary Unit	14
Figure 2.5	PEM Fuel Cell Diagram (IRD Fuel Cells A/S)	15
Figure 2.6	PEM Fuel Cell Stack - EFC GmbH	19
Figure 2.7	Fuel Cell Test Rig Schematic	20
Figure 2.8	Fuel Cell Test Rig (EFC GmbH)	21
Figure 2.9	LabView 7.0, Stack Test Rig User Interface (EFC GmbH)	22
Figure 2.10	Graph Showing the Polarisation Curve for a Typical Low Temperature, Air Pressure, Fuel Cell.	23
Figure 2.11	Polarisation Curve for the PEMFC - Variation in Coolant Flow Temperature	24
Figure 2.12	Polarisation Curve for the PEMFC - dT across the Stack	25
Figure 2.13	The PEM Fuel Cell System	26
Figure 2.14a	PEM Fuel Cell Thermal Storage	29
Figure 2.14b	PEM Fuel Cell Combi Store	29
Figure 2.15	PEM Fuel Cell Thermal Store - EFC GmbH	30
Figure 2.16a	TES Experimental Apparatus View 1	31
Figure 2.16b	TES Experiential Apparatus View 2	31
Figure 2.17	Fuel Cell Thermal Loading to a 300lt Store	32
Figure 2.18a	300lt Thermal Store Under Charging - Graph Indicating the Relationship Between Temperature and Tank Height with Time.	32
Figure 2.18b	300lt Thermal Store Under Discharge - Graph Indicating the Relationship Between Temperature and Tank Height with Time.	33
Figure 2.19	1000lt Combination Storage Tank Cross Section	34
Figure 2.20a	1000lt Combi Store Under Charging - Graph Indicating the Relationship Between Temperature and Tank Height with Time.	35
Figure 2.20b	1000lt Combi Store Under Discharge - Graph Indicating the Relationship Between Temperature and Tank Height with	36

	Time.	
Figure 3.1	Red Blood Cells	40
Figure 3.2	Clathrate Hydrate Crystals	41
Figure 3.3	Thermodynamic Functions of Multifunctional Fluids. A Phase Change Slurry can fulfil five or more functions simultaneously (see bold, green circles).	41
Figure 3.4	Classification of Thermal Energy Storage Materials (Abhat, 1982)	43
Figure 3.5	Chemical structure of Paraffin Waxes	44
Figure 3.6	Pressure-temperature diagram of pure substances (Yunun, 1989)	45
Figure 3.7	Change in Enthalpy at the Transition Temperature (Hariri, 1988)	47
Figure 3.8	Supercooling of a Phase Change Material (Burns, 1981)	48
Figure 3.9	Two Film Layer Micro-capsule	54
Figure 3.10	Microscopy of the MicroPCM and Woven Fibres	58
Figure 3.11	Outlast MicroPCM Apparel Principle of Operation	58
Figure 3.12	Daimler-Chrysler Multiphase Suspension Coolant (Pat; WO2004009728)	59
Figure 4.1	Stratification Tendencies of the MicroPCM Samples	64
Figure 4.2	XL ESEM Machine	65
Figure 4.3	Inside the ESEM – Sample and Heating Stage	65
Figure 4.4a	ESEM Image – 35°C sample @ 30°C	67
Figure 4.4b	ESEM Image – 35°C sample @ 35°C	67
Figure 4.4c	ESEM Image – 35°C sample @ 40°C	67
Figure 4.5a	ESEM Image – 50°C sample @ 45°C	68
Figure 4.5b	ESEM Image – 50°C sample @ 55°C	68
Figure 4.5c	ESEM Image – 61°C sample @ 50°C	68
Figure 4.5d	ESEM Image – 61°C sample @ 70°C	68
Figure 4.6	Pelkin Elmer - Model: Pyris 1DSC Machine.	71
Figure 4.7	Typical thermogram of a pure substance that undergoes solid to liquid transition during the heating and cooling cycle. (Aboul-Enein, S. and Olafa, S, 1991)	72
Figure 4.8	Metler AE 163 + Samples	74
Figure 4.9	MicroPCM Slurry Samples	74
Figure 4.10	DSC Thermogram for 100% 35°C MicroPCM Sample	75
Figure 4.11	DSC Thermogram for 100% 50°C MicroPCM Sample	76

Figure 4.12	DSC Thermogram for 100% 61°C MicroPCM Sample	76
Figure 4.13	DSC Thermogram of 61°C MicroPCM Through the Heating Phase and Corresponding ESEM Images Taken Through the Phase Transition	78
Figure 4.14	DSC Thermogram for 61°C MicroPCM and Slurries of 10%-40%	79
Figure 4.15	Relationship Between Mass Fraction of MicroPCM with Water and Latent Heat of Fusion	80
Figure 4.16	Schematic of TA Experimental Rig	81
Figure 4.17a	TA Sample	82
Figure 4.17b	TA Experimental Rig	82
Figure 4.18a	50°C MicroPCM TA - Heating	84
Figure 4.18b	61°C MicroPCM TA - Heating	84
Figure 4.19a	50°C MicroPCM TA - Cooling	85
Figure 4.19b	61°C MicroPCM TA - Cooling	85
Figure 4.20	Images of Bohlin Rotary Viscometer + Test Equipment	87
Figure 4.21	Water Viscosity	88
Figure 4.22	61°C MicroPCM Slurry Viscosity	88
Figure 4.23	61°C MicroPCM Slurry Viscosity	89
Figure 5.1	35°C Slurry	96
Figure 5.2	35°C n-eicosane Microscopy	96
Figure 5.3	a) One-way-flow Rig b) Closed Loop Rig.	97
Figure 5.4	Test Rig Schematic	98
Figure 5.5	Test Rig Image	98
Figure 5.6	Heater Test Section	99
Figure 5.7	Image of the DT500	100
Figure 5.8	Heat Exchanger Temperature Profiles for a MicroPCM Slurry in a Closed Loop System	102
Figure 5.9	Laboratory Room Temperature	103
Figure 5.10	Dittus+Boelter Verification	106
Figure 5.11	Closed Loop – Relationship Between Flowrate and $dT$ Across Heating Section	108
Figure 5.12	Closed Loop – Relationship Between Flowrate and Power input Across Heater Section.	110
Figure 5.13	Closed Loop – Relationship Between Flowrate and Power input Across Heater Section.	111
Figure 6.1	MicroPCM Design Procedure	116
Figure 6.2	In-Situ Micro-encapsulation Process	118

Figure 6.3	Acrylic Encapsulation Mechanism	120
Figure 6.4	Optical Set-up for the Generation of Diffraction Patterns.	121
Figure 6.5	Helos Laser Diffraction Particle Analyser	122
Figure 6.6	Perkin-Elmer Thermal Gravimetric Analyser	123
Figure 6.7	TGA – Capsule Durability	124
Figure 6.8	DSC – 40% Hexadecanol Concentration with Water	125
Figure 6.9	Thermogram – 40% Myristic Acid Concentration with Water	127
Figure 6.10	DSC – 40% Myristic Acid + Stearic Acid with water by Acrylic Polymerisation	128
Figure 6.11	PA – Myristic Acid and Stearic Acid	129
Figure 6.12	SEM – Myristic Acid @ 1000x Magnification	129
Figure 6.13	SEM – Myristic Acid @ 2000x Magnification	129
Figure 6.14	TGA – Myristic Acid MicroPCM	130
Figure 6.15	DSC – 40% Octadecanol with water by MF In-Situ	132
Figure 6.16	DSC – 40% Concentration Octadecanol + Stearic Acid with water formed by Acrylic Polymerisation	133
Figure 6.17	PA – Octadecanol + Stearic Acid	133
Figure 6.18	TGA – Octadecanol MicroPCM	134
Figure 6.19	Separation Characteristics of Octadecanol MicroPCM at 30% Concentration	135
Figure 6.20	Viscosity of Octadecanol MicroPCM	136
Figure 6.21	DSC – 100% French Paraffin	137
Figure 6.22	DSC – 40% French Paraffin and Stearic Acid with water by Acrylic Polymerisation	138
Figure 6.23	PA – French Paraffin by Acrylic Polymerisation	139
Figure 6.24	TGA – French Paraffin MicroPCM	140
Figure 6.25	Separation Characteristics of French Paraffin MicroPCM at 30% Concentration	141
Figure 6.26	Rheology of French Paraffin MicroPCM	142
Figure 7.1	Heat Flow Cycles	145
Figure 7.2	Enthalpy Curve of the French PCS with Different Concentrations of Capsules Compared with Water	147
Figure 7.3	Fuel Cell Simulator	148
Figure 7.4	LabView 7.2; Fuel Cell Simulator User Interface	149
Figure 7.5a	Fuel Cell Simulator User Interface	150
Figure 7.5b	Electromagnetic Flow Meter and Pump Power Meter	150
Figure 7.6	Fuel Cell Slurry Test Rig Schematic	152
Figure 7.7	View of Fuel Cell Slurry Test Rig	152

Figure 7.8	Figure 7.7: Fuel Cell Slurry Test Rig; Mixing Reservoir and Flow Meter	153
Figure 7.9	Figure 7.8: Fuel Cell Slurry System Through a Heating Phase	155
Figure 7.10	Baseline Study with Water; The Relationship Between Pressure Drop Through the Pump, Flow Rate and Temperature	156
Figure 7.11	MicroPCM Slurry; The Relationship Between Pressure Drop Through the Pump, Flow Rate and Temperature	156
Figure 7.12	Comparison Between the MicroPCM Slurry State of Phase and Water	157
Figure 7.13	FC Simulator Flow and Return Temperatures with the Thermal Store	158
Figure 7.14	FC Power Comparison with the Water and PCS Circuit	159
Figure 7.15	Variation in System Temperatures with the PCS	160
Figure 7.16	Variation in Specific Heat with Bulk Mean Fluid Temp	161
Figure 7.17	Equivalent Flow Rate Estimate	162

### **List of Tables:**

Table 2.1	Summary of Fuel Cell Type Characteristics (Ellis, 2002)	10
Table 2.2	Effect of Fuel Gas Constituents on FC Performance (Hirschenhofer, 1998)	18
Table 2.3	Beta FC Stack Specifications	19
Table 2.4	FC Stack Coolant Conditions Summary	37
Table 3.1	Physical Properties Data of Paraffin Waxes (Zalba, 2003)	44
Table 3.2	PCM Selection Criteria	51
Table 4.1	Specification of MicroPCMs Supplied by Outlast Technologies Inc.	62
Table 4.2	Details of measurement techniques (Abhat, 1982).Differential Scanning Calorimeter and Thermal Analysis	70
Table 4.3	Summary of MicroPCM Sample Thermograms	77
Table 5.1	Slurry Material Thermophysical Properties	96
Table 5.2	Dittus+Boelter Constants from Equation [5.11]	106
Table 5.3	Rig Pumping Power Requirement	112
Table 6.1	Rheology of French Paraffin MicroPCM	143
Table 7.1	Equivalent Flow Rate Estimate	162

## Nomenclature:

<b>Symbol</b>	<b>Term</b>	<b>Unit</b>
$A$	Surface area	$m^2$
$B$	Bias error	
$C_p$	Heat capacity	$\text{kJ/kg} \cdot ^\circ\text{C}$
$C_{pl}$	Heat capacity at constant pressure of liquid phases	$\text{kJ/kg} \cdot ^\circ\text{C}$
$C_{ps}$	Heat capacity at constant pressure of solid phases	$\text{kJ/kg} \cdot ^\circ\text{C}$
$C_{pe}$	Sum of sensible and latent effective heat capacity	$\text{kJ/kg} \cdot ^\circ\text{C}$
$C_m$	Mass fraction of PCM in suspension	
$D$	Circular diameter	$m$
$E$	Electromotive force	$V$
$F$	Faraday's constant	$\text{Cb/mol}$
$f$	Friction factor	
$\Delta g_h$	Gibbs free energy released	$J$
$h$	Heat transfer coefficient	$\text{W/m}^2 \cdot ^\circ\text{C}$
$H$	Enthalpy	$\text{kJ}$
$\Delta H$	Enthalpy change	$\text{kJ}$
$\Delta H_f$	Enthalpy of fusion	$\text{kJ}$
$\Delta H_v$	Enthalpy of vaporization	$\text{kJ}$
$I$	Current	$A$
$I_i$	Instrument reading	
$l_t$	True value	
$K_f$	Thermal conductivity of the fluid	$\text{W/m} \cdot ^\circ\text{C}$
$L$	length	$m$
$l$	litres	$l$
$M$	Mass	$\text{kg}$
$M_s$	Mass of samples	$\text{kg}$
$M_r$	Mass of reference substance	$\text{kg}$
$\dot{m}$	Mass flow rate	$\text{kg/sec}$
$N$	Quantity of material	moles
$N_u$	Nusselt number	
$P$	Pressure	bar
$\Delta P$	Pressure drop	mb
$P_r$	Prandtl number	
$\rho$	Density	$\text{Kg/m}^3$

$q_w$	Wall heat flux	W/m <sup>2</sup>
$Q$	Heat Change	J
$\dot{Q}$	Heat flow	J/s
$R$	Radius of pipe	m
$Re$	Reynolds number	
$S$	Entropy	kJ
$\Delta S$	Entropy Change	kJ
$St$	Stefan number	
$t$	Time	sec
$T$	Temperature	°C
$T_b$	Temperature of boiling	°C
$T_{BMF}$	Mean bulk fluid temperature	°C
$T_f$	Temperature of fusion	°C
$T_h$	Hot temperature	°C
$T_c$	Cold temperature	°C
$\mu$	Dynamic viscosity	Pas
$V$	Voltage	V
$V$	Volume	m <sup>3</sup>
$\Delta V$	Volume Change	m <sup>3</sup>
$Y$	Output signal displacement (DSC)	

## **Chapter 1: Introduction**

### **1.0 Introduction**

Energy is the very lifeblood of today's society and economy. Our work, leisure, and our economic, social and physical welfare all depend on the supply of energy. Yet we take it for granted – and energy demand continues to grow year after year. Traditional fossil energy sources such as oil are limited, and the growing gap between increasing demand and shrinking supply will have to be met by alternative energy sources.

Hydrogen and fuel cells are seen as positive solutions to bridging this gap between energy supply and increasing demand. Hydrogen is a clean energy carrier that can be produced from any primary energy source, and fuel cells are the most efficient device for converting hydrogen, and possibly other fuels, into electricity.

The race to the new fuel cell and hydrogen future is indeed heating up. It is clear that fuel cell technology presents the potential to create an unprecedented change in energy markets. No major energy nation or company wants to be left behind, and as a result, fuel cell R+D is growing swiftly around the globe.

### **1.1 Research Overview**

Fuel cells are poised to be the power generation systems of the 21st century (Ellis, 2002). They are intrinsically clean and highly efficient energy conversion devices that look set to replace or augment combustion engines and battery technologies in a wide range of applications. Paramount to their efficient operation, however, is to ensure thermal stability of the fuel cell stack, effective use of the electrical and thermal energy generated during the fuel conversion process, and minimising parasitic loadings from ancillary devices such as pumps. This thesis focuses on the thermal system of a PEM fuel cell. This fuel cell was the heart of a stationary 2.0kW<sub>e</sub> fuel cell system that was being developed for micro-scale cogeneration.

This thesis established that the fuel cell industry is currently "searching for methods of stabilising thermal conditions across the fuel cell" (Dr.Du, Plugpower, 2005). This was primarily to make water production within the stack more predictable and uniform. To this end; a functionally thermal fluid was developed to stabilise the temperature difference across the stack, and further, to reduce

parasitic pumping loads to improve the overall electrical efficiency of the fuel cell system.

The following sections provide a brief overview of fuel cells and the hydrogen economy, the current stage of development in thermal fluids, the project research aims and an overview of the thesis.

## 1.2 Fuel Cells

Over a century has passed since Sir William Grove used two platinum electrodes with a sulphuric acid electrolyte to generate an electric current in a reverse electrolysis process, creating what is widely regarded as the first 'fuel cell' (Refocus, 2003). However, it is only now that fuel cell technology is coming close to full commercialisation and mass adoption. In part, this has been due to improvements in the performance and reduction in the cost of fuel cells, and in part it is due to external pressures affecting global energy use, such as environmental and macro-economic conditions. Increasingly, companies and organisations are looking to the future, seeing the need for clearer ways of providing power, and joining the wave of research and development.

Fuel cells are set to pervade every application of power use, from mobile phones (figure 1.1a) and laptop computers, to cars (figure 1.1b) and buses, to houses and buildings of all scales, to large scale power generation.



Figure 1.1a: Fuel Cell Mobile Phone ([www.3G.co.uk](http://www.3G.co.uk))



Figure 1.1b: Toyota's Fine-N Hybrid Fuel Cell Car ([www.fuelcelltoday.com](http://www.fuelcelltoday.com))

### 1.3 The Hydrogen Economy

Hydrogen can be produced from carbon free or carbon-neutral energy sources or from fossil fuels with CO<sub>2</sub> capture and storage. Thus the use of hydrogen could drastically reduce greenhouse gas emissions from the energy sector.

In 1874, Jules Verne, the popular science fiction writer, published a curious book entitled "The Mysterious Island". It was dated at the time of the American civil war and focused on a small group of men that were stranded on an island after escaping confederate imprisonment (Rifkin, 2002). One day they mused about the future and a sailor named Pencroft, asked the engineer, Cyrus Harding, what might happen to American commerce if they were to run out of coal. "And what would they burn instead?" asked Pencroft. "Water," explained Harding, to everyone's surprise. Harding went on to explain:

*"Water decomposed into its primitive elements and decomposed doubtless, by electricity, which will then have become a powerful and manageable force...Yes, my friends, I believe that water will one day be employed as fuel, that hydrogen and oxygen which constitutes it, used singly or together, will furnish an inexhaustible source of heat and light, of an intensity of which coal is not capable...Water will be the coal of the future." (Verne,1874).*

This extract sets the scene for the current vision of the hydrogen economy and fuel cells. Although we are still a long way from relying solely on renewable energy to meet our complete energy needs, Verne's vision of a hydrogen future is now the subject of many corporate boardrooms across the globe (Rifkin, 2002). The realisation of the hydrogen economy, not only by Europe, but the rest of the world, has been heightened by requirements of energy security and such tragic events as 9/11, New York and the war in Afghanistan 2004.

The transition to a hydrogen economy will be arduous. It is not certain to happen, nor is it obvious how soon it could happen. The first steps have already begun, but could take many decades to complete. The transition will involve many changes over time in how hydrogen is produced, delivered, stored, and converted into electricity. The transition will also affect different industries at different stages of the transition. Figure 1.2, is from the EU Hydrogen and Fuel Cell Technology Platform and shows what these changes could be and when they might occur.

## Schedule for a Deployment Strategy

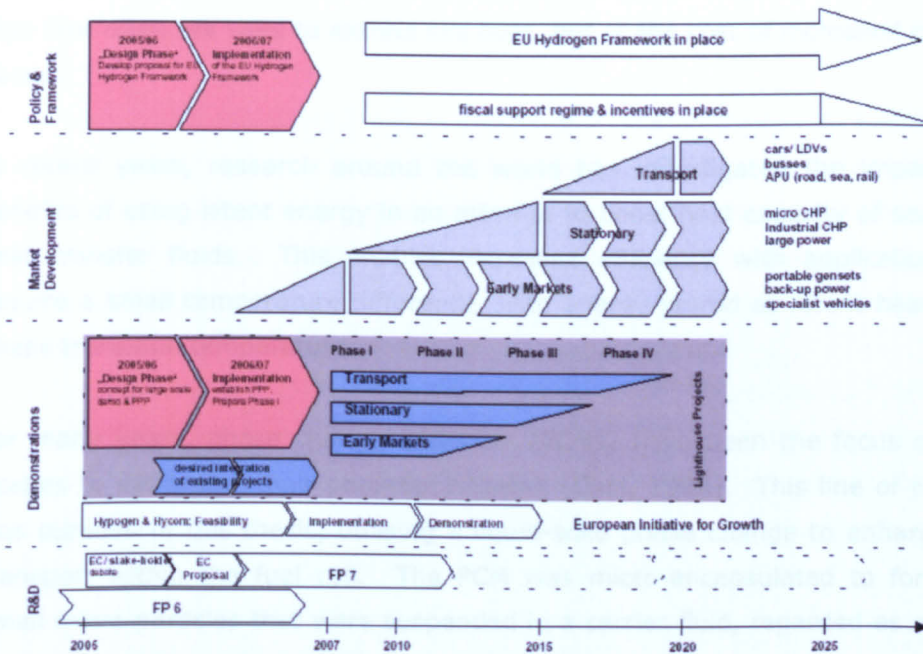


Figure 1.2: The EU Hydrogen Deployment Strategy (EU20719 EN)

## 1.4 Fuel Cell and Hydrogen Challenges

There are numerous challenges that the fuel cell and hydrogen economy must meet before full commercialisation. These are covered in more detail in the following chapters; however, all breakthroughs in this rapidly moving technology are welcome. It was considered that the use of a novel heat transfer fluid within the fuel cell system may address some gaps in performance, reliability and/or component lifetime. The following chapters focus on the development of this fluid with the fuel cell.

## 1.5 Functionally Thermal Fluids

Functionally thermal fluids typically can be employed to both physically and thermally alter the characteristics of a heat transfer fluid. They offer the opportunity to make fuel cell systems function with greater overall efficiency and reliability.

The amount of heat that can be stored by common heat transfer fluids, e.g. water or oils, depends on the useable temperature range that can be exploited and the specific heat coefficient of the fluid. The efficiency of such heat transfer fluids is poor if an application allows only a small temperature difference. Investigations in chapter 2, have shown that the smaller the temperature difference across the

fuel cell or stack, the higher and more stable the power output. This means that high flow rates are used to extract the heat, but at the cost of increased pumping power.

In recent years, research around the world has investigated the impacts and benefits of using latent energy in an attempt to boost heat capacity of secondary heat transfer fluids. This enables increased efficiency with applications that require a small temperature difference, with energy stored as latent heat at the phase transition temperature.

For many years, phase change materials (PCMs) have been the focus of these studies to determine their potential benefits (Choi, 1993). This line of research was pursued in this thesis, utilising a liquid-solid phase change to enhance heat transport within the fuel cell. The PCM was micro-encapsulated to form very small micro particles that were suspended in a carrier fluid, regarded as a micro-encapsulated Phase Change Slurry (microPCS).

### **1.6 Summary of Research Aims**

The main goal of this research undertaken was to enhance the thermal system of the fuel cell to make the overall consumer package more reliable and efficient. The integration of a functionally thermal fluid with the fuel cell was assessed in terms of pushing the boundaries of heat transfer within this emerging technology.

The project aims have been summarised as follows;

- Experimentally evaluate the fuel cell stack performance.
- Investigate functionally thermal fluids and micro-encapsulated phase change materials for fuel cell integration.
- Develop a micro-encapsulated phase change material that was specific to the operating conditions and practicalities of the fuel cell system.
- Evaluate the developed micro-encapsulated phase change material with the fuel cell system.

The thesis is divided into three research stages. The first stage, Chapter 2, analyses the proton exchange membrane fuel cell and its thermal system. The 2.0kW<sub>e</sub> fuel cell stack was experimentally evaluated. Fuel cell operating conditions and criteria for the functionally thermal fluid were established. Further experimentation on the thermal system and storage strategies revealed

favourable techniques of loading the thermal store to maximise fuel cell operation.

The second stage, Chapters 3 – 5, investigates the concept of using a functionally thermal fluid with in a pumped closed loop system. Some commercially available materials were obtained and quantitative investigations undertaken into material operation and thermal properties. An experimental test rig was designed and constructed for evaluation of the microPCS in a small scale closed loop system.

Chapters 6 and 7 were the third stage of the research. Based on the fuel cell and microPCM data obtained from the previous tests, chapter 6 indicates the design and development of a new microPCS specific for the fuel cell. Chapter 7, demonstrates the test methodology and experimental rig constructed to simulate the thermal loads from the fuel cell in practice with the microPCS.

## **Chapter 2: The PEM Fuel Cell**

### **2.0 Introduction**

The following chapter is dedicated to the fuel cell and its thermal system. Three sections are defined in this chapter, summarised as follows; A general overview of fuel cells with particular focus on the Proton Exchange Membrane (PEM) fuel cell, fuel cell experimentation and a parallel study of thermal storage with the fuel cell.

Experimental tests were conducted on the fuel cell stack over a range of thermal conditions and loads. The data established from these tests set the benchmark of operational conditions for the rest of this thesis. Experimentation revealed that the fuel cell performance was sensitive to the thermal conditions of the stack. These test further suggested that if the thermal fluid could transfer the heat under almost isothermal conditions, it could not only improve the fuel cell performance but also influence its design.

In parallel to the fuel cell testing, a study on the fuel cell thermal system and storage was undertaken. This work on the storage strategy indicated the significance of the other links in the thermal system chain, the relationship to the thermal system and its importance to the overall economic performance. The result of this work, indicated at the end of this chapter, was the selection of a novel thermal storage unit that could distribute the thermal load more effectively than a standard storage vessel, and as a result, maximise the fuel cell operational time.

### **2.1 Fuel Cell Fundamentals**

#### **2.1.1 What is a Fuel Cell?**

Fuel cells are electrochemical devices that combine hydrogen (the fuel) and oxygen to produce electricity, heat and water. A fuel cell, illustrated in figure 2.1, comprises of three key elements, an electrolyte membrane sandwiched between two electrodes, the fuel electrode (or anode) and the oxidant electrode (or cathode). The electrolyte is the substance that selectively allows the hydrogen protons to freely pass through as they move between electrodes. Electrolytes can be different substances and is usually the distinguishing factor for the various types of fuel cells. Individual fuel cells can be combined to form a fuel cell 'stack'. The number of fuel cells in the stack determines the total voltage produced by the device, and the surface area of each cell determines the current.

Fuel cells operate without combustion, so they are virtually pollution free. Since the fuel is converted directly to electricity, when compared to conventional internal combustion engine, the fuel cell can operate at much higher efficiencies than by extracting more electricity from the same amount of fuel. The fuel cell itself has no moving parts; making it a quiet and reliable source of power.

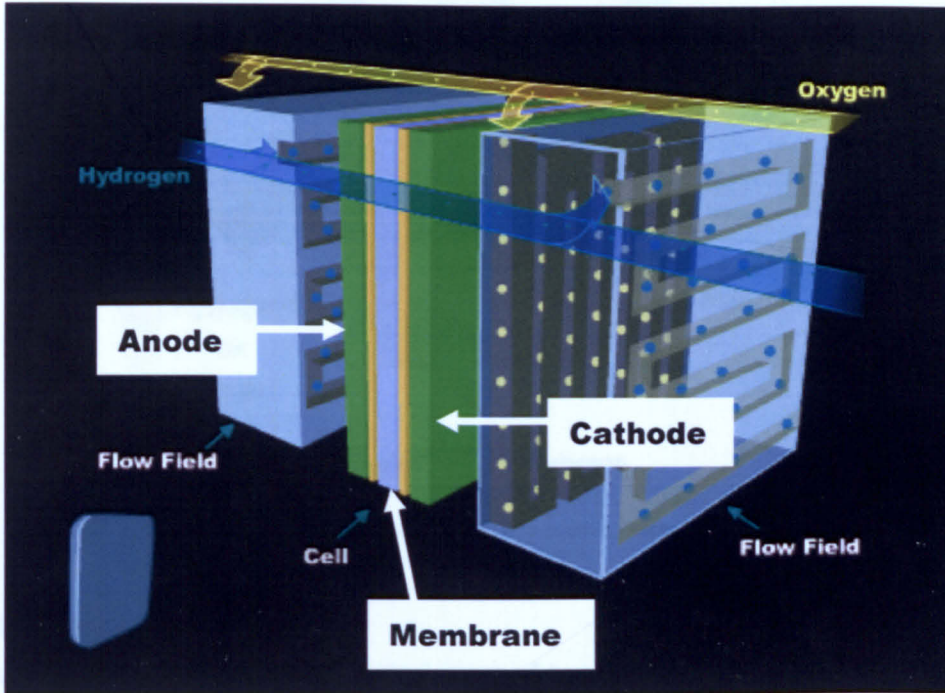


Figure 2.1: A Single Fuel Cell (Image from UTC Fuel Cells)

### 2.1.2 How does a Fuel Cell Work?

The production of energy begins when a stream of hydrogen molecules (hydrogen fuel) is forced against the fuel electrode (anode). The anode causes the hydrogen molecule to split into protons and electrons. At the same time, the cathode absorbs oxygen from air generating a potential that pulls the electrons through the external circuit. After the absorbed oxygen receives two electrons, it forms a negatively charged particle called an oxygen anion. The membranes on each side of the cell act as a 'one way valve' which blocks electrons, hydrogen gas and oxygen radicals and allows only the positively charged protons to diffuse through the membrane. The proton's migration through the electrolyte via the membrane ends by combining with the oxygen anion at the cathode to produce water and some heat. The cathode expels the water and absorbs more oxygen to

start the reaction again. By adopting a cogeneration strategy, this waste heat is captured and combined with the electrical output to provide significant efficiencies of over 90% can be achieved. Figure 2.2 illustrates the operation of a fuel cell.

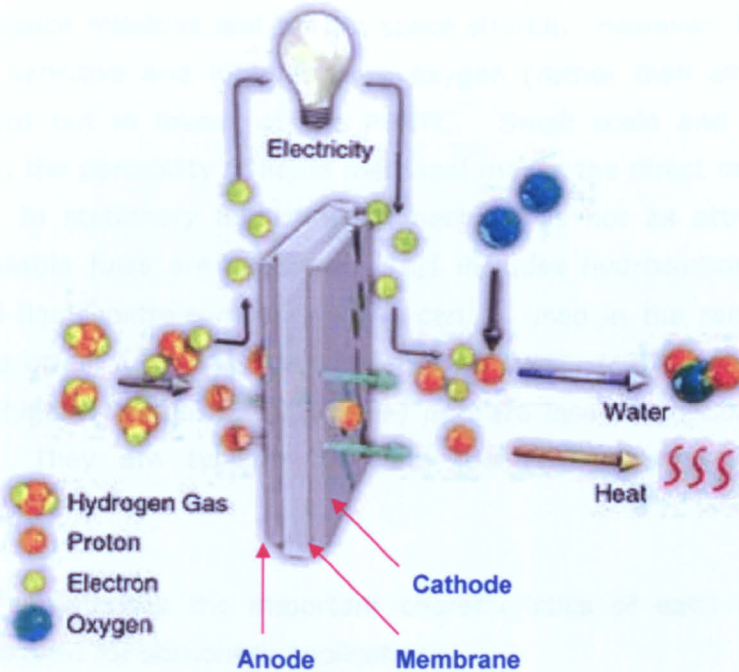


Figure 2.2: Fuel Cell Flow Diagram (Texas Fuel Cells)

### 2.1.3 Types of Fuel Cell

Each fuel cell comes with its particular set of benefits and shortcomings that lend themselves to some applications better than others. This investigation focuses on the Proton Exchange Membrane (PEM) fuel cell for small stationary systems, primarily this is for its high energy density, quick response, scalability and low operating temperature (50-90°C).

Fuel cells are most commonly distinguished by their type of electrolyte membrane and include.

- Proton Exchange Membrane Fuel Cell (PEM)
- Alkaline Fuel Cell (A)
- Phosphoric Acid Fuel Cell (PA)
- Molten Carbonate Fuel Cell (MC)
- Solid Oxide Fuel Cell (SO)
- Direct Methanol Fuel Cell (DM)

The electrolyte used in fuel cells determines the nature and purity of the fuel and oxidant, operating temperature, and design. The AFC is of historical interest as it was the first type to see practical use, serving as the primary power source on the Apollo space missions and on the space shuttle. However, this type of fuel cell is  $\text{CO}_2$  sensitive and requires pure oxygen (rather than air), hence it has been phased out in favour of the PEMFC. Small scale and portable power applications, the portability of liquid methanol makes the direct methanol fuel cell attractive. In stationary applications, methanol is not as attractive as more readily available fuels are required. This includes hydrocarbon fuels such as natural and liquid petroleum gas, which can be used in the remaining fuel cell types. The other fuel cells, that include the PAFC, MCFC and SOFC typically operate at higher temperature ( $200^\circ\text{C}+$ ) and are less susceptible to electrolyte poisoning. They are typically used in medium to large scale stationary applications.

Table 2.1, summarises the important characteristics of each of the fuel cell technologies used for stationary applications.

Fuel Cell Technology	PEM FC	PA FC	MC FC	SO FC
<b>Electrolyte</b>	Polymer Membrane	Phosphoric Acid	Molten Carbonate	Ion-conductive Ceramic
<b>Operating Temperature (<math>^\circ\text{C}</math>)</b>	50-90	200	650	800
<b>Charge Carrier</b>	$\text{H}^+$	$\text{H}^+$	$\text{CO}_3^{2-}$	$\text{O}^{2-}$
<b>Power Density (<math>\text{W}/\text{cm}^2</math>)</b>	0.3-0.8	0.1-0.3	0.1-0.2	0.1-0.3
<b>Electrical Efficiency at Full Load (%)</b>	40	45	45-50	45-50
<b>Heat Output (%)</b>	40	35	30-35	35
<b>Start-up Time</b>	Minutes	Hours	Hours	Hours
<b>Applicable Size Range (<math>\text{kW}_e</math>)</b>	1-250	100-1,000	100-2,000	5-2,000
<b>Typical Application</b>	Automotive + Small Scale Stationary	Medium Scale Stationary	Medium + Large Scale Stationary	All Stationary Sizes

**Table 2.1: Summary of Stationary Fuel Cell Type Characteristics (Ellis, 2002)**

#### 2.1.4 Inherent Strengths of Fuel Cells

Notwithstanding the technical differences across the various fuel cell types and applications, the main advantages of fuel cells are:

- **Fuel Efficiency.** Combustion technologies are theoretically incapable of providing the level of fuel/electrical efficiency that fuel cells can.
- **Flexibility.** Fuel cells offer quick response and high efficiency over various loads and do not require running at or close to peak load to deliver the required economics (Ellis, 2002).
- **Environmentally Benign.** Hydrogen produced from renewables is the cleanest solution. Although fuel cells can consume hydrocarbons like conventional combustion engines, the processes involved are very different. As a consequence they do not produce nitrogen or sulphur oxides ( $\text{NO}_x$  and  $\text{SO}_x$ ) nor do not produce particulates. Carbon dioxide is a product if hydrocarbon fuels are used, but the quantities are smaller due to higher system efficiencies.
- **High Power Density.** Particularly when compared to other electrochemical technology. In addition, fuel cells do not require recharging – ‘fuel and go’.

#### 2.1.5 Fuel Cell Technology Challenges

Cost and durability are the major challenges to fuel cell commercialisation. However, hurdles vary according to the application in which the technology is employed. The size, weight, thermal and water management are also barriers to the commercialisation of fuel cell technology dependent on the application where they are to be applied. In transportation applications, these technologies face more stringent cost and durability hurdles. In stationary power applications, where cogeneration of heat and power is desired, the use of PEM fuel cells would benefit from raising operating temperatures to supply a higher grade of thermal output. For market acceptance, stationary PEMs are expected to have a lifespan of greater than 40,000 hours of reliable operation.

The following figure 2.3, is a good representation of the present situation of one of the leading fuel cell developers, Ballard, based in Canada. They focus on PEM stack development for transport and small scale stationary applications.

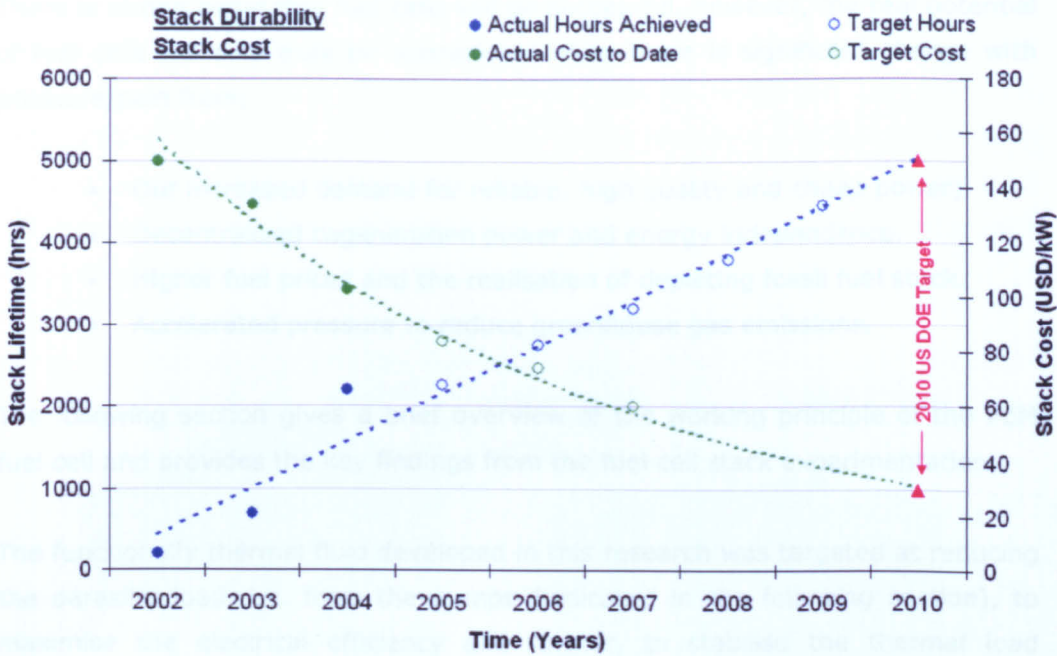


Figure 2.3: Fuel Cell Stack Durability and Cost (Ballard, 2005)

Ballard's company vision is 'Power to change the world'. As with any emerging technology, until recently, the fuel cell industry has had no established technology benchmarks or milestones against measured progress. However, the US Department of Energy (US DOE) recently updated its Hydrogen, Fuel Cells and Infrastructure Technologies Program's Multi-Year Research, Development and Demonstration Plan, written in 2003. It laid out industry targets for fuel cell cost, durability and performance. Figure 2.3 indicates the US DOE's 2010 target values for a stack lifetime at 5000 hrs and a cost of \$30 US/kW net for a fuel cell stack. Ballard's progress to date indicates that it is well on target and above the durability target trend-line at 2200 hrs in 2004. It also shows good progress with cost reductions, in 2004, hitting \$103 US/kW.

### 2.1.6 Are Fuel Cells the Future?

Although the capital costs of fuel cell systems are still well above what they need for economic viability. These prices are falling rapidly and now have great potential for being the next generation energy providers. They are essentially a first generation technology that must excel in order to effectively compete with its much more mature conventional solutions, such as the IC engine in order to be successful.

There is strong belief that fuel cells will be successful, however, the real potential of fuel cells will only truly be appreciated when there is significant change with pressure/pain from;

- Our increased demand for reliable, high quality and cheap power;
- Decentralised cogeneration power and energy independence.
- Higher fuel prices and the realisation of depleting fossil fuel stock.
- Accelerated pressure to reduce greenhouse gas emissions.

The following section gives a brief overview of the working principle of the PEM fuel cell and provides the key findings from the fuel cell stack experimentation.

The functionally thermal fluid developed in this research was targeted at reducing the parasitic load, i.e. from the pumps (indicated in the following section), to maximise the electrical efficiency and further, to stabilise the thermal load through the stack. The following experimental tests were undertaken on the fuel cell stack to investigate the effect of different thermal loading on the operational performance. This was to provide information and design criteria for selection and design of the functionally thermal fluid.

In parallel to the fuel cell tests, the thermal store was developed to be used in the thermal system and in corporation with the developed thermal fluid.

## 2.2 Proton Exchange Membrane Fuel Cell

A  $2\text{kW}_e$  PEMFC was the focus of this investigation. It was the heart of the small scale stationary system that is currently being developed for domestic cogeneration, figure 2.4. The total system was to provide a  $1.5\text{kW}_e$  and  $3\text{kW}_{\text{TH}}$  to the end domestic user. This allowed for  $500\text{W}$  of electrical energy produced from the fuel cell stack to drive parasitic components within the fuel cell system, such as pumps, valves and the computer interface.

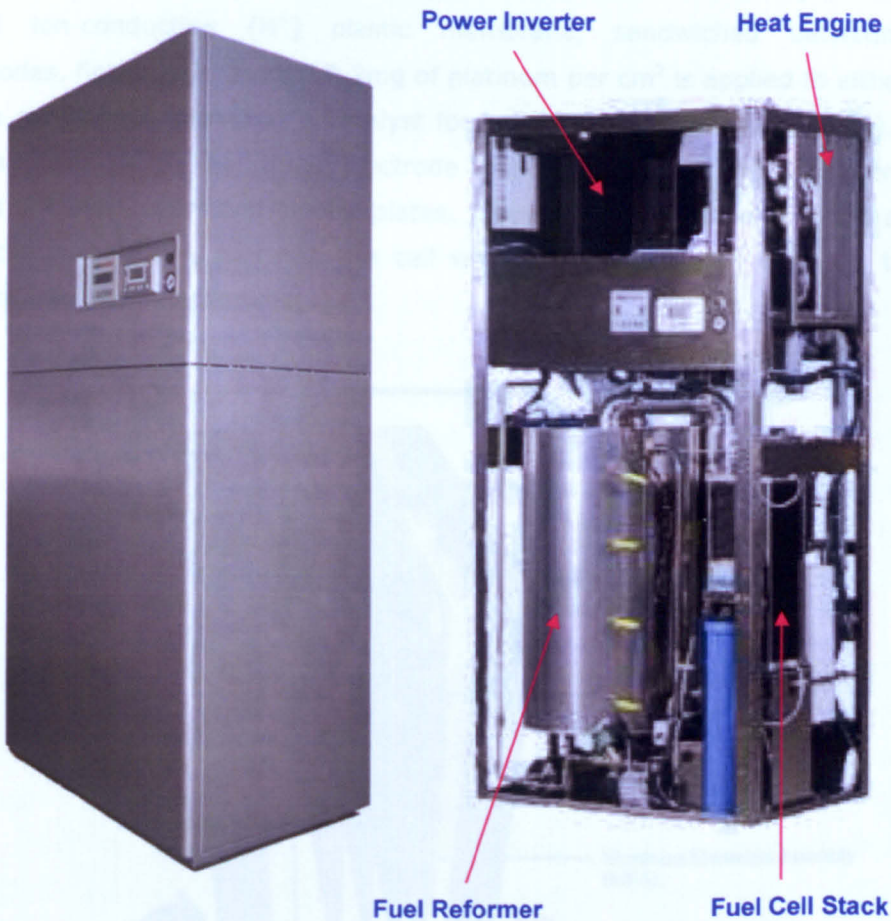


Figure 2.4: PEMFC Small Scale Stationary Unit, EFC GmbH

### 2.2.1 PEM Stack Overview

The PEM fuel cell is notable for its high current density and low operating temperatures (Larminie, 2000). These features have made this fuel cell particularly attractive in transportation and small-scale stationary applications where compact size and rapid start-up are important characteristics. The realistic possibility that this technology may achieve competitive costs, durability and reliability has attracted the attention of developers worldwide.

At the heart of the PEM fuel cell is a layered combination of electrolyte - an acid-based ion-conducting ( $H^+$ ) plastic membrane, sandwiched between two electrodes, figure 2.5. Around 0.2mg of platinum per  $cm^2$  is applied to either side of the membrane, providing a catalyst for both cell reactions (Ellis, 2002). This unit is known as the membrane electrode assembly or MEA. The MEA is encased in gas diffusion layers and bipolar plates. They are termed bipolar plates as one side channels the  $H_2$  fuel into the cell while the reverse side channels the  $O_2$  oxidant into the adjacent cell.

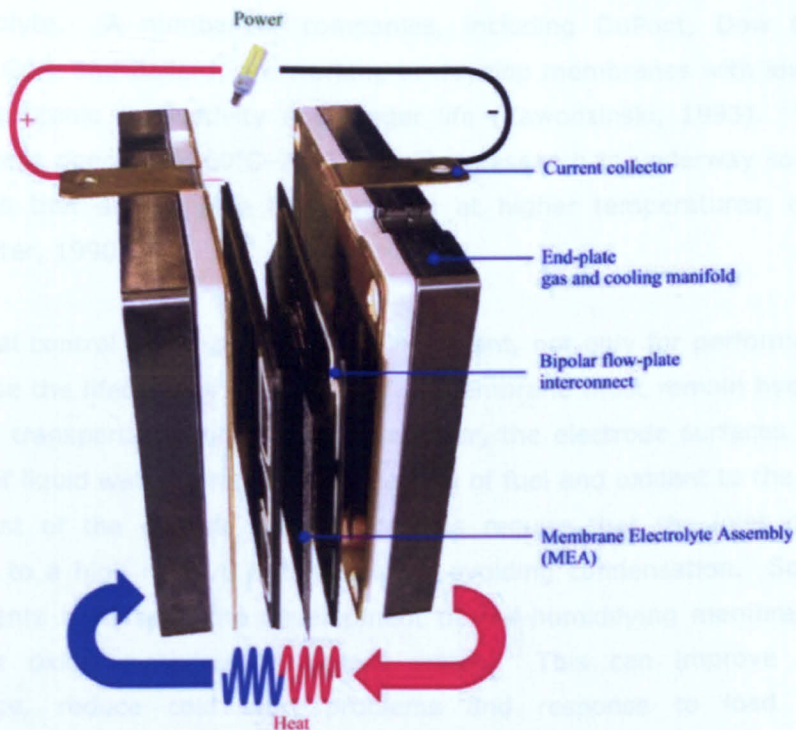


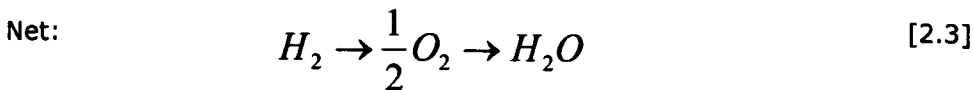
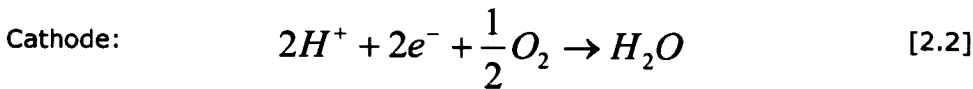
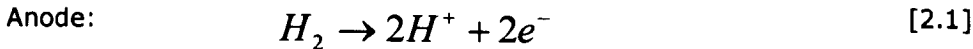
Figure 2.5: PEM Fuel Cell Diagram (IRD Fuel Cells A/S)

[www.ird.dk](http://www.ird.dk)

The PEM can operate on reformed hydrocarbon fuels, with pre-treatment, and with air. The use of a solid PEM eliminates the corrosion and safety concerns associated with the other types of fuel cell that have liquid electrolytes. At the

low operating temperature of the PEM, both the anode and cathode reactions require noble metal catalysts (e.g. typically platinum) to facilitate the reaction.

The cell reactions for a PEMFC are given by:



### 2.2.2 PEM Materials and Manufacturing

PEM fuel cells utilise a sulfonic acid membrane, typically 24 – 100  $\mu\text{m}$  thick, as the electrolyte. A number of companies, including DuPont, Dow Chemical Company, Gore and Ballard, are working to develop membranes with lower cost, improved protonic conductivity and longer life (Zawodzinski, 1993). Typically PEM fuel cells operate at 60°C–70°C, however research is underway to develop membranes that are suitable for operation at higher temperatures, closer to 100°C (Prater, 1990).

The thermal control of the stack is very important, not only for performance but to maximise the lifecycle of the stack. The membrane must remain hydrated to permit the transportation of protons. However, the electrode surfaces must be kept free of liquid water, which blocks the flow of fuel and oxidant to the reaction sites. Most of the current fuel cell designs require that the inlet gases be humidified to a high relative humidity while avoiding condensation. Some new advancements have seen the development of self-humidifying membranes that incorporate oxide materials to absorb water. This can improve the cell performance, reduce cold start problems and response to load changes (Watanabe, 1995).

The PEM stack for this investigation used a humidified gas stream to maintain saturation levels in the stack. In the test methodology, safety scripts were written into the test program to prevent flooding in the stack could reduce stack power (stopping reactions) and alternatively to prevent drying (losing the ability

to conduct protons) that permanently damages the stack. The next generation stacks will be able to operate under flooded conditions that reduce the control requirement without detrimental influence on the power output.

### **2.2.3 Fuel Cell Design Issues**

To make fuel cells economically competitive, there are many practical problems to be overcome. Of these, water management remains a key problem in PEM fuel cells and could be addressed within this thesis. At the same time many other variables must be managed, including temperature throughout the cell (which changes and can sometimes destroy a cell through drying out and thermally loading), reactant and product levels at various cells. Materials must be chosen to do various tasks which none fill completely. Durability and lifetime of the cells can be serious issues for some cells, low power densities for others. Putting all of these factors together is the key to the fuel cell success and remains the challenge for fuel cell manufacturers.

### **2.2.4 PEM Performance and Operating Conditions**

The PEM fuel cell can operate at temperatures in the range of 50°C to 90°C and at pressures of 1 to 3atm. The manufacturer of the stack tested in this study specified that the optimum temperature of the stack should be maintained at 65°C in order to maximise performance and cell durability.

In order to maximise the power output of the fuel cell, the polarisation curve (detailed further in section 2.3.8) must be kept flat and the limiting current density extended as far as possible. This goal has been pursued through the development of improved materials and better design of the fuel cell assembly by stack manufacturers. A number of studies have examined the influence of specific components of the fuel cell (e.g., membrane electrode assembly) in an effort to understand and improve the behaviour of the cell (Mosdale, 1996., Eikerling, 1998., Verbrugge, 1990., Fuller, 1993., Broka, 1997., Springer, 1991., Lee, 1998) and significant developments made in operating range and flow channel design.

The operating conditions of the fuel cell have a strong effect on its performance. Mathematical models have been proposed to describe the performance of an entire cell, including flow channels and bipolar plates, and to describe overall stack behaviour. These models permit evaluation of different operating conditions and determination of the optimum combination of operating

parameters to maximise efficiency and power density of the PEMFC (Yi, 1998., Singh, 1999., Kim, 1995., Amplett, 1995., Gurau, 1998., Bernardi, 1992).

The performance of the cell also depends on the properties of the fuel and oxidiser streams. Reformat fuels derived from hydrocarbon fuel sources contain various groups other than H<sub>2</sub> that can affect performance. For example, if the CO concentration in the fuel stream exceeds 10ppm, catalyst poisoning and severe performance degradation are experienced. Table 2.1 shows the effect of various fuel gas groups on fuel cell performance.

Gas Group	Effect
H <sub>2</sub>	Fuel
CO	Poison (>10 ppm)
CH <sub>4</sub>	Diluent
CO <sub>2</sub> and H <sub>2</sub> O	Diluent
Sulphur Compounds (e.g., H <sub>2</sub> S)	No studies found

**Table 2.2: Effect of Fuel Gas Constituents on FC Performance (Hirschenhofer, 1998)**

## 2.3 PEM Stack Experimentation

### 2.3.1 PEM Stack Description

Figure 2.6 depicts the PEM fuel cell stack that was used in this study. The picture shows the stack arrangement of cells with the Anode side on the left and the Cathode on the right. Hydrogen enters the stack from the left hand side, feeds the cells via their flow fields in parallel and excess H<sub>2</sub> leaves the stack on the right. On the Anode side, air enters from the right, is fed through the flow fields and is vented on the left.

The PEMFC Stack output was 2.0kW<sub>e</sub> and 3.0kW<sub>th</sub>. The stack manufacturer was *IRD Fuel Cells A/S*. They operate as is an independent high technology company devoted to research, development and production of fuel cell materials, fuel cells and fuel cell systems. The *IRD Group* develop and produce new fuel cell products in co-operation with fuel cell system developers (such *EFC GmbH*) and other international research groups and strategic partners to produce greater cost effectiveness, durability and reliability.

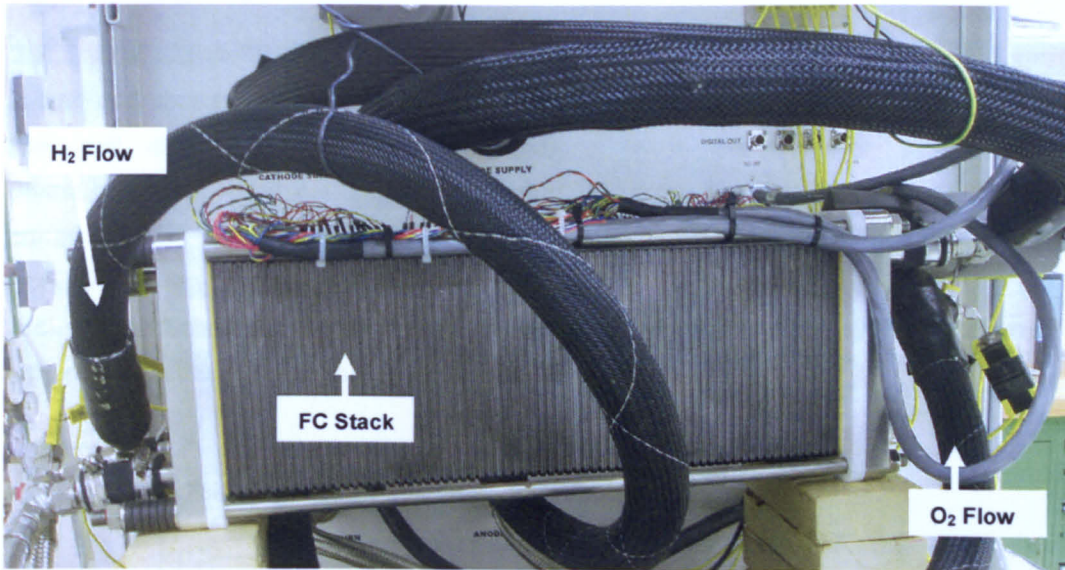


Figure 2.6: PEM Fuel Cell Stack – EFC GmbH

The stack design is "all polymer" in the sense that no metallic parts are exposed to either the fuel or the water circuits. The single-cell design is based on a polymer frame. This design allows the PEMFC stack to be easily dismantled for service or for the exchange of individual cells. The flow distribution/ interconnect plate is graphite-based for long lifetime. Each cell is fitted with an electrical connection for single-cell monitoring. The stack end plate-manifolds have a polymer-based sandwich construction which, together with the polymer frames, ensures thermal insulation and thereby good thermal management of the stack. The cells and stacks are designed with a very low pressure drop to optimise the efficiency of the auxiliary pumping equipment.

### 2.3.2 PEM Stack Specifications:

Table 2.2 provides a summary of the *IRD* stack specifications.

<b>PEM Fuel Cell</b>	
Electrical Power Output	2 kW <sub>e</sub>
Thermal Power Output	3 kW <sub>th</sub>
Number of Cells	68
Electrical Output per Cell	0.7V @ 300A
Active Cell Area	150 cm <sup>2</sup>
Working Pressure	200mb
Bipolar Plate Material	Graphite
Number of Components per Cell	5

Table 2.3: Beta FC Stack Specifications

### 2.3.3 PEM Stack Testing:

A fuel cell test rig was developed by *European Fuel Cell GmbH* and a Canadian fuel cell stack manufacturer, *Hydrogenics*, with the singular purpose of investigating the fuel cell stacks performance across the full range of operating conditions. This was to investigate the effect on performance, durability and operational ranges to integrate it with the rest of the stationary fuel cell system. A simplified schematic of the fuel cell test rig is depicted in figure 2.7. A detailed schematic of the test rig may be found in Appendix A.

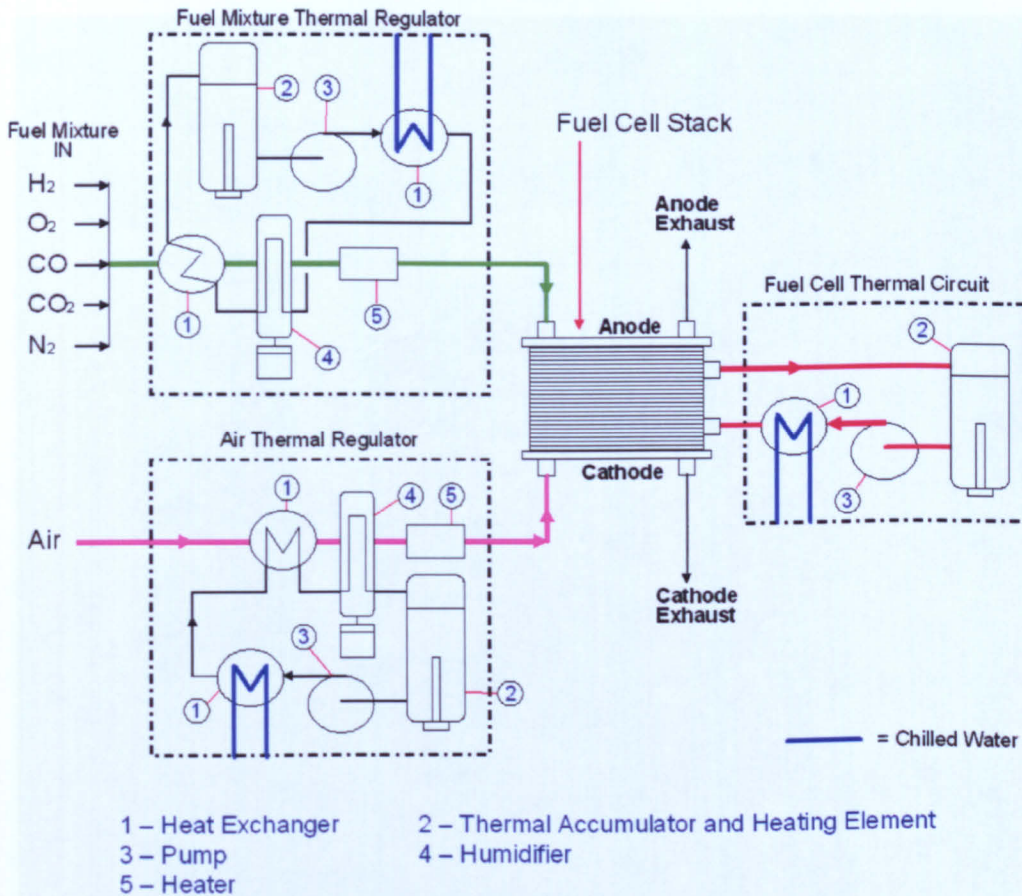


Figure 2.7: Fuel Cell Test Rig Schematic

The test rig used computer software, LabView 7.0, as a control program and user interface to control pre-programmed operational scripts through a Siemens Programmable Logic Controller (PLC). Figure 2.9 depicts a screenshot of the LabView user interface – this screen on the user interface allows the user to set the Anode and Cathode gas flow rates, pressures and gas compositions. The PLC operated the system components such as valves, pumps etc to provide the run procedures to the stack. The start-up and shut-down procedures may be found in Appendix A, along with a sample of an operation script.



Figure 2.8: Fuel Cell Test Rig (EFC GmbH)

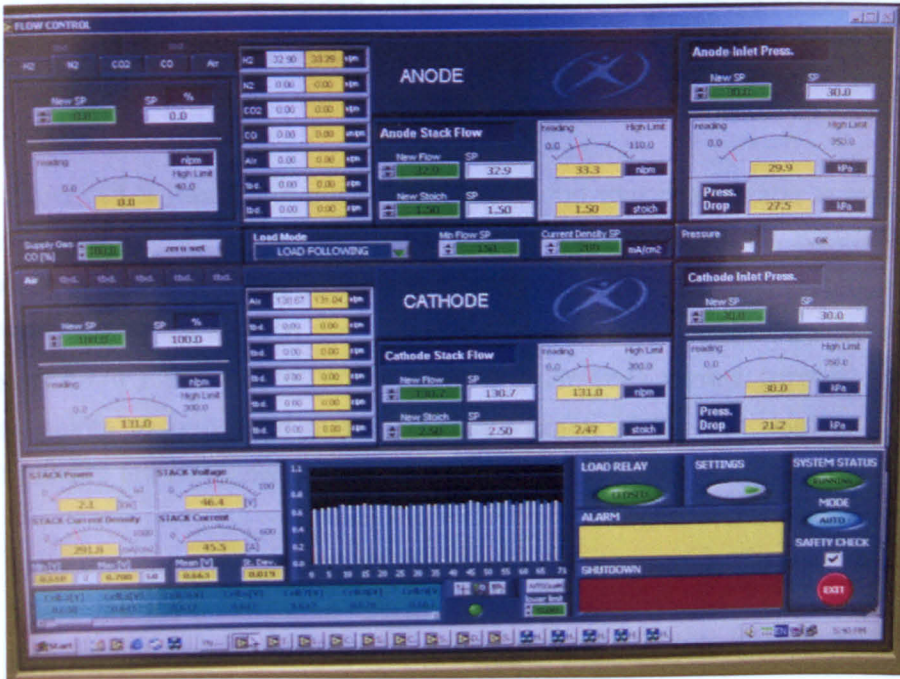


Figure 2.9: LabView 7.0, Stack Test Rig User Interface (EFC GmbH)

For the purpose of this investigation, the test stand was used to investigate the effect of a range of coolant flow conditions on the stack performance. Two tests were the main focus. The first analysed the effect of coolant flow temperature on stack performance, and the second, analysed the effect of temperature difference across the stack. The voltage and current was varied across the stack under these range of conditions to provide a polarisation curve (explained in the following section) that was used to compare performance.

### 2.3.4 Operational Fuel Cell Voltage

A common way to express the performance of a fuel cell is the steady-state voltage versus current (or current density), polarization curve.

The open circuit voltage of an electrochemical cell can be related to the theoretical free energy change of the overall electrochemical reaction of the cell as follows:

$$E = \frac{-\Delta g_f}{2F} \quad [2.4]$$

Where  $E$  is the Electromotive Force,  $-\Delta g_f$  is the Gibbs free energy released and  $F$  is Faradays constant. This gives a value of  $\sim 1.2V$  for a cell operating around  $100^\circ C$ .

When a fuel cell is made and put to use, it is found that the voltage is less than the above figure of  $1.2V$ . Figure 2.10 shows the performance of a typical single cell operating at  $65^\circ C$ , at normal air pressure. Since current generated will be proportional to active surface area, it is common to plot voltage versus current density ( $mA/cm^2$ ) and to plot power density ( $mW/cm^2$ ) versus current density. The key points to notice on this polarisation graph of the cell voltage against current density are as follows;

- Even the Open circuit voltage is less than the theoretical value.
- There is rapid initial fall in voltage.
- The voltage then falls less rapidly, and more linearly.
- There is sometimes a higher current density at which the voltage falls rapidly.

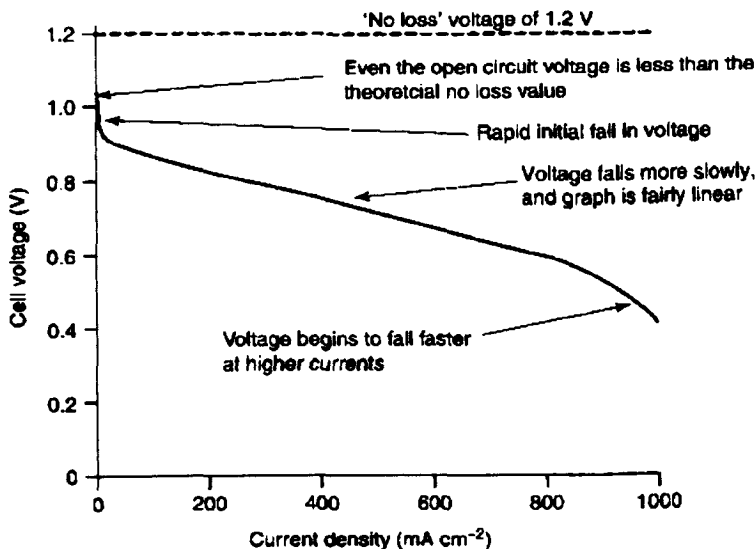


**Figure 2.10: Graph Showing the Polarisation Curve for a Typical Low Temperature, Air Pressure, Fuel Cell.**

The polarisation curve was used to present the performance of the fuel cell stack over its operating range under the examined thermal conditions.

### 2.3.5 Stack Thermal Evaluation

#### 2.3.5.1 Stack Coolant Temperature

Figure 2.11 illustrates the polarisation curve for the fuel cell stack across a range of coolant flow temperatures.

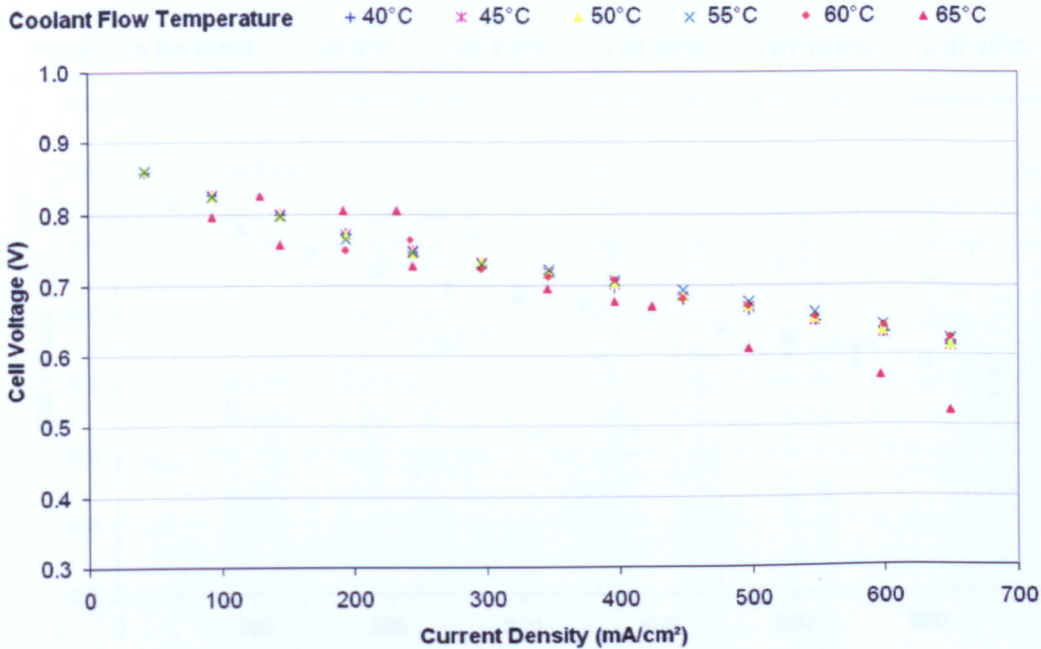


Figure 2.11: Polarisation Curve for the PEMFC – Variation in Coolant Flow Temperature

The operating temperature of the stack was maintained 0.3 bar and 65°C based on the manufacturers guidelines. It was clear that when the coolant temperature from the thermal management system rose above 60°C, there was not a sufficient coolth to maintain stack performance. The maximum coolant flow temperature was therefore no greater than 60°C, any hotter and there was a drop in the fuel cell performance. At 70°C, the fuel cell overheated and the safety script shut the fuel cell down.

#### 2.3.5.2 Temperature Difference Across the Stack

Figure 2.12 illustrates the polarisation curve for the stack with a range of temperature differences across it. The stack was maintained at 65°C and the flow rate of the coolant was varied. Results indicated that small variations in the dT across the stack did not have a significant influence on stack performance. However, when the dT across the stack was 15°C, there was a drop in performance. At a dT of 20°C, the safety script was initiated and the stack was shut down. From this result, it was concluded that with a larger dT across the

stack, different parts of the cell were at different temperatures, which had an influence on their humidification and hence output i.e. areas near the coolant inlet would be maintained at the correct temperature, however towards the exit points of the cell, the temperature of the coolant would rise and there would be reduced output.

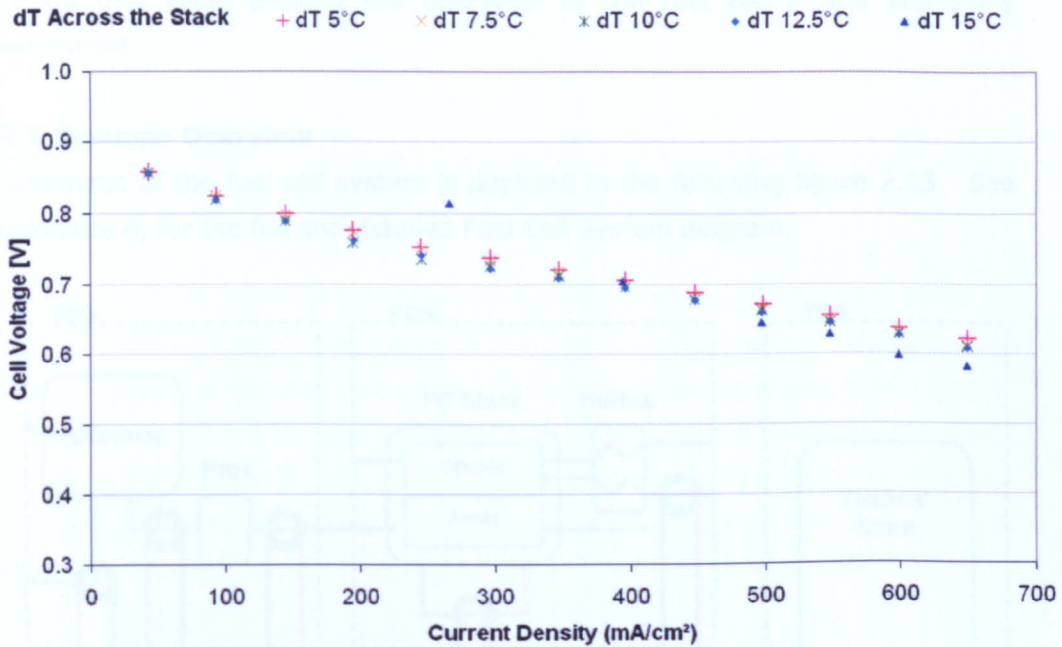


Figure 2.12: Polarisation Curve for the PEMFC – dT Across the Stack

One of the key driving factors for the research into a functionally thermal fluid for the fuel cell was to maintain the heat carrying capacity of a large dT, but to have a stable temperature through the stack and no reduction in performance. Figure 2.12 shows that in order to reduce the parasitic pumping load from the coolant and hence maximise the fuel cell efficiency, the dT was to be as large as possible without influence on stack performance. A larger dT would be a result of lower flow rates and reduced pumping load. The study showed that the largest dT through the stack using water as a coolant should be no greater than 12.5°C. Any greater than this temperature difference, the stack experienced fluctuations and a reduction in cell voltage.

## 2.4 The PEM Fuel Cell Thermal System

The following section is an overview of the experimental tests and development work undertaken on the thermal store for the fuel cell. This work was in parallel to the fuel cell testing and not only provided the operation conditions expected for the thermal system and the thermal fluid work, but revealed a successful storage strategy that could prolong the operation of the fuel cell in the stationary environment.

### 2.4.1 Systems Overview

A schematic of the fuel cell system is depicted in the following figure 2.13. See appendices A, for the full and detailed Fuel Cell System diagram.

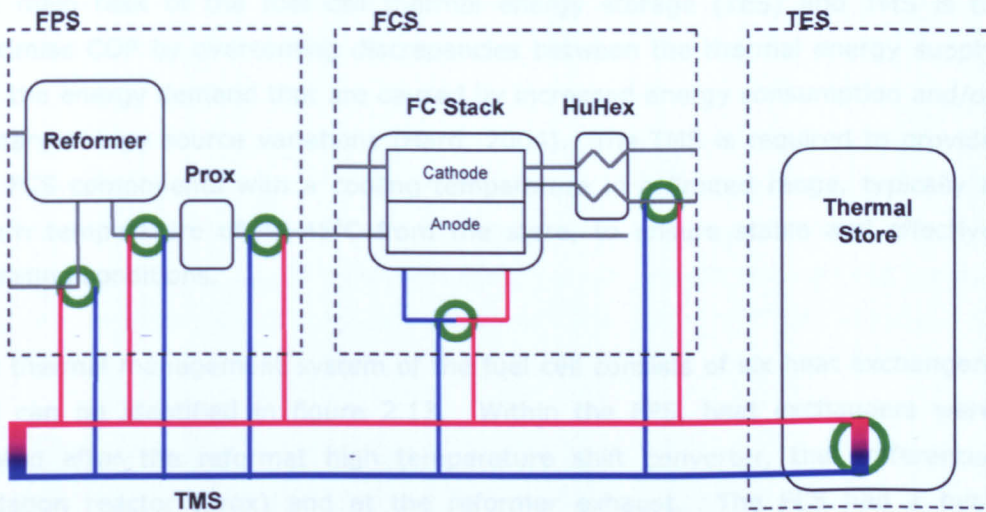


Figure 2.13: The PEM Fuel Cell System

The design of fuel cell systems is complex and can vary significantly depending upon fuel cell type and application. However, the stationary PEM fuel cell systems for this investigation consist of four basic components:

- **Fuel cell stack (FCS)**, which generates a DC current from hydrogen-oxygen electrochemical reaction; heat is exchanged via the water cooled Membrane Electrode Assembly (MEA) circuit and from the cathode return stream that has been dehumidified.
- **Fuel processor (FPS)**, which converts a hydrocarbon fuel such as natural gas into a hydrogen-rich mixture.
- **Current converter**, to regulate the output power of the cell and where necessary convert it to alternating current.

- **Heat recovery system**, to remove heat from the stack and to transfer heat amongst the various system components and for storage

The heat recovery system comprises of two major elements, the Thermal Energy Store (TES) and the Thermal Management System (TMS). The fuel cell systems also include other components and subsystems to control the fuel processing and fuel cell parameters such as humidity, temperature, gas pressure, and wastewater.

Figure 2.13 also clearly depicts the fuel cell thermal management system (TMS) for the fuel cell, which is the main subject of this investigation.

The main task of the fuel cell thermal energy storage (TES) and TMS is to maximise COP by overcoming discrepancies between the thermal energy supply and the energy demand that are caused by increased energy consumption and/or primary energy source variations (Hard, 2004). The TMS is required to provide the FCS components with a cooling temperature in a limited range, typically a return temperature of 40-45°C from the store, to ensure stable and effective operating conditions.

The thermal management system of the fuel cell consists of six heat exchangers and can be identified in figure 2.13. Within the FPS, heat exchangers were located after the reformat high temperature shift converter, the preferential oxidation reactor (Prox) and at the reformer exhaust. The FCS had a heat exchanger situated in the deionised water circuit that cools the stack and another in the cathode air exhaust. The final heat exchanger is located in the thermal store and transfers the energy from the aforementioned heat exchangers.

The thermal loading circuit consisted of five heat exchangers for extracting heat. Most of the heat was distributed around the system and the major contributor to the cogeneration supply was the fuel cell, at  $3kW_{TH}$ . The flow and return temperatures to the store were set at 65°C and 40°C respectively, based on the manufacturers operational conditions and the Fuel Cell tests in section 2.3.9.

### 2.4.2 Fuel Cell Heat Recovery System (TES) – Parallel Study

From an energy perspective the fuel cell systems are primarily used to generate electricity. However, since significant amounts of heat are generated, the energy can be used to produce steam or hot water or converted into electricity via a gas turbine or other technology. This increases the overall energy efficiency of the systems. The output temperature from the PEM is too low to generate efficient electricity therefore it is better utilised for heating purposes, which particularly suitable to the small scale stationary environment.

The TES in a stationary application should be sized and designed to overcome the discrepancies between the energy supply and the energy demand that is caused by increased energy consumption and/or primary energy source variations, such as periodic variations in outside temperature and/or solar radiation energy (Banaszek, 1990).

Thermal storage is extremely important to the success of the commercial stationary fuel cell systems. It must provide the thermal requirements to meet the demand of the end user, storing excess energy in periods of low demand to be used to meet periods of peak demand, and yet provide the fuel cell system with the essential region of operating conditions (65°C-40°C) to enhance its operation time, performance and efficiency.

### 2.4.3 Thermal Storage Overview

There are three basic methods of storing thermal energy that could be applied to a small scale stationary application, they are as follows;

- Thermo-chemically
- Sensible Heat
- Latent Heat

In a thermo-chemical heat storage process, thermal energy is absorbed or released by breaking and reforming molecular bonds in a reversible chemical reaction. In a sensible heat storage unit, thermal energy is stored by changing the temperature of the storage medium, which can be a liquid (like water) or a solid (like rock beds). The amount of energy stored in a unit depends on heat capacity of the medium, temperature changes and the amount of the storage material. In the latent heat storage, thermal energy is accumulated by means of a reversible phase change occurring in the medium. Solid-liquid transformation is

most often used to avoid large pressure vessels required for vaporisation or sublimation.

Through the comparison between the sensible and latent energy storage, it may be concluded that the latter solution is more appealing. In fact, the latent heat of most materials is much higher than their sensible heat, thus requiring a much smaller mass of storage medium for storing and then recovering a given thermal energy. Moreover, the latent heat thermal process occurs at nearly constant temperature, which is typically desirable for efficient operation of most thermal systems (Babus'.Haq, 1993, DomanÄski, 1993, Himran, 1994, Abe, 1984, Garg, 1985). This may also imply that, in principle, if PCM were to be pumped through the fuel cell stack, the heat could be absorbed from the stack at low flow rate with almost constant  $dT$ .

#### 2.4.4 Thermal Energy Storage Experimentation

The aim of the TES experimentation was to investigate strategies of energy storage to maximise the output load of the fuel cell and provide it with the optimum conditions. This was to supply the maximum storage and fuel cell operation capacity based on the return supply conditions from the store. As a result, storage strategies were examined to most effectively meet the energy demand and maximise fuel cell system output and operational hours.



Figure 2.14a: PEM Fuel Cell Thermal Storage



Figure 2.14b: PEM Fuel Cell Combi Store

The second objective was to assess and achieve good operational understanding and development of the TES to meet the energy requirements for integrating into the stationary cogeneration environment. An underlying objective of the TES strategy was to maximise the cooling to the fuel cell for as long as possible. This would enable the prolonged operation and economic running of the system especially in summer periods where there was less demand for hot water. Figures 2.14a illustrate some of the storage vessels tested and loading arrangements that were undertaken. The vessel in figure 2.14b illustrates a cut through of a store used to distribute the thermal load more effectively than a standard cylinder.

Various thermal systems and delivery strategies were investigated for use with the fuel cell, see Appendices A. These included using different sized conventional water storage tanks, 150lt, 300lt and 600lt, and also less conventional tanks. The other types of tanks had been developed for other applications such as for solar heating for domestic use. These concepts were examined and were adapted for use with the fuel cell. A concept of using Phase Change Material (PCM) encapsulated in small vessels within the storage tanks was also investigated, Appendices A.

### 2.4.5 Thermal Energy Storage Schematics

The following figure 2.15, illustrates the experimental set-up of the thermal loading circuits for the fuel cell thermal system. Figures 2.16a and 2.16b depict the experimental apparatus; this includes the fuel cell, thermal storage vessels, cooling tower, pressure regulators, pumps, flow meters, valves and piping. The equipment used for data acquisition was K-type thermocouples, Pt-100 pressure transducers and a Siemens Programmable Logic Controller (PLC).

- 1 - FC Loading Circuit
- 2 - Thermal Loading Circuit
- 3 - SpH Unload Circuit
- 4 - BBS Loading Circuit
- 5 - DHW Unload Circuit
- 6 - Internal Conductivity
- 7 - BBS Auxiliary Loading

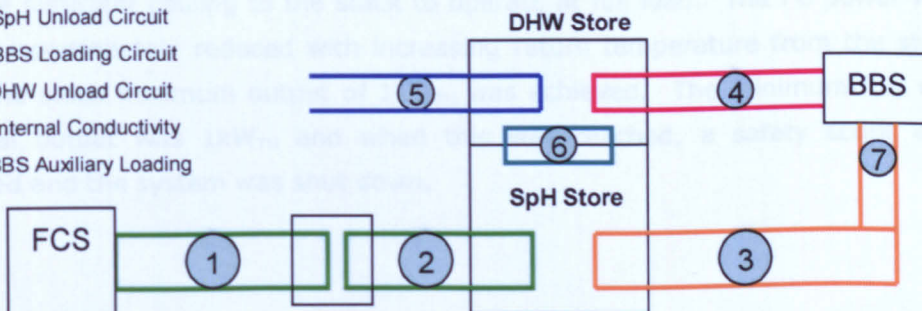


Figure 2.15: PEM Fuel Cell Thermal Store Schematic – EFC GmbH



Figure 2.16a: TES Experimentation  
Apparatus View 1



Figure 2.16b: TES Experimentation  
Apparatus View 2

## 2.4.5 Thermal Energy Storage Evaluation

### 2.4.5.1 Conventional Store Sensible Heat Storage

Tests were based on Fuel Cell System (FCS) operation with a thermal store capacity of 300 litres and a constant  $3\text{kW}_{\text{TH}}$  load, see figure 2.17. The store used was a standard solar tank with the TMS heat exchanger coil located in the lower region of the store. A period of approx 4hrs: 40mins runtime at full power was determined to be obtainable from a fully exhausted store. This corresponded to a tank temperature and cooling load temp of  $45^{\circ}\text{C}$  back to the fuel cell. After this period was met, the return flow temperature back from the store could not provide sufficient cooling to the stack to operate at full load. The FC power was then proportionately reduced with increasing return temperature from the store until the stack minimum output of  $1\text{kW}_{\text{TH}}$  was achieved. The minimum fuel cell thermal output was  $1\text{kW}_{\text{TH}}$  and when this was reached, a safety script was initiated and the system was shut down.

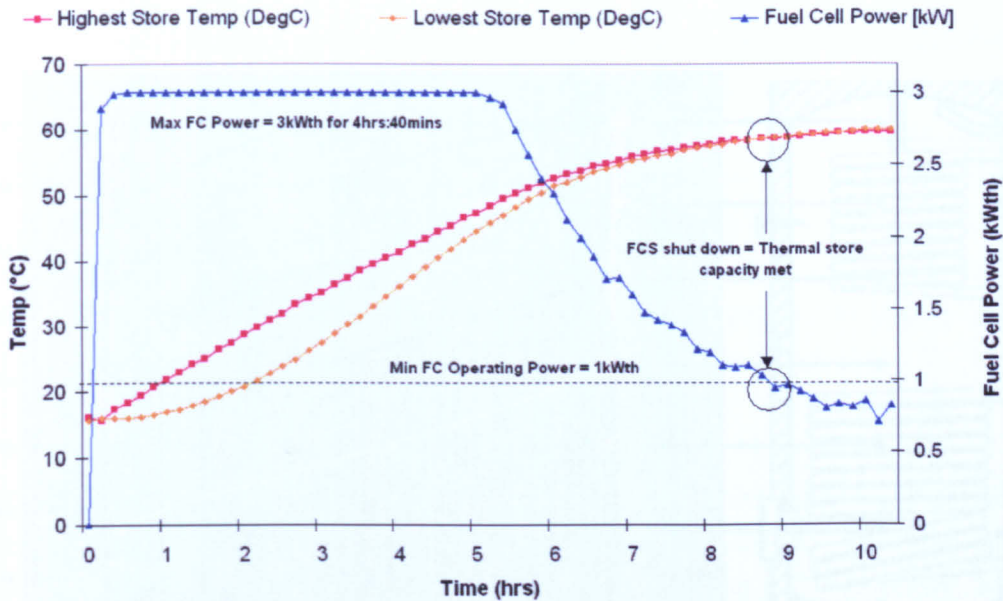


Figure 2.17: Fuel Cell Thermal Loading to a 300lt Store

The use of standard sensible heat storage tanks showed typical stratification characteristics under loading and unloading. This trend is depicted in figure 2.18a and 2.18b for the relationship between temperature, height of the tank and time under charge, and under discharge for a 300l store. The tank showed uniform heating under charging and stratification under a flow rate of 10lpm discharge. The cold water input was at the bottom of the store and the hot water was expelled at the top.

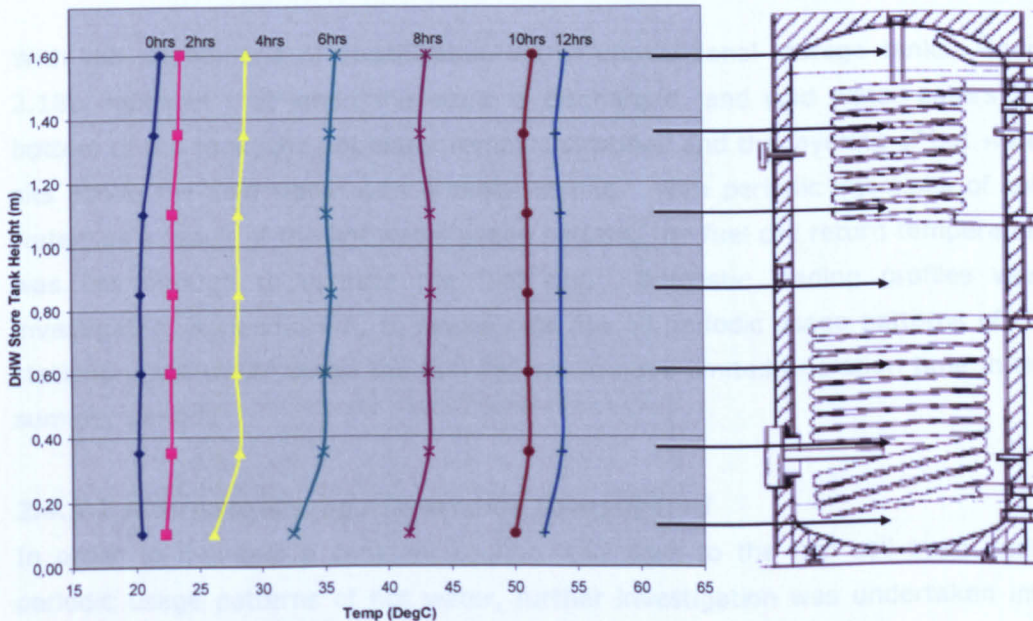
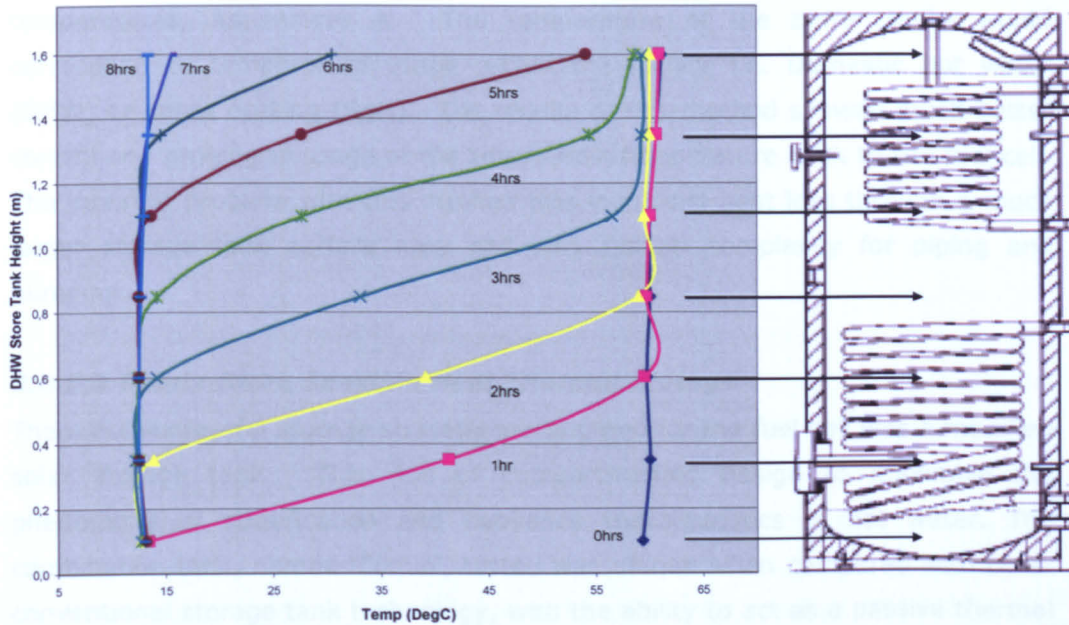


Figure 2.18a: 300lt Thermal Store Under Charging – Graph Indicating the Relationship Between Temperature and Tank Height with Time.



**Figure 2.18b: 300lt Thermal Store Under Discharge - Graph Indicating the Relationship Between Temperature and Tank Height with Time.**

Figure 2.18a identifies a uniform heating profile across the height of the tank through the charge phase. This indicates that the minimum return flow temperature to the fuel cell is the same as that of the mean storage tank temperature. Hence, whenever the mean temperature of the store rises above 45°C, the TMS will struggle to cool the fuel cell.

With the phenomena of stratification within conventional storage tanks, Figure 2.18b indicates that when the store is discharged, and cold water enters the bottom of the tank, the hot water remains stratified and the layering of hot water sits above the cold water with minimal mixing. With periodic injections of cold water, as a result of the hot water usage pattern, the fuel cell return temperature was low enough to operate the fuel cell. Domestic loading profiles were investigated, Appendices A, to reveal that due to periodic usage patterns of the stationary hot water usage the fuel cell would have limited operation time in the summer periods.

#### **2.4.5.2 Alternate Storage Strategies Investigated**

In order to maintain a constant cooling load back to the fuel cell even under periodic usage patterns of hot water, further investigation was undertaken into thermal storage strategies. This included a number of techniques such as storage

buffering that used two or more tanks to store the thermal energy at different temperatures, Appendices A. The temperature of the buffer tanks would correspond to temperature usage within the facility i.e. Domestic hot water (DHW) or space heating (SpH). The results of this method showed much better control and prolonged usage of the return flow temperature back to the fuel cell. The inherent problem with this method was increased heat loss through a much larger storage tank surface area and also system complexity for piping and pumping.

### 2.4.5.3 Combi-Store Sensible Heat Thermal Storage

The most successful storage strategy investigated for the fuel cell was a modified solar storage tank. This was of compartmented design to maximise the phenomena of stratification and buoyancy characteristics of hot water. The combination tank, named 'Combi', tested was unique when compared with other conventional storage tank technology, with the ability to act as a passive thermal manager of the system based on the simple thermodynamic laws.

The store had a unique construction with a smaller DHW store encapsulated within a larger stratified store that was used for Space Heating. Other features included a compartmented lower heating coil and specific inlet and outlet flow distribution channels within the store. This enabled variations in thermally charged and uncharged regions. Figure 2.19, illustrates cross sections of the Combi tank identifying its various compartments and distribution channels.

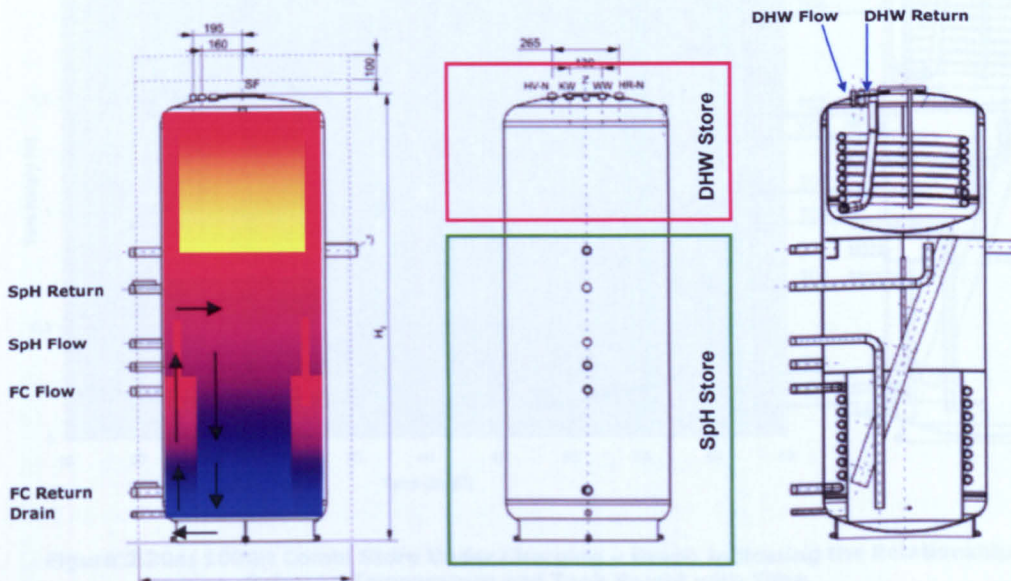
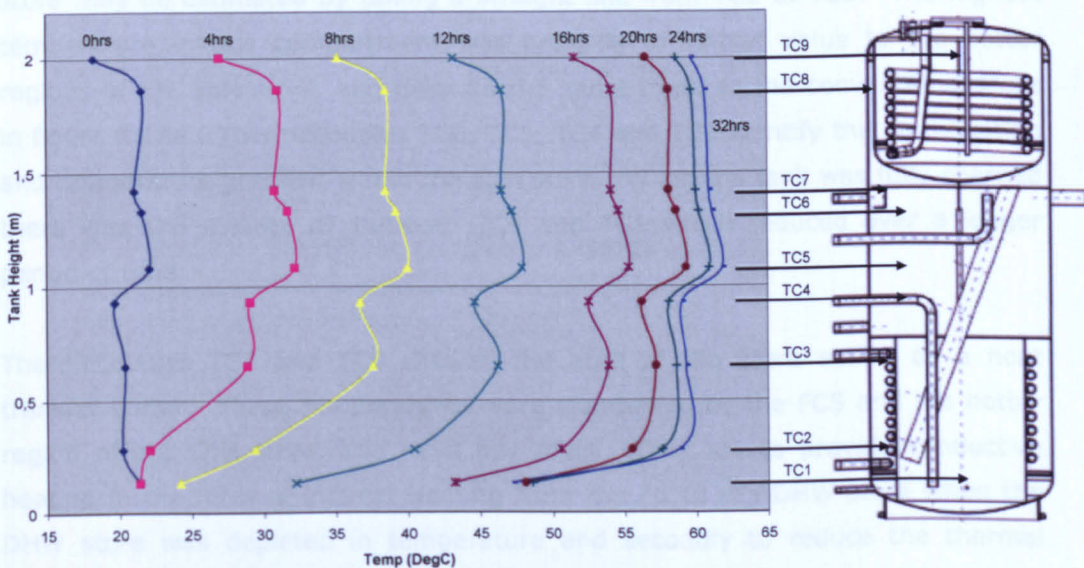


Figure 2.19: 1000lt Combination Storage Tank Cross Section

There were two key components to the success of the store's thermal management. The first was the location of the DHW store, that was typically at higher temperatures ( $\approx 60^{\circ}\text{C}$ - $65^{\circ}\text{C}$ ) and surrounded by a similar temperature store to minimise heat loss, and the second, was the flow region of buoyant heated water around the FCS heating coil at the bottom of the tank to provide flow currents and sufficient cooling back to the FC Stack.

The Fuel Cell heat exchanger coil was isolated from the stratified larger store to produce an alternative heat flow path. This region operated parallel to the stratified store by utilising its coldest area to provide cooling, and as greater  $dT$  as possible between the FCS carrier fluid and the store temp. This enhanced heat transfer and provided a low carrier fluid return temperature to the FCS, and hence prolonged FC operation. The water, once heated by the FCS coil was then distributed to the higher hotter regions of the SpH stratified store via tube diffusers.

Figures 2.20a and 2.20b illustrate the charge and discharge profiles for a 1000lt combination store. The graphs identify the relationship between temperature and height of the tank with time.



**Figure 2.20a: 1000lt Combi Store Under Charging - Graph Indicating the Relationship Between Temperature and Tank Height with Time.**

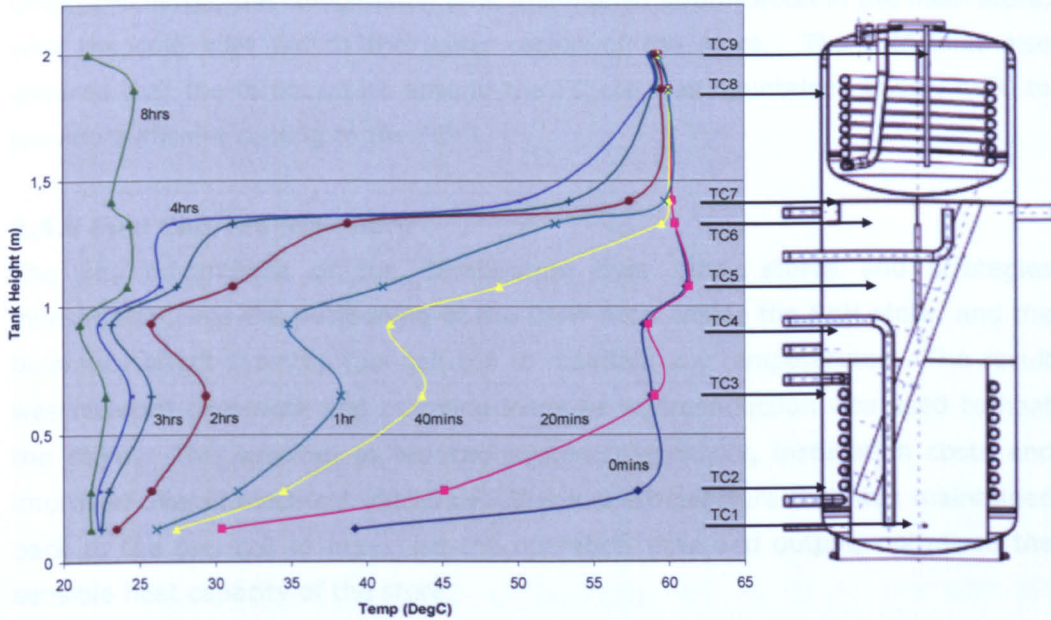


**Figure 2.20b: 1000lt Combi Store Under Discharge - Graph Indicating the Relationship Between Temperature and Tank Height with Time.**

Figure 2.20a illustrates the relationship between temperature, height of node and time during the 3kW FC charge period. It identifies four heating regions within the store – The first is the FC heating coil compartment. The stratification in this store may be estimated by taking a straight line from TC2 to TC3. The highest temperature in this compartment was typically of similar value to the hotter regions of the SpH store, and followed the same trend as the conventional store in figure 2.18a. Thermocouples TC6, TC5, TC4 and TC1 identify the stratification and temperature gradient within the SpH store. When the tank was fully charged there was still a large  $dT$  between TC4 and TC1 which reduced over a longer period of time.

Thermocouples TC7 and TC8 showed the area of the store acting as a heat transfer buffer. These temperatures were maintained by the FCS and the hotter region of the SpH store, and have key roles. They are to provide conductive heating in the form of indirect heating from the FC to the DHW store when the DHW store was depleted in temperature and secondly to reduce the thermal losses when the store was fully charged. The final region to identify was the DHW store that was a few degrees lower in temperature than the hotter parts of the SpH store. This was due to the positioning of the thermocouple (TC9) within the store as it is positioned in the mid centre away from the heated walls.

Under discharge, the combination tank maintained stratification in the main store, with the cold inlet fed to the lower region of the store. The cold inlet also ensured that the temperature around the FC coil was maintained below 45°C to provide sufficient cooling to the FC.

#### 2.4.6 Fuel Cell TES Summary

The key advantages of the Combi-store over other stores and strategies investigated, was the positioning of the DHW store inside the SpH store, and the buoyancy effect over the fuel cell coil to maintain low temperatures. The result was reduced pipe-work and pumping loads as wall conduction was used to heat the store. This resulted in reduced system complexity, installation costs and improved overall electrical efficiency. The low temperature that was maintained back to the fuel cell to maximise the operation time and output, optimised the sensible heat capacity of the store.

The 1000lt store was very much oversized for a typical small stationary system; however, this was the only size available for experimentation. From the results of this storage study, a 400lt store was put into prototyping and production for use and to be sold with this PEMFC for domestic scale stationary systems.

#### 2.5 FC Stack and Thermal Store Design Conditions Summary

The following conditions, table 2.3, were used for development of the functionally thermal fluid for use with the fuel cell stack, based on experimental testing and the manufacturer's guidelines.

<b><i>PEM Fuel Cell</i></b>	<b><i>Operational Temperature</i></b>
FC Operating Temp	65°C
Coolant flow max temp	40°C
Coolant flow min temp	60°C
Optimum coolant flow temp	55°C
Maximum coolant dT	12.5°C
Coolant return temp max	65°C

**Table 2.4: FC Stack Coolant Conditions Summary**

## **2.6 Fuel Cell Concluding Remarks**

Fuel cells are poised to be the power generation technology of the 21<sup>st</sup> century. They are clean, efficient and suitable for a wide range of applications. In order for them to achieve this, a number of challenges must be overcome, including cost, reliability and lifetime.

This chapter gave an overview of the fuel cell and analysed the fuel cell stack itself. This highlighted the operational temperatures and characteristics of the stack and influence on performance. These operational conditions would be the basis for the design and development of the functionally thermal fluid that was aimed at improving the performance of the fuel cell.

In parallel, the thermal system was experimentally evaluated and a novel fuel cell thermal strategy developed. This storage technique was to be used with the commercially available system. The thermal store was an important link between the fuel cell and the thermal transfer circuit, regulating the stack temperature and providing the cogeneration link to the end user.

The thermal energy storage would be balanced with the thermal fluid, and is a simple solution to correcting the mismatch between the supply and demand of energy. It was noted that this element should not be overlooked for successful integration of the FCS with the stationary application. From the experimental tests, a strategy and thermal store was integrated that could maximise the operational time and performance of the fuel cell through effective distribution of the thermal energy.

## **Chapter 3: Functionally Thermal Fluids**

### **3.0 Introduction**

Multifunctional (thermal) fluids and suspensions, also named “intelligent fluids”, yield new classes of fluids with improved (thermal) properties. These fluids can be designed to optimally fulfil particular objectives. Most commonly seen in refrigeration and air-conditioning, these can be used to enhance thermal conductivity of a fluid, improve heat transfer characteristics, increase thermal energy storage capacity, stabilise temperatures and reduce pressure drops.

In conventional thermal energy systems, many applications often operate by using the sensible heat of a single-phase working fluid (e.g. water, oil) which mostly require high volumetric flow rate. Increasing the convective heat transfer coefficient of a working fluid would permit the use of a smaller volumetric flow rate which would reduce pumping power.

This chapter reviews the current status of research on thermal energy transportation using functionally thermal fluids. These fluids are a mixture of a heat transfer medium such as water and another material with or without phase change as a latent heat storage material.

Functionally thermal fluids offer an attractive opportunity for the fuel cell; to enhance thermal energy transportation and heat transfer of heat exchangers to reduce system size, volume and pumping loads. Hence, reduce system cost, improve thermal stability and increase the overall electrical efficiency.

The following sections provide an overview of functionally thermal fluids and focuses on a specific fluid that was proposed to be developed for the fuel cell system. This fluid combined latent and sensible energy to maximise the thermal capacitance and heat transfer of the thermal fluid through the fuel cell system.

### **3.1 Functionally Thermal Fluids**

An elegant example of one of the most intelligent fluids is in the biological engineering world, namely blood in living creatures, pictured in figure 3.1. Blood, functions as a carrier fluid of both thermal energy and other material such as oxygen, nutrients, water etc. It comprises of formed elements such as red blood cells, white blood cells and platelets suspended in plasma. It transports oxygen from the lungs and nutrients from the intestines to the cells, and removes carbon

dioxide and other products to the secretion organs (lungs, kidneys) etc. (Egolf, 2001). In comparison to most fluids applied in technical systems, blood exhibits a wide range of functionalities and makes them look particularly inferior.



**Figure 3.1: Red Blood Cells**

Other intelligent fluids used in commercial applications can include functional fluids like electro-rheological fluids and magnetic fluids whose flow behaviour is controlled from the outside by an electric or magnetic field (Inaba, 2000).

The use of functionally thermal fluids offers attractive opportunities for effective usage of the low-grade thermal energies exhibited by some cogeneration, renewable energy systems and the PEM fuel cell. At present thermal energy is most commonly stored and transported using hot and cold water as sensible heat, and as ice and steam in the latent heat state. However, it is often difficult to apply these materials to wide demand as there are limitations of operational range. This results in them having certain constraints on their potential range of application. Therefore, in order to breach this gap, it is necessary to develop compound fluids that are made by mixing a thermal fluid and other different materials, such as phase change (solid-liquid).

Typically functionally thermal fluids are classified into either sensible heat fluids or latent heat fluids. Sensible fluids may be aqueous polymer solutions, aqueous surfactant solutions or a mixed fluid of liquid and fine particles. The latent heat fluids comprise of a mix of a working fluid and a solid-liquid phase change material.

Several review articles exist presenting overviews of the different kinds of latent heat multi-functional fluids. One of the earliest and most well known is by Inaba (2000).

Inaba distinguishes the following fluids;

- Ice Slurries
- Micro-encapsulated Slurries
- Micro-emulsions
- Clathrate Slurries (fig 3.2)
- Shape-stabilised Paraffins
- Carbon Dioxide Slurries

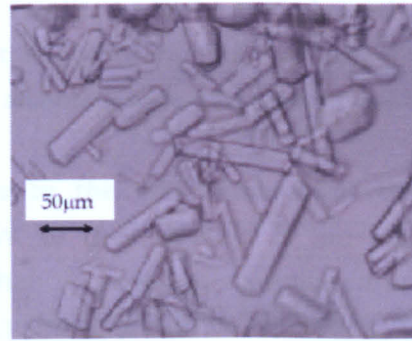


Figure 3.2: Clathrate Hydrate Crystals

All these fluids show enhanced thermal energy densities due to a change of phase, e.g. a solid-liquid transition or a similar physical and/or chemical bonding of molecules, which stabilises the temperature in the working domain around a mean (melting) temperature  $T_m$  with a total (melting) range  $T_r$ .

Regardless of the differences in existing compositions, the above fluids all have in common the notion of combining multiple functionalities in a fluid with the intention of customising it for a relevant temperature range of a thermal process and fulfilling the transport and the storage of thermal energy within a single suspension. In this sense, with regards to the relevant temperature range, ice slurry (PCS), is suitable for refrigeration or freezing process.

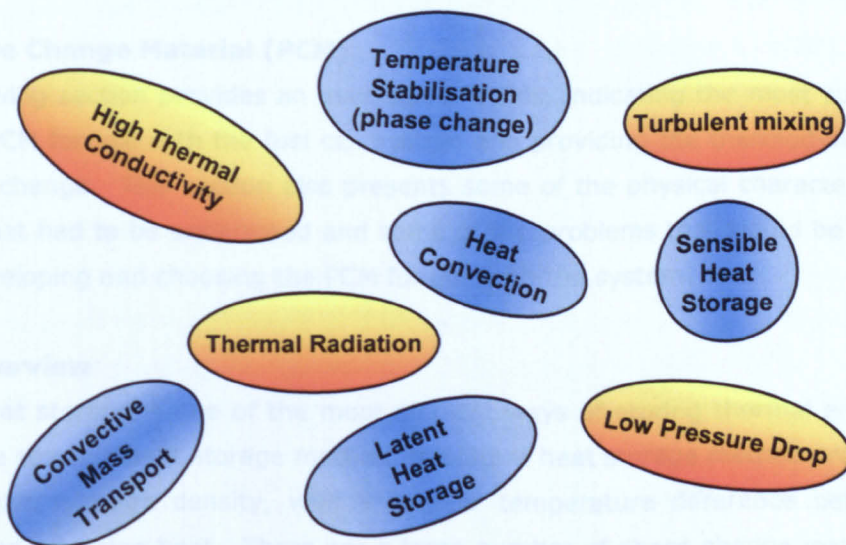


Figure 3.3: Thermodynamic Functions of Multifunctional Fluids. A Phase Change Slurry can Fulfil Five or More Functions Simultaneously (see Blue Circles) (Abhat, 2000)

Figure 3.3, depicts the thermodynamic functions that are desired of multifunctional thermal fluids. It can be seen that five or more of the highlighted functions can be met by phase change slurries alone.

Inevitably, there could be some drawbacks to the use of some of these functionally thermal fluids. The key element to their success is the match between the fluid and the application. The enhanced fluid may be required to be designed very carefully to the operation of the system for it to be beneficial. This could have a very positive influence at the optimum conditions, however, could restrict or reduce the performance of the system if it were to operate outside these boundaries. Water has a high specific heat, over a larger temperature range, water alone may perform better than for example a PCM and water mix. In this scenario, the greater sensible capacity of the water that would be displaced by the PCM could more than exceeds the gain in latent storage over a large temperature range.

To fully and successfully integrate the functionally thermal fluid with the fuel cell, it is very important that the operating conditions and fluids thermo-physical properties can successfully fuse. The following sections provide an overview of phase change materials and their principle of operation. The remainder of this chapter focuses on the use of phase change material as a functionally thermal fluid.

### **3.2 Phase Change Material (PCM)**

The following section provides an overview of PCMs, indicating the most suitable class of PCM for use with the fuel cell system and providing the thermodynamics of phase change. This section also presents some of the physical characteristics of PCM that had to be understood and some of the problems that would be faced when developing and choosing the PCM for use with the system.

#### **3.2.1 Overview**

Latent heat storage is one of the most efficient ways of storing thermal energy. Unlike the sensible heat storage method, the latent heat storage method provides much higher storage density, with a smaller temperature difference between storing and releasing heat. There are a large number of phase change materials that melt and solidify at a wide range of temperatures, making their use favourable in a number of applications. Paraffin waxes are cheap and have good

thermal energy storage density but low thermal conductivity and, hence require large surface area if they are to make successful PCM.

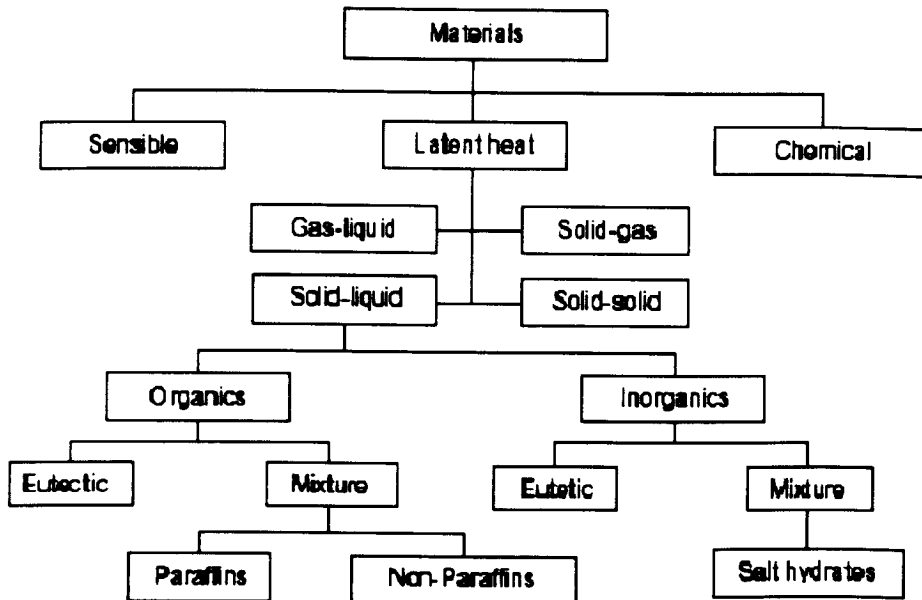


Figure 3.4: Classification of Thermal Energy Storage Materials (Abhat, 1982)

Non-paraffin waxes are thermally comparable to paraffin's and exhibit many of their favourable cycling characteristics, however they are much more costly. Hydrated salts have larger energy storage density and higher thermal conductivity but experience supercooling and phase segregation, and hence, their application requires the use of some nucleating and thickening agents. The different classes of PCM are identified in Figure 3.8 with reference to thermal energy storage materials.

### 3.2.2 Paraffin Wax

Paraffin's are substances that have a waxy constancy at room temperature. They contain major components called alkanes characterised by  $C_nH_{2n+2}$ ; the n-alkane content in paraffin waxes usually exceeds 75% and may reach 100%. Another primary component of paraffin waxes is straight-chain hydrocarbons with only a small amount of branching, such as 2 methyl groups, near the end of the chain. The more carbon atoms in their chain, the higher is the melting temperature of the paraffin. This applies only for n-alkanes, which have single, non-branching carbon chains. Alkanes with the number of carbon atoms between 14 and 40, posses melting points between 6°C and 80°C (EPST, 1971). Figure 3.5, illustrates the structure of Paraffin wax; the longer the chain, the higher the melting point.

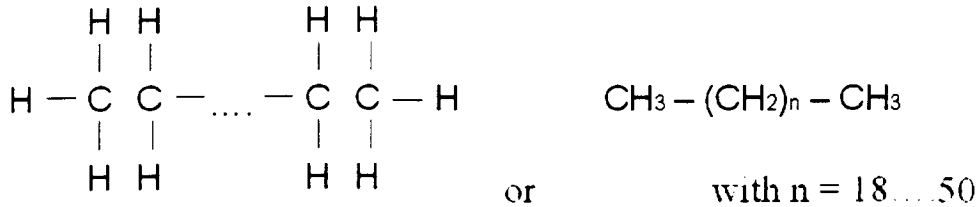


Figure 3.5: Chemical structure of Paraffin Waxes

Some of the paraffin waxes investigated for heat storage applications include commercial waxes, *n*-eicosane and *n*-octadecane. Paraffin is found to exhibit many desirable characteristics of phase change substances; high heat of fusion, negligible supercooling, low vapour pressure when molten, chemically inert and stable, self nucleating, no phase segregation and commercially available at reasonable cost (Abhat, 1982). In a large thermal store, it is less desirable than the other PCMs due to its low thermal conductivity, however under micro-encapsulation, the thermal conductivity is much greater. Unlike the other PCMs, the paraffin is water insoluble, which means it is ideal for use with current micro-encapsulation technology. Paraffin waxes are listed in the following table 3.1.

Compound	Melting temperature (°C)	Heat of fusion (kJ/kg)	Thermal conductivity (W/m K)	Density (kg/m <sup>3</sup> )
Paraffin C <sub>14</sub>	4.5	165	n.a.	n.a.
Paraffin C <sub>15</sub> -C <sub>16</sub>	8	153	n.a.	n.a.
Polyglycol E400	8	99.6	0.187 (liquid, 38.6°C) 0.185 (liquid, 60.0°C)	1125 (liquid, 25°C) 1228 (solid, 3°C)
Dimethyl-sulfoxide (DMS)	16.5	85.7	n.a.	1009 (solid and liquid)
Paraffin C <sub>15</sub> -18	20-22	152	n.a.	n.a.
Polyglycol E600	22	127.2	0.189 (liquid, 38.6°C) 0.187 (liquid, 67.0°C)	1126 (liquid, 25°C) 1232 (solid, 4°C)
Paraffin C <sub>17</sub> -C <sub>18</sub>	22-24	189	0.21 (solid)	0.760 (liquid, 70°C) 0.900 (solid, 20°C)
1-Dodecanol	26	200	n.a.	n.a.
Paraffin C <sub>12</sub>	28	244	0.148 (liquid, 40°C)	0.774 (liquid, 70°C)
	27.5	243.5	0.15 (solid) 0.355 (solid, 25°C)	0.814 (solid, 20°C)
1-Tetradecanol	38	205		
Paraffin C <sub>14</sub> -C <sub>18</sub>	42-44	189	0.21 (solid)	0.765 (liquid, 70°C) 0.910 (solid, 20°C)
Paraffin C <sub>20</sub> -C <sub>21</sub>	48-50	189	0.21 (solid)	0.769 (liquid, 70°C) 0.912 (solid, 20°C)
Paraffin C <sub>23</sub> -C <sub>24</sub>	58-60	189	0.21 (solid)	0.795 (liquid, 70°C) 0.920 (solid, 20°C)
Paraffin wax	64	173.6 266	0.167 (liquid, 63.5°C) 0.346 (solid, 33.6°C) 0.339 (solid, 45.7°C)	790 (liquid, 65°C) 916 (solid, 24°C)
Polyglycol E600	66	100.0	n.a.	1085 (liquid, 70°C) 1212 (solid, 25°C)
Paraffin C <sub>21</sub> -C <sub>30</sub>	66-68	189	0.21 (solid)	0.830 (liquid, 70°C) 0.930 (solid, 20°C)
Biphenyl	71	119.2	n.a.	991 (liquid, 73°C) 1166 (solid, 24°C)

n.a.: not available

Table 3.1: Physical Properties Data of Paraffin Waxes (Zalba, 2003)

To use paraffin as a microPCM for heat storage specifically in liquids, it is necessary to prevent agglomeration of the particles. Due to the encapsulation, it is possible to disperse the paraffin in water and the melt it without any interaction between the PCM and the carrier fluid. The consistency of dispersion ranges from a liquid similar to water at low capsule fraction, to a viscid slurry like consistency with larger fractions of capsules.

### 3.2.3 Thermodynamics for Latent Heat Storage

The following review on the basic thermodynamics for latent heat storage is based on studies of Hariri (1988) and Yanus (1989). A substance can exist at three different phases; liquid, solid and vapour. The three phases may exist together in equilibrium but the two phases are more common. Figure 3.6 illustrates the pressure-temperature diagram of a pure substance, called the phase diagram (three phases are separated from each other by three lines). Along the sublimation line the solid and vapour phases exist in equilibrium, along the fusion (or melting) line the solid and liquid phases exist in equilibrium, and along the vaporisation line the liquid and vapour phases are in equilibrium. These three lines meet at the triple point, where all three phases coexist in equilibrium. The vaporisation line ends at the critical point because no distinction can be made between liquid and vapour phases above the critical point.

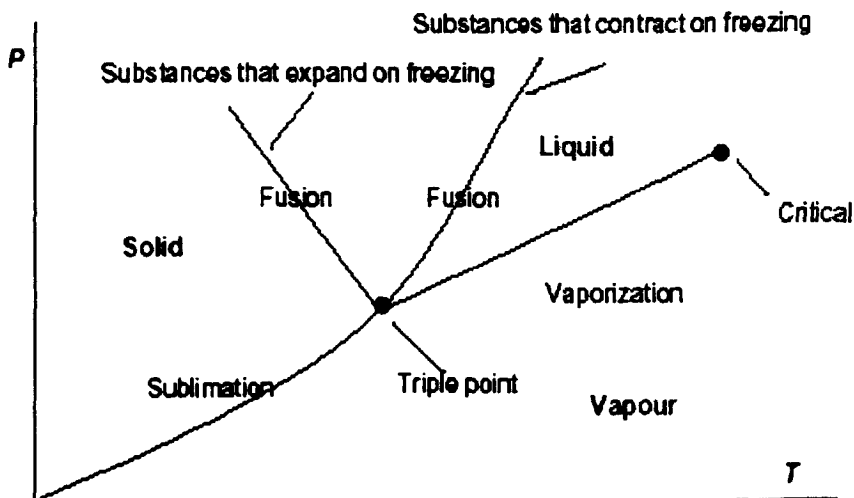


Figure 3.6: Pressure-Temperature Diagram of Pure Substances (Yunus, 1989)

Under equilibrium conditions two phases of the same substance exist at the specified temperature and pressure. Enthalpy, entropy and Gibbs function (an indication of the amount of energy in a system) are three thermodynamic extensive (mass dependent) properties of matter. The Gibbs function difference is the driving force for phase change, just as the temperature difference is the driving force for heat transfer. "the two phases of a pure substance are in equilibrium when each phase has the same value of specific Gibbs function" (Yunus, 1989). This is due to having the two phases at the same pressure and temperature. This fact is relevant to different solid phases of a pure substance and is important in metallurgical applications of thermodynamics. It can be expressed as:

$$G = H - TS \quad [3.4]$$

Where  $H$ , is the Enthalpy in energy/mass,  $T$ , Temperature and  $S$ , the Entropy in energy/mass temperature.

The Clapeyron equation is another important thermodynamics relation for understanding a phase change process. It involves the saturation pressure and temperature, the change of enthalpy associated with a change of phase and the specific volume of the two phases.

During a phase change process, the pressure is the saturation pressure, which depends on the temperature only and is dependent of the volume. Consider the third Maxwell relation;

$$\frac{dP}{dT} = \frac{\Delta S}{\Delta V} \quad [3.5]$$

Where  $dp/dT$  is the slope of the pressure-temperature diagram, which is independent of the volume,  $\Delta S$  the entropy change and  $\Delta V$  the volume change for the phase transition. By substituting entropy with the latent heat of phase transition  $\Delta H$  divided by the temperature  $T$  at which the change is occurring, we obtain;

$$\frac{dP}{dT} = \frac{\Delta H}{T\Delta V} \quad [3.6]$$

This is called the Clapeyron equation which applies to any change of state; fusion, vaporisation, sublimation and changes between crystallisation forms. This is an important thermodynamic reaction since it enables us to determine the enthalpy of vaporisation at a given temperature by simply measuring the slope of the saturation curve on the P-T diagram and the specific volume of saturated liquid and saturated vapour at the given temperature.

### 3.2.4 Nucleation and Supercooling

The total amount of heat stored by any substance in a solid phase when the temperature is increased from  $T_s$  to the temperature of boiling  $T_b$  via the temperature of fusion  $T_f$  can be expressed as;

$$Q = n \int_{T_s}^{T_f} C_{ps} dT + n\Delta H_f + n \int_{T_f}^{T_b} C_{pl} dT + n\Delta H_v \quad [3.7]$$

Where  $n$  is the quantity of the material in moles,  $C_{ps}$  and  $C_{pl}$  the molar heat capacity at constant pressure of the solid and liquid phases (sensible heat), respectively,  $\Delta H_f$  the enthalpy of fusion, and  $\Delta H_v$  the enthalpy of vaporisation. The second and fourth terms indicate the amount of heat involved in the phase change at the points of melting and boiling, respectively (Mayhew, 1980).

Figure 3.7, shows the change in enthalpy according to the transition temperature. The enthalpy  $H$  has an infinite slope at the fusion temperature,  $T_f$ , and this kind of phenomena called "first order phase transition". It has the implication that the heat capacity,  $C_p$  (defined as the gradient of enthalpy with respect to temperature), becomes also infinite.

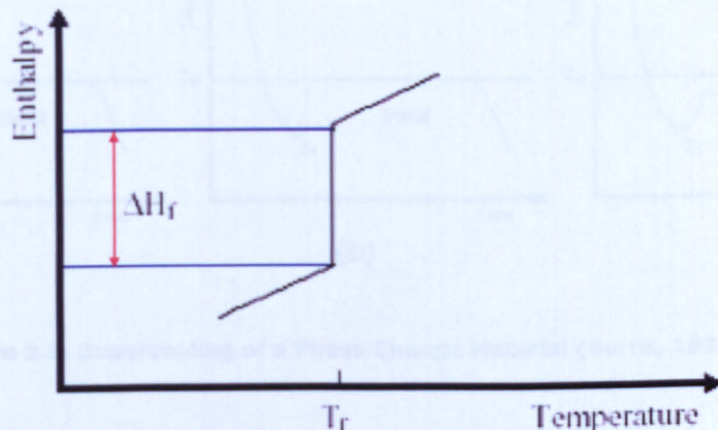


Figure 3.7: Change in Enthalpy at the Transition Temperature (Hariri, 1988)

The physical reason for this trend is the addition of heat to a system at its first order transition temperature is used in pushing the transition rather than in changing the temperature of the system. It follows that a first order transition may be characterised by an infinite heat capacity at the transition point. This is the reason why phase change materials are attractive as heat storage media.

### 3.2.4 Nucleation and Supercooling

Nucleating and crystal growth are characteristic terms that refer to and accompany conduction heat transfer and the formation of solid mass as it liberates heat. During heat gain, where melting occurs, nucleation does not exist because convective heat transfer enhances the process.

During the solidification process of a PCM, nuclei must form and grow for the crystallisation to continue. There are many PCMs which have the disadvantage of the tendency to supercool upon liberation of heat. This characteristic is quite apparent in PCMs such as salt-hydrates compounds, where the temperature drops below their transition temperatures, as it leads subsequently to the delayed development of the crystallisation process (Burns, 1981).

For example, as seen in figure 3.8, supercooling at point  $S_c$  can be noted as soon as the temperature drops. There are three ways of describing supercooling and the crystallisation process; Curves (a) and (b) indicate that, due to poor rate of nucleation, the liquid phase supercools to point  $S_c$  then the crystallisation begins. This is followed by a period where the two curves stabilise, at the transition (melting)  $T_m$ , until they drop again.

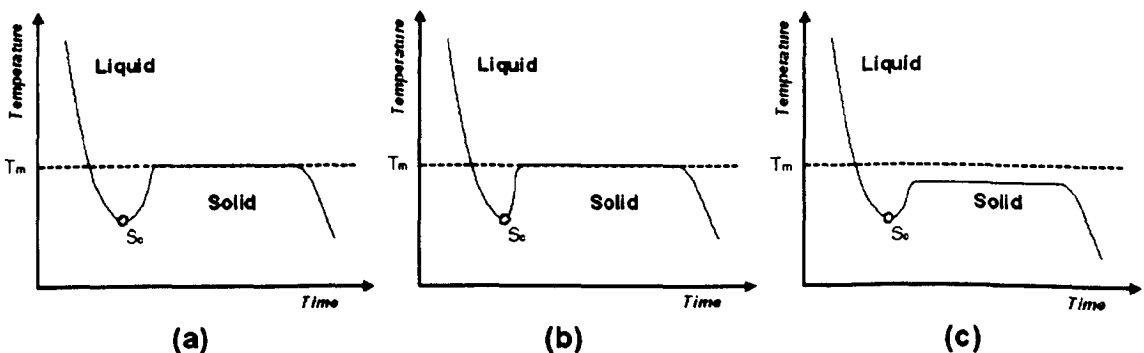


Figure 3.8: Supercooling of a Phase Change Material (Burns, 1981)

The difference between curves (a) and (b) is that in the former (a) case, nucleation is slower either because of high content of water which leads to lower thermal diffusivity, or because of some distribution in the molecular structure of the material due to impurities. In the latter (b) case, the material attains the temperature  $T_m$  quickly, indicating higher thermal diffusivity.

Curve (c) indicates that supercooling in both liquid and solid phases appear. This can be attributed to poor rate of crystal growth, as it continues below the transition (melting)  $T_m$  line for period of time until the rate of heat removal overcomes the latent heat of solidification. Therefore, it can be assumed that poor nucleation in the solidification of PCM leads to poor rate of crystal growth, hence poor material thermal performance.

Since solidification involves nucleation, numerous nucleating additives have been investigated in order to reduce supercooling. A nucleating agent is a material having a crystal structure similar in lattice spacing to that of the phase change substance. They serve as nuclei for the PCM crystals to grow on them during freezing of the PCM and are also termed as seed-crystals (Abhat, 1982). Ryu (1992) studied various inorganic salt hydrates as a latent heat storage medium. He found that, for thickened Glauber's salt, Borax could reduce supercooling of the salt from 15°C to 3-4°C. Three different powders of carbon (1.5-6.7  $\mu\text{m}$ ), copper (1.5-2.5  $\mu\text{m}$ ) and titanium dioxide (2-200  $\mu\text{m}$ ) were found to reduce the supercooling of thickened hydrated salt  $\text{Na}_2\text{HPO}_4 \cdot 12\text{H}_2\text{O}$ . By adding 2 wt% potassium sulphate, the supercooling of salt  $\text{CH}_3\text{COONa} \cdot 3\text{H}_2\text{O}$  was reduced from 20°C to 2-3°C, also.

An investigation of the supercooling phenomenon by Yagamishi (1996) showed that of the size of microspheres ranging from 5-100  $\mu\text{m}$ , the crystallisation temperatures are lower as the microspheres size decrease. He points out that the supercooling increased with reducing the size of the microcapsule because the number of nuclei in each droplet size reduces.

### **3.2.5 Stratification + Agglomeration**

Stratification (or irreversible phase change) is usually associated with phase separation after it cycles through the phase change process a number of times. This phenomena limits the usefulness of the PCM. For example, Glauber's salt has an incongruent melting point, and as its temperature increases beyond the melting point it separates into a liquid phase and a solid. Since the density of the

solid is higher than the density of the solution, phase separation occurs. As a consequence, the salt settles to the bottom of the tank. With complete stratification, the storage ability of the PCM decreases about 40% (Hariri, 1988).

To overcome the problem, the addition of suspension media or thickening agents to the PCM could be used to prevent separation of the solid and liquid phases. The use of a thickener also can assist to suspend the nucleating agents within the PCM, otherwise they have a tendency to collect at the bottom of the container due to differences in density. Thickening agents do, however, displace a part of the PCM in the heat store, thus reducing the volumetric heat capacity of the store (Abhat, 1982).

Several techniques have been tried for preventing phase separation, which results in loss of storage capacity, i.e. rotating storage devices and direct contact heat transfer. Another approach is to store PCM solutions in shallow pans or a long thin tube (Hariri, 1988). In addition, the favourable technique of micro-encapsulating the PCM within a small plastic shell avoids the phase separation. Results tested by Burns (1981) showed that more than 2,000 cycles of PCM encapsulated, changed phase without any separation.

These above issues are eliminated if the PCM is encapsulated. Microencapsulating the PCM for the purpose of this investigation eliminates any separation within the microcapsule, combined with the use of the paraffin's which are less susceptible to the problem. The only stratification issues that may occur could be a result of the capsule being less dense than the carrier fluid. This would cause buoyant characteristics of the microcapsules in the working fluid and separation and clogging. This would have to be solved before the slurry could have prolonged use within the fuel cell.

### **3.2.6 Requirements of the PCM for the Fuel Cell**

The selection of any candidate paraffin PCM could be exclusively made on the suitability of its thermal properties. These properties included the heat of fusion and transitional temperatures. During the selection procedure the great number of candidates was reduced substantially when other factors, such as safety, cost, encapsulation and physical properties were considered. Comprehensive records of the thermo-physical properties of these materials were published, for example, by Humphries and Griggs (1977) and Abhat (1983). The following table 3.1,

summarises the selection criteria, that should be satisfied by any candidate PCM for use in a slurry; these fall into five groups of properties.

Properties	
<b>Thermal</b>	<ul style="list-style-type: none"> <li>• High Latent Heat of Fusion</li> <li>• High Specific Heat</li> <li>• Good Thermal Conductivity</li> </ul>
<b>Physical</b>	<ul style="list-style-type: none"> <li>• Total Congruent Melting</li> <li>• Low Volume Change</li> </ul>
<b>Kinetic</b>	<ul style="list-style-type: none"> <li>• No Supercooling</li> </ul>
<b>Chemical</b>	<ul style="list-style-type: none"> <li>• Long-term Chemical Stability</li> <li>• Non-corrosive (if possible)</li> <li>• Non-inflammable</li> </ul>
<b>Economic</b>	<ul style="list-style-type: none"> <li>• Available</li> <li>• Cheap</li> </ul>

**Table 3.2: PCM Selection Criteria**

### 3.3 Phase Change Slurries

The amount of heat that can be stored by common heat transfer fluids, e.g. water or oils, depends on the usable temperature range that can be exploited. The efficiency of such heat transfer fluids is poor if applications allow only a small temperature difference. One solution to increase the efficiency of such applications is to use phase change materials, the so-called PCMs. The energy that can be stored at the phase transition e.g. from solid-liquid, of some materials is very high. Paraffin is a PCM that can be pumped through pipes when it is microencapsulated and dispersed in a carrier fluid, e.g. water. These mixtures of PCMs and carrier fluids are called phase change slurries (PCSs). A key driver is that PCMs can provide high heat density and smaller temperature variation.

In recent years, researchers around the world have investigated the impacts and benefits of Phase Change Materials (PCMs) in an attempt to boost the heat capacity of secondary heat transfer fluids. For many years, PCMs have been studied to determine their benefits in district cooling systems (Choi, 1993). Recently research activities have demonstrated that the heat capacity of a heat transfer fluid can be increased by up to four times by adding PCMs to cooling systems (Bo, et al, 1999).

PCMs can be encapsulated in small micro-spheres and suspended in a working fluid to form a slurry. This is intended to improve the thermal characteristics of a heat transfer fluid through use of the associated latent heat of fusion to enhance the thermal storage capacity of the fluid. Microencapsulated PCM (MicroPCM) slurries have indeed become a viable option for heat transfer processes in recent years. MicroPCM slurry also has unique characteristics that can increase the thermal capacity of heat transfer fluids by providing latent heat capacity at a temperature different to the phase change point of the carrier fluid.

In order to successfully adapt the microPCM slurry to the fuel cell system, the microPCM thermal and fluid properties, and their effectiveness in heat transfer must be fully characterised and understood.

### **3.4 Micro-encapsulation of PCMs**

The following section provides an overview of microPCMs and their use as a functionally thermal fluid.

#### **3.4.1 Overview**

MicroPCMs are very attractive since the rate of heat transfer per unit volume to or from the material in the particles is high, and the ratio of surface area to volume of the small particles is large, (Charunyakorn, 1991). In addition, encapsulating the PCM in small capsules can eliminate any segregation during phase change that may be caused by changes in density.

The use of microPCM particles suspended in a single-phase working fluid can provide additional thermal capacity from the latent heat associated with the solid-liquid phase change. Although the latent heat of fusion is generally less than that of vaporisation and sublimation, the change in volume of the phase change materials during fusion or solidification is usually very small, which is easier to contain and control in a system such as the fuel cell.

The slurry may also serve as both energy storage and heat transfer media, and the requirement of separate heat transfer media is therefore eliminated. Many conventional systems using the sensible heat of a single-phase working fluid alone, often operate at a high-volume flow rate to provide the desired operational conditions. As a result, systems can consume large amounts of pumping power.

Using the PCS can increase the convective heat transfer coefficient through increasing the effective thermal capacity of the working fluid, thus allowing the use of a smaller volumetric flow rate, and hence, reducing the system volume and pumping-power requirement.

Micro-encapsulation techniques are well developed, mainly by the pharmaceutical industries, because they were used to produce pills, copy papers, composites, powders, coatings, foams and fibres. Furthermore, they were applied to clothing for a heat capacity enhancement (Colvin et al, 2003). A newer application is plastic microcapsules, containing PCM, floating in a carrier fluid for thermal energy transportation. Advantages to encapsulation include; the PCM is completely encapsulated and, therefore, shows a higher thermal cycling resistance and doesn't separate, as displayed in larger phase change systems. Importantly, the capsules are sufficiently resistant to the shear stresses occurring in the pumps to make them viable in pumped systems. The smaller the capsules are, the greater their resistance towards destruction (Colvin et al, 2003). By micro-encapsulating the PCM, the core material is always separated from the carrier fluid, preventing its deposition and clogging of system components.

### **3.4.2 Description**

The latent heat microcapsule is made from encapsulating a fine phase change material with a thin film. A typical method of encapsulation is coacervation that makes the latent heat microcapsule by solidifying the coating deposition covered around the core of fine spherical phase change material in a cooling process (Processes explained in detail in chapter 6). Figure 3.4 shows the cross section of a single microPCM particle. Particle diameters can range from one to several hundred microns. The core PCM constitutes approximately 80-90% of the particles weight.

Capsule material is very thin and is a member of a hydrophilic group. The capsule material is constructed by double thin films in which the outside thin film is a hydrophilic polymer such as polystyrene or polyamide, and the inside one is a hydrophobic polymer like fluoride as shown in figure 3.9.

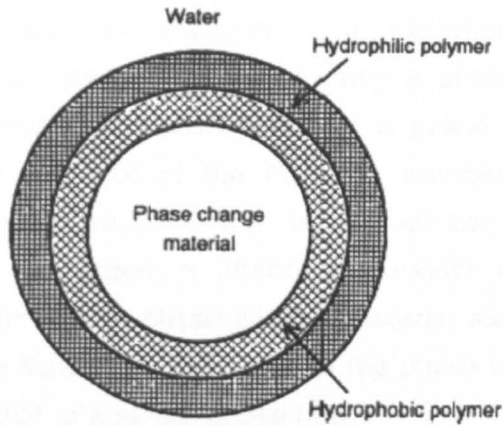


**Figure 3.9: Two Film Layer Micro-capsule**

Generally, for the stable dispersion of microcapsules in water, there are a number of determining factors such as capsule density, the carrier fluid density, however, to aid dispersion the average diameter of the particles has a tendency to be in the range of 1-5 $\mu\text{m}$  and surfactants may be added into the carrier fluid as a dispersant agent (Inaba, 2000).

The physical strength of the microcapsule can be controlled by the film thickness. This can range from 2nm to 10nm, and as a result the thermal resistance is very small.

### 3.4.3 History

Many researchers have shown advantages and possible utilisation of encapsulating PCM in small capsules. The earliest study concerning the thermal use of microPCM as a heat transfer medium was for General Electric Inc, by Mehalick and Tweedie (1979). The use of fluidised particles to enhance heat transfer for applications such as space cooling systems was not new (Hendel, 1965), but the use of microscopic particles, which were encapsulated liquids under warm conditions, was very new.

Since 1983, The Small Business and Innovation Research (SBIR) program for NASA demonstrated the effectiveness of this novel coolant to significantly enhance effective thermal capacitance. This development enabled the reduction of weight and volume of thermal energy systems used in spacecrafts (Kasza, 1985). It was also reported that the convective heat transfer coefficient of the working fluid increased as a result of the increase in effective thermal conductivity and capacitance.

Chen, 1987, carried out an analytical and experimental study on the augmentation of laminar flow heat transfer using a phase change slurry. He found that the completed heat transfer rate for a phase change slurry flow is proportional to the square root of the Reynolds number (Re), and inversely proportional to the cubic root of the Jakob number (Ja) of the slurry. Charunyakorn, 1991, developed a theoretical model describing the force convective heat transfer with a phase change material slurry in a circular duct flow and found that the Nusselt number (Nu) of the phase change slurry flow was 2-4 times higher than that of a single-phase flow.

Recently more papers have been published concerning thermal advantages of using microPCM to enhance the convective heat transfer of a working fluid [Roy (1991, 1997), Colvin (1992), Goel et al (1994), Choi (1994) and Yamagishi (1996)]. However, most have not addressed some of the key practical issues of integrating such a fluid into conventional systems. These issues are to be explored later in the thesis.

#### 3.4.4 Experimentation

A limited number of journal articles present and discuss heat transfer and pressure drop characteristics of microPCMs, however the research has brought to light very important issues concerning the PCMs effectiveness in improving heat capacity. Several publications indicate the importance of key parameters such as the Stefan number (St), mass fraction, and the PCM latent heat of fusion in improving performance (Roy and Avanic, 2001). The Stefan number is defined as:

$$St = \frac{C_p \left( q_w \frac{R}{k} \right)}{c_m \lambda} \quad [3.1]$$

Where,  $C_p$ ,  $q_w$ ,  $R$ ,  $k$ ,  $c_m$ , and  $\lambda$  are the specific heat of suspension, wall heat flux, radius of pipe, thermal conductivity of suspension, mass fraction of PCM in suspension, and latent heat of fusion of PCM, respectively. It relates specific heat to latent heat of fusion. According to Goel et al. (1994), St should be less than 1 for optimal effectiveness.

From the heat capacity point of view, higher mass fractions and latent heat of fusion values are preferred because they increase heat capacity of the slurry

(Choi, 1993). Alternatively, higher mass fractions increase apparent viscosity, which translates into higher needs for pumping power (Bellas, et al., 2002, Choi, 1993, Choi, et al., 1991).

Very few journal articles concerning microPCM physical properties have been published. Roy and Sengupta (1991) conducted an experimental study to evaluate the properties of microPCMs with two characteristic thicknesses that made up between 15% and 30% of the total volume of each microcapsule. A differential Scanning Calorimeter (DSC – explained in detail in chapter 4) was used to determine their thermal properties. Yamagishi, et al.(1996) presented experimental results indicating that MicroPCM particle size does not affect melting temperature and latent heat of fusion. However, the degree of supercooling or the difference between crystallisation and melting temperature points increased with particle size,  $d_p$ , was less than 100 $\mu\text{m}$ .

The researchers also tested nucleating agents with molecular structure similar to the PCM molecules and were able to suppress supercooling considerably. Yamagishi, et al. (1999), presented empirical data for microencapsulated Octadecane obtained by using DSC equipment, a Couette viscometer (Yamagishi, et al. 1996), and pressure drop data. Results indicated that an ionic surfactant can decrease the apparent viscosity of the slurry and turn it into Newtonian-like fluid at high mass fractions (20-30%). As a result, Yamagishi, et al. (1999) used the Vand model (Vand, 1945) to predict the relative viscosity of the microPCM slurry at different volume fractions.

Ohtsubo, et al. (1991) presented experimental data that explained why microcapsules structurally failed. It became evident after several experiments that as  $D_p/th_p$  increases, the percentage of broken capsules increases, where  $D_p$  and  $th_p$  are microcapsule diameter and thickness, respectively.

Based on observations and past research activities (Roy and Avanic, 1997), the microPCM walls do not have a significant impact on the heat transfer process. For microcapsules (less than 20 $\mu\text{m}$ ) filled with n-tetradecane, the calculated Biot number is less than 0.1, which is primarily due to the smallness of the microcapsules. Results also indicate that the Reynolds number is not an independent parameter for the heat transfer process. Yamagishi, et al (1996) indicates that the slurry approximately follows the Blasius equation:

$$f = 0.0791 \text{Re}^{-0.25} \quad (\text{in turbulent flow}) \quad [3.2]$$

$$f = 64/\text{Re} \quad (\text{in laminar flow}) \quad [3.3]$$

Where,  $f$  and  $\text{Re}$  are friction factor and Reynolds number, respectively. Findings indicate that an optimum point of operation exists that represents a trade-off between microcapsule concentration and pressure drop, to maximise heat transfer without severely penalising the pumping power.

Experimental data with pressure drop showed that when no heat transfer took place, the friction factor of the microPCM slurry followed the same behaviour as pure water at different mass fractions as described by the Blasius equation. It was concluded that viscosity increased non-linearly with mass fraction. No evidence of pressure drop fluctuations could be found when the PCM melted within the micro particles, and a constant relative viscosity was observed when the slurry temperature increased (Yamagishi, 1996). It was also observed that when the slurry velocity approached 2-2.5m/s at 30% volume fraction, pressure drop decreased, indicating that the slurry became laminarised. The authors concluded that because the particles were smaller than the turbulent length scale, turbulence was suppressed and pressure drop reduced.

### 3.4.5 MicroPCM Applications

Currently there are no microPCM slurries being used in commercial applications. Recent activity and development in the shell formation technology for the application in the following section 3.6.2, over the past 2 years has seen improved encapsulation techniques and capsule durability. These have had a knock on effect to the slurry research, and yet, whilst no applications have become commercial, new patents have been established by leading companies such as DaimlerCrysler, section 3.6.2.

#### 3.4.5.1 Clothing

The large microPCM industry has emerged over the past two years. This has primarily been in the field of utilising microPCMs in apparel to regulate temperature. The microPCM is embedded with textile fibres, illustrated in figure 3.10, and operate as a thermal shock absorber by slowing the rate of

temperature change within a wearer's personal microclimate. It reduces the rate at which a person will over heat or get cold.

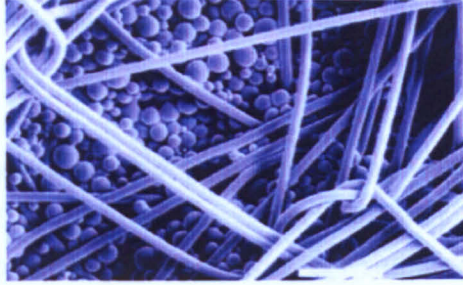


**Figure 3.10: Microscopy of the MicroPCM and Woven Fibres**

Three years after the completion of a contract with NASA, a Boulder, Colorado-based firm acquired from Triangle Research and Development Corporation the exclusive patent rights for incorporating phase-change technology in commercial fibres and fabrics. They formed the company Outlast Inc. with a niche market to use phase-change technology to enhance the comfort levels for individuals with active outdoor lifestyles.

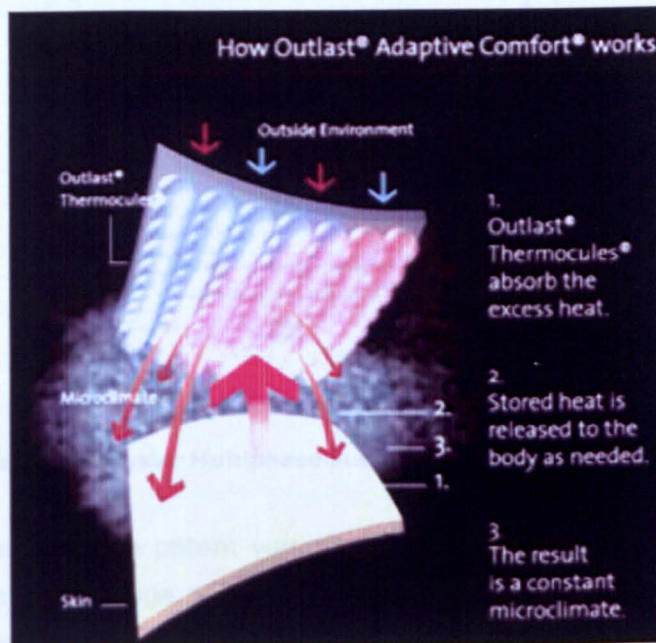


**Figure 3.11: Outlast MicroPCM Apparel Principle of Operation**

Outlast's first products were gloves and since then have expanded into a vast potential of product lines for their materials. These have included motorbike, sports and safety clothing. They have recently also entered strategic partnerships with over 200 premium-brand leaders in North America, Europe, and

Asia, such as: Adidas, Bugatti, Burton, Kenneth Cole, Lands' End, Nordstrom, Rainforest, The North Face, Timberland, and Weatherproof. Expanding beyond consumer apparel, Outlast material has been considered by General Motors as the material of choice for leather bucket seats in the conceptual design of future Hummer H2 sports utility models.

### 3.4.5.2 DaimlerChrysler Multiphase Suspension Coolant

In early 2004 U.S. car manufacturer DaimlerChrysler, established an International Patent on the use of a microPCM slurry as an engine coolant. The principal was very similar to that for the fuel cell slurry in this investigation with the exception of different operation temperatures and system components. Figure 3.12 illustrates the principal outlined in the patent.

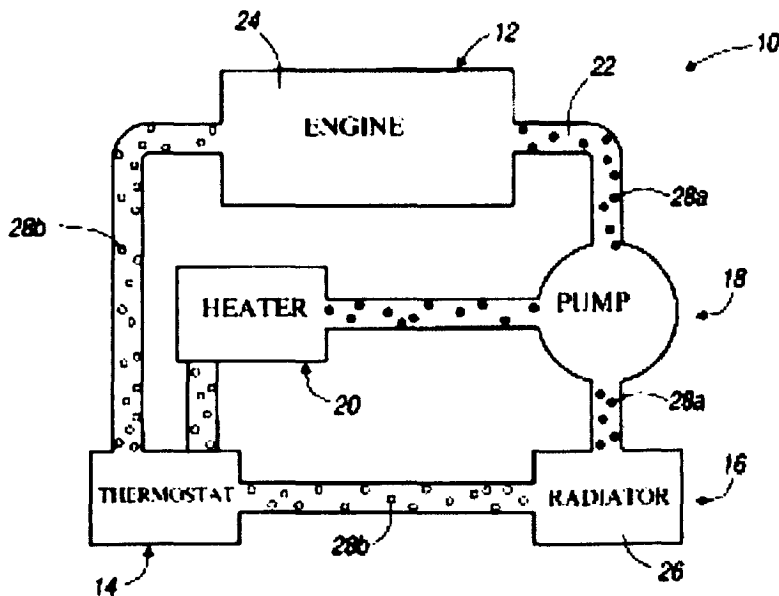


Figure 3.12: Daimler-Chrysler Multiphase Suspension Coolant (Pat; WO2004009728)

The slurry disclosed in the patent was to use a polymer encapsulated solid-liquid or a solid-solid phase change material for use in a fluid coolant for an engine heat exchange system. The resulting coolant would have a higher heat transfer rate than a conventional fluid due to the utilisation of the heat of fusion of the material. Thus providing, improved coolant properties and allowing down sizing of the coolant pump and subsequent reduction of parasitic loading. Engine heat up time would also be increased due to the lower coolant flow rate and heat transfer capability at below the operating range temperatures.

### **3.5 Concluding Remarks**

Functionally thermal fluids have been the focus of this chapter. It has identified a range of fluids that could be developed for use with the fuel cell. The microPCM was particularly attractive to maximise the thermal characteristics of the working fluid by using latent energy. This offers an attractive opportunity for the fuel cell; to enhance thermal energy transportation and heat transfer of heat exchangers to reduce system size, volume and pumping loads. Hence, reduce system cost, improve thermal stability and increase the overall electrical efficiency.

Large research activities in Japan, the United States and at present also in Europe are directed on the development of multifunctional and "intelligent" fluids. These developments are leading to highly improved fluids compared to the conventional sensible heat fluids. The advancement on capsule production for clothing has strengthened the economics for use as a slurry, with improved availability and cost. This has also increased the interest and has aided the development of stronger capsules for resistance to pumping loads.

The use of latent energy microPCM slurry has promising potential to impact thermal system that require improved efficiency, reduced size and thermal stability. The strength of the capsules, the high thermal capacity and the free choice of melting temperatures allows the fluid to be fine tuned to the technical application. This would be a particular advantage where there is a need to reduce pumping loads, systems thermal stability and system size as a result of increased thermal capacity and heat transfer. A fine tuned slurry could significantly benefit an application where only a small  $\Delta T$  was available and has the potential to operate almost isothermally. The remainder of this thesis investigates the feasibility of using a microPCM slurry to improve the performance of a fuel cell.

This chapter has identified that there is an ever-increasing demand on the systems used today to become more efficient and reliable. The use of functionally thermal fluids and latent energy is a stepping-stone to achieving this goal. In terms of the fuel cell, it is the ideal platform to incorporate a state of the art fluid with cutting edge technology. The microPCM slurry has the chance to enhance the fuel cell efficiency and stability, yet be at the forefront of system developments.

## Chapter 4: Thermal Properties Investigation of Microencapsulated Phase Change Material (MicroPCM) Slurries

### 4.0 Introduction

Chapter 3 has shown that the use of functionally thermal fluids, and specifically, the latent energy of fusion can have significant advantage in thermal systems to maximise both energy conversion and conservation. The work outlined in this chapter concerns the experimental investigation of such materials, and focuses on the thermal properties of currently available microPCM for use as a slurry in a fuel cell thermal circuit. The aim of this investigation was to broadly outline the different thermal properties and characteristics of the microPCM and determine their suitability for use with the fuel cell.

Various measurement techniques were implemented. There are many methods for obtaining the thermo-physical properties of PCMs. The choice of method type to be adopted depended on its suitability, accuracy and cost. Some properties, such as melting points, density and, heating and cooling curves can be measured directly using standard laboratory equipment. Other properties can not be measured directly, but require more complex, purposely designed and expensive instruments such as Scanning Electron Microscopy (SEM) or sophisticated computer driven Differential Scanning Calorimeters (DSC) and Viscometers.

The following chapter identifies;

- **Surface Morphology** - Visual identification at microscopic level of the microPCM surface morphology. This experimentation was the first in any literature reviewed to capture the microPCM structure as it undergoes phase transition, also identifying a 15% increase in volume between solid-liquid state.
- **Thermal** - Thermodynamic properties, such as the thermal capacitance, phase transitional temperature ranges, trends and peaks were investigated using two different techniques, DSC and Thermal Analysis (TA).
- **Physical** - Rheological studies established a relationship between slurry concentration and viscosity to establish a compromise between thermal capacity improvement and the increase in effective pumping load.

In the first part of this work, the materials under investigation are reviewed, followed by the presentation of some of the experimental work carried out and results obtained from the thermo-physical properties of the microPCMs.

**4.1 MicroPCMs Investigated**

The PCM used in this preliminary evaluation chapter was paraffin wax. The advantages of microencapsulating this paraffin wax for the fuel cell slurry were its high latent heat of fusion, high specific heat and thermal conductivity, a high density with low volume change during phase change and non-hazardous nature. For these preliminary tests, the microcapsules were manufactured by and obtained from Outlast Technologies Inc. Three samples were examined; they were distinguished primarily by their melting points of 35°C, 50°C and 61°C. The specifications for the microPCM samples are detailed in table 4.1. The microPCM samples are referred to in the rest of this chapter by their phase change temperatures rather than their chemical PCM name.

	<i>Paraffin Wax PCM</i>	<i>Melt Temp (°C)</i>	<i>Density (kg/m<sup>3</sup>)</i>	<i>Specific Heat (kJ/kg°C)</i>	<i>Thermal Conductivity (W/m°C)</i>	<i>Latent Heat (kJ/kg)</i>	<i>C.A.S.No</i>
1.	<i>n</i> -eicosane	35	899	2.14	0.179	180	112-95-8
2.	C23/27 Alkane Mix	50	894	2.13	0.178	160	9002-88-4
3.	Octacosane	61	912	2.14	0.179	186	630-02-4

**Table 4.1: Specification of MicroPCMs Supplied by Outlast Technologies Inc.**

The manufacturer stated that the paraffin was encapsulated “in millions of durable capsules of 15-40µm in diameter, and the PCM comprised 80-85% of the materials weight. The PCM was encapsulated in an impermeable shell with a wall thickness of less than one micron”. The capsule wall was made up of a flexible and strong-thermoset plastic wall and was claimed by the manufacturer to pass through 150,000 freeze/thaw cycle tests with minimal degradation under thermal and pressure (sub 5bar) operations.

As described chapter 3.0 on the applications for microPCMs, the 35°C and 50°C samples had been developed for use in clothing to buffer the temperature. This did however mean that the capsules that were used have been developed to be robust but have not been tested for resistance to pumping stress.

The 61°C sample was different to the other two samples. It had been developed for a confidential military application. On mixing with water, it had different buoyancy characteristics to the other samples. This topic is covered later in the chapter however; the 35°C and 50°C samples had a tendency to separate when mixed with water, while the 61°C exhibited Newtonian behaviour. This was to be a desired characteristic for use as a PCS and suggested that it had been developed for a pumped slurry system.

## **4.2 MicroPCM Slurry Thermo + Physical Evaluation**

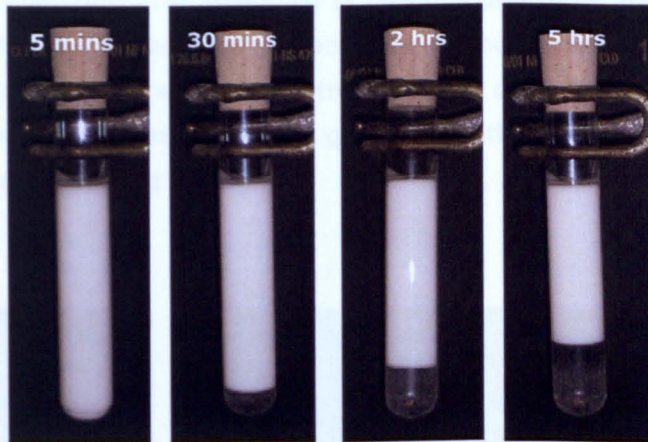
**4.2.1 Overview** Melting and freezing characteristics of PCM involve behaviours such as melting and freezing ranges, congruency of melting, nucleation characteristics, super-cooling of the melt and stability to thermal cycling. For tuning to the fuel cell system and assurance of the long term performance of a latent heat system, it would be important to understand the melting and freezing behaviours of heat-of-fusion substances, and in particular the reproducibility of such processes under repeated melting and freezing cycles.

**4.2.2 Carrier Fluid** The MicroPCM was suspended in a working fluid to enhance the overall energy transportation medium. The slurry combines two useful functions of both thermal energy storage and heat transport. In order to select a fluid as a heat transfer medium, Goel (1994) notes that there are two main criteria; high thermal conductivity and high specific heat. However, as the microPCM samples would be used as the heat transfer medium in the phase change slurry, the selection of the working fluid was governed by the other important aspects; the compatibility with the PCM and the capsule wall. Water was chosen as the carrier fluid and could be used without any inconvenience. It was easy to handle, had low viscosity and no effect on the PCM or capsule wall.

**4.2.3 Initial Observations** At the outset, it was useful to consider some of the interesting issues that occurred in the study. As the capsules of PCM are suspended in the working fluid and forced to circulate through a closed loop circuit for heating and cooling operations, one immediate consideration was the structural stability of the microPCM to withstand the stress in shear flow imposed by the pump, and volumetric expansion due to phase change (under heating). This would be important because microstructure in colloidal suspensions can be strongly distorted by a moderate shear flow (Blawdziewicz, 1996). However, it was claimed by the manufacturer that the capsule wall was flexible and strong and had been tested through 150,000 cycles showing minimal degradation.

Another issue would be the stratification of solid particles in the suspended fluid caused by gravity or centrifugal forces. After the microPCM powder and water were stirred together with a degree of homogeneity, phase separation could occur in as short a period as five minutes; this was particularly the case with the 50°C sample, figure 4.1. The capsules generally floated to the surface of the slurry as they possessed a lower density than the water in which they were suspended (see figure 4.1). In operation, this problem could be eliminated if the Reynolds number of the main flow in pipes is sufficiently high to ensure the solid particles experience continual state of diffusion. For systems operating at low Reynolds number, a mixing device may be required for stirring the slurry in a reservoir. Both the 35°C and 50°C samples exhibited the phase separation when left stationary for a prolonged period; however the 61°C sample showed promising Newtonian characteristics and remain mixed indefinitely. This was to be further examined in chapter 5.

35°C MicroPCM @30%  
Concentration



50°C MicroPCM @30%  
Concentration

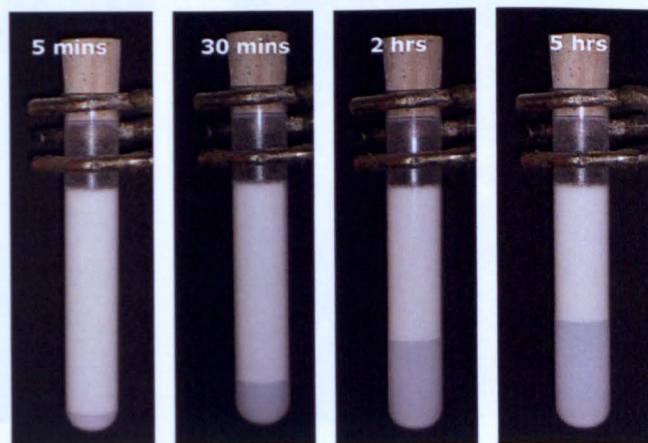


Figure 4.1: Stratification Tendencies of the 35°C and 50°C MicroPCM Samples

### 4.3 Surface Morphology

**4.3.1 Aim** To Investigate the size, structure and surface morphology of the microPCMs at microscopic level.

**4.3.2 Background** Microscopists use several types of microscopes to collect required data. The device used in this investigation was an Environmental Electron Scanning Microscope (ESEM). The ESEM has evolved from the desire by microscopists to have the best of two worlds: optical microscopy and scanning electron microscopy. The model used for this study was the XL ESEM series machine. A review and outline of the general principals and applications of ESEM may be found by (Danilatos, 1991). Figure 4.2 depicts the ESEM machine and figure 4.3, the sample and heat stage that enters the pressurised chamber.

An ESEM allows the examination of surfaces of practically any specimen, wet or dry, insulating or conducting, because it allows the introduction of a gaseous environment in a specimen chamber. The tolerance of gaseous pressures above 600Pa (4.6 Torr) allows the maintenance of a saturated vapour pressure at temperatures above the freezing point and, hence, the presence of liquid water. The presence of positive ion supply from the ionized gas ensures the suppression of negative charge build up on insulating specimens.



Figure 4.2: XL ESEM Machine

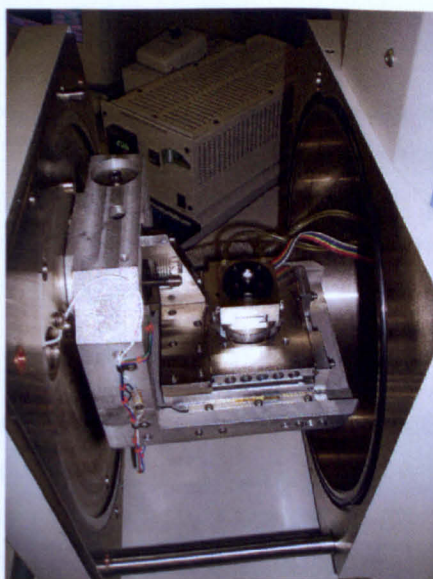


Figure 4.3: Inside the ESEM – Sample and Heating Stage

The XL ESEM in particular was an ideal tool for analysing the microPCM at microscopic level. It had a special heating stage, called the Peltier stage that allowed the unique analysis of varying the temperature of the sample. This was normally used for varying the image quality; however, in this case it was used to capture images of the microPCM phase change, before, during and after the phase transition. The beam damage was also very low compared with that of standard SEM that would require the material to be coated in gold. All previous literature (Colvin, 1980, Yamagashi, et al., 1996) had images of the microPCMs in a gold coating whereas the images obtained were of non-treated samples.

Standard SEM results are directly related to how samples are presented or prepared. Some samples may not easily pump down to high vacuum and will develop artefacts when prepared for this mode of operation. Some need to be kept wet (not freeze dried) to get the correct results. The ESEM used offered the opportunity for investigating samples that are prone to give off contaminants, are prone to become contaminated and are beam sensitive to be studied.

**4.3.3 Methodology** The samples were taken from dried microPCM and placed on a sample pan in the heating stage of the ESEM. The ESEM was pressurised to 3.2mb and images were initially captured at ambient temperature. The Peltier stage was then used to take the sample up through its phase transition and images were captured of the microPCM capsules as they changed state.

**4.3.4 Evaluation of Results** The following images (figures 4.4a, 4.4b and 4.4c) depict the 35°C microPCM sample at 500x magnification, as they passed through their phase transition, from solid to liquid. In accordance with the literature study, it could be seen clearly that the microcapsules were spherical and appeared to be encapsulated with a plastic shell material.

Identified from the images were indentations in the capsules walls. This appeared to reduce with the increase in temperature as the PCM was taken through its corresponding phase change temperature. This suggested that when the capsule wall was indented, the PCM was in solid phase, and when it melted and expanded, the capsule wall accommodated this expansion. The increase in shape corresponded to the relevant phase change temperature of the samples and was not caused by any other influences such as beam damage. An approximate gain of 15% in capsule volume was evaluated.

These images provided evidence that the PCM contained within the flexible plastic shell of the capsule expanded and contracted dependent on its state of phase. This trend was also evident for the other capsule examined, pictured in figures 4.5a and 4.5b.

The surface roughness of the microPCMs varied amongst the three samples examined. The 35°C sample appeared to be very smooth with few blemishes. The other two samples, the 61°C and in particular the 50°C samples had a rougher appearance. This may have been a result of different encapsulation techniques, and/or how well the plastic film encapsulated the PCM. The surface roughness of the microPCMs may also have an influence on the viscosity of the PCS, examined in section 4.4.

It was also clear from the ESEM images that for all three samples, there was a large variation in diameter of the capsules, this was typically from 5-50µm. The mean capsule size was ~30µm.

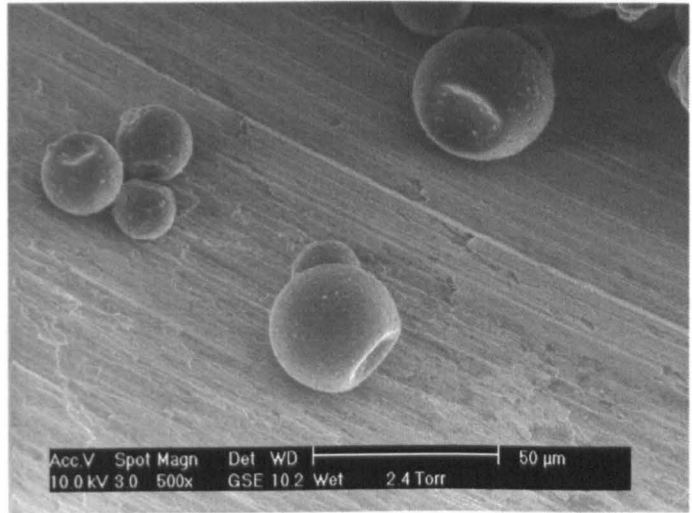


Figure 4.4a: ESEM Image – 35°C sample @ 30°C

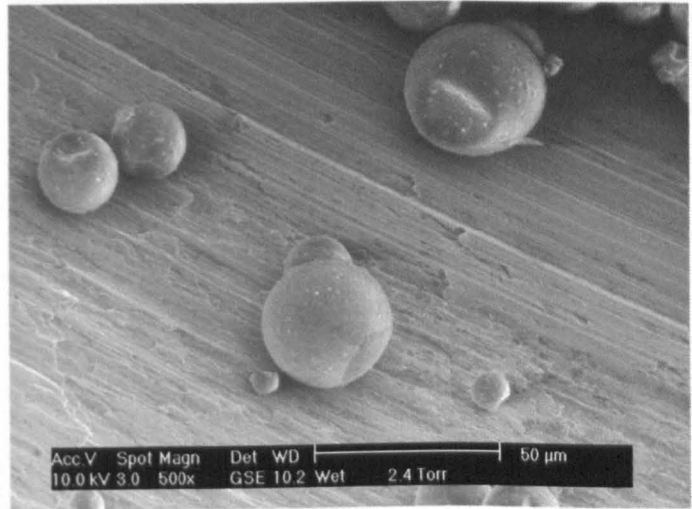


Figure 4.4b: ESEM Image – 35°C sample @ 35°C

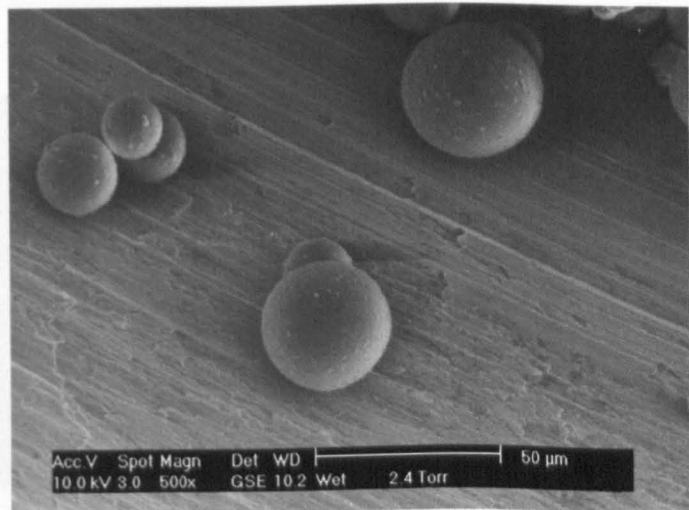


Figure 4.4c: ESEM Image – 35°C sample @ 40°C

Images of the 61°C sample are pictured in Figure 4.5c and 4.5d before and after phase change. They have also been superimposed on figure 4.13, with the corresponding DSC thermogram to demonstrate the change in enthalpy with the change in size of the capsules as they undergo a change of phase.

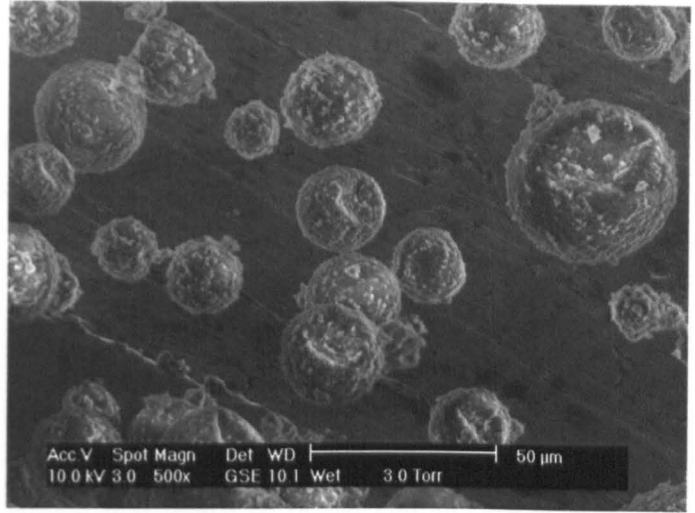


Figure 4.5a: ESEM Image – 50°C sample @ 45°C

The 61°C also appeared to have small pieces of material mixed with it, figure 4.13. The 61°C microPCM was discovered to be neutrally buoyant when mixed with water. It was thought that these small pieces of material were silica that was encapsulated with the microPCMs at the manufacture in order to raise the density of the capsule to match that of water.

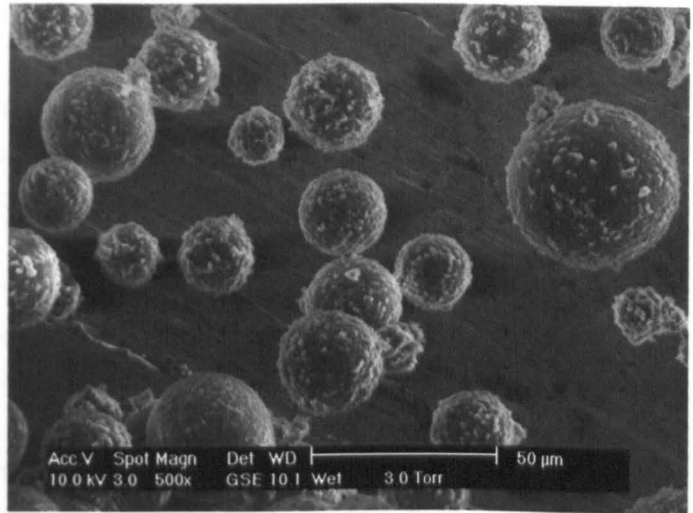


Figure 4.5b: ESEM Image – 50°C sample @ 55°C

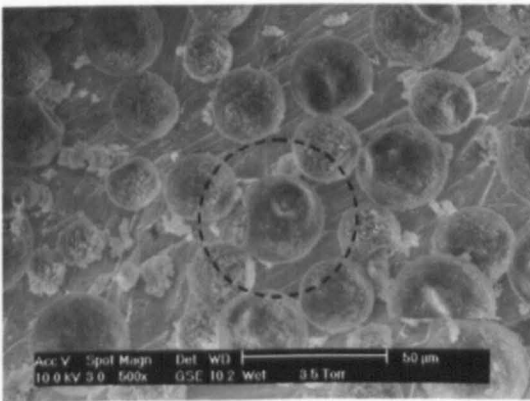


Figure 4.5c: ESEM Image – 61°C sample @ 45°C

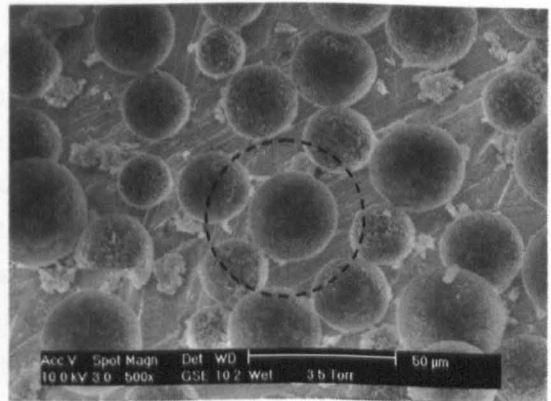


Figure 4.5d: ESEM Image – 61°C sample @ 70°C

**4.3.5 ESEM Summary** The ESEM study was very useful for visually exploring the microPCM as it undertakes its phase change and recognising the change in capsule size. This was to have implications on system design and the effect on system pressures (chapter 7). The 61°C particles appeared to be encapsulated with another material which may account for its neutral buoyancy when mixed with water.

#### **4.4 Latent Heat of Fusion**

**4.4.1 Aim** To determine the thermodynamic properties and characteristics of the microPCM. This included the thermal capacitance, phase transitional temperature ranges, trends and peaks of phase change. This was also to give a better understanding of the applicable temperature ranges and characteristics for use with the fuel cell system.

**4.4.2 Background** The determination of the latent heat of fusion is not simple. It requires a temperature control system to bring the test samples to its melt temperature. A method for measuring the amount of heat absorbed at this temperature is required and is usually complicated. Latent heat is derived indirectly from calculations based on other variables or from specialised equipment. One simple method consists of placing the test material in an insulated refractory container with differential thermocouple junctions inside and outside the container (Hale et al, 1971). The container with the sample is placed in a furnace where the heating rate is controlled so that a constant temperature gradient is maintained across the container walls. The heat flow to the sample is thus almost constant and the heat received by the sample in a given time is determined. The time the sample takes to go through a given temperature interval is proportional to the heat gained and is a measure of the heat capacity.

The time of a temperature arrest is directly proportional to the latent heat of fusion. Primary two measurement techniques are employed for the determination of the heat of fusion, melting temperature and super-cooling characteristics; Differential Scanning Calorimetry (DSC) and Thermal Analysis (TA). The two methods distinguish themselves in terms of the type of measurements made, the quantity of the sample in the tests and the speed with which results can be obtained. Table 4.2, is outlined by Abhat (1982), which gives details of the TA measurement in comparison with the DSC technique.

Measurement Technique		
	Differential Scanning Calorimetry (DSC)	Thermal Analysis (TA)
<b>Apparatus Design</b>	Pelkin Elmer Model: Pyris 1	Glass tube, Flat glass containers of Finned heat pipe heat exchanger
<b>Quantity of Substance</b>	1-10mg	10g-10kg
<b>Measurements Made</b>	Temporal variation of the thermal energy exchanged with the sample to undergo heating or cooling at a constant rate. The output of the measurements is the energy-time diagram, also called thermogram.	Temporal variation of temperature at selected locations within the heat substance resulting from energy input/output of the sample. The output of the measurements is the temperature-time diagram.
<b>Data Evaluated</b>	<ul style="list-style-type: none"> <li>-Form of the endothermic and exothermic peaks on the thermogram.</li> <li>- Melting point/range.</li> <li>- Freezing point/range.</li> <li>- Degree of supercooling.</li> <li>- Heats of fusion and solidification.</li> <li>- Specific heat as a function of temperature.</li> </ul>	<ul style="list-style-type: none"> <li>- Shape of the temperature-time diagram, melting and freezing plateaus, homogeneity of the original substance following melting, etc.</li> <li>- Melting point/range</li> <li>- Freezing point/range</li> <li>- Degree of supercooling</li> <li>- Congruent/incongruent melting</li> </ul>

**Table 4.2; Details of Differential Scanning Calorimeter and Thermal Analysis measurement techniques (Abhat, 1982).**

Both Methods were employed to analyse the microPCMs. The DSC provided accurate measurements and trends whilst the TA highlighted issues that were to be addressed before system integration. This included separation and agglomeration trends.

**4.5 Differential Scanning Calorimetry**

**4.5.1 Aim** To determine and compare the thermodynamic properties, such as the thermal capacitance, phase transitional temperature ranges, trends and peaks of phase change.

**4.5.2 Background** A Differential Scanning Calorimeter (DSC) is a useful instrument for measuring heat of fusion and specific heat, which provides quick and reliable results in the form of energy-time diagrams (thermograms). Evaluation of the thermograms yields precise values of the phase transition temperatures during melting and freezing, the specific heats of fusion and solidification, and the specific heat variation as a function of temperature (Abhat, 1982). Usually the quantity of the sample used in the tests are very small, e.g. 1-10mg. Experiments can be made in hermetically sealed pans with a choice of atmosphere with a range of heating rates. The DSC is, however, a severe test for substances that supercool, since the supercooling tendencies are maximised due

to small quantities of the samples and the poor nucleation conditions in the DSC testing pans. Some DSC machines have the additional feature of low temperature auxiliary equipment using liquid nitrogen, i.e. that could test microPCMs with phase change temperatures below ambient temperature. The following figure 4.6, depicts the DSC machine used for this investigation.



Figure 4.6: Pelkin Elmer - Model: Pyris 1DSC Machine.

In DSC, the sample material is subjected to a linearly increasing temperature rate ( $dT/dt$ ), and the heat flow rate ( $dQ/dt$ ) into the sample is continuously measured; this heat flow rate is proportional to the instantaneous specific heat,  $C_p$  of the sample.

A primary temperature control system controls the average temperature of the two samples, using platinum resistance thermometers and heating elements embedded in the sample holds. A secondary temperature control system measures the temperature difference between the two sample holders, and adjusts this difference to zero by controlling a differential component of the total heating power. This differential signal displacement output is measured and recorded, in the form of thermograms (Perkni-Elmer DSC-2 Operation Manual, 1974).

Aboul-Enein and Olofa (1991), gave a description of a typical thermogram, as shown in figure 4.7, whereby the total energy (latent heat of fusion) associated

with the phase transition can be determined by integrating the area under the Endothermic (heating) or Exothermic (cooling) peaks between the deviation of the points from the baseline. The specific heat of the sample material, for any given temperature range, can be given from;

$$C_p(T) = \left\{ \frac{M_r \cdot C_p(T)_r}{M_s} \right\} \cdot \left| \frac{Y_s \pm Y_{pan}}{Y_r \pm Y_{pan}} \right| \quad [4.1]$$

Where  $C_p$  is the Specific Heat as a function of temperature (kJ/kg-K),  $M_s$  is the Mass of the samples (mg),  $M_r$  is the Mass of reference substance (mg); and  $Y$  is the Output signal displacement of thermogram at a given temperature.

This technique has been adapted in the present work as will be described in section 4.5.3.

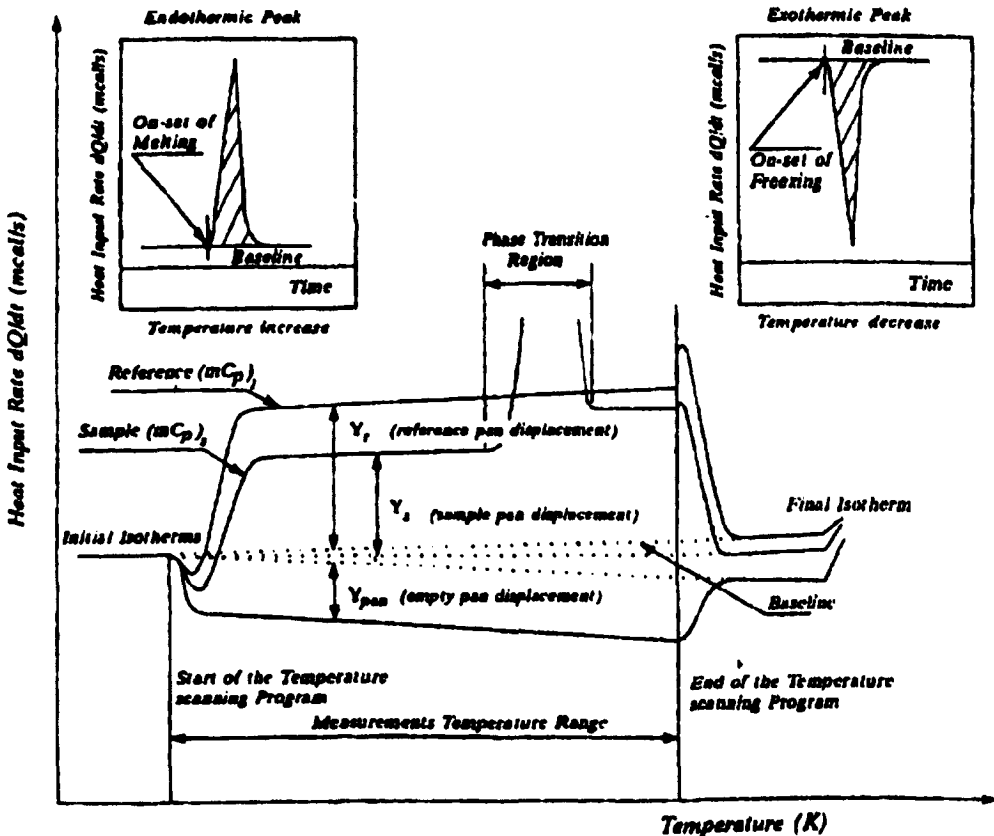


Figure 4.7: A Typical Thermogram of a Pure Substance that Undergoes Solid to Liquid Transition During the Heating and Cooling Cycle. (Aboul-Enein and Olofa, 1991)

**4.5.3 Methodology** Experiments were conducted to study the latent heat of fusion and changes in melting point of the available paraffin microPCM's. A DSC manufactured by Perkin Elmer (Model: Pyris 1), figure 4.6, from the School of Materials and Manufacture, University of Nottingham, was used for the investigation. This machine also had the capability of cooling the samples below ambient using nitrogen gas to ensure that the all phase change transitions were identified. This was particularly relevant to the lower temperature microPCMs under investigation.

The three samples of 100% concentration MicroPCM particles were examined. The thermal behaviour was also investigated at different slurry concentrations of microPCM mixed with water as the carrier fluid. These concentrations were at 10%, 20%, 30% and 40% wt, microPCM to water.

In DSC measurement, the microPCM sample and reference material were heated at a constant rate of 5.0°C/min. The temperature difference between them was proportional to the difference in heat flow between the two materials. The latent heat of fusion was calculated using the area under each peak of the DSC thermograms and the melting temperature was identified by the temperature established by the thermograms at the peak point. The experiments were performed under heating and cooling mode to investigate the supercooling phenomena.

The test procedure took the samples from ambient temperature down to 5°C. The heating phase took the sample from the 5°C to 80°C at heating rate of 5°C/min. The sample was held at 80°C, and then the cooling phase took the sample at the same heating rate back down to 5°C. This process was repeated for all of the samples.

**4.5.4 Sample Preparation (DSC);** The size of samples tested were in the region of 5-15mg. This size was obtained simply for the 100% microPCM test as no mixing was required, however to sample various concentrations of MicroPCM and water, an alternative technique was used. To provide samples with an accurate consistent mix of MicroPCM and water, the methodology was to mix a larger mass of material (summing 100g) and then take a small sample of that mass for testing i.e. a 20% solution of MPCM in water, 20g of MicroPCM was measured and added to 80g of water.

When the MicroPCM was first mixed with water, it was observed that consistent mixing was not achieved as the MicroPCM would repel the water and remain in a powdery state on the surface. In order to assist in the mixing it was necessary to heat the water. It was first considered that the water temperature should be above the phase change temperature of the PCM to enable thorough mixing, however this was not the case with the higher temperature 50°C and 61°C MicroPCM as a temperature of 45°C proved adequate.

An electronic set of scales, figure 4.8, was used to measure the solutions accurate to 0.01g. Firstly a 150ml plastic container was used for mixing, this was placed on the scales and torn to produce a summed value. The corresponding MicroPCM weight by mass was measured into the container on the scales. The water was heated using a hot plate to a temperature of 45°C and added to the MicroPCM. Rather than measure the volume of water it was more accurate to measure it by weight as it was added to the MicroPCM. This eliminated the error caused from the corresponding expansion and contraction of the water as it was heated and would cool. The containers were then shaken until the solution was fully mixed (typically 20-30 seconds).

The sample containers that were used in the DSC machine were small aluminium pans of approximately 23mg in weight, consisting of a base pan and lid. Each pan was weighed before the sample input using electronic weigh accurate to 0.01mg. The inner diameter and height of the containers were measured at 5 and 2mm, respectively.



Figure 4.8: Metler AE 163 + Samples



Figure 4.9: MicroPCM Slurry Samples

The samples were placed in the pan using a syringe of 15ml capacity. The solution container was again shaken for 30 seconds to ensure complete mixing and three loads of the syringe were plunged to again assure a consistent mix before the sample was taken.

The lid was placed on the pan and sealed using a crimping machine. The sample and pan were then weighed so that the sample weight was calculated by subtracting the weight of the pan.

**4.5.5 Calibration** A baseline test was run as a reference before the sample tests were ran. This involved heating the two sample pans with no material. This was repeated a second time to ensure repeatability.

**4.5.6 Evaluation of DSC Results** Figures 4.10, 4.11 and 4.12, show the DSC thermograms of the samples 35°C, 50°C and 61°C respectively. This plots the rate of energy absorption against temperature. One thermal cycle was conducted shown as a heating and cooling curve. The latent heat of fusion was observed as the curves rapidly rose when the MicroPCM melted under heating (indicated as positive heat flow) and rapidly fell as the particles re-crystallised under cooling (indicated as negative heat flow). The latent heat of fusion of the sample was measured from calculating the area underneath the curve.

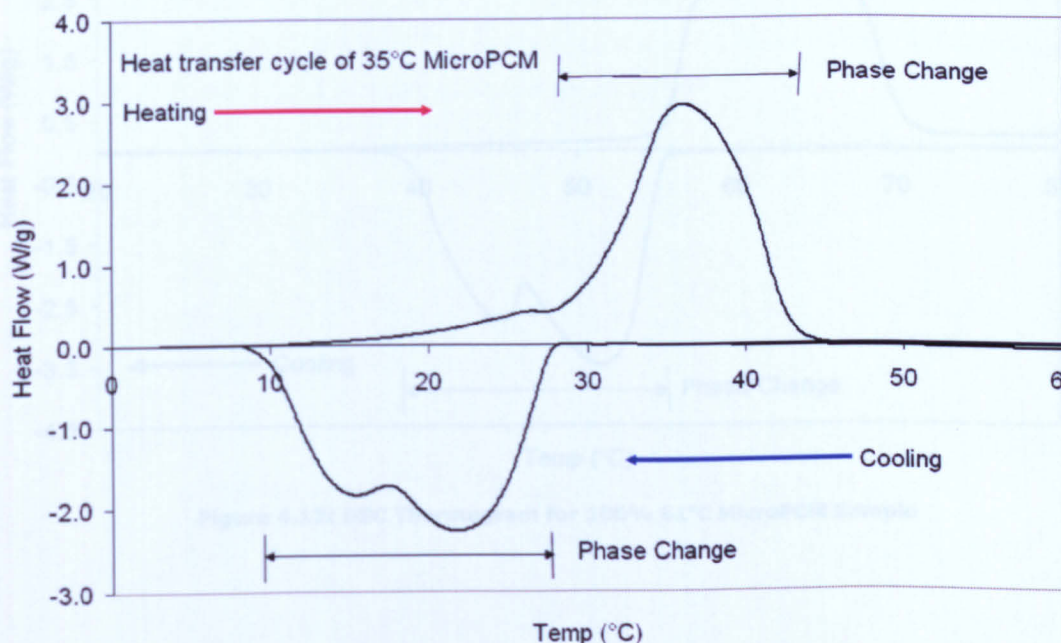


Figure 4.10: DSC Thermogram for 100% 35°C MicroPCM Sample

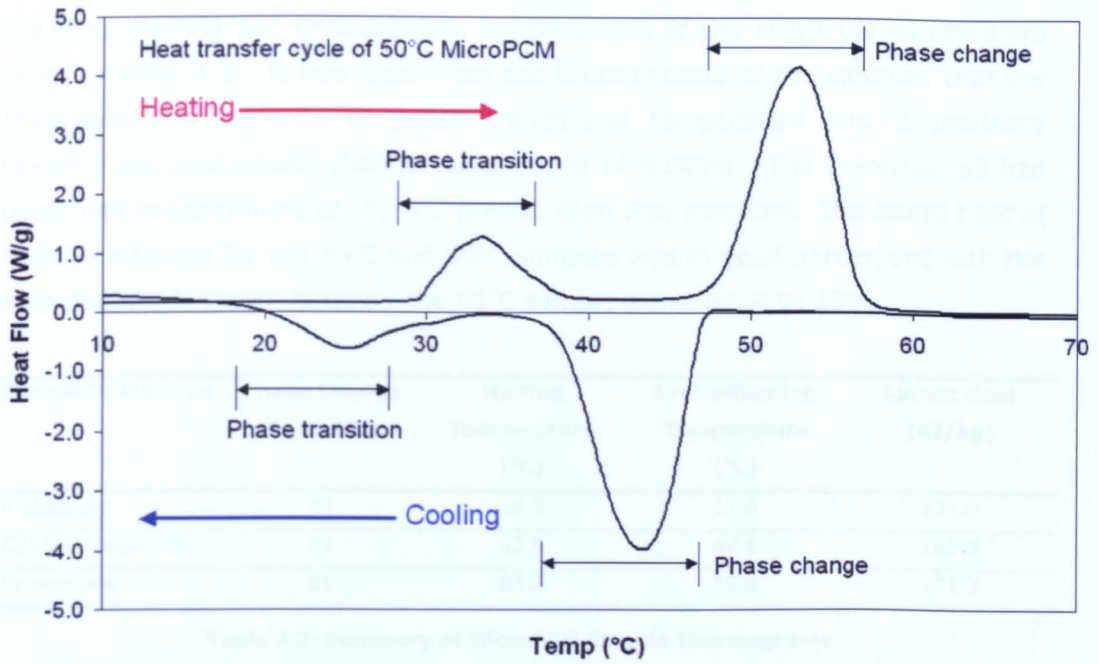


Figure 4.11: DSC Thermogram for 100% 50°C MicroPCM Sample

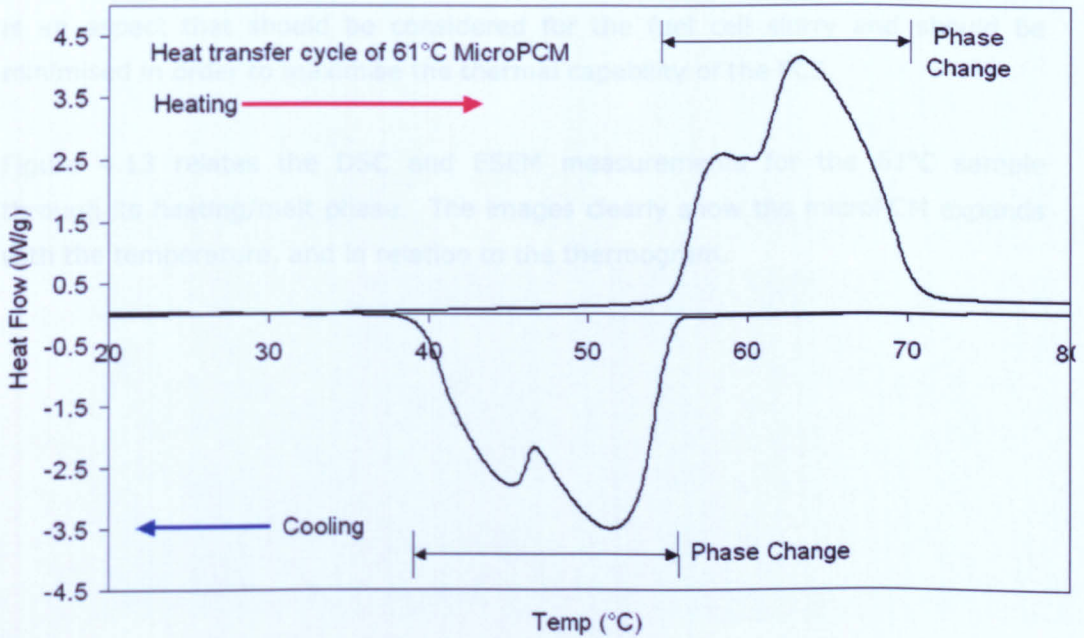


Figure 4.12: DSC Thermogram for 100% 61°C MicroPCM Sample

**4.5.7 Summary of DSC Thermograms** The measured latent heat of fusion and the peak melting and crystallisation temperatures of the microPCM samples are given in table 4.3. It was clear from the thermograms of the samples that the manufacturer's guidance of phase transitional temperature had a tendency towards the peak phase change temperature of melting. The materials all had peak melt temperatures of 1°C-3°C greater than that specified. The latent heat of fusion measured for the 35°C and 50°C samples was in good agreement with the manufacturer's specs; however the 61°C sample exceeded it by 19%.

MicroPCM Material	Phase Change Temp (°C)	Melting Temperature (°C)	Crystallisation Temperature (°C)	Latent Heat (kJ/kg)
<i>n</i> -eicosane	35	36.2	27.6	171.0
C23/27 Alkane Mix	50	52.9	47.6	160.8
<i>Octacosane</i>	61	63.2	55.9	221.3

**Table 4.3: Summary of MicroPCM Sample Thermograms**

The crystallisation temperatures were lower than the melt temperatures by up to 9°C for the 35°C sample, indicating the supercooling phenomena. This melt range is an aspect that should be considered for the fuel cell slurry and should be minimised in order to maximise the thermal capability of the PCS.

Figure 4.13 relates the DSC and ESEM measurements for the 61°C sample through its heating/melt phase. The images clearly show the microPCM expands with the temperature, and in relation to the thermogram.

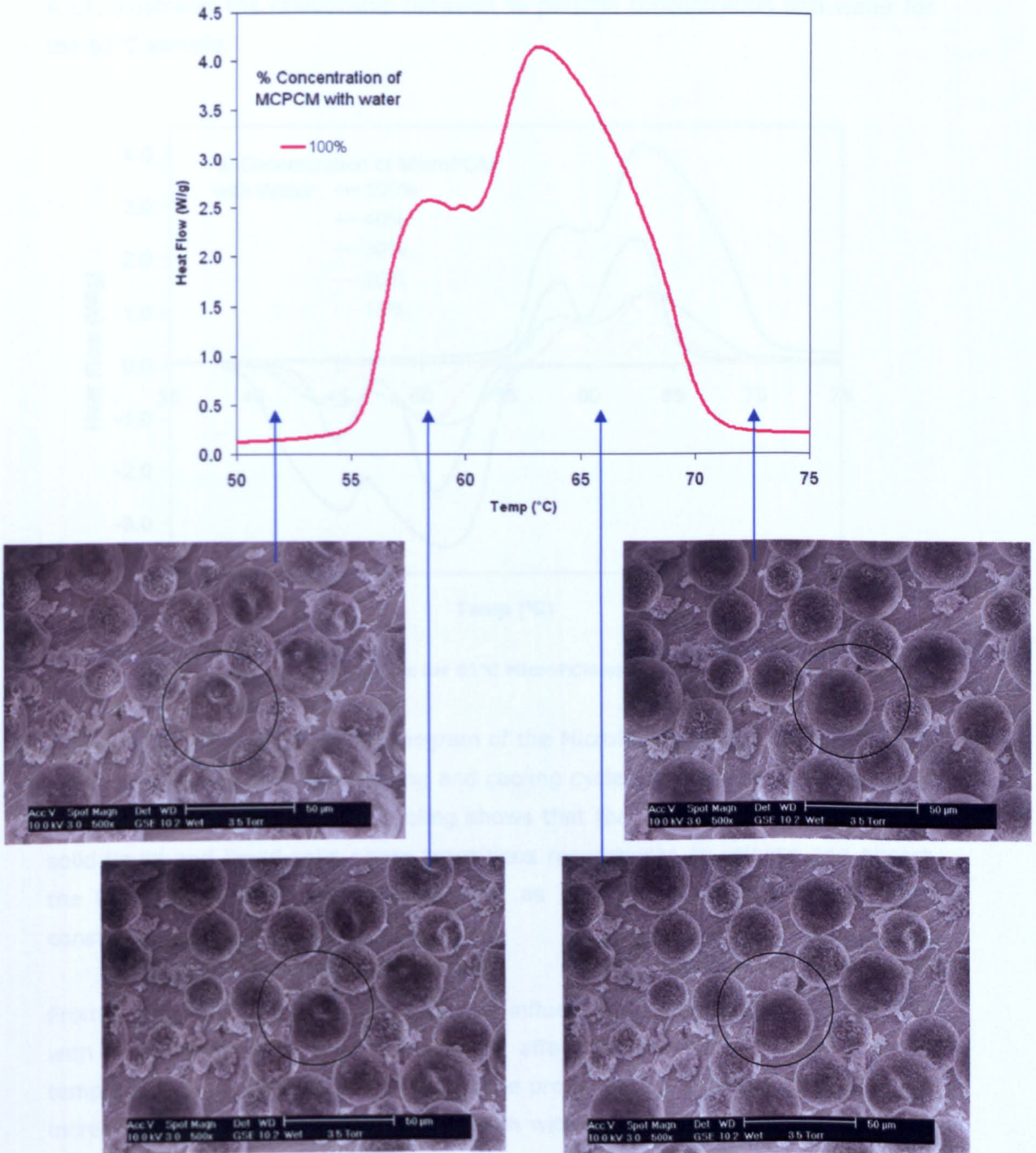
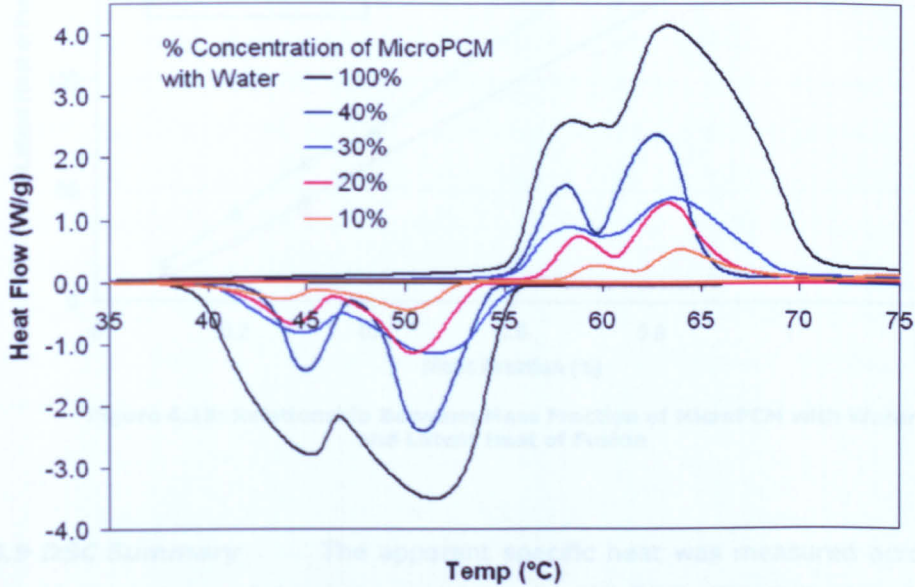


Figure 4.13: DSC Thermogram of 61°C MicroPCM Through the Heating Phase and Corresponding ESEM Images Taken Through the Phase Transition

**4.5.8 Evaluation of DSC Results**

The three microPCM samples were mixed with water at concentrations of 40%, 30%, 20% and 10% by wt. Figure 4.14, illustrates the relationship between % paraffin concentration and water for the 61°C sample.



**Figure 4.14: DSC Thermogram for 61°C MicroPCM and Slurries of 10%-40%**

Figure 4.14 shows the DSC thermogram of the MicroPCM slurries (10%-40%) and water through its complete heating and cooling cycle. Evaluation of the peaks of 63°C on heating and 54°C on cooling shows that the paraffin wax undergoes its solid-liquid and liquid-solid phase transitions respectively, to release and absorb the latent heat of fusion. In contrast, as seen from the figure, the water constituent exhibits just sensible heat.

From figure 4.14, it can be seen that the influence of mass fraction of microPCM with water does not have a significant affect on the melt or crystallisation temperatures. Figure 4.15 summarises the proportional relationship between the increase in amount of latent heat of fusion with the increase in mass fraction of microPCM.

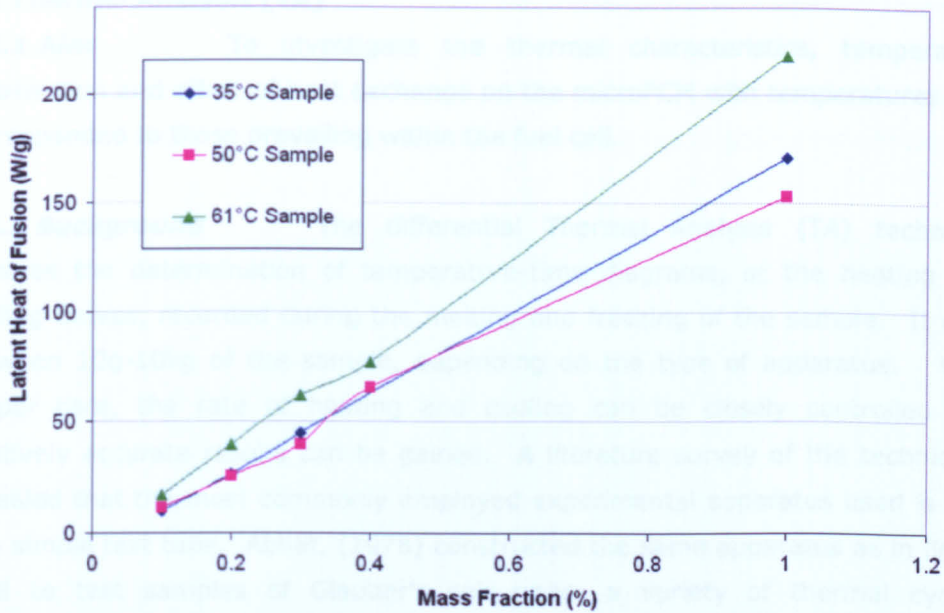


Figure 4.15: Relationship Between Mass Fraction of MicroPCM with Water and Latent Heat of Fusion

**4.5.9 DSC Summary** The apparent specific heat was measured across the phase change region of the three samples using the DSC. The data obtained was in good agreement with the manufacturers specification with the exception of the 61°C sample which had 19% greater latent heat capacity. From the DSC results, we can see that the transport of the slurry can be significantly enhanced by introduction of the latent heat from the microPCMs. The investigation demonstrated the different phase change relationships and ranges, which should be refined to maximise the slurry use with the fuel cell.

Figure 4.16: Schematic of TA Experimental Rig

**4.5.2 Sample Preparation** The samples were prepared using the same technique as outlined in section 4.5.1.

**4.5.3 Methodology** The MicroPCM slurries of 10%, 20% and 40% concentrations were evaluated using the TA technique. The 10% concentration did not show significant interest in the temperature variation. A cylindrical glass tube (10mm  $\phi$  x 150mm) was used as a container for the microPCM slurries. The temperatures were measured using 4-type thermocouples located at the centre of the tube. The glass tube filled with the slurry was initially

## 4.6 Thermal Analysis (TA)

**4.6.1 Aim** To investigate the thermal characteristics, temperature stabilisation and effect of heat exchange on the microPCM with temperatures that corresponded to those prevailing within the fuel cell.

**4.6.2 Background** The differential Thermal Analysis (TA) technique involves the determination of temperature-time diagrams, or the heating and cooling curves, recorded during the melting and freezing of the sample. It uses between 10g-10kg of the sample, depending on the type of apparatus. With proper care, the rate of heating and cooling can be closely controlled and relatively accurate results can be gained. A literature survey of the techniques revealed that the most commonly employed experimental apparatus used is that of a simple test tube. Abhat, (1978) constructed the same apparatus as in figure 4.16 to test samples of Glauber's salt under a variety of thermal cycling conditions.

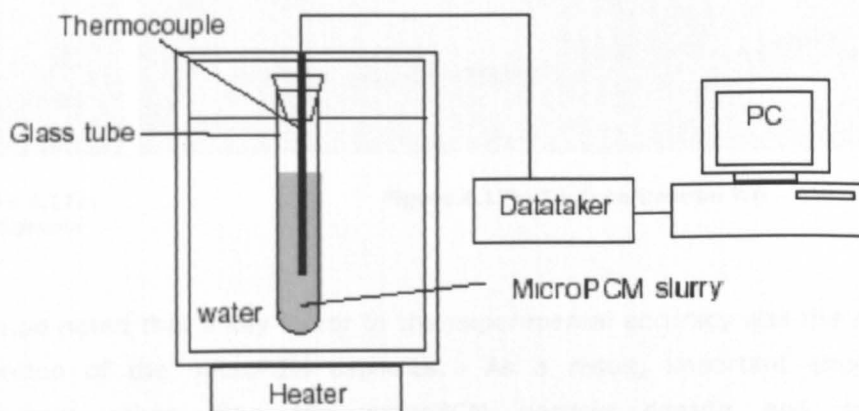


Figure 4.16: Schematic of TA Experimental Rig

**4.6.3 Sample Preparation** The samples were prepared using the same technique as outlined in section 4.5.4.

**4.6.4 Methodology** The MicroPCM slurries of 20%, 30% and 40% concentrations were evaluated using the TA technique. The 10% concentrations did not show significant influence on the temperature variation. A cylindrical glass tube (10mm  $\varnothing$  x 150mm) was used as a container for the microPCM slurries. The temperatures were measured using K-type thermocouples located at the centre of the tube. The glass tube filled with the slurry was initially

submerged in a bath kept at 40°C using an immersion thermostat. In order to heat the sample, the tube was transferred to another bath kept at 65°C (see figure 4.17a). Once the sample was fully heated, to complete the heating cycle and initiate the cooling phase, the sample was transferred back to the 40°C bath.



Figure 4.17a:  
TA Sample



Figure 4.17b: TA Experimental Rig

It can be noted that a key factor to the experimental accuracy was the mixing or separation of the microPCM capsules. As a result, important experimental parameters other than the microPCM particle density and separation characteristics, were the duration of test and quantity of sample. The longer the duration of experiment the more time the particles had to separate. Using a smaller quantity of sample (25g), the test took less time and could be done before stratification occurred. One drawback of using this smaller sample quantity was that the constant temperature region was less apparent.

Trial and error was used to achieve a balance between sample quantity and test duration and suggested the use of a sample quantity of 100g and test duration of 6mins. In the temperature-time diagram, as the sample undergoes phase transition, this may be determined by observing the temperature as practically constant over a duration of time (this temperature corresponds to the

melting/freezing temperatures). Care was taken to ensure that the same sample quantity was the same for each test.

**4.6.5 TA Experimental Observations** Figures 4.18a and 4.18b show typical heating curves for the 50°C and 61°C samples respectively, obtained during TA measurements with 20%-40% microPCM slurries and for pure water. Figures 4.19a and 4.19b show the cooling curves for the respective PCSs (10% microPCM slurry was ignored in the TA test as the energy transportation was slight in comparison to water determined in the previous DSC tests). As seen in the figure, the microPCM did not show the long and flat freezing/melting plateaus, as expected. However, it could be observed that the slurries exhibited narrow freeze/melting ranges, which signified a phase change transition.

Supercooling was not clearly shown in the figure 4.19 as seen in the DSC tests. Compared with water, the slurries had more energy transport as they maintained a larger temperature difference in both the heating and cooling curves (as the rate of heat transfer depends on the temperature difference between the system and the surroundings). The higher the concentration of microPCM, the greater the temperature difference between the PCS and the bath, and the greater rate of heat transfer.

In terms of energy storage, the microPCM slurry also provided a higher heat capacity compared with water. This can be seen in figure 4.18, where the curves for the slurries lagged behind that of the water. This implies that they have a higher heat capacity, which took longer time to transfer all the heat. For example, compared with water, the 30% microPCM slurry took approximately one minute longer to reach 60°C as its temperature reached the surrounding bath temperatures (it was seen that the time period was longer at the melt/freezing temperature corresponding to the phase transition).

This seems very attractive since we can store more heat in the microPCM slurry within a smaller space and can bridge the time gap between energy requirements and energy use. It also has the unique advantage of maintaining a larger temperature difference in heat exchange components and hence could improve overall heat transfer.

TA Temperature Variations of MicroPCMs Under Heating

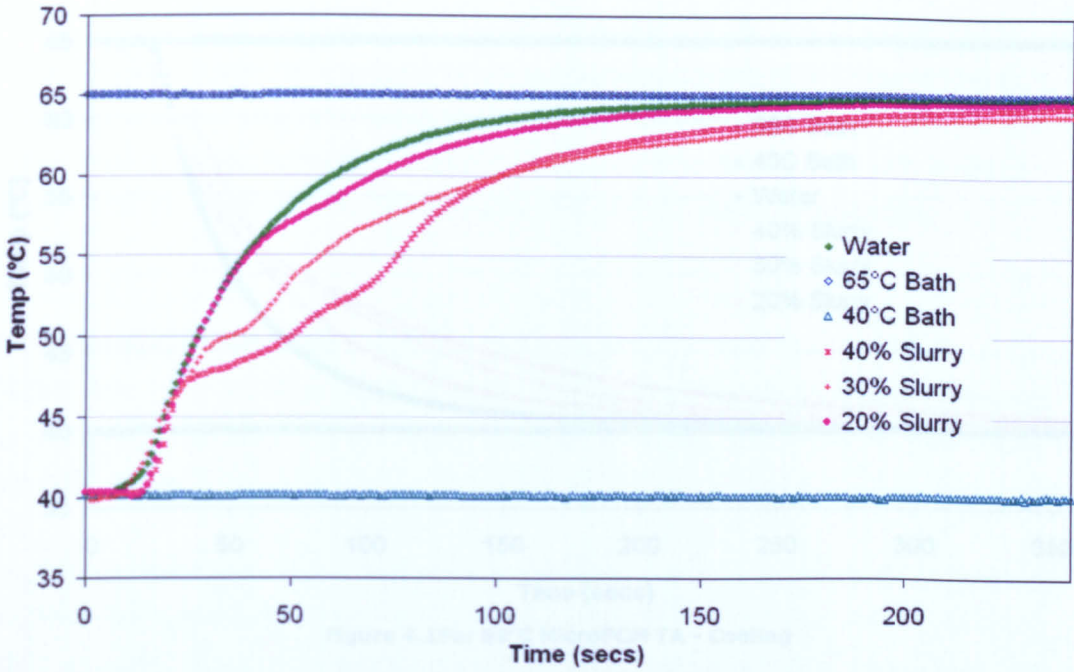


Figure 4.18a: 50°C MicroPCM TA - Heating

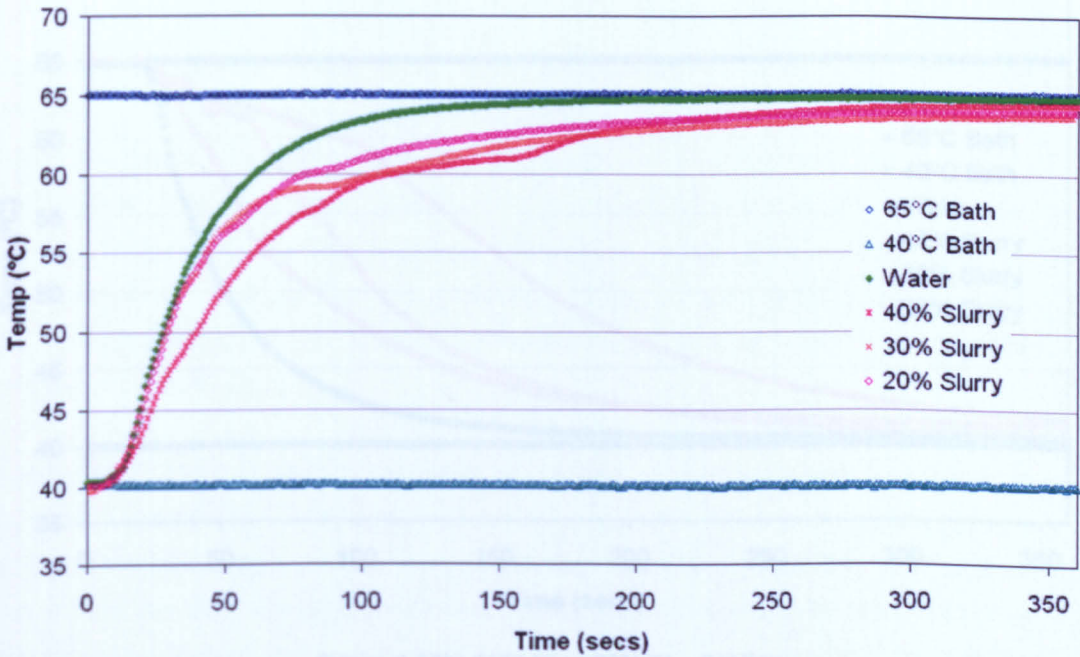


Figure 4.18b: 61°C MicroPCM TA - Heating

## TA Temperature Variation of MicroPCMs Under Cooling

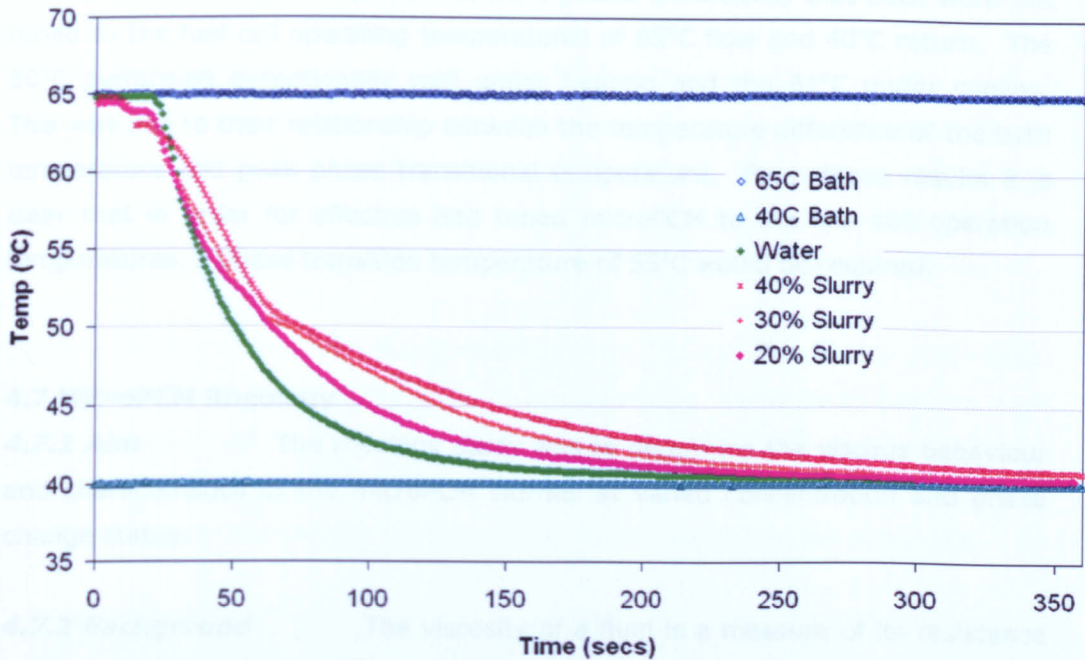


Figure 4.19a: 50°C MicroPCM TA - Cooling

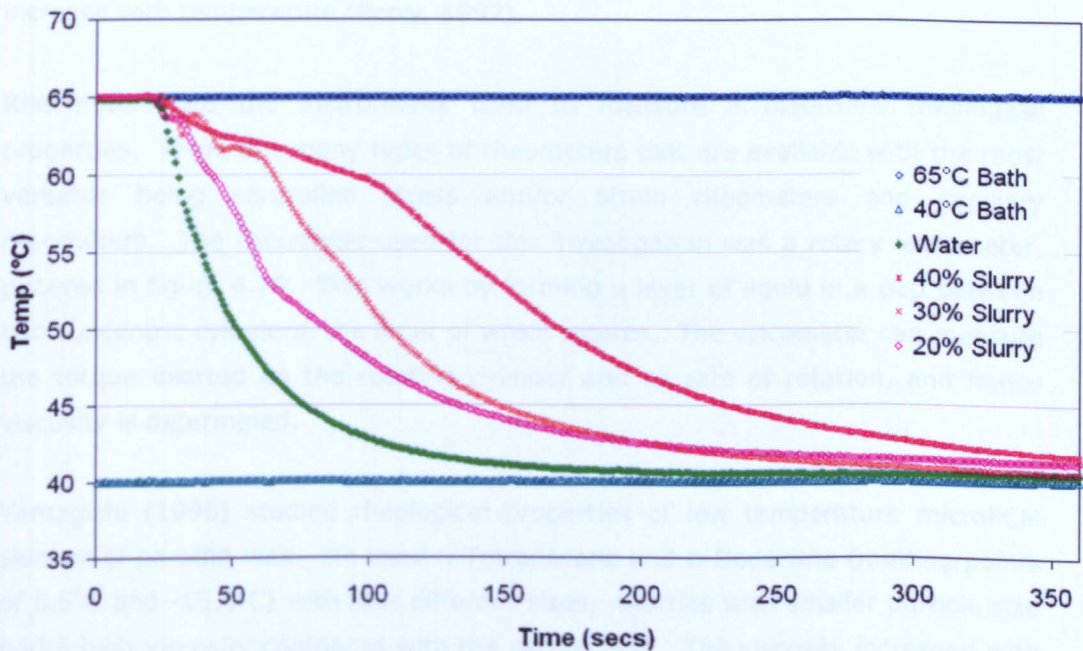


Figure 4.19b: 61°C MicroPCM TA - Cooling

**4.6.6 TA Summary** It was clear from the TA results for the two micro PCMs under investigation (61°C and 50°C phase transitions) that both were not tuned to the fuel cell operating temperatures of 65°C flow and 40°C return. The 50°C performed exceptionally well under heating and the 61°C under cooling. This was due to their relationship between the temperature difference of the bath temperature and peak phase transitional temperature. From these results it is clear that in order for effective and tuned microPCM to the fuel cell operation temperatures, a phase transition temperature of 55°C would be required.

## **4.7 MicroPCM Rheology**

**4.7.1 Aim** The rheology study was to determine the viscous behaviour and characteristics of the microPCM slurries at varied concentration and phase change states.

**4.7.2 Background** The viscosity of a fluid is a measure of its resistance to flow represented by a ratio of shear stress to shear rate. It is widely observed that viscosity tends to be a strong function of temperature. It is shown that the viscosities of liquid decrease with temperature, whilst the viscosities of gases increase with temperature (Perry, 1997).

Rheometers are the instruments used to measure a material's rheological properties. There are many types of rheometers that are available with the most versatile being controlled stress and/or strain rheometers and capillary rheometers. The rheometer used for this investigation was a rotary viscometer, pictured in figure 4.20. This works by forming a layer of liquid in a gap between two concentric cylinders, the inner of which rotates. The viscometer can measure the torque exerted on the rotating cylinder and its rate of rotation, and hence viscosity is determined.

Yamagishi (1996) studied rheological properties of low temperature microPCM slurries of paraffin wax. He used n-Tetradecane and n-Dodecane (melting points of 5.5°C and -15.5°C) with four different sizes. Slurries with smaller particle size had a high viscosity compared with the carrier fluid. The viscosity increased with the decrease in the shear rate i.e. non-Newtonian behaviour. The microPCMs used in this study had a similar range of particle size, 5-40µm. It was also observed (similar to the observations in section 4.2) that MicroPCM slurries had a tendency to get sticky when left stationary and started to stratify. Yamagishi also

stated that, in contrast, the slurries were easily moved under homogeneity (low viscosity in high shear).

**4.7.3 Methodology** Viscosities of the microPCM slurry were measured using a Bohlin Visco 88 BV viscometer from the School of Materials, University of Nottingham. This device was a rotational viscometer and is pictured in figure 4.19. All three samples (35°C, 55°C and 61°C) were measured at the range of concentrations, 10%, 20%, 30% and 40% slurry (wt.% of microPCM with water).

Tests were carried out with the temperatures of the slurry at above and below the melting temperature of the paraffin wax samples. These temperatures were 25°C to ensure solid state and at 75°C for liquid state. This was to study the effect of the suspended particles with liquid or solid core. A temperature bath was used to heat and maintain the samples to the desired test temperatures.



Figure 4.20: Images of Bohlin Rotary Viscometer + Test Equipment

**4.7.4 Evaluation of Rheology Results** A baseline study was initially conducted with water, this was used to calibrate the rheometer and set a benchmark for the PCS concentrations under investigation. Figure 4.21 illustrates the relationship between viscosity with increasing shear for the two temperatures investigated. It demonstrates that the viscosity of water reduces with increased temperature.

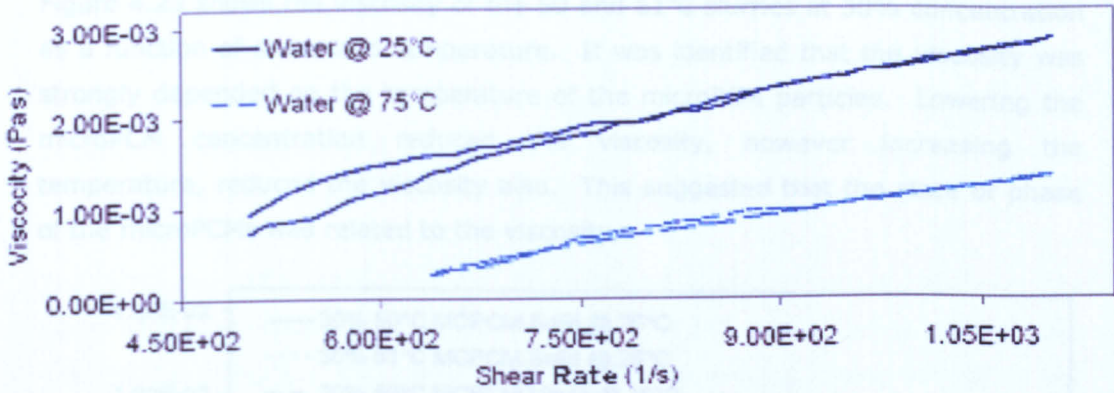


Figure 4.21: Water Viscosity

A trend shown with all the microPCM samples was the increase in viscosity with slurry concentration. Figure 4.22 identifies this trend with the 61°C sample at 25°C. As with the baseline water tests, the highest viscosities were at the lower temperature band when the microPCM was in its solid state. The increase in viscosity with slurry concentration appeared to be exponential, with marginal increase between 10%-20% concentrations and increasing exponentially with the 30% and 40% concentrations. Figure 4.22 indicates that the 30% slurry was 52% more viscous than the 20% slurry. The 40% slurry was 261% greater than the 30% slurry and was out of the scale of figure 4.22.

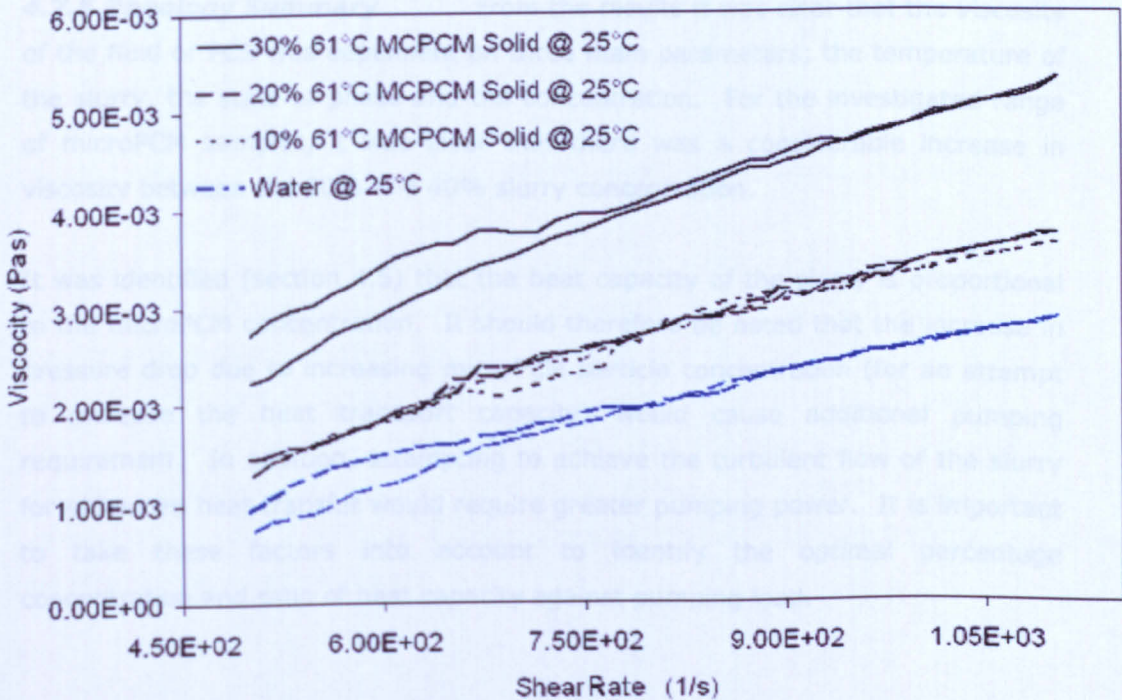


Figure 4.22: 61°C MicroPCM Slurry Viscosity

Figure 4.23 shows the viscosity of the 50 and 61°C slurries at 30% concentration as a function of shear and temperature. It was identified that the viscosity was strongly depended on the temperature of the microPCM particles. Lowering the microPCM concentration reduced the viscosity, however increasing the temperature, reduced the viscosity also. This suggested that the state of phase of the microPCMs was related to the viscosity.

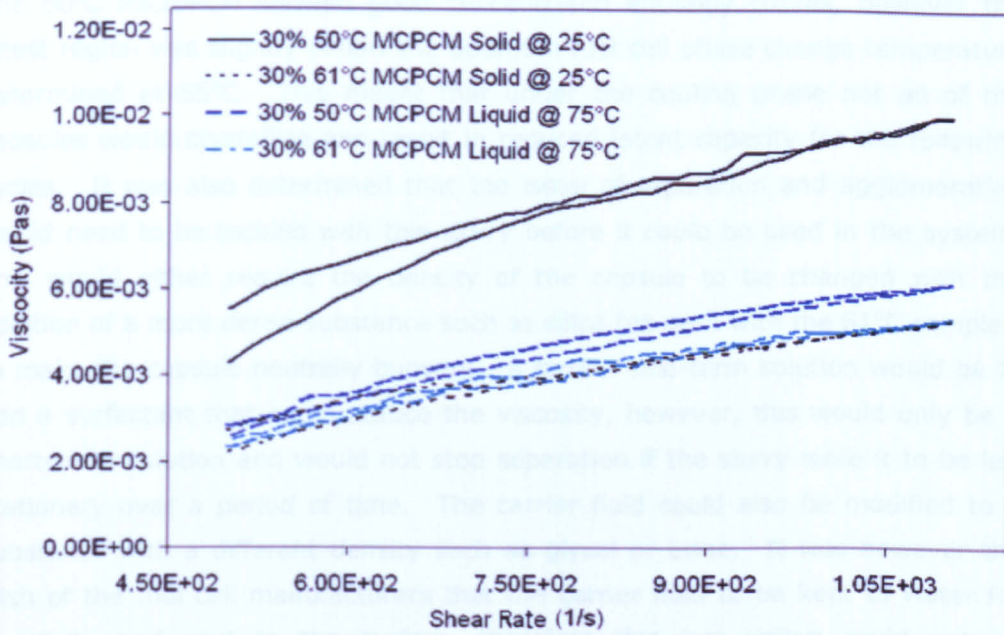


Figure 4.23: 61°C MicroPCM Slurry Viscosity

#### 4.7.5 Rheology Summary

From the results it was clear that the viscosity of the fluid or PCS was dependent on three main parameters; the temperature of the slurry, the state of phase and the concentration. For the investigated range of microPCM samples, it was clear that there was a considerable increase in viscosity between the 30% and 40% slurry concentration.

It was identified (section 4.5) that the heat capacity of the slurry is proportional to the microPCM concentration. It should therefore be noted that the increase in pressure drop due to increasing microPCM particle concentration (for an attempt to increase the heat transport capacity) would cause additional pumping requirement. In addition, attempting to achieve the turbulent flow of the slurry for enhanced heat transfer would require greater pumping power. It is important to take these factors into account to identify the optimal percentage concentration and ratio of heat capacity against pumping load.

#### **4.8 Concluding Remarks**

This chapter has given an overview of the thermo-physical tests undertaken on some commercially available microPCMs. This established the operating principles of the microPCMs and enhanced the understanding in order to establish criteria for developing a microPCM for the fuel cell.

The 50°C microPCM showed good concentrated enthalpy curves, however the latest region was slightly below the optimum fuel cell phase change temperature determined at 55°C. This meant that under the cooling phase not all of the capsules would crystallise and result in reduced latent capacity for the following cycles. It was also determined that the issue of separation and agglomeration would need to be tackled with this slurry before it could be used in the system. This would either require the density of the capsule to be changed with the addition of a more dense substance such as silica (as seen with the 61°C sample), to make the capsule neutrally buoyant. A further mid-term solution would be to add a surfactant that could reduce the viscosity, however, this would only be a short-term solution and would not stop separation if the slurry were it to be left stationary over a period of time. The carrier fluid could also be modified to a substance with a different density such as glycol or brine. It was however the wish of the fuel cell manufacturers that the carrier fluid to be kept to water for simplicity and cost to the system, therefore this last option could not be considered.

The use of the 35°C microPCM was eliminated for use with the fuel cell primarily as its phase change temperature was below the range of the fuel cell. Its physical and buoyancy characteristics observed in slurry state were identical to the 50°C microPCM and therefore faced the same physical stability issues.

The 61°C microPCM proved to be significant in this investigation and showed very positive thermal properties, rheology and neutral buoyancy characteristics. Its capacity to remain neutrally buoyant was the one key factor that none of the other slurries were capable of, and would be essential in the fuel cell system. As this sample was specially manufactured and was only available in this one off sample, no more was available for further testing. Chapters 6.0, covers the development work to produce a microPCM that had similar characteristics based on this 61°C microPCM sample.

From the tests, it is clear that the investigated microPCS is advantageous to applications where only a small temperature difference can be used, and therefore particularly attractive to the fuel cell. In an application with a high  $\Delta T$ , water as a very cheap heat transfer fluid has clear advantages in comparison to the microPCS. The PCSs do, however, promise advantages particularly in low temperature applications, in combination with water where only a small  $\Delta T$  is permitted.

The approximately isothermal temperature profile can reduce the  $dT$  across the fuel cell and improve its performance. It also has the potential to save electricity through reduced pumping loads, and as a consequence, reduced system size and component costs of the fuel cell system.

For the PCS and integration with the fuel cell, from these tests, it may be seen that the pressure drop depends on the concentration and also the phase state of the slurry (at certain flow rates). The heat capacity of the slurry is proportional to the microPCM concentration. It should therefore be noted that the increase in pressure drop due to increasing microPCM particles (in an attempt to increase the heat transport capacity for example) would cause additional pumping requirement. In addition, attempting to achieve the turbulent flow of the slurry for enhanced heat transfer would require greater pumping power. It is important to take these factors into account for the best suited percentage concentration and ratio of heat capacity against pumping load.

## **Chapter 5: An Investigation of MicroPCM Slurry in a Closed Loop Thermal System**

### **5.0 Introduction**

From chapter 4, it could be seen that the addition of microPCM can significantly enhance the thermal capacity of the working fluid with the inclusion of latent heat. This chapter studies the feasibility of using a microPCM slurry containing the phase change material mixed with water as the carrier fluid in a closed loop system. The 35°C microPCM, that was studied in chapter 4, was used in this test. Although this material had a phase change temperature well below the optimum fuel cell temperature, it was the only material that was readily available in the quantity required and was low in cost.

The effects of repeated use of liquid-solid phase change particles upon melting and solidifying in a PCS were studied using a small scale rig with a closed loop circuit. The primary parameters for the investigation were the degree of slurry concentration and flow rate. The heat transportation of the slurry was measured in order to determine the additional thermal capacity of the fluid in relation to the slurry concentration and flow rate. The practicalities of using such a slurry in the system was further assessed.

### **5.1 Experimental Aim**

The aim of the test was to investigate the thermal and physical operation of the microPCM slurry in a pumped system. The microPCM was commercially available however was not suitable for use with the fuel cell, 55°C, as the phase change temperature was too low, at 35°C. It was selected however, to provide a better understanding of the practicalities of using the microPCM as a slurry and further analyse and quantify its thermal capabilities. The point of interest was the comparison between the use of the sensible and latent heat compared to a single-phase sensible fluid, namely water. A further objective was to determine any issues associated with the use of a PCS that may have implications on its suitability for use in the fuel cell system.

Recently, more papers have been published on theoretical or experimental approaches to clarify the merits of this medium. These studies have focused more

on heat capacity and heat transfer coefficients. Although they indicate promising applications, they are limited in scope. The data necessary for engineering design of a thermal-energy system using microPCM slurry is still not yet available in literature. The major challenge is to apply liquid-solid microPCM to a convectional pumped heat transfer loop and overcome practical implications such as durability, clogging, component suitability and lifetime.

This chapter provides some further background of microPCM slurry operation and theory. The experimental apparatus and methodology has been explained and was developed in order to answer the hypothesis. The test rig was verified using the Dittus+Boelter heat transfer equation. Results and conclusions were made from the results achieved from the test rig.

## **5.2 Slurry Performance:**

When the PCMs are properly selected and encapsulated, it is possible to achieve remarkable improvements in the heat storage and the transport capability of the fluid slurry. Equation [5.1] is the familiar relation describing the rate of heat storage within a material as its temperature increases.

$$\dot{Q} = \dot{m}C_p\Delta T \quad [5.1]$$

The effective thermal capacity of a two-component material is therefore proportional to the ratio of the rate of heat transfer and its temperature change, as described by equation [5.2].

$$C_{pe} = \dot{Q} / \dot{m} \cdot \Delta T \quad [5.2]$$

Expressing the heat transfer sum of the sensible and latent components, the effective heat capacity  $C_{pe}$  becomes;

$$C_{pe} = \bar{C}_p + \frac{xf\lambda}{\Delta T} \quad [5.3]$$

Where  $\bar{C}_{pe}$  is the weighted average of the components,  $x$  the fraction of capsules undergoing phase change,  $f$  the capsule loading fraction and  $\lambda$ , the latent heat capacity.

It can be seen that the latent capacity is comparably very large at small temperature differences ( $\Delta T$ ), but the contribution it makes to the weighted average heat capacity decreases as  $\Delta T$  grows.

The Nusselt number,  $N_u$ , and convective heat transfer coefficient,  $h$  are related to the Prandtl number,  $Pr$ , and heat capacity, as shown in equation [5.4] (Rogers, 1967) for laminar flow.

$$N_u = \frac{hl}{k_f} = f \left[ (N_{Nu} \cdot N_{Pr})^{1/3} \right] \quad [5.4]$$

Where  $Pr$ , is the Prandtl number ( $Pr = \mu C_p / k_f$ ),  $\mu$ , is the dynamic viscosity,  $k_f$ , is the thermal conductivity of the fluid,  $l$ , the length of test section and  $Re$ , the Reynolds number. It is therefore expected that  $h$  will be enhanced with an enhancement of  $C_p$ .

### **5.3 Review of Previous MicroPCM Slurry Closed Loop Experimental Work**

Microencapsulation of phase change materials allows the continual separation of the melted core material from the circulating carrier fluid, thus avoiding the collection or deposition of the core material in undesirable areas of the system. During early experiments for NASA and USAF, Colvin and Mulligan in 1986, 1987, demonstrated that the enhancement of heat capacity with their PCM slurries (PCS) could significantly exceed ten times that of water and that these significantly higher heat transfer rates could also be obtained under practically isothermal conditions.

Key parameters affecting the heat storage performance of the microPCM slurry include the bulk Stefan number and the slurry concentration. The bulk Stephan number may be defined as the ratio of sensible heat capacity of the suspension to its latent heat capacity. Charunyakorn (1991) noted that the bulk Stefan number significantly dominates the heat transfer performance of the microPCM slurry. The Nusselt number can be considerably improved by 1.5-2.5 times through reducing the

bulk Stefan number, which corresponds to the increase in latent heat of the slurry. The effect of increasing the concentration is two-fold; it decreases the Stefan number and raises the conductivity enhancement factor.

Goel (1994) also showed that the bulk Stefan number is the most dominant parameter. His results showed that up to 50% reduction in the wall temperature rise can be obtained by using the microPCM suspension in place of a single-phase fluid. He concluded that for the best results, the bulk Stefan number should be maintained low ( $Ste \leq 1.0$ ). This could be achieved either by selection of the PCM, such that its ratio of latent heat to sensible heat capacity is high, by increasing the concentration of the microPCM or by reducing the pipe radius. The concentration does play an indirect role in heat transfer through the bulk Stephan number.

Choi (1994) studied the effects of PCM-water slurry on the convective heat transfer coefficient in a turbulent flow and suggested that the effect of latent heat on the local heat transfer coefficients may also depend upon the slurry flow structure. Yamagishi (1999) investigated the effect of turbulent and laminar slurry flows on local heat transfer coefficients. His results interestingly showed that when flows of microPCM slurry are at approximately the same mean flow velocity, the flow of higher particle fraction of 15% has a lower heat transfer augmentation than a 7% microPCM slurry. This was because the flow of 7% slurry had a higher Reynolds number than that of the 15% slurry. However, if the particle volume fraction is the same for both laminar and turbulent flows, the heat transfer in the turbulent flow is more effective than that in the laminar flow. The heat transfer augmentation associated with phase change depended not only on the fraction of solid particles in the slurry but upon the degree of turbulence.

The effect of pipe-to-particle diameter ratio and degree of homogeneity of the suspension did not have significant effect on the heat transfer characteristics of the phase change slurry (Goel, 1994). Two other parameters that could be negligible are the particle-to-fluid thermal conductivity ratio and modified particle Peclet number (Charunyakorn, 1991).

## 5.4 Experimental Investigation of a Small Scale Closed Loop System

### 5.4.1 Microcapsules and Slurry Physical Properties

The MicroPCM used for this study was a paraffin wax of *n*-eicosane with a melting temperature of 35°C. The paraffin wax was encapsulated in a capsule of 15-40microns in diameter. Water was used as the carrier fluid with a 10%-40% wt concentration of microPCM. The properties are shown in the table 5.1. Figures 5.1 and 5.2 depict the 35°C microPCM sample mixed with water and under ESEM imaging, respectively.

Material		Density $\text{kg}\cdot\text{m}^{-3}$	Specific Heat $\text{J}/\text{kg}\cdot^{\circ}\text{C}$	Thermal Conductivity $\text{W}/\text{m}\cdot^{\circ}\text{C}$	Latent Heat $\text{kJ}\cdot\text{kg}^{-1}$	Viscosity $\text{mPa}\cdot\text{s}$ @ $25^{\circ}\text{C}$
n-eicosane (35°C)	(Solid)	850	1,800	0.340	223	-
	(liquid)	780	2,200	0.150	-	-
Melamine-formaldehyde Shell		1,490	1,670	0.420	-	-
Water (@ 25°C)		997	4,180	0.610	-	0.87
MicroPCM Particle	(Solid)	1,000	1,754	0.310	167	-
	(liquid)	936	2,014	0.144	-	-
MicroPCM Slurry	0.1	998	4,009	0.597	14.8	1.18
Fraction	0.2	998	3,680	0.541	30.3	4.26
	0.3	989	3,489	0.483	43.6	10.4
	0.4	982	3,279	0.451	62.1	16.1

Table 5.1: Slurry Material Thermophysical Properties (Outlast, 2004)



Figure 5.1: 35°C Slurry

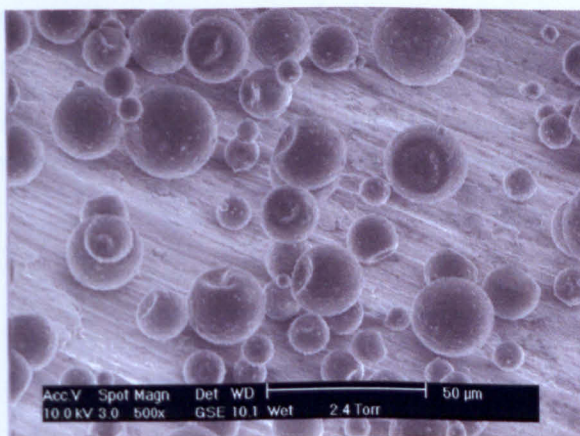


Figure 5.2: 35°C n-eicosane Microscopy

### 5.4.2 Apparatus and Methodology

This study employed a small-scale rig with a closed loop circuit, see Figure 5.3b, rather than a one-way flow rig, see Figure 5.3a, as used in most previous studies to date. This is to circulate the slurry through; both a heating test section and a cooling section (as used in real system applications), and back to a main reservoir. The slurry was thermally investigated and the practical effects of the repeated circulation of the slurry with liquid-solid phase change particles upon melting and solidification were investigated.

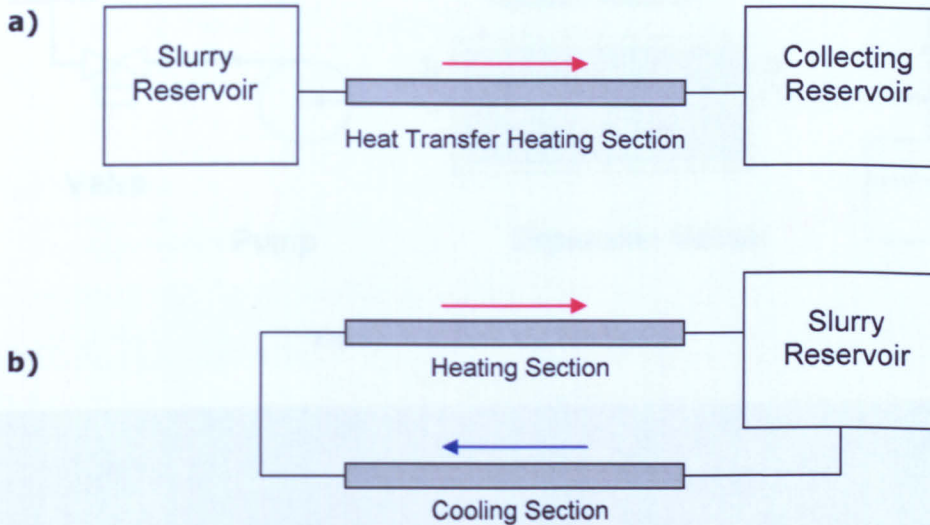


Figure 5.3: a) One-way-flow Rig b) Closed Loop Rig.

Figure 5.4 and 5.5 show a schematic diagram and an image of the experimental apparatus of the system. The thermal loop comprises of a heating section that is charged from an electric heating element, a fan assisted cooling section, a slurry reservoir, a pump with power meter, breather valve, expansion vessel, tubing, a voltmeter, ammeter and AC power supply.

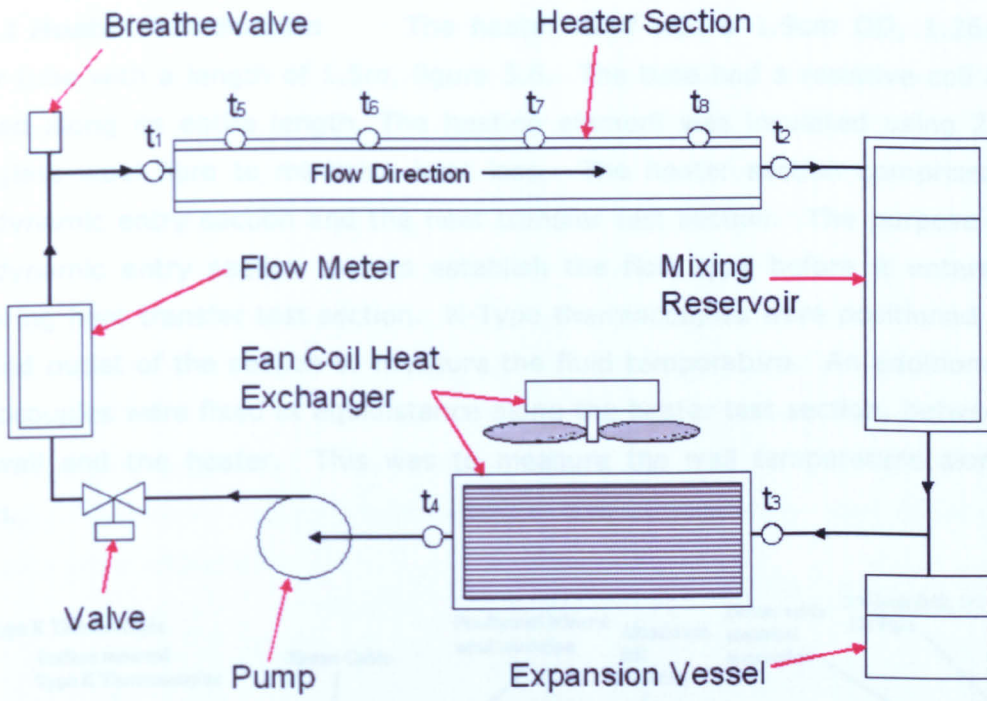


Figure 5.4: Test Rig Schematic

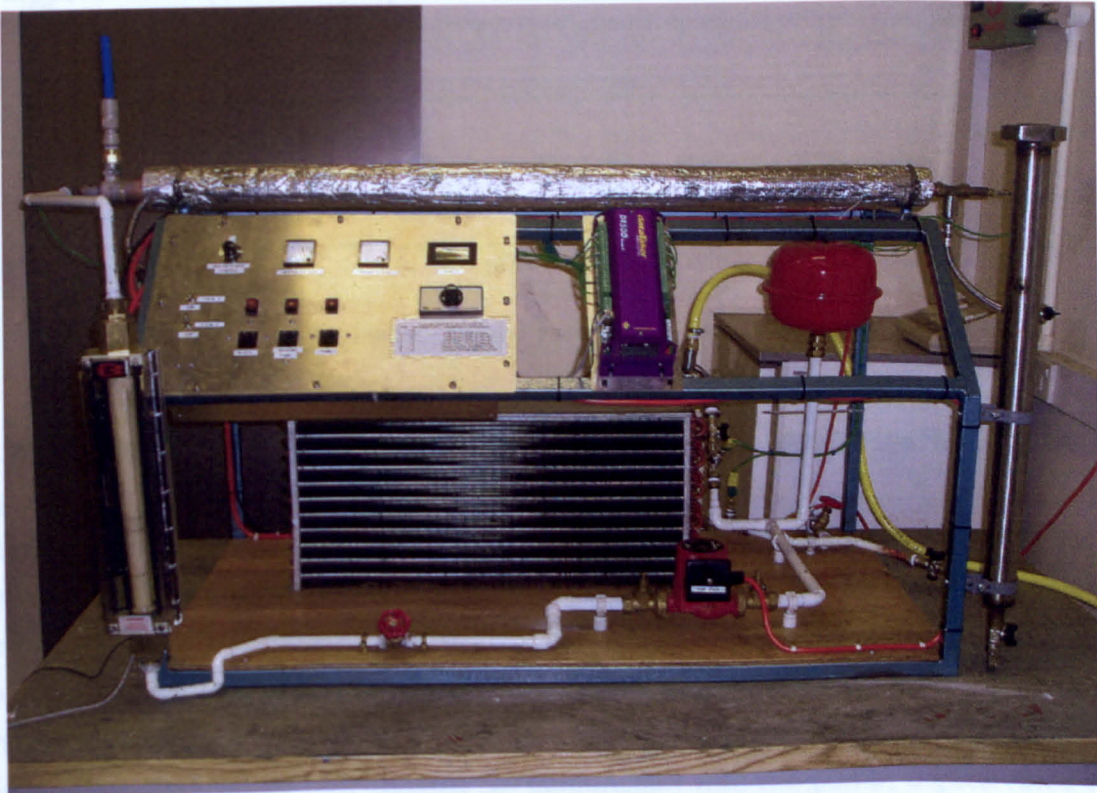


Figure 5.5: Test Rig Image

**5.4.2.1 Heater Test Section** The heater itself was a 1.9cm OD, 1.26cm ID copper tube with a length of 1.5m, figure 5.6. The tube had a resistive coil heater wrapped along its entire length. The heating element was insulated using 2.54cm thick glass wool fibre to minimise heat loss. The heater section comprised of a hydrodynamic entry section and the heat transfer test section. The purpose of the hydrodynamic entry section was to establish the flow type before it entered the measuring heat transfer test section. K-Type thermocouples were positioned at the inlet and outlet of the section to measure the fluid temperature. An additional four thermocouples were fixed at equidistance along the heater test section, between the tube wall and the heater. This was to measure the wall temperature along the section.

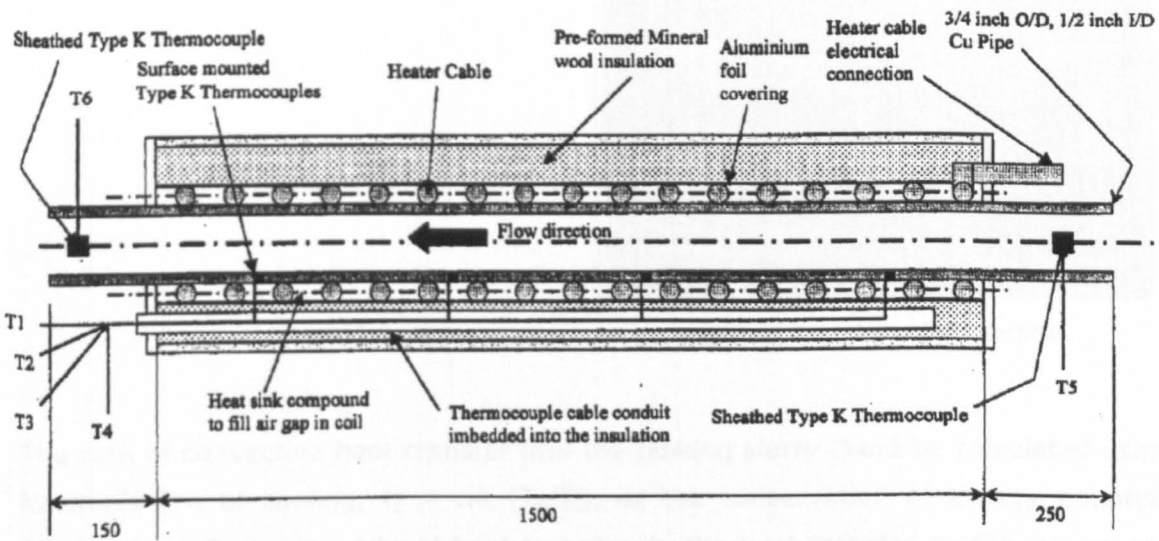


Figure 5.6: Heater Test Section (Hard, 2003)

**5.4.2.2 Pump** Various pumps were considered for use in the system, this ranged from standard commercially available and economically priced pumps to more specialist pumps. These specialist pumps included progressive cavity and diaphragm pumps that would have reduced shear exerted on the slurry in order to enhance slurry lifetime. For this investigative study, a centrifugal pump was used in order to expose the capsules to a relatively harsh pumping regime to observe how they coped under this level of shear. The pump had three speed settings that were used to set the desired flow ranges. In conjunction with the pump, a gate valve was used to throttle the flow and fine-tune the flow rate.

**5.4.2.3 Other Components** to cool the slurry and complete the thermal loop, a fan coil heat exchanger unit was used. The mixing reservoir was situated after the heating section and supplied the cooling section with the slurry. The purpose of the reservoir was to aid mixing the slurry to provide a consistent concentration of microPCM. It also aided the loading process of the microPCM slurry to the system. Other components included a breath valve to eliminate air in the system, an expansion vessel to account for variations in pressure. Further valves were used to isolate sections of the system for filling and mixing the slurry and for cleaning.

**5.4.2.4 Data Acquisition** A Datalogger, figure 5.7, model DT500 was used to monitor the thermocouple outputs and used to determine that steady state conditions were established.



Figure 5.7: Image of the DT500

The rate of convective heat transfer into the flowing slurry could be calculated using Newton's law of cooling,  $Q = hA (T_s - T_f)$ , or the conservation of energy equation [5.1], where  $Q$  was the rate of heat transfer,  $h$ , the heat transfer coefficient,  $m$ , the mass flowrate,  $C_p$ , the specific heat,  $A$ , the surface area and  $T$ , temperature.

In the case of pure water, the local bulk mean temperature was easily estimated from a linear temperature rise along the heater test section under the condition of uniform heat flux. When no phase change was involved in the slurry, the temperature at any location in the test section can be readily calculated. However, when a phase change did occur, the temperature rise across the melting temperature of n-eicosane was not linear because of the latent heat (neither the local heat transfer coefficient, nor the thermal capacity was constant along the flow direction).

The experiment was conducted to monitor the rate of heat transfer into the system provided by the heater. The bulk mean temperature of the fluid or slurry was controlled to 35°C, which corresponded to the peak melting temperature of the PCM. For the first test, the flow rate was varied to measure the relationship between flow rate and the  $\Delta T$  across the heating sections. A second test was undertaken by varying the power input from the heater to maintain the constant  $\Delta T$ 's over the range of flow rates. For repeatability this was undertaken twice using water to establish baseline conditions. The test was repeated using the slurry at the range of wt concentration of 10%, 20%, 30% and 40%.

Notably, the experiment was carried out under steady state conditions, in which the temperature through the controlled system did not change with time. In order to ensure steady state the system conditions were closely monitored with a minimum settling period of 5 minutes established between setting the conditions and taking readings.

#### **5.4.3 Slurry Tuning:**

The bulk mean temperature of 35°C for the slurry through the heat transfer section was determined by the peak melt temperature from the DSC analysis. This temperature was very important in order to tune the slurry to the system.

Figure 5.8, distinguishes between the conditions for flow through a closed loop circuit. Figure 5.8a, and 5.8d, show the temperature cycling of a circulating loop for a microPCM slurry operating at either above or below the critical melting point of operation. Figure 5.8b, shows a balanced microPCM operating around the melting temperature of the core material. Whilst most of the heat transport is within the latent heat particles, some of the transported heat is sensible and there is a finite thermal gradient across the system. Figure 5.8c, illustrates an ideal or optimal "tuned" state where the temperature gradient within the fluid is practically zero. At this level, all of the heat transport is via the latent energy storage within the microPCMs, the temperature throughout the closed loop is essentially isothermal, and the fluid exhibits its maximum thermal capacitance. A US patent was awarded to the TRDC regarding this operation of microPCM slurry coolant (Colvin and Mulligan, 1990).

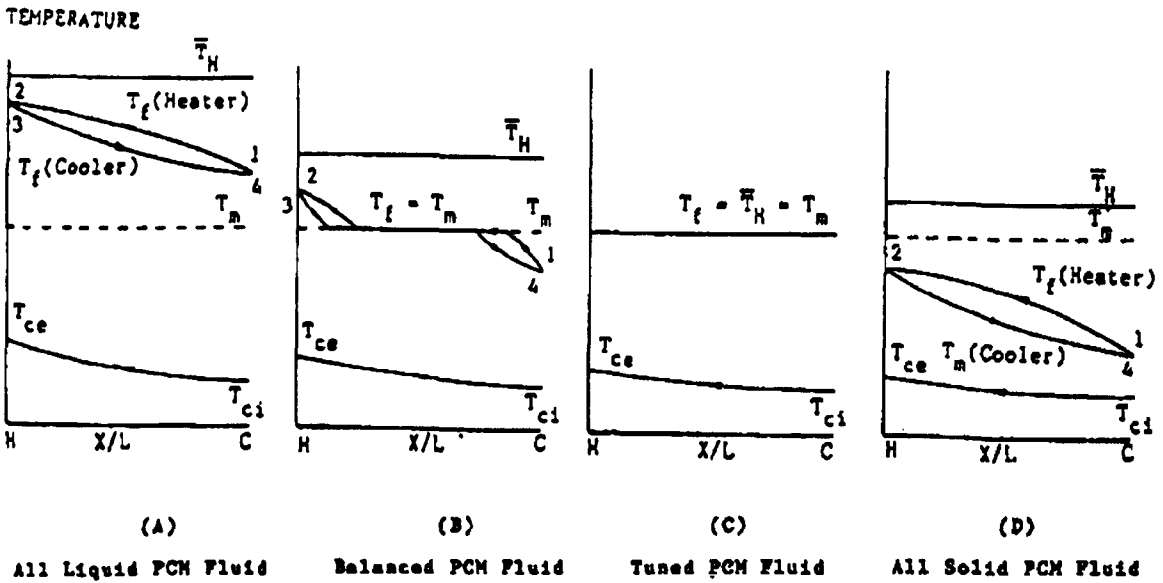


Figure 5.8: Heat Exchanger Temperature Profiles for a MicroPCM Slurry in a Closed Loop System (Colvin, 1993)

Figure 5.8, highlights the importance of a tuned system. If the system operational temperatures are outside that of the phase change range then the slurry may only operate in the sensible zone which in turn is not as effective as just using water alone and has additional pumping requirement.

#### 5.4.4 Equipment Calibration + Experimental Uncertainties:

Errors are inherent in all measurement. Even under ideal conditions, repeated measurements of reference standard, such as a standard mass placed on a scale, will give a slightly different instrument reading. Thus, the accuracy of the device used in the present study was calibrated to minimise these errors. Thermocouples were calibrated against the known temperatures of ice and boiling point of water. The bias error (Miller, 1989) for the devices can be calculated as follows;

$$B = \frac{I_i - I_t}{I_t} \cdot 100 \quad [5.5]$$

Where B, is the Bias error,  $I_i$ , the Instrument actual reading and  $I_t$ , the True value.

With a positive bias, the instrument is said to be reading high, and with a negative bias reading low. In the experiment, the operating temperature range was 10-75°C,

and the average error of calibration of any thermocouple was found to be  $\pm 0.251^{\circ}\text{C}$ . The figure falls well within the limit error from the manufacturer's specifications of  $\pm 0.375^{\circ}\text{C}$ .

The flowmeter was calibrated using a static weight method to establish the relationship between the meter indicated flow rate and the measured true rate. The working fluid was diverted into the collecting tank for a fixed period. It was then measured with the fluid static in the tank. The net mass of fluid was divided by the measured time period to obtain the true mass flow rate. The average error was determined to be  $-4.5\%$ , which agreed well with the manufacturer's claim of  $\pm 7\%$ .

As the cooling element of the system was a fan coil rather than for example, chilled water. The rig was susceptible to instability due to room temperature. The laboratory was heated via a gas heater that was set to maintain a temperature of  $23^{\circ}\text{C}$ . It can be seen from figure 5.9, that the room temperature was stable at  $23^{\circ}\text{C}$ , however, there were periodic injections of heat from the heater. It was therefore necessary to ensure that whenever steady state measurements and recordings were taken, that the heater was not in operation.

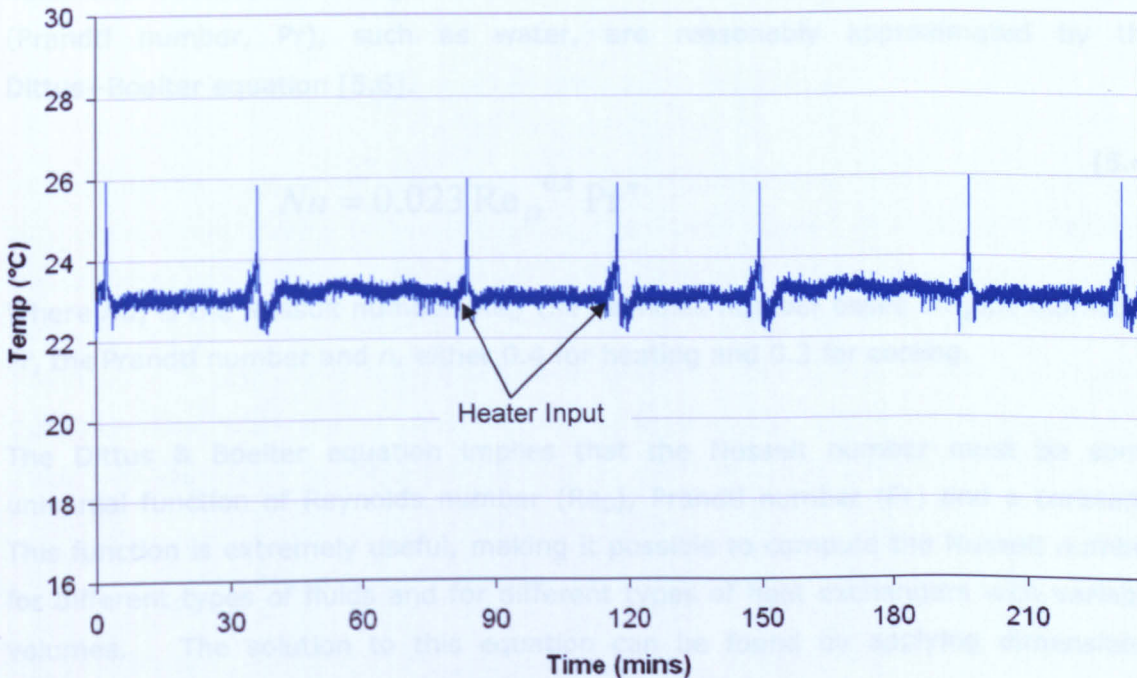


Figure 5.9: Laboratory Room Temperature

To validate the experimental procedures and to establish a baseline for bulk fluid temperatures and heat transfer coefficients, a comparison between pure water and slurry were made. Water tests were repeatedly conducted over the flow rate range of 2-6 lpm.

To ensure that the baseline water tests were providing significant and accurate results, the data were used to verify the heat transfer coefficient equation of Dittus+Boelter (Dittus, 1930).

### **5.5 Slurry Test Rig Verification with Dittus+Boelter**

This section verifies the Slurry Rig with the Dittus+Boelter Equation for heat transfer coefficient. This equation was used as a base methodology for ensuring that the test equipment gave results that agreed with this well-established general equation.

This study considered the case of hydro-dynamically and thermally fully developed laminar and turbulent flows in a pipe of constant wall heat flux to illustrate potential advantages of microPCM slurries over an alternative coolant, water. The non-dimensional heat transfer coefficient (Nusselt number,  $Nu$ ) for turbulent flows of fluids with moderate and high ratios of momentum diffusivity to thermal diffusivity (Prandtl number,  $Pr$ ), such as water, are reasonably approximated by the Dittus+Boelter equation [5.6].

$$Nu = 0.023 Re_D^{0.8} Pr^n \quad [5.6]$$

Where  $Nu$ , is the Nusselt number,  $Re_D$ , the Reynolds number based on pipe diameter,  $Pr$ , the Prandtl number and  $n$ , either 0.4 for heating and 0.3 for cooling.

The Dittus & Boelter equation implies that the Nusselt number must be some universal function of Reynolds number ( $Re_D$ ), Prandtl number ( $Pr$ ) and a constant. This function is extremely useful, making it possible to compute the Nusselt number for different types of fluids and for different types of heat exchangers with variable volumes. The solution to this equation can be found by applying dimensional analysis;

Considering,

$$\Pi_1 = F(\Pi_2, \Pi_3) \quad [5.7]$$

In this case,

$$\Pi_1 = Nu = \frac{hD}{k} \quad [5.8]$$

$$\Pi_2 = Re_D \quad [5.9]$$

$$\Pi_3 = Pr \quad [5.10]$$

The Dittus+Boelter equation may be defined as follows using the following constants;

$$Nu = A Re_D^a Pr^b \quad [5.11]$$

In order to solve the equation in the experimental apparatus the Prandtl number was kept constant. This could be maintained under a range of experimental conditions if the difference between the inlet and outlet temperatures were maintained. This was initially done keeping a Bulk Mean Fluid Temperature ( $T_{bmf}$ ) of 35°C and repeated with a  $T_{bmf}$  of 30°C. The 35°C test would also correspond to the peak phase change temperature of the slurry to be used in the latter investigation.

Measurements were taken when the test rig achieved steady state. For each flow rate under investigation between 2-6lpm, the heater power was varied in order to maintain the constant  $T_{bmf}$ . Once the  $T_{bmf}$  had stabilised at a set flow rate and power input, it was possible to record the temperature distribution along the heated tube assembly. It was from this relationship between wall temperatures and  $T_{bmf}$  at different flow rates and power settings that was the key interest in order to determine the values to verify the equipment with the Dittus & Boelter equation.

### 5.5.1 Dittus+Boelter Evaluation

Figure 5.10, illustrates the relationship between the logarithmic values of the Reynolds number against the Nusselt number for the two  $T_{bmf}$ s under investigation. From the equations of the lines it is possible to determine and verify the constants (A) and (a) in equation [5.11].

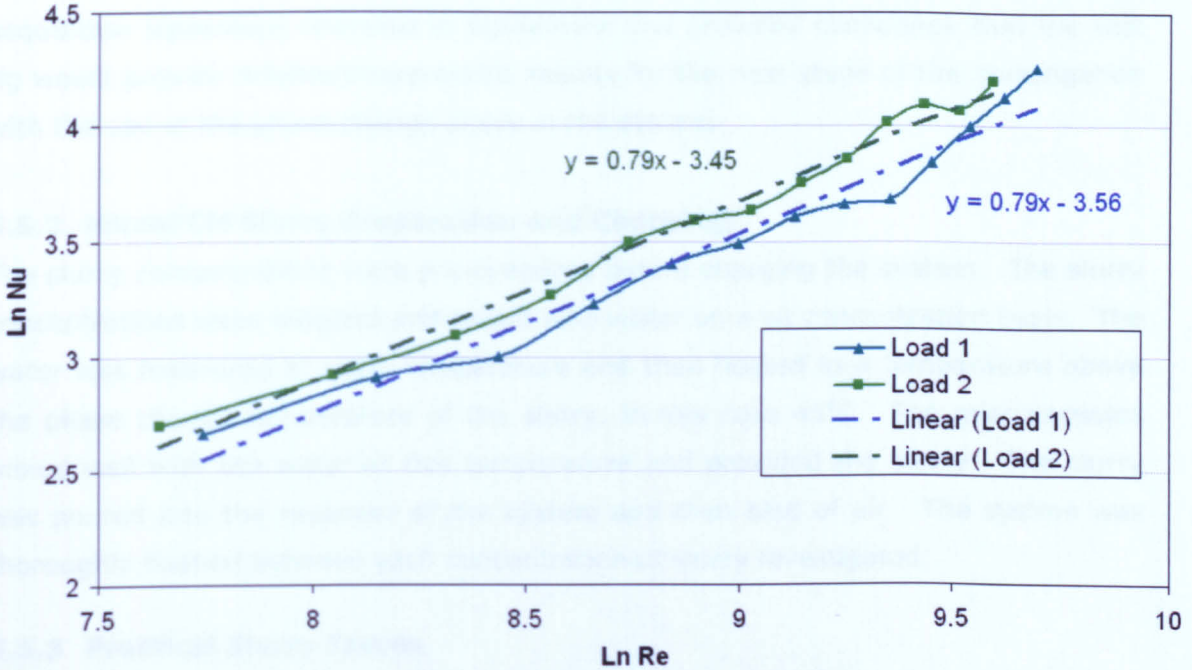


Figure 5.10: Dittus+Boelter Verification

The following table (5.2) summarises the values achieved from this study.

$T_{bmf}$	A	a
Dittus + Boelter Equation	0.023	0.8
30°C	0.035	0.79
35°C	0.037	0.79

Table 5.2: Dittus+Boelter Constants from Equation [5.11]

These results indicate that the test rig did operate in good agreement with the Dittus+Boelter equation. Constant (a) showed extremely good correlation with the Dittus+Boelter constant with an error of 2.25%. Constant (A) for the Re number showed good agreement, however the discrepancies may be put down to the

assumption made that it was independent of the Prandtl number. As the Prandtl number was assumed constant by maintaining the  $T_{b,mf}$ , the Dittus+Boelter equation is a general function of the flow and is most likely the reason for the difference in value of constant A.

The validation of the Dittus+Boelter equation suggested that the rig and data acquisition equipment operated in agreement and provided confidence that the test rig would provide reliable/interpretable results for the next stage of the investigation with the use of the phase change slurry in the system.

### **5.5.2 MicroPCM Slurry Preparation and Charging;**

The slurry concentrations were pre-prepared before charging the system. The slurry concentrations were weighed and mixed with water on a wt concentration basis. The water was measured at room temperature and then heated to a temperature above the phase change temperature of the slurry, in this case 45°C. The microcapsules mixed well with the water at this temperature and provided the slurry. The slurry was poured into the reservoir of the system and then bled of air. The system was thoroughly flushed between each concentration of slurry investigated.

### **5.5.3 Practical Slurry Issues**

Operational problems encountered during the experimental measurements are summarised as follows. In an initial test, there were problems concerned with the use of a variable flow meter. A float in a transparent tapered tube made a very simple flow meter, however after prolonged use the microPCM would stick to it producing more drag and indicating a higher flow rate. The slurries containing higher concentrations of suspended particles had a tendency to build up layers of agglomerate and reduced its accuracy.

As the flow rate was varied, the float rose or dropped along a guide rod. In the case of just using water, there was no sticking and the float easily moved through the full range. It also provided good accuracy with the calibration method described in section 5.5.4. To solve the problem of agglomeration of the float, the flow meter was changed for a larger model with a more substantial float, this solved the agglomeration problem. Only with the 40% slurry, careful observation of the float was required to ensure that it was not stuck and providing accurate results.

## 5.6 Evaluation of Slurry Performance Data

### 5.6.1 Slurry Temperature Difference

Two tests were undertaken to evaluate the performance of the slurry compared with the use of pure water as a thermal fluid. The first test was to evaluate the effect of flow rate and slurry concentration on the temperature difference ( $\Delta T$ ) through the heater test section. The heater input was kept constant at 3kW and the  $\Delta T$  was measured with varied flow rate. Figure 5.11; demonstrates the range of  $\Delta T$ s achieved with different concentrations of the slurry, and compared with water. Between flow rates 2l and 6l, there was a significant reduction in  $\Delta T$  across the section which suggested that with increased slurry concentration, the slurry operated more isothermally.

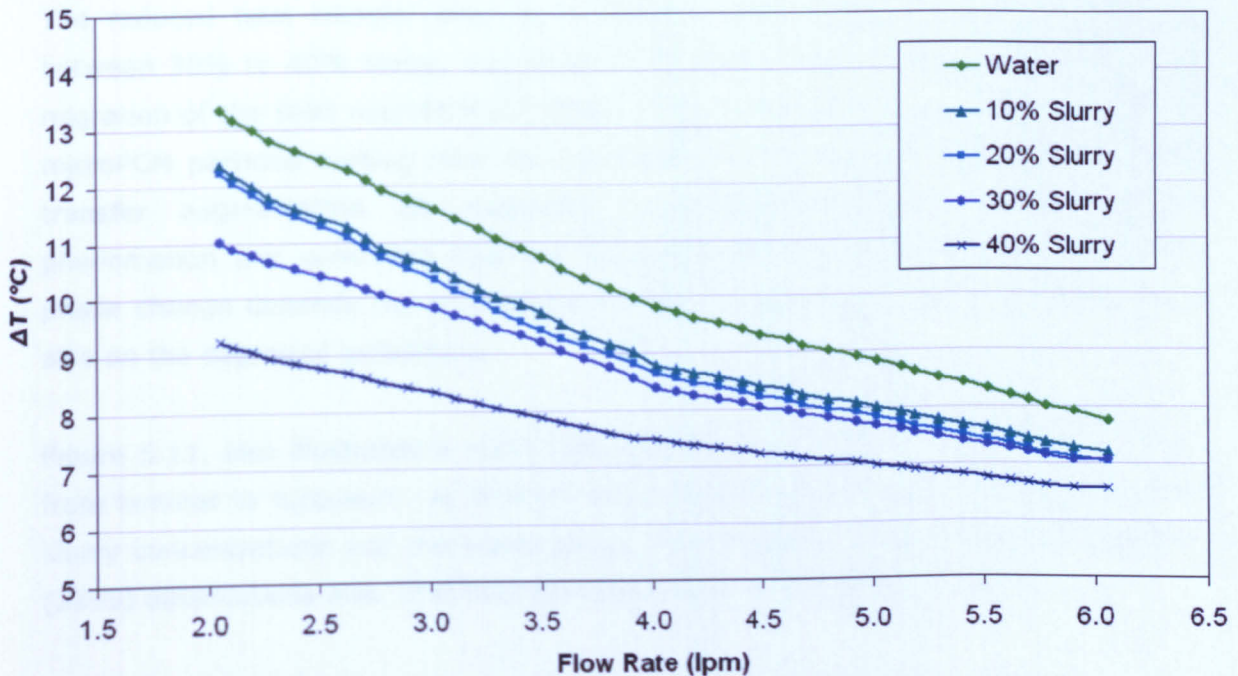


Figure 5.11: Closed Loop – Relationship Between Flowrate and  $\Delta T$  Across Heating Section

With water alone and at high flow rates, 6l, the temperature difference between the outlet and inlet was smaller compared with the smaller flow rates, 2l, as a result from the increased mass flow rate. The use of phase change particles in the form of the slurry was found to decrease the  $\Delta T$  between the outlet and the inlet from the

heat exchanger, because the slurry had greater thermal capacity than the water. When the microPCM was pumped around the system, most of the energy was absorbed by the phase change particles associated with the PCM melting.

There was a large gap between the  $\Delta T$  for 40% slurry in comparison with the 10%, 20% and 30% slurries. This suggested that it was unrelated to the increase in thermal capacity from the additional phase change material and more as a consequence of reduced heat transfer. This was confirmed by the second test to reveal that between 30% and 40%, at 2lpm, there was only a 3.4% increase in thermal input, whilst increasing the concentration from 20% to 30%, there was a 14.6% increase.

The reduced heat transfer may be a result of the sudden increase in viscosity between 30% to 40% slurry, measured in chapter 4, and could impede the radial migration of the solid microPCM particles. This would decrease the number of solid microPCM particles melting near the tube wall, and as a result, decrease the heat transfer augmentation as measured. Yamagishi (1999) reported similar phenomenon and concluded that the heat transfer augmentation associated with phase change depends not only on the fraction of solid particles in the slurry, but also on the degree of turbulence.

Figure 5.11, also illustrated a trend that may be a result of a change in flow type, from laminar to turbulent. At 4l there was a clear change in gradient for all of the slurry concentrations and the water tests. This suggestion aligns with Yamagishi's (1999) observations also, that heat transfer is related to flow formulation.

### **5.6.2 Thermal Input**

The aim of the second test was to investigate the additional thermal storage/transportation capabilities of the microPCM slurry under various concentrations and in comparison to water. This was achieved through maintaining the  $\Delta T$  through the heater section and varying the heater power input with slurry concentration. Steady state was achieved and the resultant heater power for each slurry concentration was measured and used to compare the additional thermal energy required to maintain the  $\Delta T$ . Figure 5.12, illustrates these results.

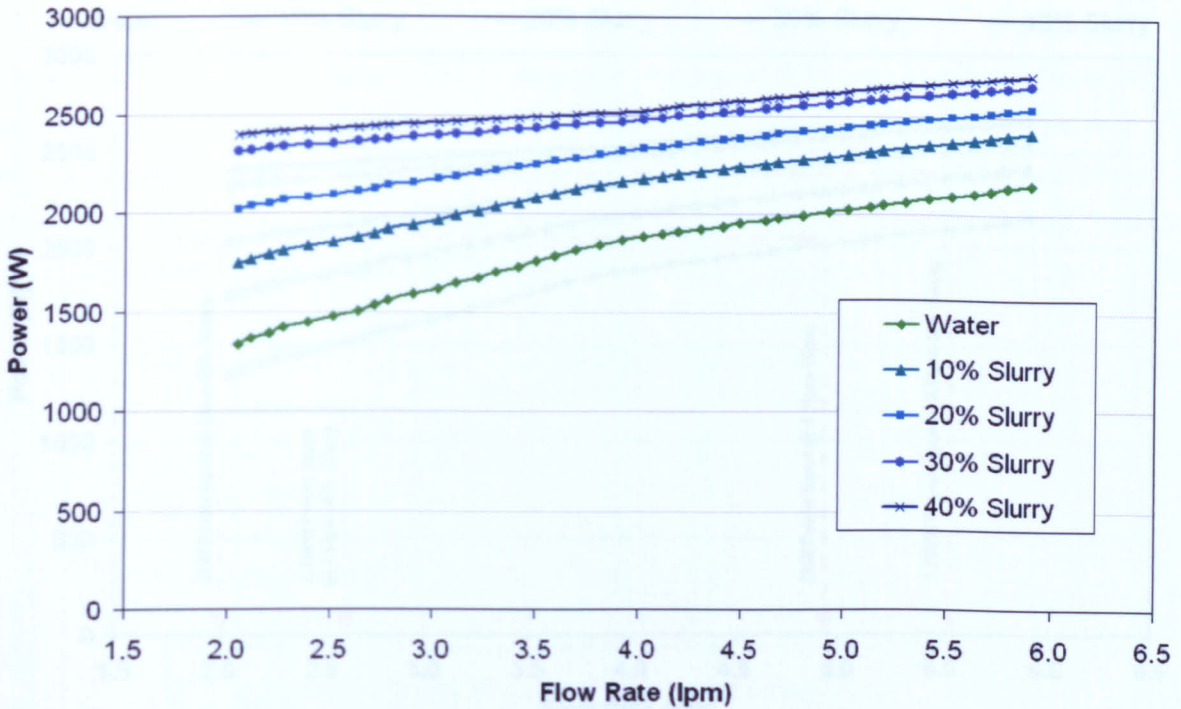


Figure 5.12: Closed Loop – Relationship between Flowrate and Power input Across Heater Section.

The results from the test were very positive with a significantly greater thermal input required to maintain the temperature difference over using water alone. Thus, the use of latent heat provided by the microPCM was found to improve the performance of heat transportation of the slurries over the use of pure water. For example, at 2.6l, the heat transportation of the 30% microPCM slurry was approximately 57% higher than that of pure water, being 3.94kW compared to 2.51kW respectively.

It can be seen that with increased flow rate, the power input increased. The percentage improvement in power input over water also changed with flow rate. Over all of the flow rates under investigation, the thermal input was greater for the slurry, however the largest improvements were observed at the slower flow rates. At 2l, the 30% slurry showed a 73% improvement over water, at 3.0l, 48.1%, 4l, 31.5% and at 6l, 23.4%. This suggested that residency of the slurry in the heating section had an influence on the thermal capability. It appeared that the longer the residency period of the microPCM in the heater section, the greater the percentage of phase change material melted and hence use of the large latent capacity available.

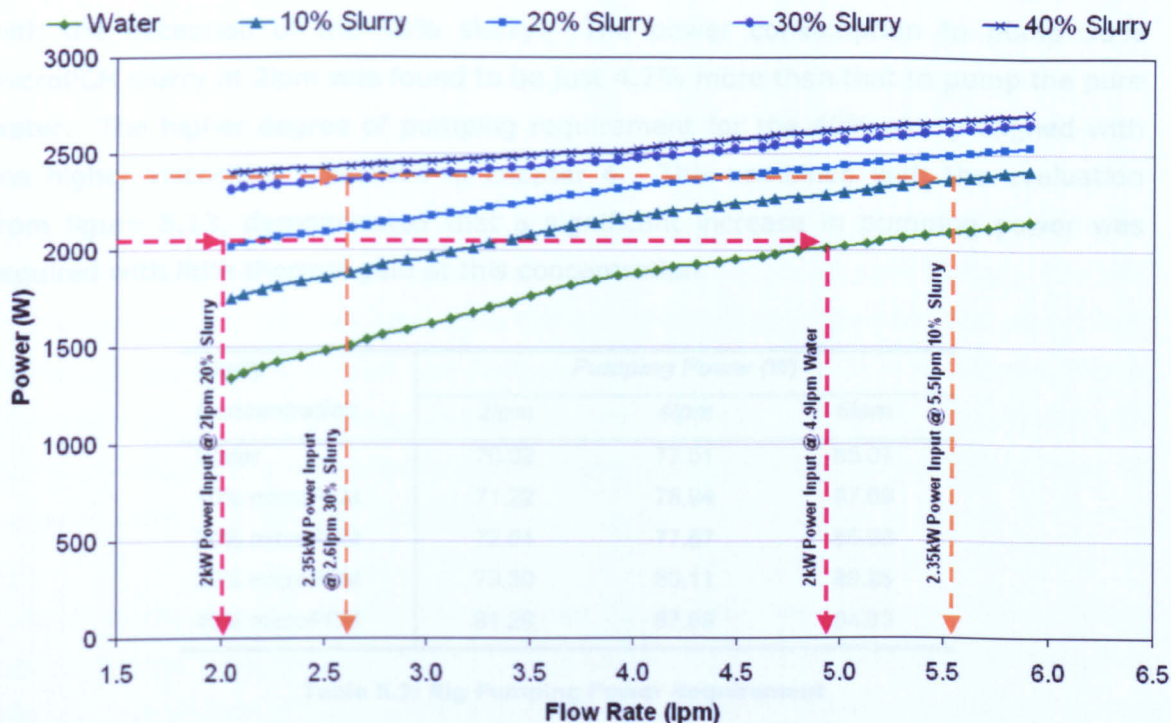


Figure 5.13: Closed Loop – Relationship Between Flowrate and Power input Across Heater Section.

This trend would also be evident in meeting the aims of the investigation, to reduce pumping loads, with a 20% slurry operating at 2.0l, this could transfer the same thermal energy as water at 4.9l. Even greater flow rate reductions could be achieved with a 30% slurry over water.

### 5.6.2 Operational Challenges

The trend observed with  $\Delta T$  test could also be observed in the power test with a change in gradient at 4l. It is assumed that this is a result of a change in flow type from laminar to turbulent. From figure 5.13, it can be seen that the change in flow type maintained a larger thermal input than that which would have been a result of interpolation from the laminar flow trend.

### 5.6.3 Pumping Power

Table 5.3 indicates the energy consumption of the pump for pure water and the microPCM slurries across the concentrations investigated. The higher flow rates necessitated increased pumping power as illustrated in the table. However, it is interesting to note that the increase in pressure drop due to the high concentration

of microPCM, see table 5.3, did not give a significant increase for pumping power, with the exception of the 40% slurry. The power consumption to pump 30% microPCM slurry at 2lpm was found to be just 4.7% more than that to pump the pure water. The higher degree of pumping requirement for the 40% slurry aligned with the higher viscosities measured in chapter 4. This combined with the evaluation from figure 5.13, demonstrated that a significant increase in pumping power was required with little thermal gain at this concentration.

<b>Slurry Concentration</b>	<b>Pumping Power (W)</b>		
	<b>2lpm</b>	<b>4lpm</b>	<b>6lpm</b>
Water	70.02	77.51	85.01
10% microPCM	71.22	78.94	87.69
20% microPCM	72.61	77.87	85.66
30% microPCM	73.30	80.11	86.28
40% microPCM	81.29	87.69	94.83

**Table 5.3: Rig Pumping Power Requirement**

The slurry concentration that had the most favourable trade-off between thermal improvement, pumping load and general operation characteristics was the 30% slurry. This had significant improvement in thermal capacity with only a 1.5-4.7% increase in pumping power. The results in table 5.4 showed that the microPCM slurry did not provide savings in pumping power compared just using water alone due to the increase in viscosity of the working fluid.

**5.7 Operational Challenges**

Practical pumping and application fuel cell suitability issues. One of the major problems or challenges encountered during the experimentation was stratification and agglomeration of the particles. This was caused by gravimetric forces on the slurry as the microcapsules were slightly less dense than water and therefore showed buoyant characteristics. This was not an issue when the slurry was in motion and being pumped, however, when left stationary for any long periods of time, the system had a tendency to cream and clog. This was particularly evident in the 40% slurry; after 40hrs of operation in the system, the slurry showed signs of particle build up in parts of the system that resisted the flow and hence reduced the slurry flow rate.

As the flowrate increased, the heat transportation also increased. However, as expected, it did require more pumping power. In addition, a higher concentration of microcapsules signified large energy storage capability of the suspension. On the other hand, the drawback was that it led to increased viscosity of the suspension, which required more pumping power, and at high concentrations, non-Newtonian behaviour. From the investigation it could be seen that the 10%, 20% and 30% slurries did have significant thermal improvements over using pure water. The use of the 40% slurry was not attractive due to its clogging tendencies and significant increase in pumping load over the less concentrated slurries. It also showed only a small increase in thermal performance over the 30% slurry. The 30% slurry showed the best trade-off between maximising thermal capacity for a reasonable level of pressure drop as a result of viscosity.

Capsule durability was also under investigation in this test. Although the capsules were only run for a relatively small period of time compared with typical operating life in a real system. There were no severe indications of capsule breakdown. Only with the 40% slurry was there any symptoms. It was observed at this concentration a thin layer of wax floating at the surface of the reservoir. Further investigation would be required to match capsule durability and pumping technique to ensure that the capsules would remain structurally in-tacked in the system, yet prove a pumping solution that was cost effective. Previous experimental work by Colvin and Muligan (1993) showed that after 8,000-10,000 freeze-thaw thermal cycles of their microPCM particles, there was no significant degradation in slurry or loss in thermal performance.

## **5.8 Concluding Remarks**

This chapter studied the performance of the microPCM slurry as a functionally thermal fluid in a small-scale closed loop system. The parameters of interest were the slurry concentration and flow rate. The following conclusions can be made from this experimental study.

- Phase Change Slurries can enhance fluid based heat transfer.
- The same amount of energy can be transported with less fluid flow with the use of latent energy – less energy for pumping required (viscosity trade off).
- Microencapsulated paraffin is a viable PCS.

- More research and development is needed for; Phase change temperature optimisation to the fuel cell, better material properties for neutral stability and capsule strength.

The heat transportation from the functionally thermal fluid containing the microPCM could be significantly enhanced compared with the use of pure water. For example, at 2.6lpm the heat transportation of the 30% slurry was approx 57% higher than that of pure water. This significant increase in thermal capacity of the working fluid due to the use of phase change material could permit the use of a smaller flow rate, which in turn could save on the pumping power. For example, to deliver 2.0kW of heat, the 20% microPCM slurry of 35°C paraffin wax could allow use of a flow rate of 2.0lpm instead of 4.9lpm with the use of pure water. The result, based on the pump power data, would achieve a 12% reduction in pumping power (from 81.26W to 72.61W). It must be noted that this small scale rig had a relatively small system volume compared with the fuel cell system studied in this thesis; therefore it may be assumed that larger absolute saving could be made in a larger pumping regime.

The next stage of the research and development of the phase change slurry for a PEM fuel cell was to develop a suitable phase change microcapsule. The microcapsule had to be tuned to the fuel cell operational temperature, be neutrally buoyant to overcome the issues of separation and agglomeration and be durable enough for suitable system life expectancy.

If these particle characteristics could be achieved, this investigation has shown that the phase change slurry could reduce the fuel cell systems pumping load to improve its overall electrical efficiency. It could also reduce system size and aid to stabilise the system temperature through minimising temperature differences and fluctuations.

## Chapter 6: MicroPCM Development for a PEM Fuel Cell

### 6.0 Introduction

This chapter gives an outline of the development of a microPCM and PCS specifically designed to operate and investigate with the fuel cell system. Investigation and selection of PCM was undertaken with preliminary tests to identify suitable PCMs for encapsulation. Further to this, favourable PCMs were encapsulated and developed. These included the PCMs; Hexadecanol, Myristic Acid, Octadecanol and a paraffin wax composite named "French Paraffin". Each were developed and assessed both thermally and from a practicality standpoint for use with the fuel cell system.

Substantial work was carried out to fully characterise and develop a microPCM slurry to suit the thermal conditions of the fuel cell and address the practical pumping issues. For this study, the microPCM particles were developed and produced using two different methods. The choice of method was related to the type of material that was being encapsulated. These two methods are explained further in section 6.4, and include the more common process of in-situ micro-encapsulation with Melamine-formaldehyde (MF) and the less common, acrylic polymerisation.

### 6.1 MicroPCM Development Process

The approach depicted in figure 6.1 shows the design process undertaken for the microPCM development. These steps were taken to achieve the stated goals; selection of a phase change material (PCM) with the desirable phase transition and melting point, an appropriate nucleating agent, and a desirable particle size range. The samples produced were thermally tested to determine their degree of supercooling, enthalpy, temperature range and homogeneity. Successful batches were subjected to a durability test to determine the strength of the encapsulation. Both experimental procedures are explained in detail later in this chapter.

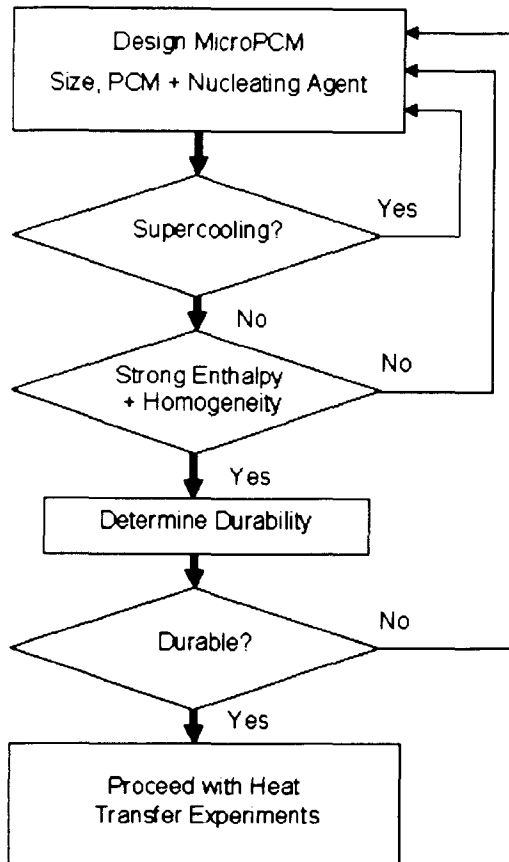


**Figure 6.1: MicroPCM Design Procedure**

The following sections highlight some of the key developments and problems faced during the identification and production of a suitable microPCM for use with the fuel cell.

## 6.2 Fuel Cell Slurry Criteria

From the experimental tests conducted on the PEM fuel cell, the operating temperatures and optimal conditions were identified. Essentially, the key temperatures for the thermal circuit that the slurry would replace, was a flow and return temperatures of 65°C and 40°C respectively. The microPCM therefore had to have its phase transitions within this operating range to be fully tuned and optimised to the system. The other criterion from the fuel cell perspective was on a physical bias rather than thermal, that it could not agglomerate and clog, which would cause serious operational problems.

### 6.3 Phase Change Material Design

Selection of phase change material was paramount to the success of the microPCM to be used in the system. Thermally, the phase change material had to have its phase transitional temperatures tuned to the fuel cell. From the fuel cell evaluation the peak transitional temperature was selected to be within the range of 50-55°C. The latent heat of fusion was to be as high as possible and the boiling point was to be greater than 200°C for durability. The density of the PCM was desired to be as close to water as possible, 1.0 g/cm<sup>3</sup>, so that once encapsulated and mixed with water, was neutrally buoyant.

In order to have a successful encapsulation process, the PCM had to meet a number of basic requirements. The PCM had to be water insoluble. This was required otherwise neither of the encapsulation processes could take place. The density of the material was also an issue for the Acrylic polymerisation as a stable emulsion of PCM and water had to be produced before encapsulation could occur.

With an economic bias, the phase change material had to be readily available and also cost effective. This was to ensure economic viability and availability for use with the fuel cell system. The range of PCM was restricted to paraffin waxes (rather than organic salt) from a safety aspect so that it was non-hazardous and non-corrosive.

Appendix B identifies a list of potential phase change materials with associated thermal properties. The Phase Change Materials that were selected for further investigation and development were; Hexadecanol, Myristic Acid, Octadecanol and paraffin composite - French Paraffin. All are water insoluble, have phase transitional temperatures around 55°C and good enthalpies.

## 6.4 Encapsulation Processes

Two methods were adopted to encapsulate the PCM. The capsules produced by these processes can be distinguished by their shell type and also their particle size. The first method is known as in-situ micro-encapsulation, figure 6.2, and is more commonly used for ink printing and characterised by its Melamine-Formaldehyde shell. As seen and tested in the previous chapters 4 and 5, the  $\eta$ -eicosane capsules investigated had been encapsulated by the manufacturer using this process and with this material. Typically, the particle size for this type of microcapsule ranged from 20-100 $\mu\text{m}$  as identified by the ESEM. The second method was Acrylic Polymerisation (illustrated in figure 6.3). This was favourable as it has a acrylic polymer shell and forms smaller capsule size at 2-20 $\mu\text{m}$ . Preliminary tests with samples clearly identified that when mixed in slurry form with water, the particles acted colloiddally with minimal separation and clogging.

### 6.4.1 In-Situ Microencapsulation

This process involves the production of microcapsules by polymerisation of melamine formaldehyde in an aqueous medium containing dispersed particles of a liquid to be encapsulated (US Patent, 4,396,670). Figure 6.2 depicts this process.

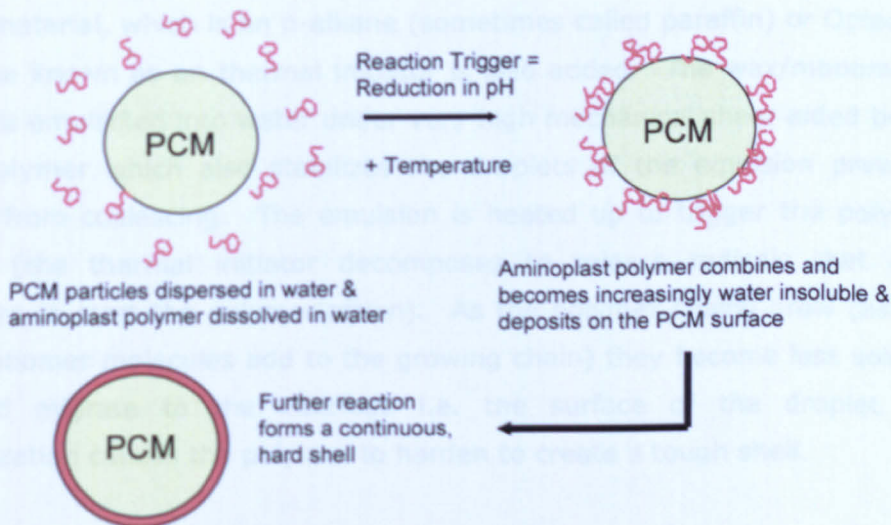


Figure 6.2: In-Situ Micro-encapsulation Process (Cibasc, 2005)

The Melamine-formaldehyde (MF) process: PCM is emulsified into water using a surface active polymer that also stabilises the droplets of the emulsion preventing them from coalescing. A melamine-formaldehyde pre-condensate is added which dissolves in the water. The pH is reduced to  $\sim 4$  to trigger a condensation reaction, whereby smaller melamine-formaldehyde molecules combine to form larger polymeric molecules. The temperature is gradually increased, to speed-up the rate of reaction. As the reaction proceeds (and the molecules grow) the growing molecules reduce in water solubility and migrate and deposit on the surface of the PCM droplet. Eventually the entire surfaces of the droplets are coated with polymer. Further reaction hardens the polymer into a tough shell.

### **6.4.2 Acrylic Encapsulation**

The Acrylic (ACR) microencapsulation process: depicted in figure 6.3. Acrylic monomers combine to form long chain "polymers" in polymerization reactions. All manner of polymers and copolymers (where more than one monomer type is used) are made for many different applications. Copolymers can be tough, flexible and water insoluble/impermeable or can be very water soluble. For microencapsulation, monomers are used that give the tough, flexible, water-insoluble polymers that form the shell of the capsule. Firstly, acrylic monomers are dissolved in the molten phase change material, which is an n-alkane (sometimes called paraffin) or Octadecanol. A substance known as a thermal initiator is also added. The wax/monomer/initiator solution is emulsified into water under very high mechanical shear aided by a surface active polymer which also stabilizes the droplets of the emulsion preventing the droplets from coalescing. The emulsion is heated up to trigger the polymerization reaction (the thermal initiator decomposes to release radicals that react with monomers to start the polymerization). As the polymer chains grow (as more and more monomer molecules add to the growing chain) they become less soluble in the PCM and migrate to the interface i.e. the surface of the droplet. Further polymerization causes the polymer to harden to create a tough shell.

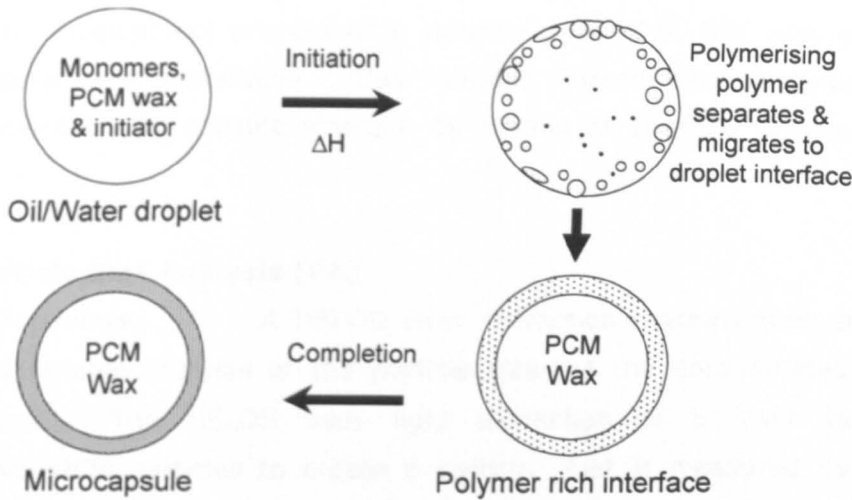


Figure 6.3: Acrylic Encapsulation Mechanism (Cibasc, 2005)

#### 6.4.3 Summary of Encapsulation Process's

Both methods are capable of producing significantly durable capsules, identified by Thermal Gravimetric Analysis (TGA), covered in section 6.5.1, however the Acrylic method was more favourable from a health perspective as it was less harmful if inhaled. The smaller particles produced using this method showed more neutrally buoyant characteristics, suggesting that this would be more feasible for the fuel cell system.

The definitive factors that determined which encapsulation method was used was related to the physical properties of the phase change material that was identified. Good MF shells could be produced only with materials that were polar. The ACR method was dependant on producing an emulsion of phase change material and water that was stable. If this could not be made and separation occurred, the ACR method could not be used.

## 6.5 Methodology and Apparatus

To aid the development process of a suitable microPCM, DSC was used, and two further tests were introduced. This included Particle Size Analysis (PA) and a measurement of the capsule strength by means of Thermal Gravimetric Analysis (TGA).

### 6.5.1 Particle Size Analysis (PA)

**6.5.1.1 Overview** A HELOS laser diffraction machine was used to give a quick and reliable analysis of the particle sizes of the encapsulated PCMs under development. The HELOS uses light diffraction of a laser beam on the sample/microPCM particles to create a pattern, that is measured by an array of detectors. Software provided with the HELOS was used to obtain the particle size distributions. Figure 6.4 illustrates a picture

During the last 25 years laser diffraction has asserted itself against all established methods because of its simple operation and wide usage possibilities for most materials from under  $0.1\mu\text{m}$  to the centimetre range.

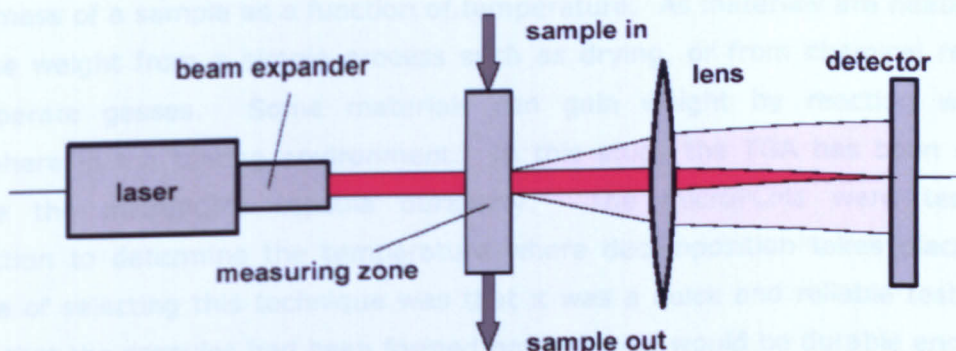


Figure 6.4: Optical Set-up for the Generation of Diffraction Patterns.

The traditional set-up for the particle light interaction is shown in figure 6.4. The basic principle is light scattering the edges of particles. After focusing the light in the centre of the detector, the scattering effect leads to signals on the non-central elements of the detector. The optical set-up is referred to as Fourier-optics (M. Heuer).

**6.5.1.2 Methodology** The microPCM analysed was placed on the measuring zone and selected at a feed rate of 35% of the maximum rate. The samples were passed into an air stream, where it was subjected to high shear forces (3.0 bar). A vacuum (90-100 mbar) was used to draw the particles into the path of a He-Ne laser beam. The diffraction of the laser beam by the particles created a pattern measured by an array of 32 detectors that was a function of size. Software provided with the HELOS was used to obtain the particle size distributions. Figure 6.5 illustrates a picture of the HELOS PA machine.



**Figure 6.5: Helos Laser Diffraction Particle Analyser**

## 6.5.2 Thermal Gravimetric Analysis (TGA)

### 6.5.2.1 Overview

Thermal Gravimetric Analysis (TGA) is a measurement of the mass of a sample as a function of temperature. As materials are heated, they can lose weight from a simple process such as drying, or from chemical reactions that liberate gasses. Some materials can gain weight by reacting with the atmosphere in the testing environment. In this study the TGA has been used to indicate the microPCMs capsule durability. The microPCMs were tested to destruction to determine the temperature where decomposition takes place. The purpose of selecting this technique was that it was a quick and reliable test and to ensure that the capsules had been formed properly and would be durable enough for pumping without mechanically testing them in the circuit. Figure 6.6 shows an image of the Perkin-Elmer Thermal Analysis Machine used.



Figure 6.6: Perkin-Elmer Thermal Gravimetric Analyser

#### 6.5.2.2 Basic Principle

A sample of the test material is placed into a suspended high aluminium cup that is suspended from an analytical balance located outside the furnace chamber. The balance is zeroed, and the sample cup is heated according to a predetermined thermal cycle. The balance sends the weight signal to the computer, along with the sample temperature and the elapsed time. The TGA curve plots the TGA signal, converted to percent weight change on the Y-axis against the reference material temperature on the X-axis.

#### 6.5.2.3 Methodology

After the sample (5-15mg) had been placed on the testing pan and suspended inside the temperature programmable furnace, it was heated through a predetermined temperature profile and continuously purged to remove volatilised products. Its weight was continuously monitored and plotted as a function of time or temperature. The temperature profile took the sample to 110°C and held for 1 min. It was then heated from 110°C to 500°C at a heating rate of 20°C/min.

The thermal gravimetric analysis (TGA) method could be used to detect any thermally induced changes in the sample that produced weight variation and any significant amounts of gaseous components. The following graph, figure 6.7, compares the TGA for the microPCM capsule used in the closed loop study (chapter

5) in comparison to one of the preliminary capsules produced with Myristic Acid in this study.

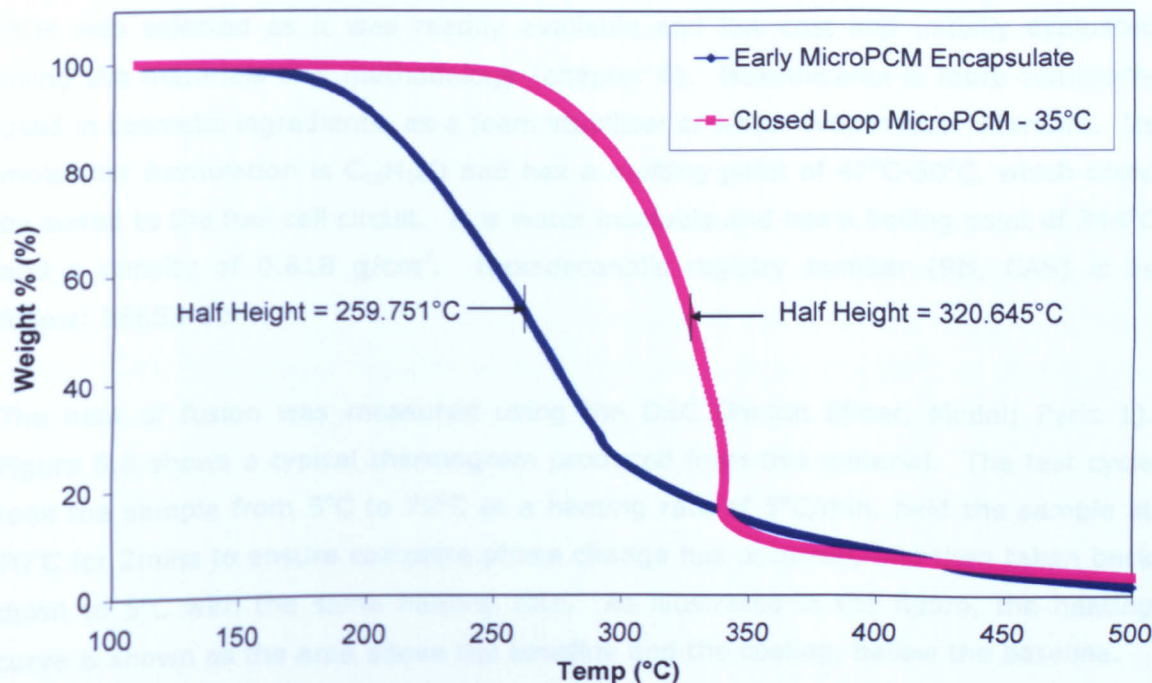


Figure 6.7: Thermal Gravimetric Analysis of Capsule Durability

It can be seen from this graph that the capsule used for the closed loop study, the 35°C,  $\eta$ -eicosane significantly outperformed the early Myristic Acid capsules produced for this study. The  $\eta$ -eicosane, decomposed with a half-life of 321°C compared with 260°C for the Myristic Acid. From preliminary experimental testing on the microPCM used in chapter 4, it was deemed that a capsule must have a half-life of greater than 300°C to be approved of as durable enough to move on to the next stage of testing in the mechanically pumped fuel cell system.

### 6.5.3 Preliminary Tests with Hexadecanol

One of the first PCMs under investigation was Hexadecanol. This was encapsulated using MF as the shell type and was thermally evaluated using the DSC machine. This PCM was selected as it was readily available and low cost and initially evaluated using the materials test methodology (chapter 4). Hexadecanol is more commonly used in cosmetic ingredients, as a foam stabiliser or water evaporation retardant. Its molecular formulation is  $C_{16}H_{34}O$  and has a melting point of  $47^{\circ}C$ - $50^{\circ}C$ , which could be suited to the fuel cell circuit. It is water insoluble and has a boiling point of  $344^{\circ}C$  and a density of  $0.818 \text{ g/cm}^3$ . Hexadecanol's registry number (RN, CAS) is as follow: 36653-82-4.

The heat of fusion was measured using the DSC (Perkin Elmer, Model; Pyris 1). Figure 6.8 shows a typical thermogram produced from this material. The test cycle took the sample from  $5^{\circ}C$  to  $70^{\circ}C$  at a heating rate of  $5^{\circ}C/\text{min}$ , held the sample at  $70^{\circ}C$  for 2mins to ensure complete phase change has occurred, and then taken back down to  $5^{\circ}C$  with the same heating rate. As illustrated in the figure, the heating curve is shown as the area above the baseline and the cooling, below the baseline.

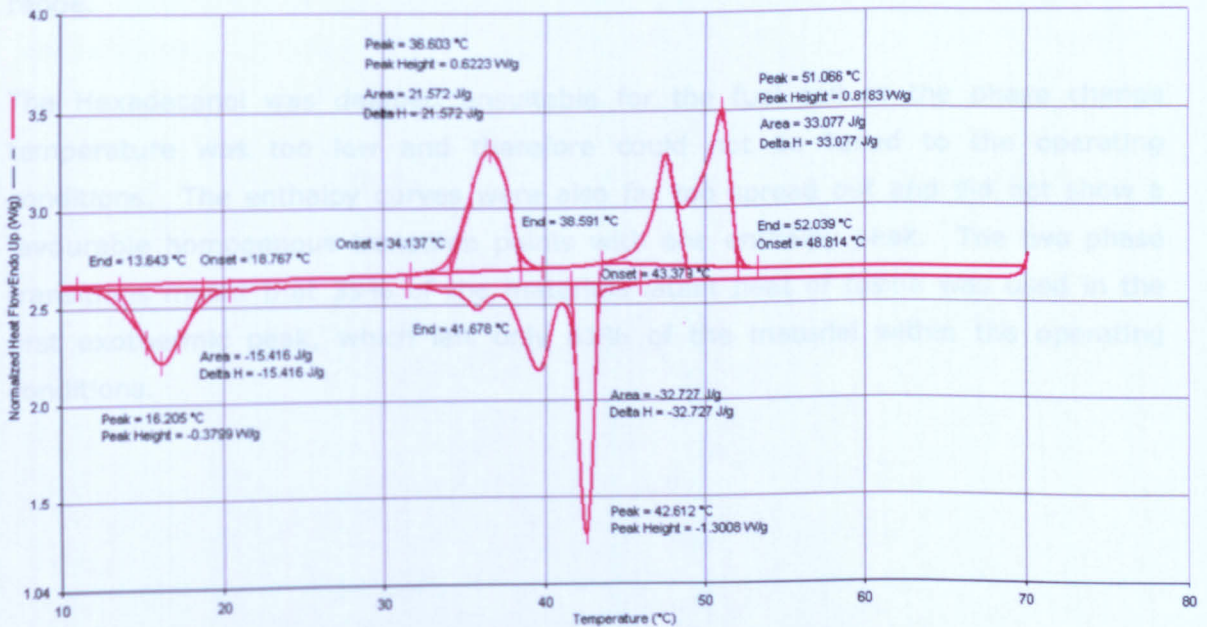


Figure 6.8: DSC – 40% Hexadecanol Concentration with Water

It can be seen that the melting and crystallisation phases are spread out over a large temperature range; 32°C to 52°C for heating and 43°C to 13°C under cooling, with no definitive phase transition temperature. These temperatures were significantly lower than that stated by the materials manufacturers. The thermographs experienced a lot of noise when compared with previous DSC experimental analysis with the microPCMs investigated in the chapter 4.

From figure 6.8 it is also clear that there were two phase transitions taking place within the material. The first exothermic peak was 21.6 J/g at 36.6°C and its endothermic peak was 15.2 J/g at 16.2 °C, the second, was a double exothermic peak at 51°C with 33 J/g with a corresponding endothermic peak at 43.6°C of 33 J/g also. These two main transitions were caused by impurities in the Hexadecanol composition that may have occurred in the encapsulation process.

The phase transitional temperature of the Hexadecanol was too low for use with the fuel cell as all the phase transition occurred below 52°C under heating conditions and started to re-crystallise at 43°C. This would mean that the PCM would melt, however, would not re-crystallise within the 65°C to 45°C operational temperature range.

The Hexadecanol was deemed unsuitable for the fuel cell as the phase change temperature was too low and therefore could not be tuned to the operating conditions. The enthalpy curves were also far too spread out and did not show a favourable homogenous transition points with one enthalpy peak. The two phase transitions meant that 39% of the materials latent heat of fusion was used in the first exothermic peak, which left only 61% of the material within the operating conditions.

## 6.6 Myristic Acid

Myristic Acid, also known as n-Tetradecanoic acid, is essentially a 14-Carbon, a saturated fatty acid that occurs in most animal and vegetable fats, particularly butterfat and coconut, palm, and nutmeg oils. It is also used to synthesise flavour and as an ingredient in soaps and cosmetics (Dorland). Registry number (RN, CAS): 544-63-8. It is a white solid that was primarily selected in this study because it had a melting point of between 52°C-54°C. This phase transitional temperature was well suited to the fuel cell operating conditions. Its molecular formulation is  $C_{14}H_{28}O_2$  and it has a boiling point of 250°C. The density of this PCM is  $0.87g/cm^3$  and it is water insoluble.

**6.6.1 Development** Encapsulation was first attempted by the process of Acrylic polymerisation; however, encapsulation was poor as a stable emulsion could not be produced with the time constraints available. The Myristic Acid was therefore encapsulated with the MF shell.

**6.6.2 DSC** Figure 6.9, illustrates the Myristic Acid encapsulated with an MF shell. It can be seen that it exhibited a very favourable exothermic peak with a peak phase change temperature of 54.5°C and an enthalpy of 75.9 J/g at 40% concentration with water.

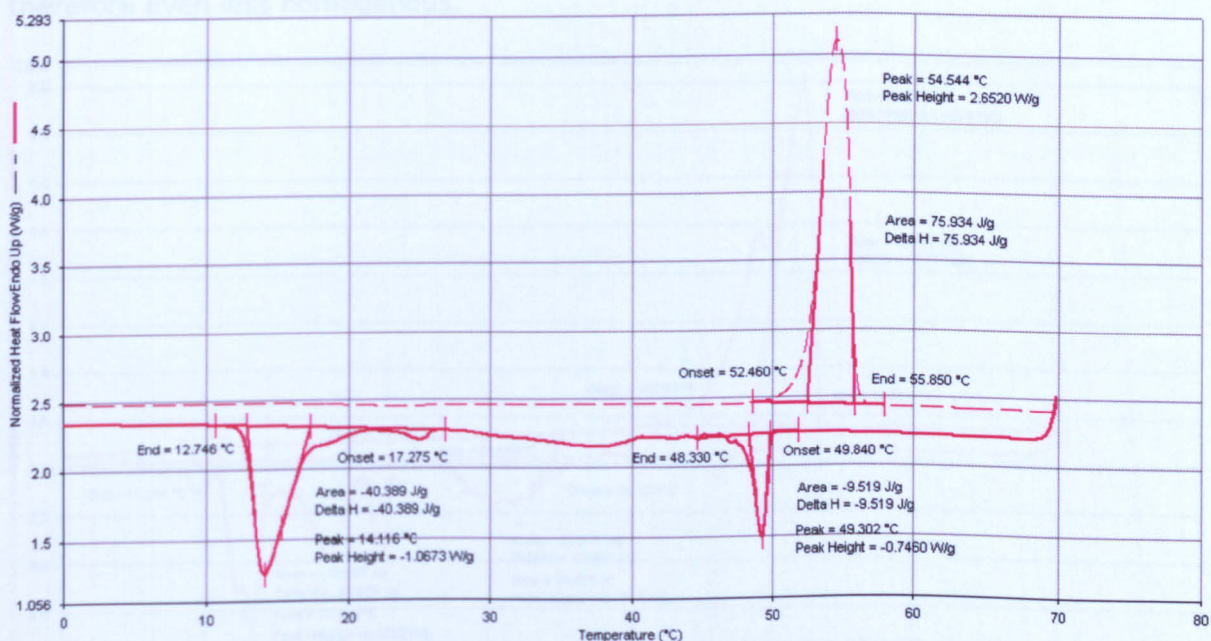


Figure 6.9: Thermogram – 40% Myristic Acid Concentration with Water

The Myristic Acid however, did not perform very well under cooling and severely suffered from supercooling. There was initial promise with the crystallisation onset at 49.8°C although there was only a small phase change of 9.5 J/g that took place. The rest of the crystallisation took place at 14.1°C, which was well below the fuel cell operating conditions.

**Combating the Supercooling Effect;** Supercooling may be clearly identified in figure 6.9. The aim of the first stage of the development process (figure 6.1) was to overcome this supercooling that took place. Investigation into the supercooling phenomena revealed US patent 5456852, it stated that this could be reduced by the introduction of a nucleating agent.

Figure 6.10, illustrates the thermogram produced when encapsulating the Myristic Acid and nucleating agent, Stearic Acid. The exothermic peak was very similar to that of figure 6.9, with a peak at 52.3°C and enthalpy of 73.7 J/g. The stearic acid with a phase transitional temperature of 49°C produced the double exothermic peak. The nucleating agent did alter the exothermic curves and reduce the supercooling, however not significantly enough to bring the crystallisation phase into the fuel cell operating range. The main exothermic peak was similar to figure 6.9, although the nucleating agent caused more noise or latent interactions. The cooling phase was therefore even less homogenous.

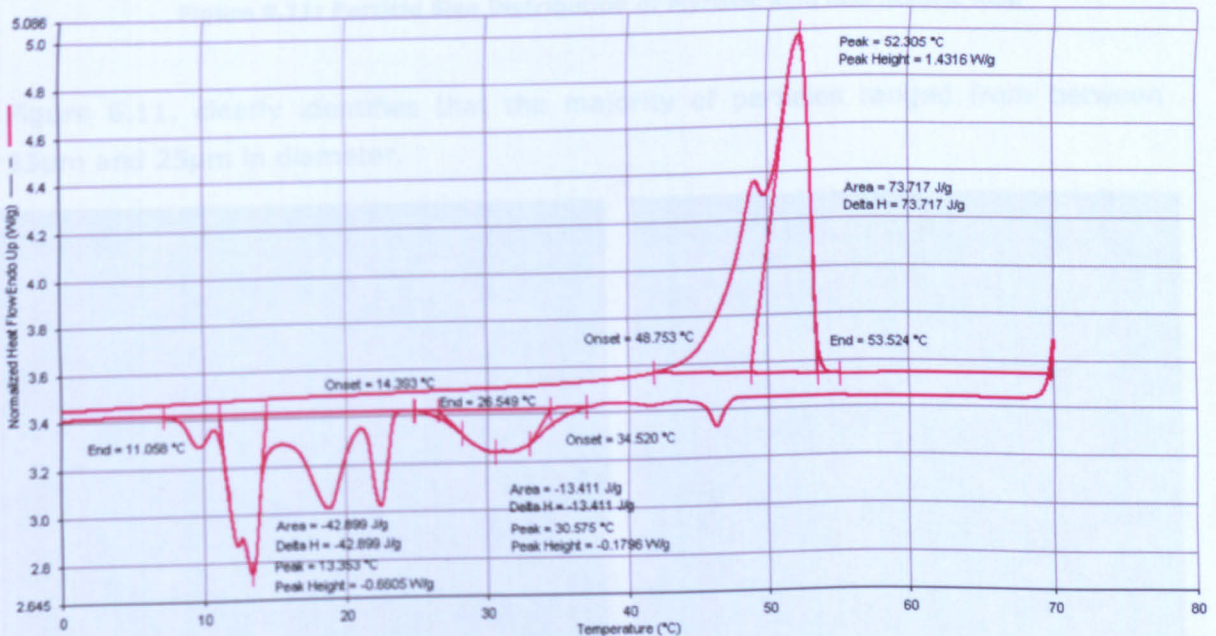


Figure 6.10: DSC – 40% Myristic Acid + Stearic Acid with water by Acrylic Polymerisation

From this thermogram, figure 6.10, it was clear that the encapsulated Myristic acid would not be suitable for use with the fuel cell. Primarily this was due to the large difference between the endothermic and exothermic peaks. The cooling phase was significantly outside the fuel cell lower operating temperature.

### 6.6.3 Particle Size Analysis

Particle size analysis was undertaken to determine the particle size distribution created by the In-situ process with Myristic Acid and Stearic Acid with an MF shell. Figure 6.11, illustrates the size distribution curve. The mean particle size was  $26\mu\text{m}$  in diameter and ranged from  $1\mu\text{m}$  to  $30\mu\text{m}$ .

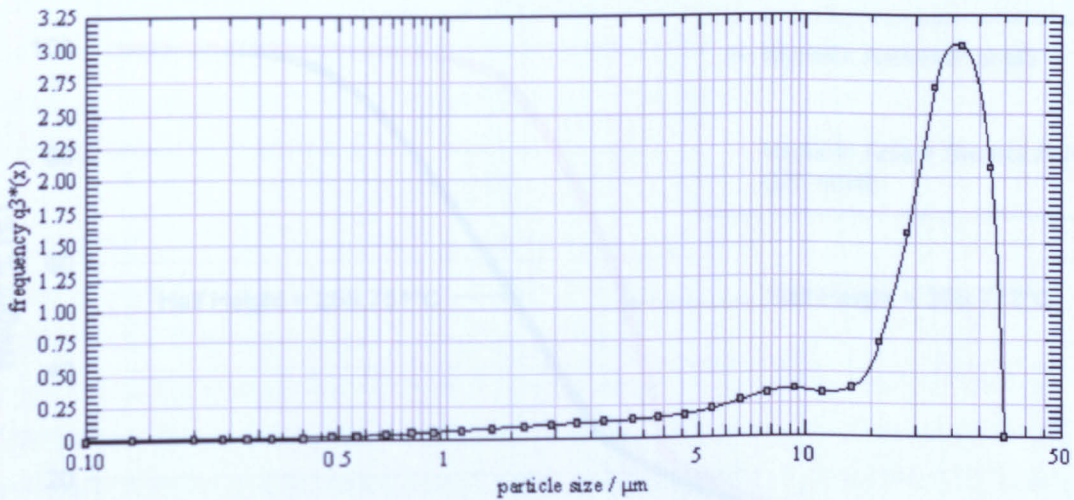


Figure 6.11: Particle Size Distribution of Myristic Acid and Stearic Acid

Figure 6.11, clearly identifies that the majority of particles ranged from between  $15\mu\text{m}$  and  $25\mu\text{m}$  in diameter.

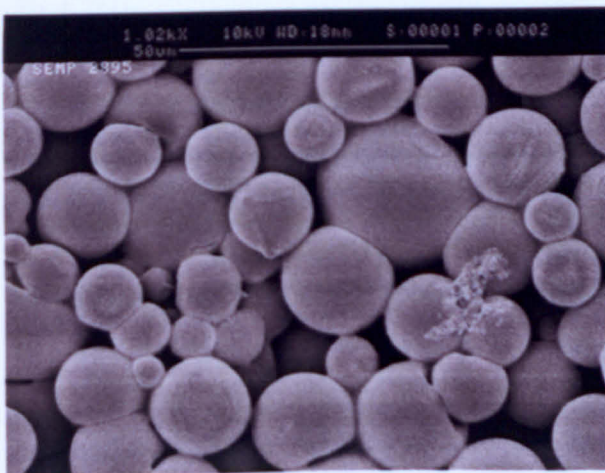


Figure 6.12: SEM - Myristic Acid @ 1000x Magnification

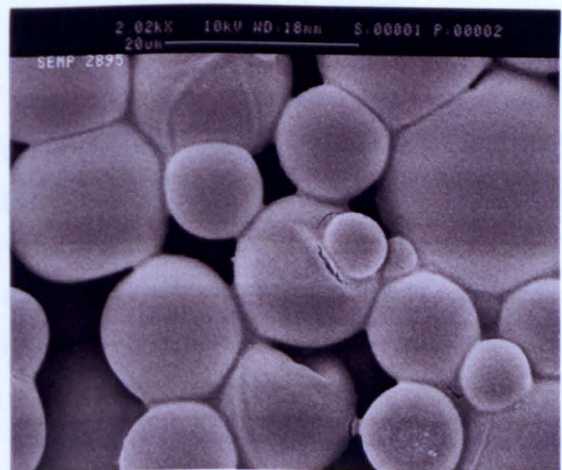


Figure 6.13: SEM - Myristic Acid @ 2000x Magnification

Figure 6.12 and 6.13 show Scanning Electron Microscope images of the sampled particles at two levels of focus. These images verify the particle size distribution produced from the HELOS diffuser.

### 6.6.4 Thermal Gravimetric Analysis

Figure 6.14, identifies two Myristic samples tested using the TGA process. It can be seen that the original Myristic Acid did not encapsulate very well and had a half-life of 260°C. The latter sample with a combination of Myristic and Stearic Acid made a more durable shell with a half life of 309°C.

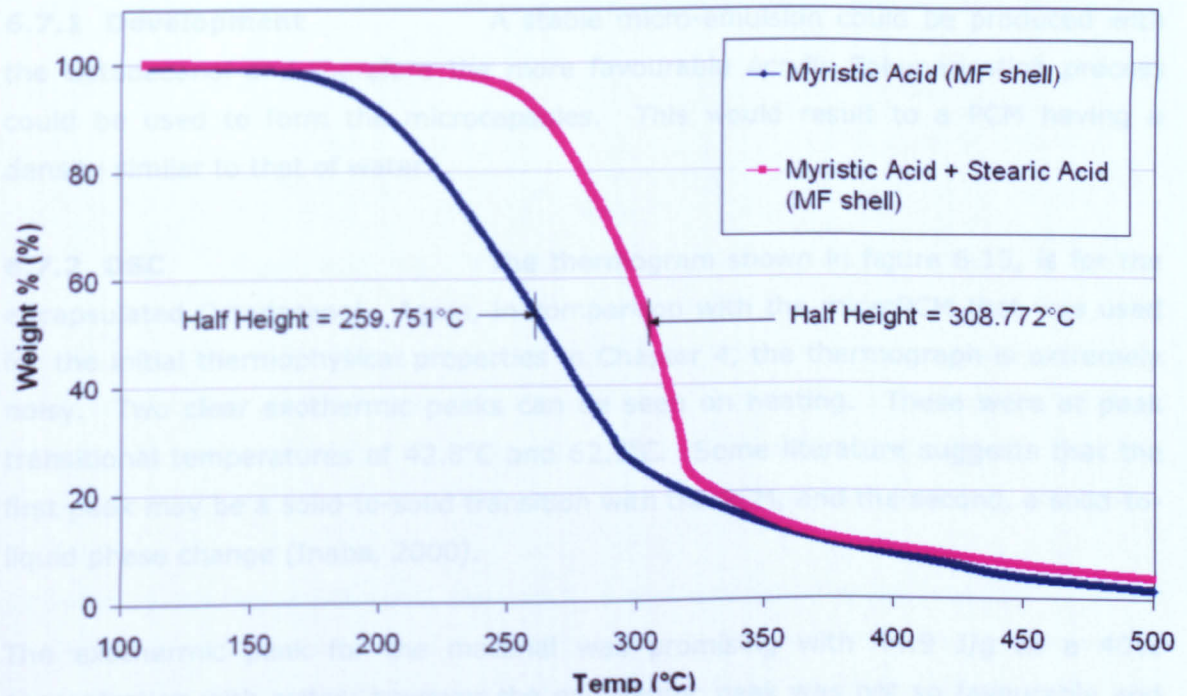


Figure 6.14: Thermal Gravimetric Analysis of Myristic Acid MicroPCM

### 6.6.5 Myristic Acid Summary:

Investigation with Myristic Acid showed that under heating it performed well enough to be integrated with the fuel cell. It had a good enthalpy peak with a small range. The Myristic did, however, suffer from severe supercooling and even with the introduction of a nucleating agent (Stearic acid), this effect could not be reduced significantly enough. Myristic acid does show potential although the problem of supercooling would have to be overcome. Detailed development of the PCM,

however, was outside the scope of this investigation. With its current formulation it could not therefore be selected as a viable PCM for the fuel cell system.

## **6.7 Octadecanol**

Octadecanol is also known as Octadecyl alcohol or pure Stearyl alcohol. Registry number (RN, CAS): 112-92-5. Its molecular formulation is  $C_{18}H_{38}O$  and is a white crystalline solid. It was chosen for its availability and melting point temperature of 55°C-58°C. It is insoluble with water, has a density of 0.81 g/cm<sup>3</sup> and has a boiling point of 300°C.

### **6.7.1 Development**

A stable micro-emulsion could be produced with the Octadecanol and therefore the more favourable Acrylic Polymerisation process could be used to form the microcapsules. This would result to a PCM having a density similar to that of water.

### **6.7.2 DSC**

The thermogram shown in figure 6.15, is for the encapsulated Octadecanol. Again, in comparison with the microPCM that was used for the initial thermophysical properties in Chapter 4, the thermograph is extremely noisy. Two clear exothermic peaks can be seen on heating. These were at peak transitional temperatures of 42.8°C and 62.5°C. Some literature suggests that the first peak may be a solid-to-solid transition with the PCM, and the second, a solid-to-liquid phase change (Inaba, 2000).

The exothermic peak for the material was promising with 44.9 J/g at a 40% concentration with water; however the exothermic peak was not so favourable and exhibited a wide range of phase transition with two peaks on cooling. This did however all occur within the fuel cell temperature range of 65°C and 40°C.

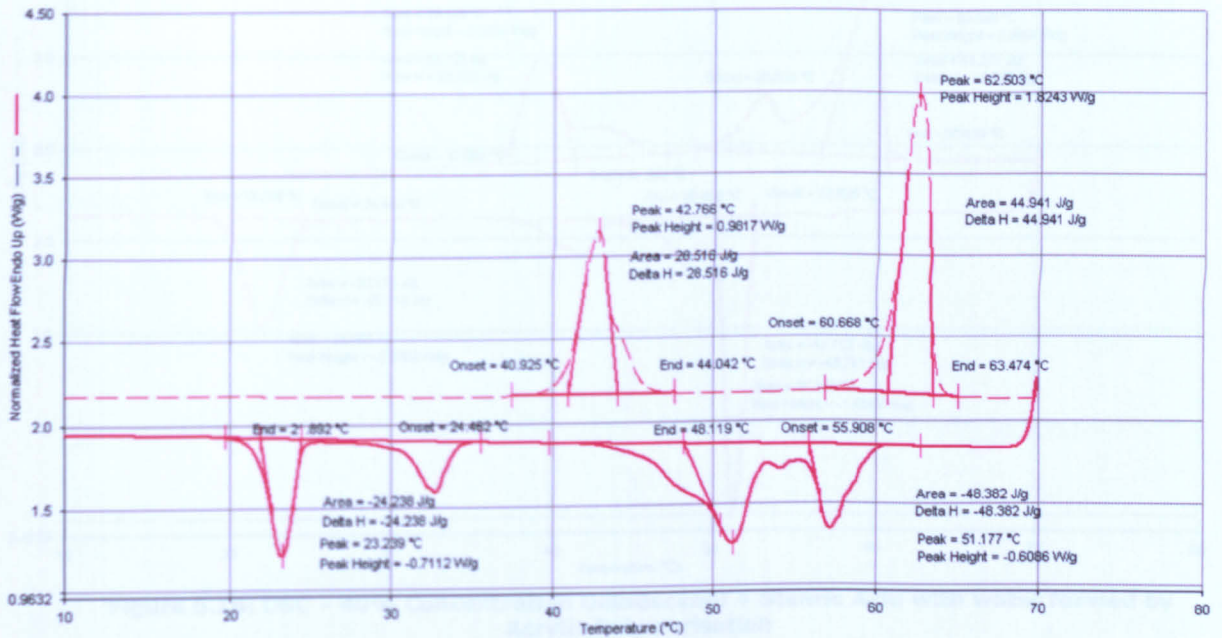


Figure 6.15: DSC – 40% Octadecanol with water by MF In-Situ

The aim for the next stage of this development was to improve the exothermic liquid-solid phase transition so that it was more homogenous and had a smaller range. To ensure that the material was tuned to the fuel cell, it was desired that the exothermic peak was reduced by a few degrees so that it would fully melt.

In order to achieve these aims, the addition of a nucleating agent was investigated. Again, the nucleating agent added was Stearic Acid and the resultant thermogram is illustrated in figure 6.16. This showed much of the desired effects. It had significant influence on the supercooling effect and produced a homogenous exothermic peak that mirrored the exothermic peak with 43.8 J/g compared to the 45.3 J/g respectively. All of the solid-liquid-solid phase transition occurred over the desired 55°C operating temperature. This suggested that although there was the solid-solid phase transition that couldn't be harnessed, the rest could be well tuned to the fuel cell conditions.

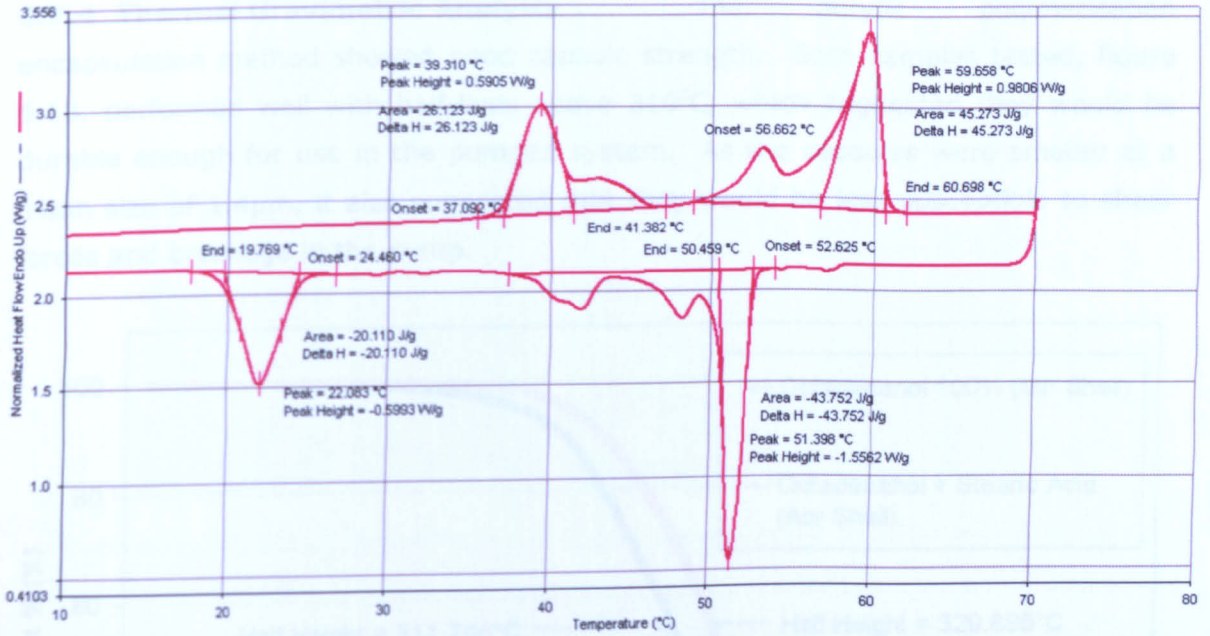


Figure 6.16: DSC – 40% Concentration Octadecanol + Stearic Acid with water formed by Acrylic Polymerisation

**6.7.3 Particle Size Analysis**

The Octadecanol was encapsulated using the Acrylic Polymerisation process. Compared to the In-situ process with an MF shell, the acrylic process produced smaller capsules. As previously stated, this was a primary reason for using this process. The particle size distribution is illustrated in figure 6.17. The mean particle size was 1.4µm and they ranged from 0.4µm to 5µm in size.

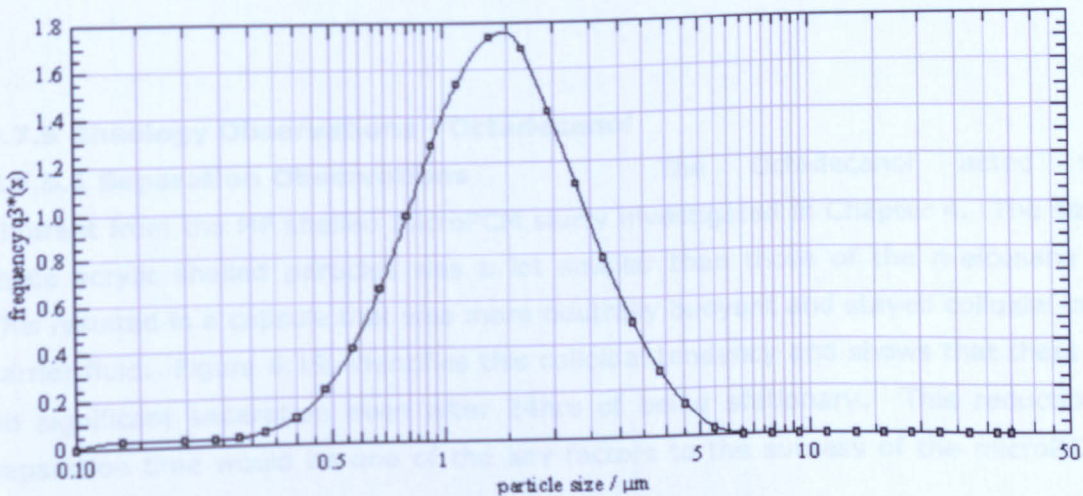


Figure 6.17: Particle Size Distribution of Octadecanol + Stearic Acid

### 6.7.4 Thermal Gravimetric Analysis

The acrylic polymerisation encapsulation method showed good capsule strength. Both samples tested, figure 6.18, performed well with half-lives above 310°C, which suggested they would be durable enough for use in the pumped system. As the capsules were smaller at a mean size of 1.4µm, it also suggested that they would be less susceptible to shear forces and breakage in the pump.

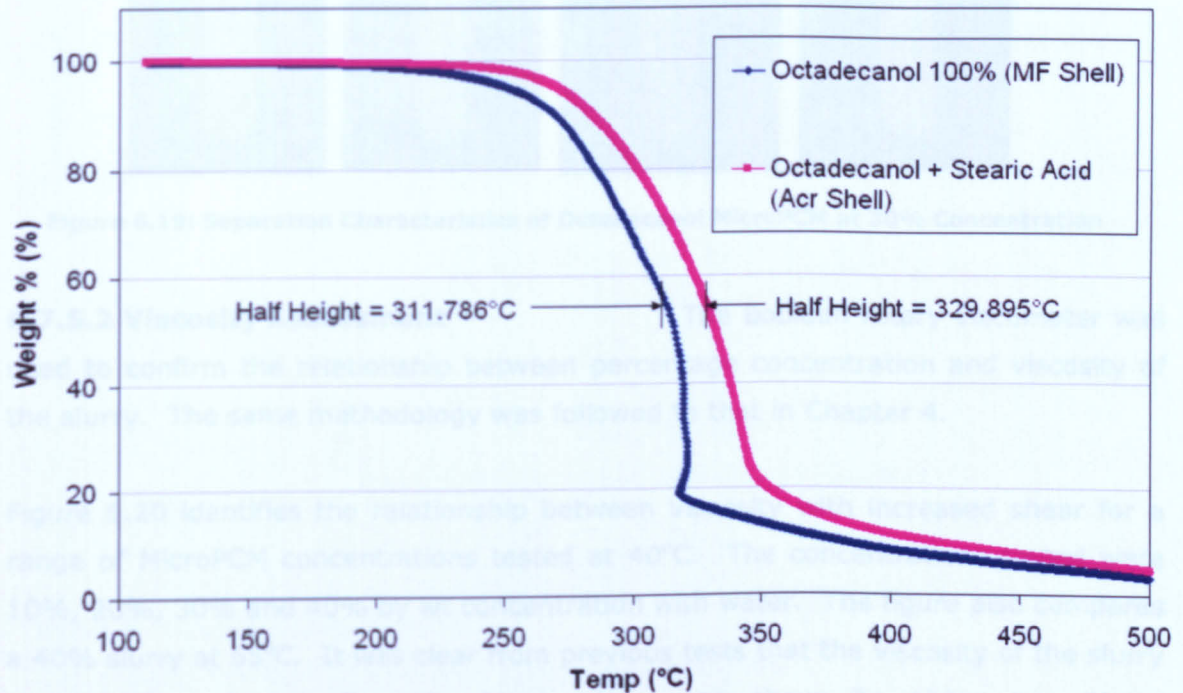


Figure 6.18: Thermal Gravimetric Analysis of Octadecanol MicroPCM

### 6.7.5 Rheology Observations - Octadecanol

#### 6.7.5.1 Separation Observations

The Octadecanol acted very different from the MF shelled microPCM slurry investigated in Chapter 4. The size of these acrylic shelled particles was a lot smaller than those of the n-eicosane MF. This resulted in a capsule that was more neutrally buoyant and stayed colloidal in the carrier fluid. Figure 6.19, identifies this colloidal tendency and shows that there was no significant separation even after 24hrs of being stationary. This reduction of separation time would be one of the key factors to the success of the microPCM in the fuel cell circuit.

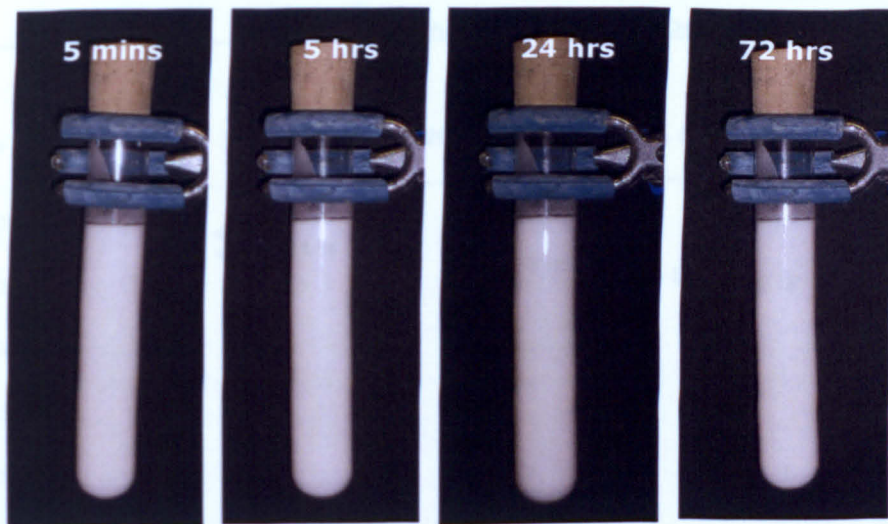


Figure 6.19: Separation Characteristics of Octadecanol MicroPCM at 30% Concentration

#### 6.7.5.2 Viscosity Assessment

The Boolean rotary viscometer was used to confirm the relationship between percentage concentration and viscosity of the slurry. The same methodology was followed to that in Chapter 4.

Figure 6.20 identifies the relationship between Viscosity with increased shear for a range of MicroPCM concentrations tested at 40°C. The concentrations tested were 10%, 20%, 30% and 40% by wt concentration with water. The figure also compares a 40% slurry at 65°C. It was clear from previous tests that the viscosity of the slurry significantly reduces when the temperature was above its phase transitional temperature, so therefore the more significant results for pumping load investigation was when the slurry was operating at the lower range of temperature – 40°C. It was clear that even a 40% slurry at 65°C, it was less viscous than a 30% slurry at 40°C.

From figure 6.20 it can be seen that the viscosity of the slurry at 40°C gradually increase with increase concentration between 10-30%, however there is a significant increase when the concentration was taken up to 40%. This suggests that in the fuel cell system the slurry should have a no greater concentration than 30% otherwise significant pumping load and clogging may occur. It also suggested that the best trade off between maximising thermal capacity and minimal pumping load would be achieved with a 30% slurry.

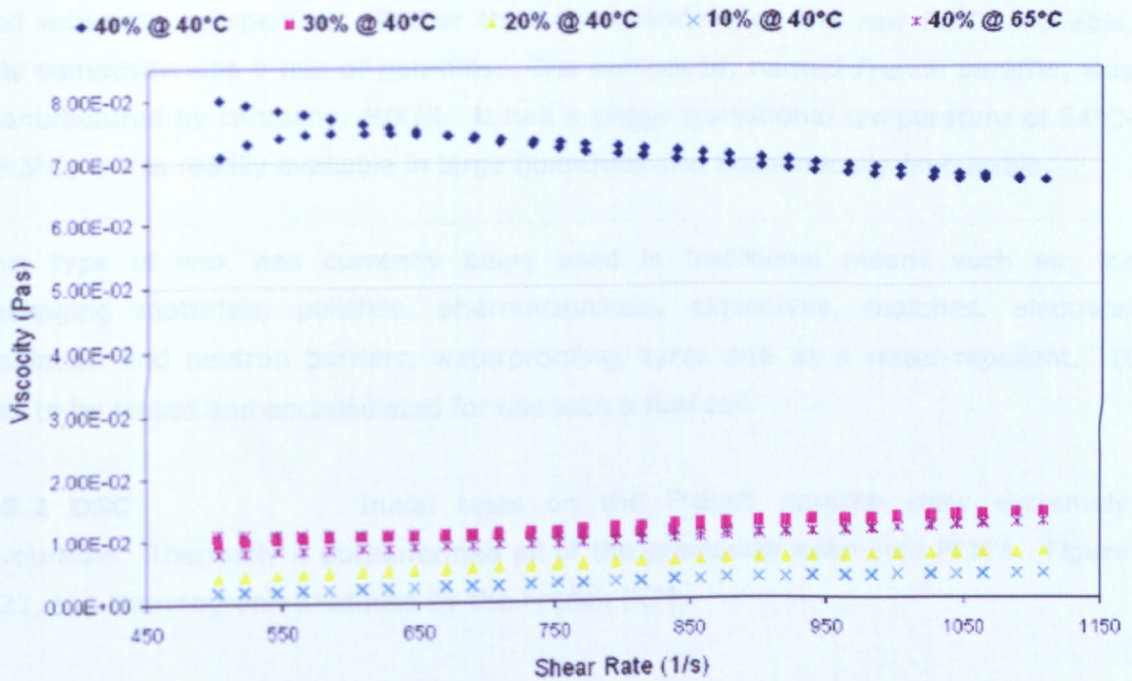


Figure 6.20: Viscosity of Octadecanol MicroPCM

### 6.7.6 Summary - Octadecanol

The encapsulation of Octadecanol proved successful and met the criteria demanded in the design process. It showed excellent rheological behaviour at 30% and met the durability tests with the TGA. Thermally, it provided an homogenous thermogram with the nucleating agent overcoming the issue of supercooling. The thermal capacity was not one of the highest; however the phase transitional temperature and range should be very tuned to the fuel cell design temperatures. This sample was to be scaled up in the laboratory for further tests in the fuel cell system (Chapter 7).

## 6.8 French Paraffin

The French Paraffin wax composite proved to be a breakthrough from a materials and economic perspective. Rather than concentrating on the raw PCMs available, this composite was a mix of paraffins. The composite, named French paraffin, was manufactured by company, *MIKIR*. It had a phase transitional temperature of 54°C-56.5°C; it was readily available in large quantities and economically favourable.

This type of wax was currently being used in traditional means such as; for packaging materials, polishes, pharmaceuticals, explosives, matches, electrical insulation and neutron barriers, waterproofing, tyres and as a water-repellent. It was to be tested and encapsulated for use with a fuel cell.

### 6.8.2 DSC

Initial tests on the French paraffin were extremely favourable. Thermally it outperformed all of the previously examined PCM's. Figure 6.21, is a thermograph produced by the French PCM.

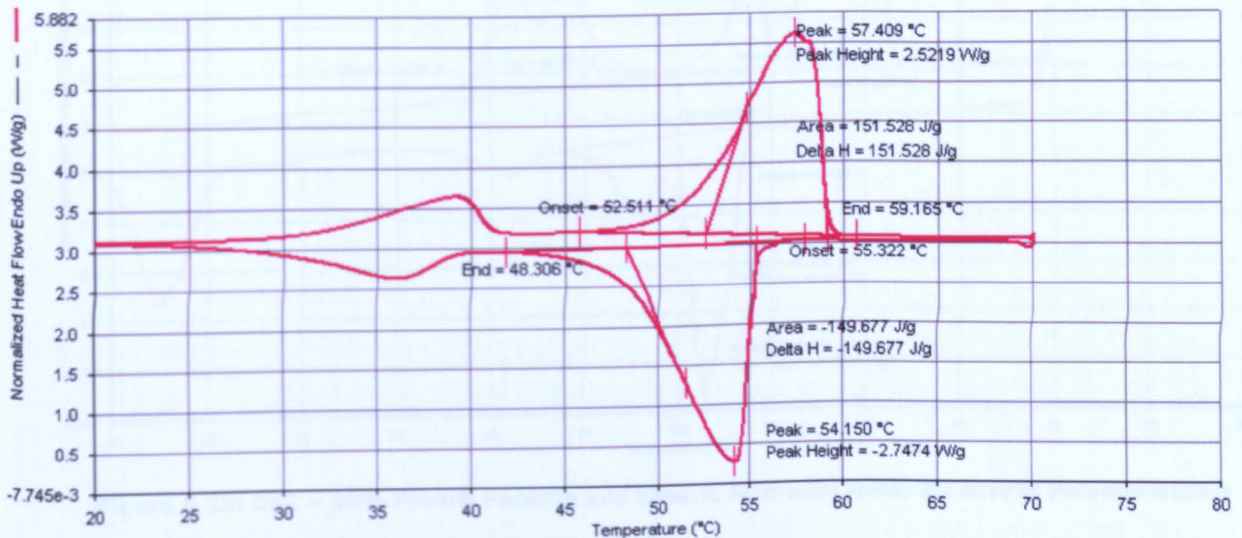


Figure 6.21: DSC – 100% French Paraffin

Figure 6.21, shows an ideal phase transitional temperatures of 55°C and exhibited large enthalpy curves operating over a small range. It showed a very small temperature difference between the peak endothermic curve and the peak exothermic curve of just 3.3°C.

The thermograph also identifies a small solid-to-solid phase transition at 37°C, however this was ignored as it was outside the fuel cell operating range.

The next stage of the development stage was to encapsulate the French paraffin using one of the encapsulation methods. The acrylic polymerisation method was chosen as a stable emulsion could be formed and the decision was based on the successful rheological test of the Octadecanol slurry.

Initial encapsulation was poor and showed significant supercooling tendencies. As previously used, Stearic acid was included in the encapsulation to act as a nucleating agent. This reduced the supercooling effect and resulted in the following thermograph, figure 6.22.

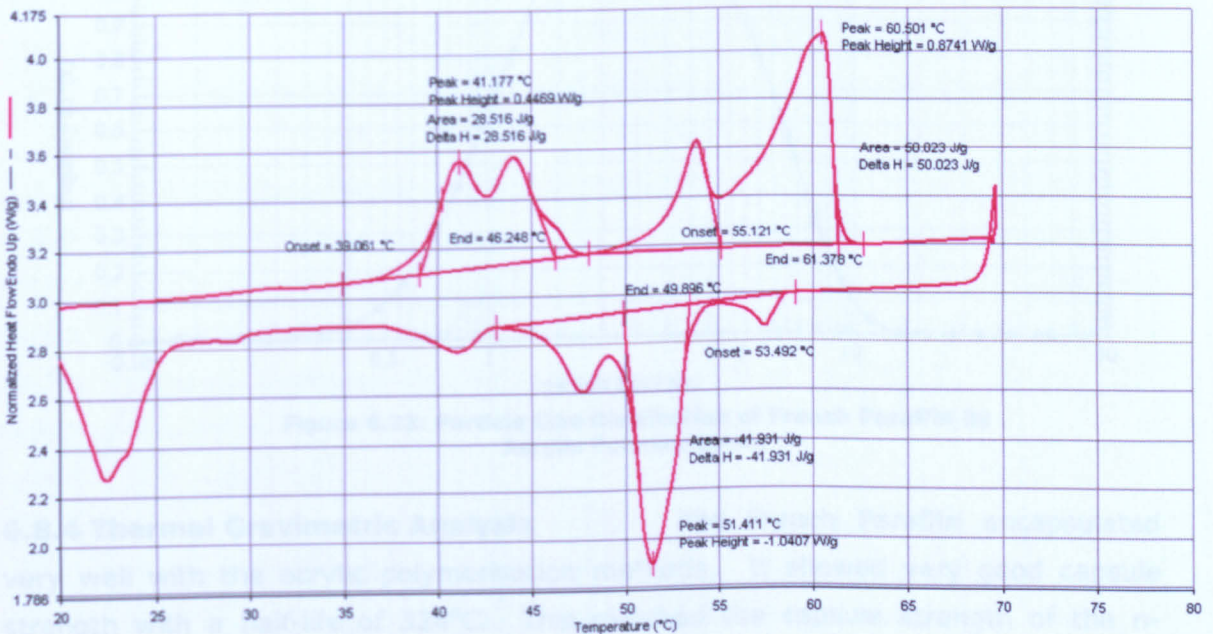


Figure 6.22: DSC – 40% French Paraffin and Stearic Acid with water by Acrylic Polymerisation

Although the thermograph in figure 6.22 was not as clean as that of figure 6.21 and had a wider transitional range, it still had all of its liquid-to-solid and solid-to-liquid phase change within the fuel cell operating conditions.

The exothermic peak has a peak transitional temperature of 60.5°C with an enthalpy of 50 J/g. The exothermic peak was at 51.4°C and enthalpy of 41.9 J/g. Thermally

the French paraffin showed that it was well suited to the fuel cell operating temperatures.

### 6.8.3 Particle Size Analysis

A HELOS laser diffraction machine showed that the particle size distribution for the sample was uniform and there were no anomalous sized particles. The mean particle size of the French Paraffin wardrobe measured to be  $2\mu\text{m}$  in diameter. They ranged in size from  $0.5\mu\text{m}$  to just over  $10\mu\text{m}$ . The distribution also showed that there was greater variation and less frequency around the mean diameter size when compared to the Octadecanol sampled that was encapsulated the same way.

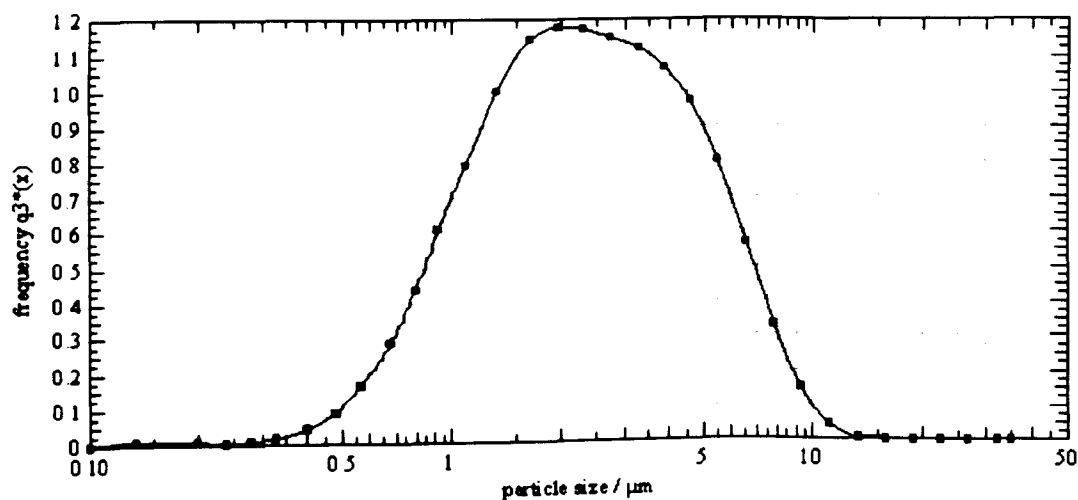


Figure 6.23: Particle Size Distribution of French Paraffin by Acrylic Polymerisation

### 6.8.4 Thermal Gravimetric Analysis

The French Paraffin encapsulated very well with the acrylic polymerisation methods. It showed very good capsule strength with a half-life of  $324^\circ\text{C}$ . This matched the capsule strength of the n-eicosane previously tested by 2%, suggesting that it would be durable enough for use in the pumped system. As the capsules were smaller at a mean size of  $1.4\mu\text{m}$ , it also suggested that they would be less susceptible to shear forces and breakage in the pump, like the Octadecanol.

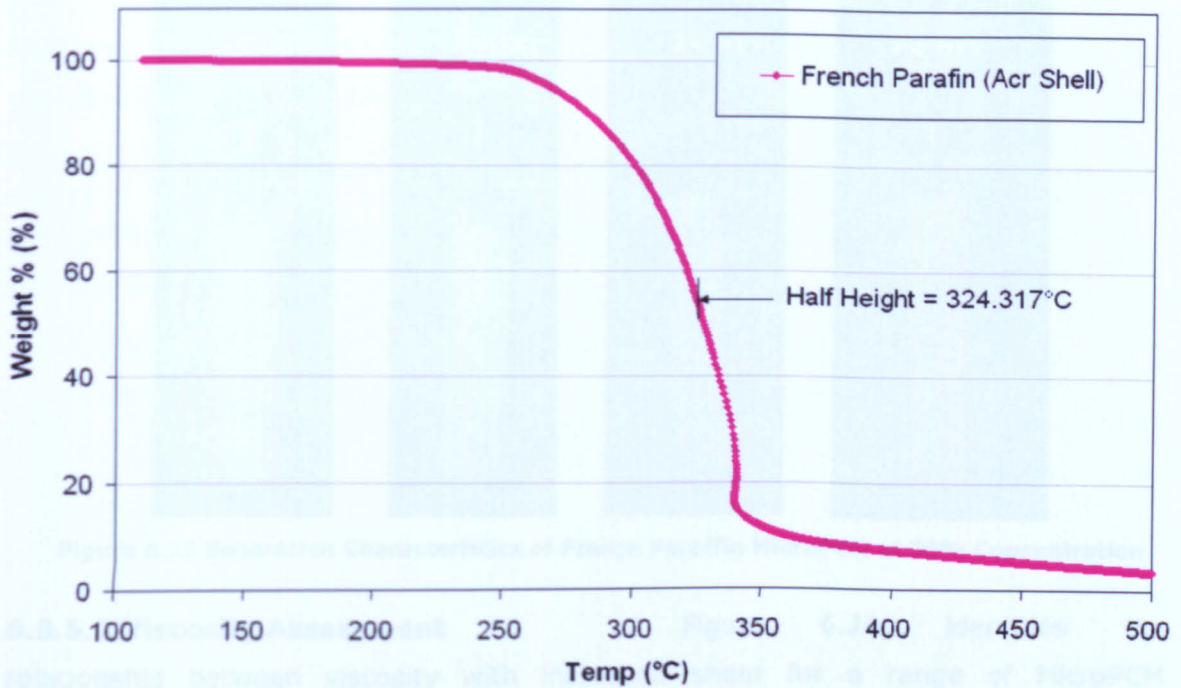


Figure 6.24: Thermal Gravimetric Analysis of French Parafin MicroPCM

### 6.8.5 Rheology Observations – French Parafin

#### 6.8.5.1 Separation Observations

The French Parafin appeared to be less viscous than the other slurries produced. As the particles were very small they produced a slurry that resembled a similar consistency to milk. It showed excellent neutral buoyancy characteristics and showed no sign of separation. Figure 6.25, indicates this trend.

The French paraffin slurry exhibited excellent buoyancy characteristics and remained stable and viscous for a long period of time. Its key disadvantage was its long-term stability, and when left for a period of time greater than 72hrs, it would start to severely agglomerate and bond to itself. It would very slowly cream on the surface and bond to produce a hard crust. Once bonded, it was extremely hard to separate. This agglomeration would need to be addressed before practical long-term use in the fuel cell.

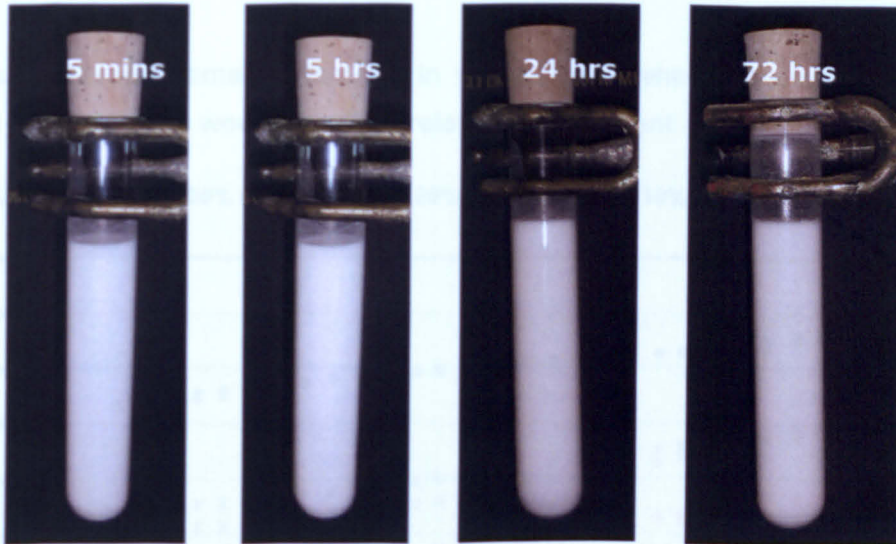


Figure 6.25 Separation Characteristics of French Paraffin MicroPCM at 30% Concentration

#### 6.8.5.2 Viscosity Assessment

Figure 6.26, identifies the relationship between viscosity with increased shear for a range of MicroPCM concentrations tested at 40°C. Using the same methodology and comparison as used for the Octadecanol, the concentrations examined were 10%, 20%, 30% and 40% by wt concentration with water at 40°C. The figure also compares the 40% slurry at 65°C.

As stated from the observations in 6.8.5.1, the rheology assessment provided experimental evidence that the viscosity was less than that of the other slurries examined. At 30% concentration it was 1.52 times less viscous than Octadecanol and a significant 5.01 times less viscous than the n-eicosane that was used in the closed loop study. This would have considerable implications on pumping load reductions with a slurry compared to the other microPCMs.

The profiles indicated in figure 6.26 show that there was an increase in viscosity with increase in concentration of the microPCM particles with water. However, this increase was significantly less than the other slurries examined. It could be seen from the figure that for every 10% increase in concentration of the slurry, the viscosity doubled. At 40% concentration, the slurry still showed that it would be viscous enough to be used in the pumped fuel cell system. Even at this concentration, it was still 2.76 times less viscous than a 30% n-eicosane slurry and just 1.83 times more viscous than the 30% Octadecanol. From the analysis it could also be seen that

there was a relatively small difference in viscosity for when the slurry was in solid and liquid states, which would result in relatively consistent pumping loads.

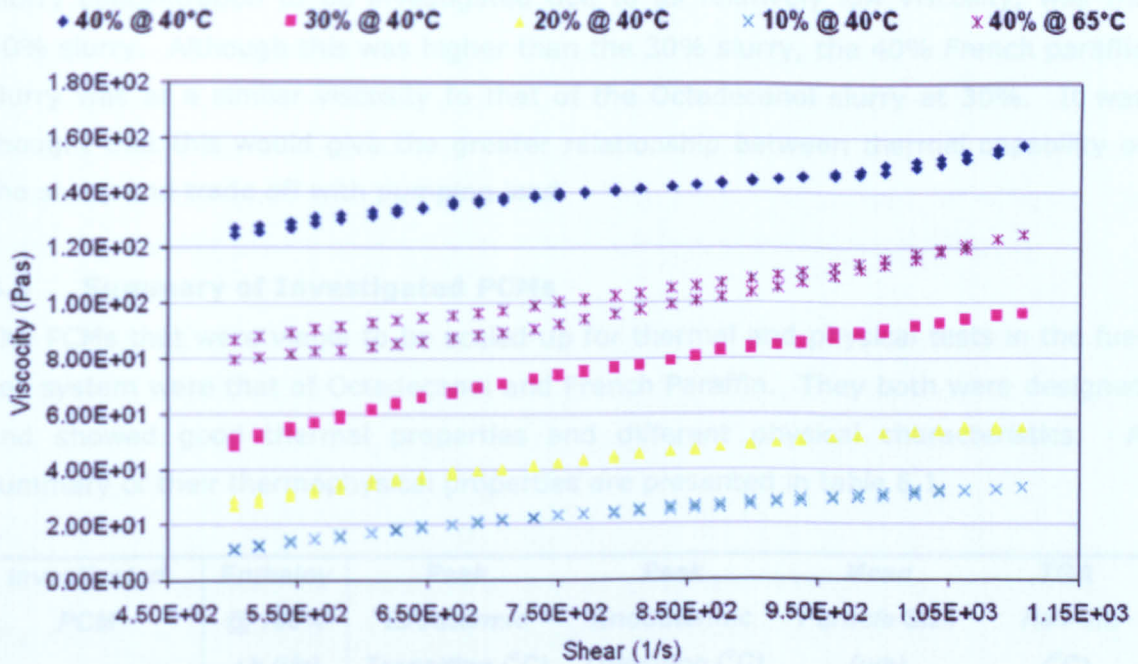


Figure 6.26: Rheology of French Paraffin MicroPCM

This suggests that in the fuel cell system the slurry should have a greater concentration than 30% otherwise significant pumping load and clogging may occur. It also suggested that the best trade off between maximising thermal capacity and minimal pumping load would be achieved with a 30% slurry.

### 6.8.6 Summary – French Paraffin

Encapsulation of the French Paraffin made a thermo-physically favourable microPCM that could be used in the fuel cell system. Thermally it showed a phase transitional temperature of 55°C and it had good, homogenous enthalpy curves. Although it was observed on the thermographs that the curves exhibited noisy areas, it was thought that this would be reduced with further development. The viscosity of the slurry was low compared to the other slurries investigated and it showed good neutral buoyancy with minimal separation over short to medium term time periods. The issue of long term instability and agglomeration would need to be addressed for a viable long term presence in the fuel cell.

The production of the French Paraffin slurry was to be scaled up to a larger batch to be investigated further with the fuel cell system (Chapter 7). It was decided that the slurry concentration to be investigated due to its relatively low viscosity, was the 40% slurry. Although this was higher than the 30% slurry, the 40% French paraffin slurry was at a similar viscosity to that of the Octadecanol slurry at 30%. It was thought that this would give the greater relationship between thermal capability of the slurry and trade off with pumping load.

### 6.9 Summary of Investigated PCMs

The PCMs that were viable to be scaled up for thermal and physical tests in the fuel cell system were that of Octadecanol and French Paraffin. They both were designed and showed good thermal properties and different physical characteristics. A summary of their thermophysical properties are presented in table 6.1.

<i>Investigated PCM</i>	<i>Enthalpy @ 100% <math>\Delta h</math> (J/g)</i>	<i>Peak Exothermic Transition (<math>^{\circ}C</math>)</i>	<i>Peak Endothermic Transition (<math>^{\circ}C</math>)</i>	<i>Mean Particle Size (<math>\mu m</math>)</i>	<i>TGA Half-life (<math>^{\circ}C</math>)</i>
Octadecanol	114.3	59.7	51.4	1.4	329.9
French Paraffin	151.53	60.5	51.4	2	324.3

Figure 6.1: Rheology of French Paraffin MicroPCM

### 6.10 Concluding Remarks

Two microPCM slurries were produced that were favorable both thermally and physically and were specific to the fuel cell operational conditions. Significant progress was achieved to develop these slurries, however they were far from ideal and displayed inherent strengths and weaknesses. One was stronger thermally, yet displayed weaker physical characteristics of separation and clogging (French composite), and the other, stronger physically, remaining colloidal and mixed, yet thermally weaker (Octadecanol).

These candidate microPCMs were tested in a simulated fuel cell system (chapter 7). With greater time and research input into the development of these materials, other nucleating agents and additives could be investigated to improve on these characteristics further. For the purpose of this investigation it can be concluded that suitable microPCMs can be modified and developed to suit the operational characteristics of the PEM fuel cell.

## Chapter 7: Fuel Cell Slurry

### 7.0 Introduction

An experimental rig was constructed to examine the operation of the fuel cell with the two favourable microPCMs that were developed in chapter 6. The previous experimental work of chapter 5 examined the heat transfer characteristics of a low temperature commercially available PCS. This work had proven to enhance the thermal capacitance and heat transfer characteristics of the working fluid.

The aim of this study was therefore to assess the thermal and physical practicalities of using the microPCM slurry with the fuel cell system, along with its required mode of operation to maximise the latent energy from the slurry and maintain fuel cell conditions.

This chapter includes an overview of the experimental background, followed by a description of the system that was designed and built. Results indicated that the gain in thermal capacity with the PCS over using water was equal to that of the measured additional pump load from the slurry. An increase in the slurry concentration in the rig and/or improvement in the microPCM thermal capacity in the lab, would achieve pump savings.

### 7.1 Experimental Background

To assess thermal characterisation of the PCS, the flow rate and the inlet and outlet temperatures of each heat exchanger were measured. The primary side of the Fuel Cell heat exchanger circuit used pure water, whereas the secondary side of the heat exchange loop contained the test microPCM slurry. Water was initially examined in the heat exchange loop for a baseline study. The sensible heat capacity ( $C_p$ ) of the capsule fraction was calculated as 2.4kJ/kgK. For water, the heat flow was computed as follows;

$$\dot{Q}_{pri/sec\_water} = \dot{m}C_p(T_h - T_c) \quad [7.1]$$

Where,  $T_h$  and  $T_c$  were equal to the hot and cold temperatures of the heat exchangers inlet and outlet,  $\dot{m}$  is the mass flow and  $\dot{Q}$  the heat flow on the primary side or secondary side of the heat exchanger. The heat flow on the slurry side  $\dot{Q}_{Slurry}$  is computed for the capsule fraction of  $x_{capsule}$  by;

$$\dot{Q}_{Slurry} = x_{capsule} \dot{m} C_{p_{capsule}} (T_h - T_c) + (1 - x_{capsule}) \dot{m} C_{p_{water}} (T_h - T_c) \quad [7.2]$$

Because the measured temperature indicates only sensible heat flow, it was necessary to recompute the latent heat using the heat transfer characteristics of the heat exchanger. To do that, first of all the heat transfer characteristic was ascertained with water also in the slurry loop. The heat flow was increased by heating up the inlet water of one heat exchanger on the fuel cell side stepwise, while the inlet temperature on the slurry side remained constant. The heat flow cycles are illustrated in figure 7.1.

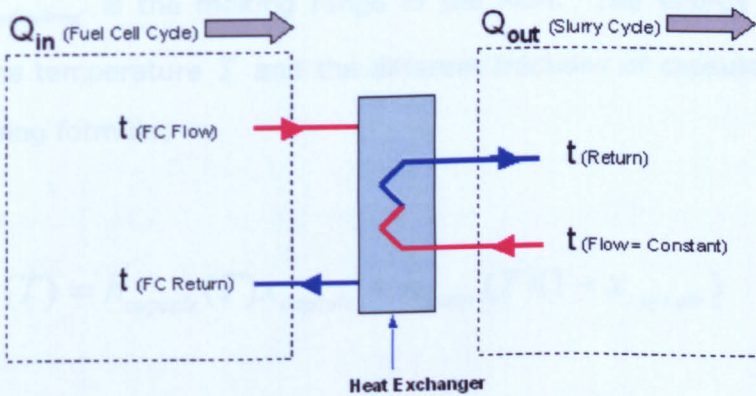


Figure 7.1: Heat Flow Cycles

The heat flow was calculated for each temperature by equation [7.1]. Since heat losses are the same with the slurry under identical *boundary conditions* (same mass flow and ambient temperatures), the heat flow difference between the water in the slurry-cycle  $\dot{Q}_{slurry-cycle_{water}}$  and the measurements with PCS in the slurry-cycle  $\dot{Q}_{slurry-cycle_{PCS}}$ , equation [7.2] must be stored as latent heat  $\dot{Q}_{latent}$ .

$$\dot{Q}_{latent} = \dot{Q}_{slurry-cycle_{water}} - \dot{Q}_{slurry-cycle_{PCS}} \quad [7.3]$$

With the adjusted mass flow and known capsule concentration, it was possible to compute the specific heat of melting  $\Delta h_{capsules}$  and to validate the capacity for latent heat storage in the slurry by comparison with the DSC measurements.

$$\Delta h_{capsules} = \frac{\dot{Q}_{latent}}{\dot{m}(x_{capsule})} \quad [7.4]$$

The capacity of the slurry to store heat was therefore;

$$Q_{PCS} = x_{capsule} \Delta h_{capsule} + C_{p_{water}} \Delta T_{area-of-melting} \quad [7.5]$$

Where,  $\Delta T_{area-of-melting}$  is the melting range of the PCM. The energy content of the slurry  $h_{PCS}$ , the temperature  $T$  and the different fractions of capsules can be found with the following formula;

$$h_{PCS}(T) = h_{capsule}(T)x_{capsule} + h_{water}(T)(1 - x_{capsule}) \quad [7.6]$$

Where,  $h$  is the enthalpy per kilogram for the capsules or water and  $T$ , the temperature in °C. Figure 7.2 shows different enthalpy curves for slurries with different capsule fraction for the French MicroPCM in comparison to water. Enthalpy values were derived from the DSC tests, this method is commonly known and used for simulations of PCMs (Lamburg, 2003).

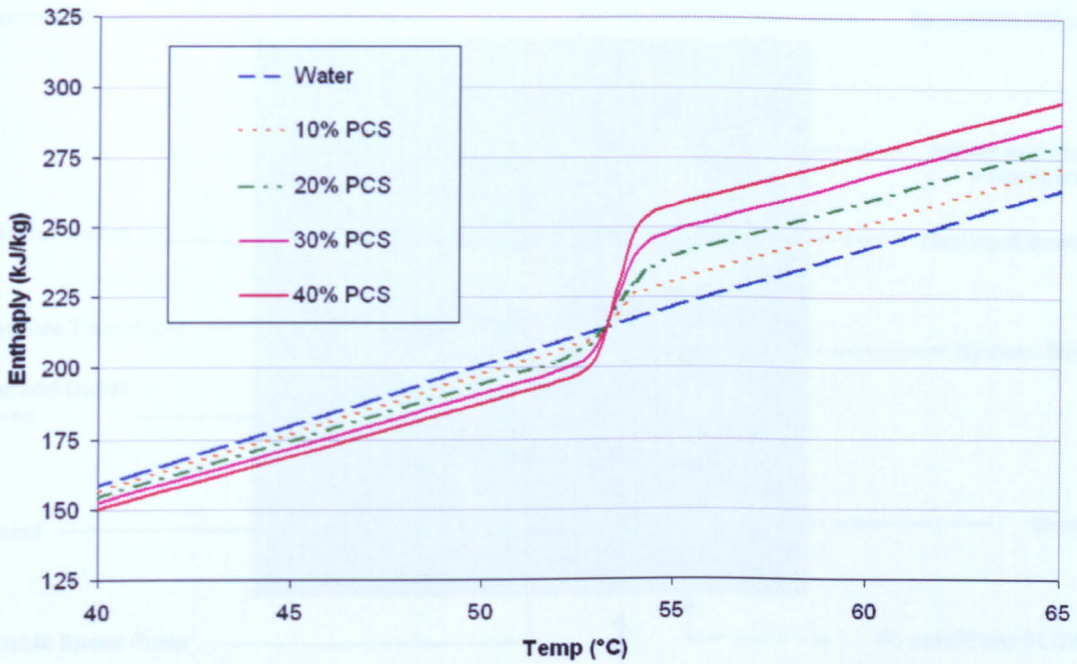


Figure 7.2: Enthalpy Curve of the French PCS with Different Concentrations of Capsules Compared with Water

## 7.2 Experimental System Design

An experimental test rig was developed to examine the microPCM Slurry in a system that simulated the operating conditions of the fuel cell. The rig consisted of three major elements, a fuel cell simulator to represent the loading to and from the fuel cell, the PCS heat transfer circuit that was made up of specialised slurry components, and a thermal load, which was either a thermal store or heat exchanger load.

### 7.2.1 Fuel Cell Simulator

It was not practical to stage initial experimental tests of the slurry within the fuel cell due to cost and technical implications. To simulate the thermal operation of the fuel cell, a separate experimental test rig was developed in collaboration with *EFC GmbH*. Figure 7.3 illustrates the fuel cell simulator (FCSim). The FCSim was designed to mimic the operational characteristics thermally from the fuel cell. It could provide constant and part load conditions. The major systems included the process technology of the water heating circuit and the control and switching system.

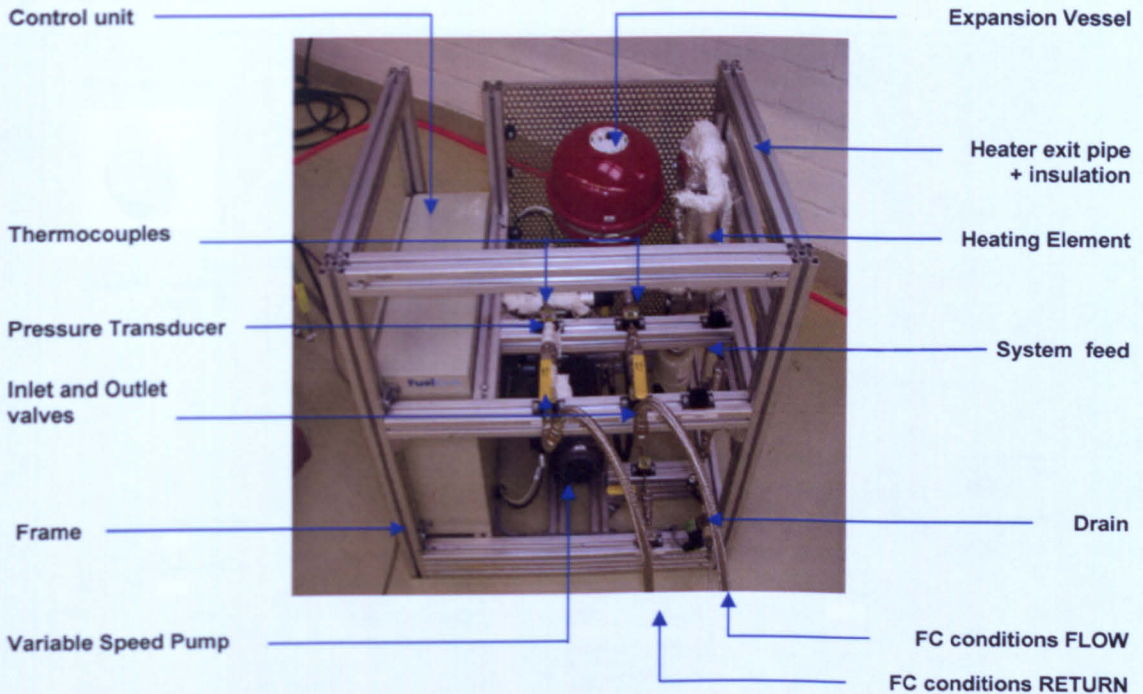


Figure 7.3: Fuel Cell Simulator

The water processing circuit was pressurised to 1.5bar and consisted of a 3kW electric heating element, pump, expansion vessel, electromagnetic flow meter, pressure transducers, actuator valves, K-type thermocouples, a breather valve and pressure release valve. See Appendices C for detailed diagrams.

A control system, user interface and control programming were developed using the computer software, LabView V7.2. This enabled automatic control of the fuel cell system via Siemens Simantic Net Software and the Siemens Program Logic Controller (PLC). Figure 7.4 illustrates the user interface that was constructed to control the FCSim. See Appendices C, for control system overview.

### 7.2.3 Data Acquisition

A Siemens PLC was used to control the system illustrated in Figure 7.3a. This controller was the same as the one used to control the actual fuel cell system. It communicated with the PC via Siemens Simantic Net software. The computer program LabView 7.2, is a powerful graphical programming language that was used to send control signals via the Simantic net software and for data acquisition.

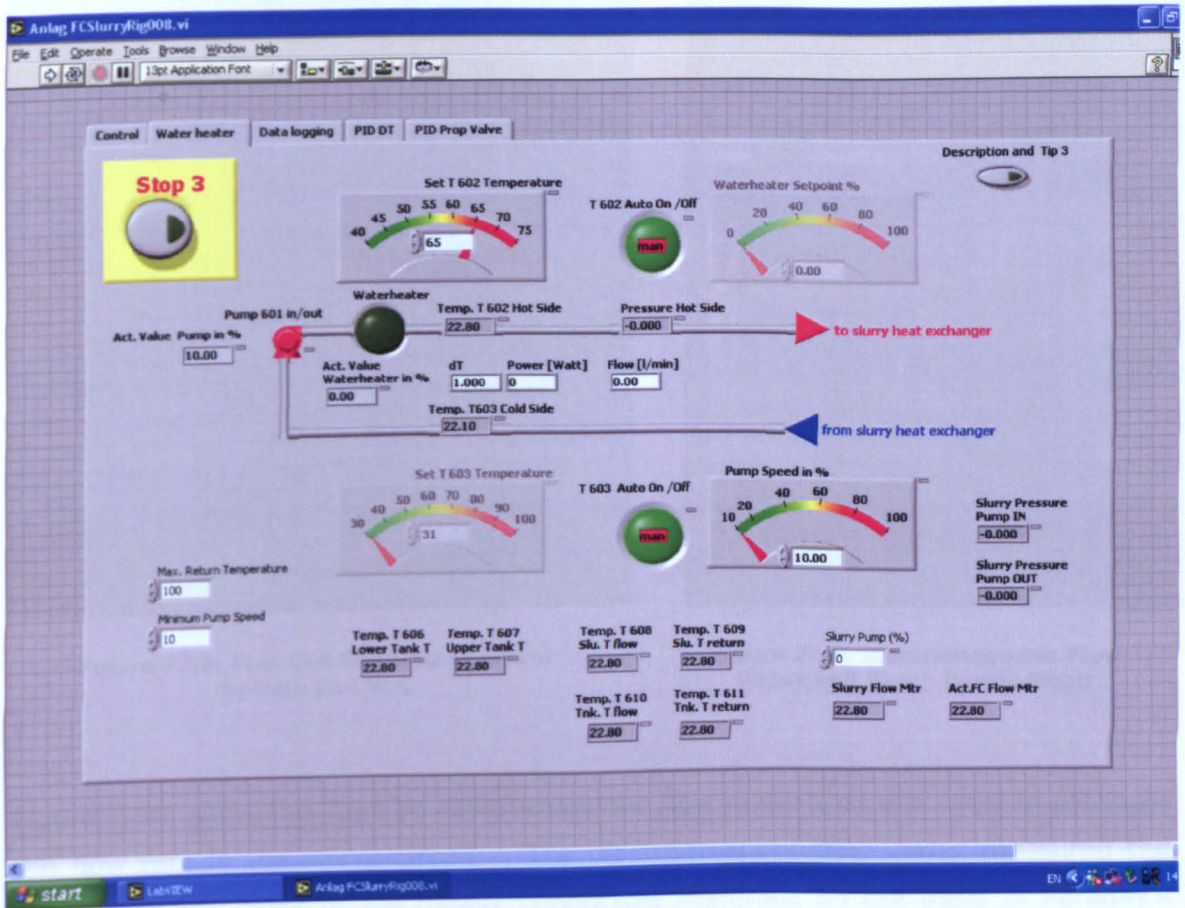


Figure 7.4: LabView 7.2 Fuel Cell Simulator User Interface

### 7.2.2 Slurry Pump

To minimise shear force on the micro-capsules, a Moyno Progressive Cavity pump was selected. It had a large pump cavity, ideal for use with high-viscosity or particulate-laden fluids. The pump delivered repeatable, pulse-less flow with no variation in fluid volume or velocity. The pump speed was controlled via a Schneider Electric speed controller and the power was monitored with a VIP ONE power meter, indicated in figure 7.5b.

### 7.2.3 Data Acquisition

A Siemens PLC was used to control the system, illustrated in figure 7.5a. This controller was the same as the one used to control the actual fuel cell system. It communicated with the PC via Siemens Simantic Net software. The computer program LabView 7.2, is a powerful graphical programming language that was used to send control signals via the Simantic Net software and for data acquisition.



**Figure 7.5a: Fuel Cell Simulator Control System and PLC**

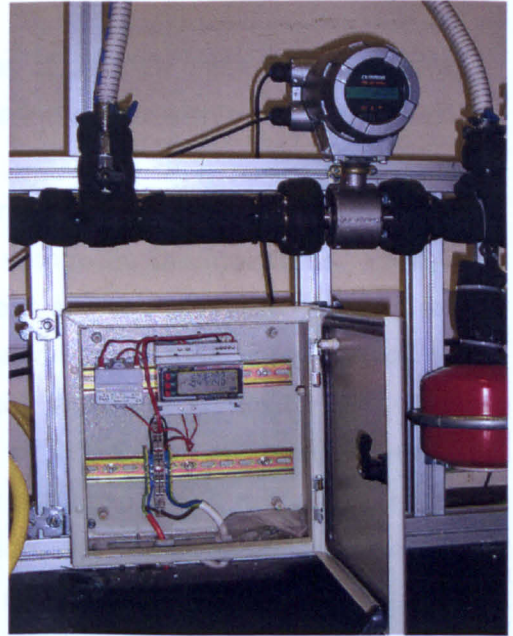


**Figure 7.5b: Electromagnetic Flow Meter and Pump Power Meter**

### 7.5 Experimental System Description

Figure 7.4 and 7.7 illustrate the schematic diagram of the experimental apparatus.

Figure 7.5b, show the Toshiba electromagnetic flow meter that was used to measure the flow rate in the slurry circuit. The electromagnetic flow meter measured the volumetric flow rates of electrically conductive materials on the basis of Faraday's Law of Electromagnetic induction. The device consisted of two units: the detector, through which the fluid to be measured flows, and the converter, which receives the electromotive force signals from the detector, then converts the signal into a 4-20mA DC signal.

Features that the flow meter had were particularly desirable to the slurry test rig.

These included:

- Fluid flow is not obstructed and pressure loss is negligible.
- The working fluid's temperature, pressure, density or flow conditions have no effect on the accuracy of the flow meter.
- The flow meter output is directly proportional to the process flow rate, thus providing an output that is easy to read.
- High accuracy,  $\pm 0.5\%$  of rate possible for 0.3-10m/s velocity range (FMG-400).
- Suitable for measurement of liquids containing solids (such as sludge or slurries).

This was enabled by signal processing capabilities of the flow meter. This ensures a stable output based on the original noise-suppression circuit within the flow meter.

Temperatures were recorded using K-Type thermocouples that were positioned at the inlet and outlet of each heat exchanger and within the thermal store. Pressures within the circuit were monitored for safety reasons and to determine pressure drops across components within the system. The pressure drops under investigation were through the slurry pump and across a 2m straight section of 20mm ID pipe. Druck pressure transmitters were used with a range of 0.1-1 bar, with an accuracy of 0.2%. The pressure transducers and flow meter produced a 4-20mA signal that was converted to data acquisition units. Calibration was undertaken based on the specifications provided by the manufacturer and calibration results were validated by using plain water.

### **7.3 Experimental System Description**

Figures 7.6 and 7.7 illustrate the schematic diagram of the experimental apparatus and view of the experimental rig. The rig consisted of two closed loop circuits, the primary Fuel Cell circuit and the Slurry circuit. The primary circuit was connected to a flat plate heat exchanger that was loaded via the FCSim loop. The slurry circuit transferred the thermal energy from the FCSim heat exchanger to either a storage vessel or a water cooled flat plate heat exchanger.

The thermal load had two modes of operation, either fed directly to a thermal storage vessel or to a separate water cooled heat exchanger. The storage vessel was connected in line, to simulate the practical situation of loading from the fuel cell and simulated the return temperatures/conditions from the store. The heat exchanger was used to set steady state conditions for analysis of heat flow between the fuel cell and the slurry loops. A bypass circuit with a 2m straight pipe test section was also included to analyse the slurry flow characteristics.

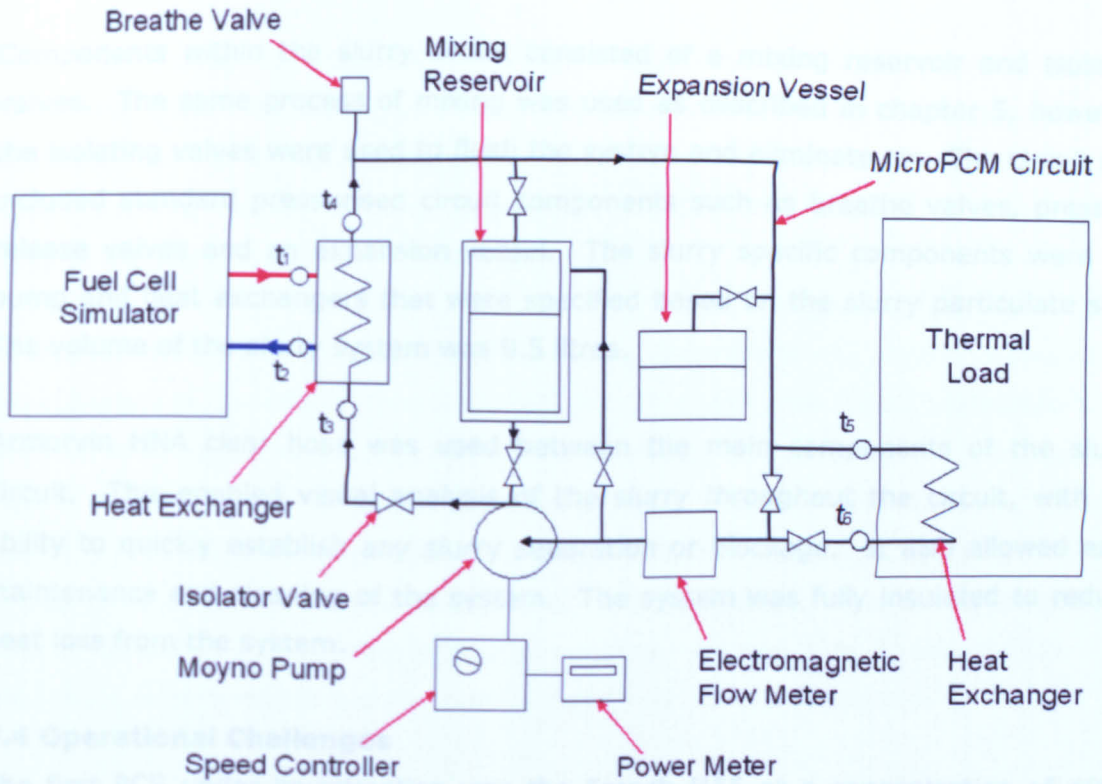


Figure 7.6: Fuel Cell Slurry Test Rig Schematic

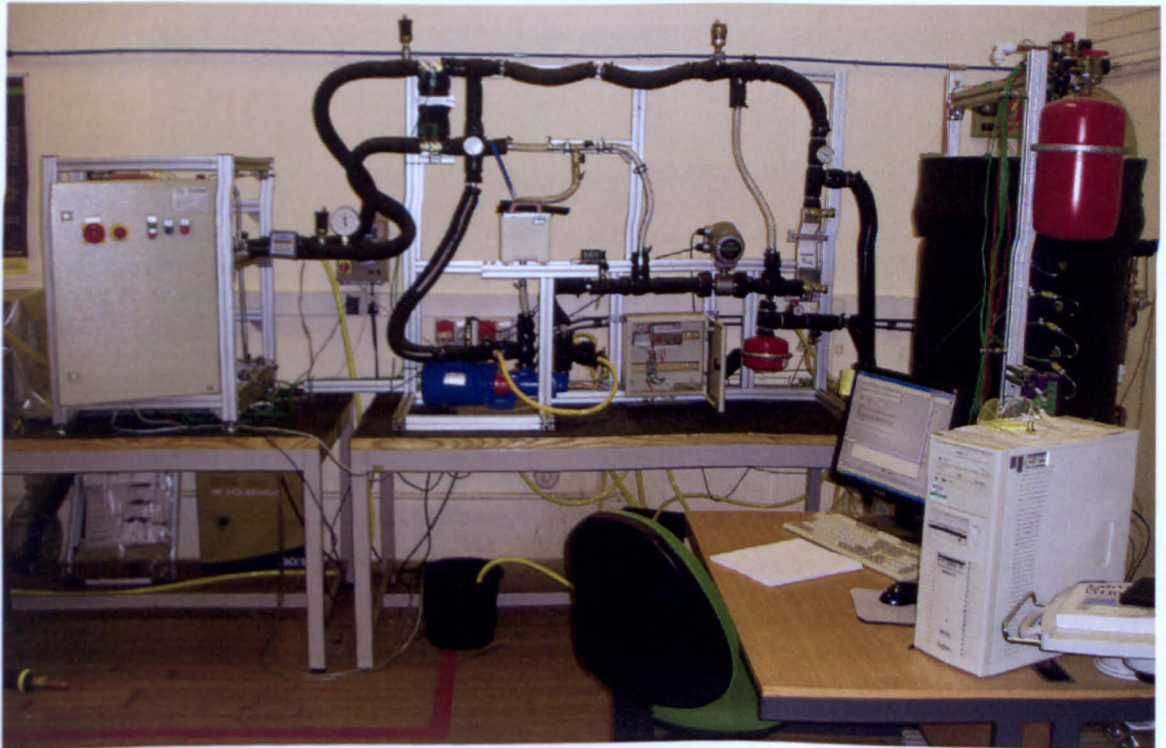


Figure 7.7: View of Fuel Cell Slurry Test Rig

Components within the slurry circuit consisted of a mixing reservoir and isolation valves. The same process of mixing was used as described in chapter 5, however, the isolating valves were used to flush the system and eliminate air. The circuit also included standard pressurised circuit components such as breathe valves, pressure release valves and an expansion vessel. The slurry specific components were the pump and heat exchangers that were specified based on the slurry particulate size. The volume of the slurry system was 9.5 litres.

Armorvin HNA clear hose was used between the main components of the slurry circuit. This enabled visual analysis of the slurry throughout the circuit, with the ability to quickly establish any slurry separation or blockage. It also allowed easy maintenance and cleaning of the system. The system was fully insulated to reduce heat loss from the system.

#### 7.4 Operational Challenges

The first PCS under investigation was the French M55 at a concentration of 40%. The aim of the test was to maximise the thermal and physical characteristics of the slurry in the circuit. Figure 7.8 pictures the M55 slurry in the test rig.



Figure 7.8: Fuel Cell Slurry Test Rig; Mixing Reservoir and Flow Meter

The French M55 showed the most favourable thermal characteristics, however physically it was less favourable, with a tendency for particulate separation when left stationary for periods of time greater than 48hrs. Previous tests with the Boolean Viscometer, revealed promising rheological characteristics at 40% concentration as long as the slurry remained agitated and active.

The preliminary thermal tests and cycling were undertaken and the M55 appeared to be operating successfully. It was heated through phase transitional temperature and showed a marginal increase in slurry flow rate due to the reduced viscosity; these results were observed in section 6, when in liquid phase. Problems occurred when the PCS was lowered in temperature down through to its solid phase. The PCS appeared to become more tacky than had previously been experienced in the solid phase. The slurry then coagulated and became un pump-able in the system. The blockages were terminal and the system had to be flushed of the slurry.

To avoid making the same mistake with the Octadecanol, a 25% concentration was used in the system to prevent agglomeration. Although the rheology studies, chapter 6, revealed that the viscosity does not significantly increase until over 40% concentration, the 25% was used to ensure some thermal and physical results were identified, and not necessarily the optimum concentration.

Thermally, the Octadecanol had reduced latent capacity compared with the French M55, however physically; it was neutrally buoyant and did not suffer from the separation and clogging tendency that the French M55 had. Therefore was expected to act more favourably in the slurry system.

The Octadecanol slurry was pumped constantly for several weeks at a range of flow rates. At a flow rate of 5lpm, this gave approx, 31.5 cycles per hour. The microPCMs showed no indication of cell degradation or agglomeration around the circuit over this period.

A further operational characteristic of the slurry was a change in system pressure dependent on the phase state of the slurry. Figure 7.9 shows a dynamic operation of the slurry rising in temperature as the thermal store reaches capacity. It indicates that when the slurry was below the phase change temperature and in solid phase,

the system pressure was 16% lower than when the slurry was in liquid phase and above the phase change temperature.

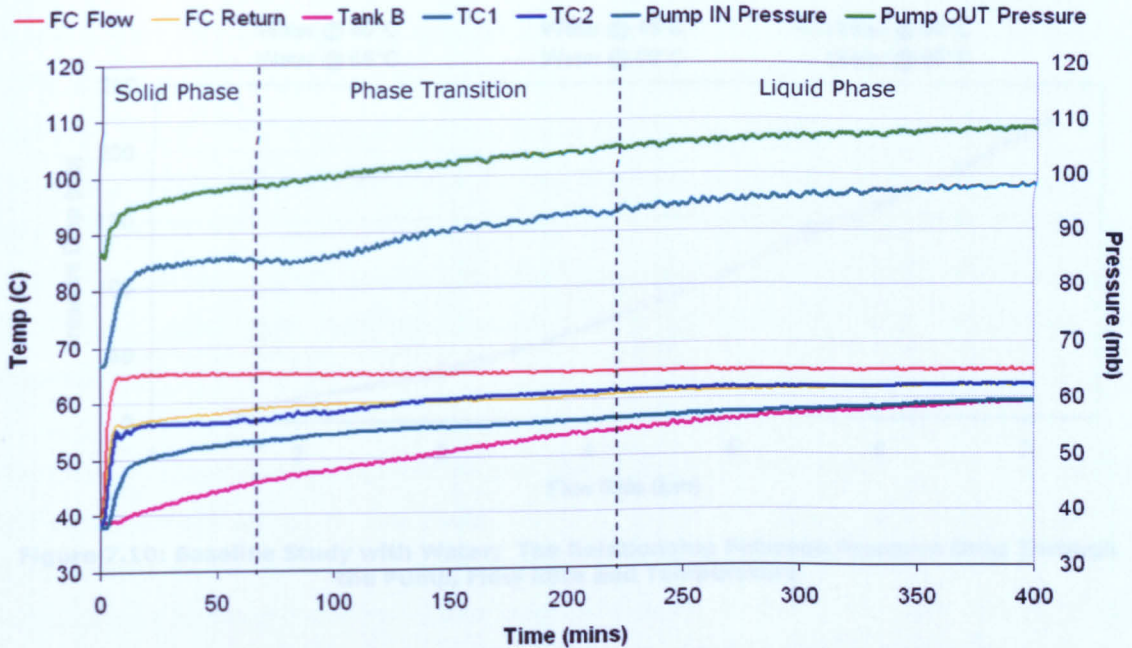


Figure 7.9: Fuel Cell Slurry System Through a Heating Phase

This increase in pressure could be accounted by the 5-15% increase in the capsule size as the PCM changed from solid to liquid state, as identified by the ESEM in chapter 4. The increase in pressure of the system would not have any implications on the pumping efficiency of the system as long as the  $dP$  across the pump remained the same. Figure 7.9 indicates that there is no significant change in the  $dP$  across the pump with the increase in pressure with temperature.

## 7.5 Pressure Drop Measurement

Tests were conducted with the Octadecanol at 25% concentration with water. To investigate the pressure loss of the PCS under both liquid and solid phase conditions, the test rig was maintained at steady state conditions and recordings were taken at ramped  $5^{\circ}\text{C}$  increments across the fuel cell operating temperature of  $40^{\circ}\text{C}$  to  $65^{\circ}\text{C}$ .

### 7.5.1 Pressure Drop Across the Pump

In order to assess the influence of the PCS on pumping and power requirements, both the pressure drop across the pump and the electrical power consumption of the pump were monitored. Initial baseline tests were conducted with water as a

comparison to the slurry. Figure 7.10 indicates the relationship between pressure drop and flow rate in relation to the temperature for the water baseline tests.

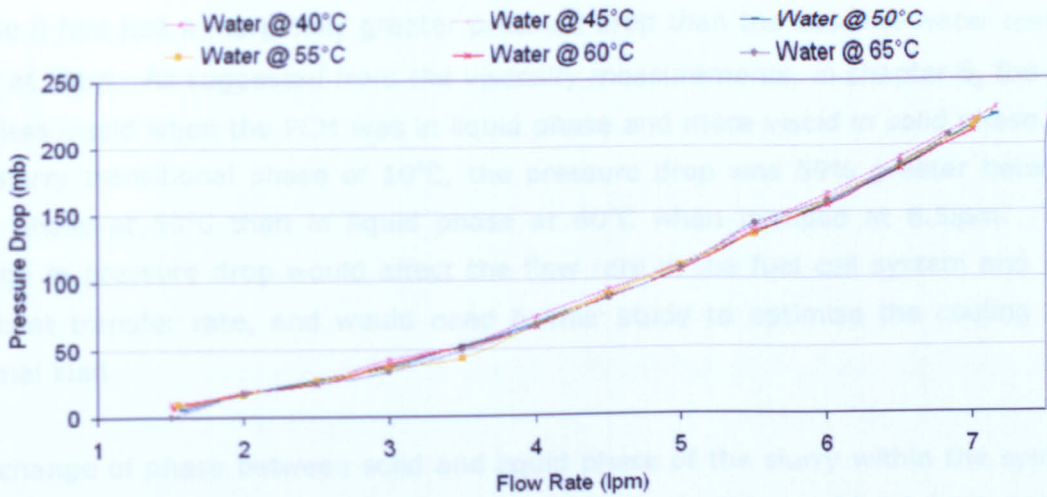


Figure 7.10: Baseline Study with Water; The Relationship Between Pressure Drop Through the Pump, Flow Rate and Temperature

figure 7.10 shows that the pressure drop through the pump increased over the range of flow rates and was independent of the water temperature. Figure 7.11 in comparison, identifies the pressure drop through the pump with the PCS at different flow rates and temperatures.

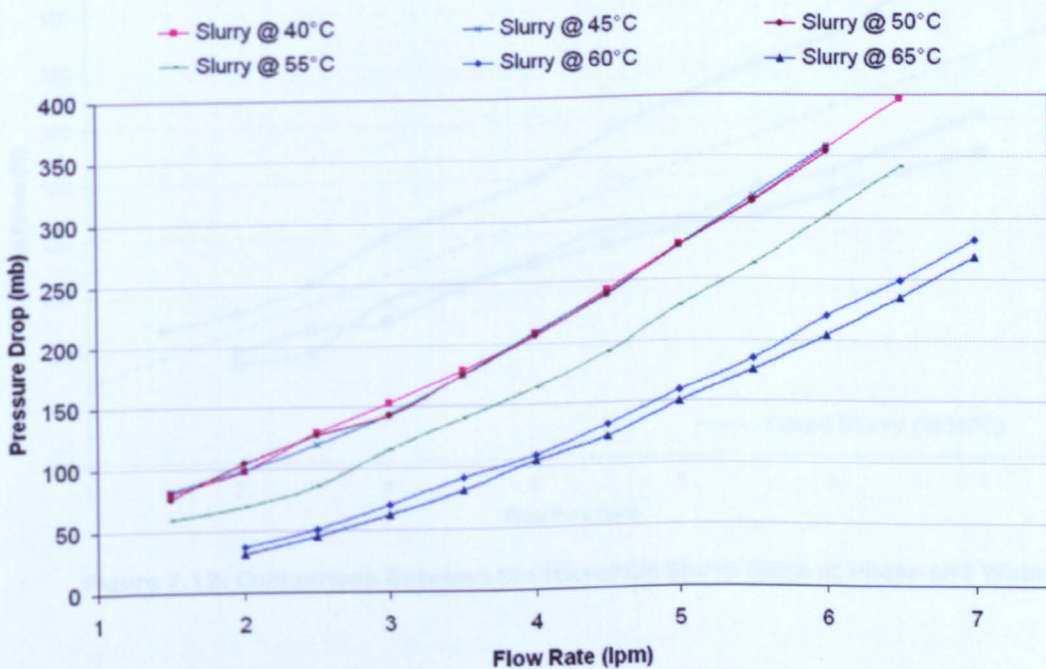


Figure 7.11: MicroPCM Slurry; The Relationship Between Pressure Drop Through the Pump, Flow Rate and Temperature

It can be seen from this figure 7.11 that the PCS follows the same gradual increase in pressure drop with flow rate, however, the PCS pressure drop was not independent of temperature. The results indicated that when the PCS was in liquid phase it had just a marginally greater pressure drop than the baseline water tests of 19% at 5lpm. As suggested from the viscosity measurements, in chapter 6, the PCS was less viscous when the PCM was in liquid phase and more viscous in solid phase. In the slurry transitional phase of 10°C, the pressure drop was 59% greater between solid phase at 50°C than in liquid phase at 60°C when pumped at 6.5lpm. This change in pressure drop would affect the flow rate in the fuel cell system and also the heat transfer rate, and would need further study to optimise the cooling and thermal load.

The change of phase between solid and liquid phase of the slurry within the system had a significant affect on the pressure drop, however, this would not have such a significant affect on the power consumption of the pump. Figure 7.12 illustrates the pump power consumption for slurry over the range of flow rates and compares the slurry in liquid phase, in solid phase and with the water baseline.

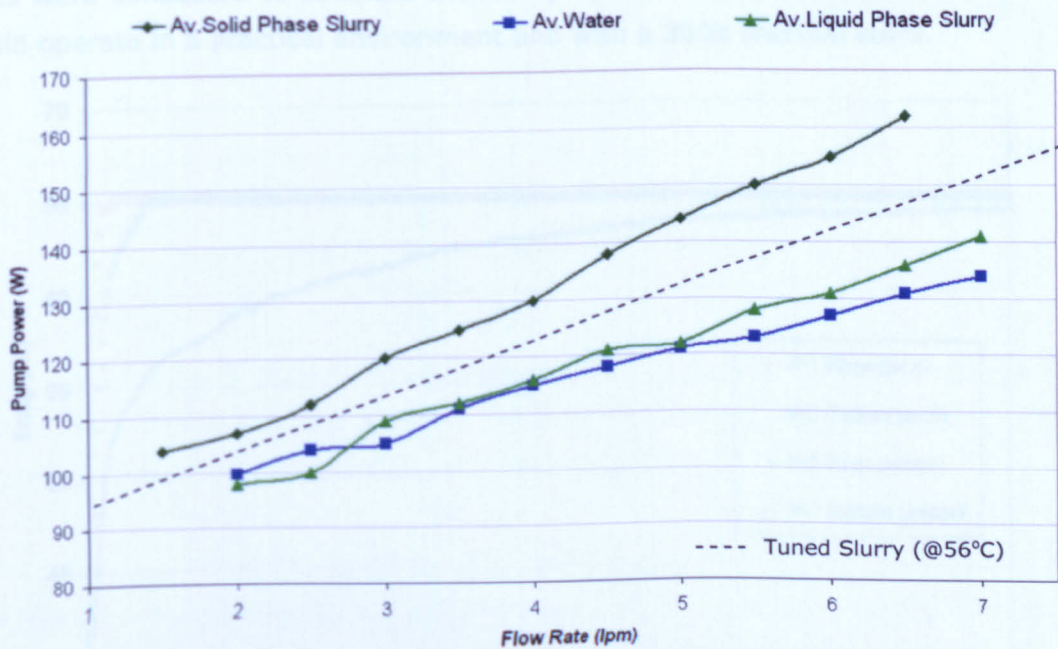


Figure 7.12: Comparison Between the MicroPCM Slurry State of Phase and Water

Between flow rates 2-5lpm the power consumption of the pump was very similar between the water and the slurry in liquid phase. Above 5lpm the liquid phase slurry consumed only marginally more power. At 6.5lpm the solid phase slurry consumed just 19% more power than the slurry in liquid phase, although having a 59% greater pressure drop. If the slurry were to operate at the lower flow rates, even at 4lpm there was only a maximum of 12% more power consumption.

the larger of T.

These results suggest also that if the thermal capacity of the slurry improves the heat transfer and can enable reduced flow rate, (as seen in chapter 5) the increased power consumption from the slurry will still be less than the equivalent water flow rate that would be required. For the power consumption to be less, the slurry must operate at between 0.5-1lpm less than the equivalent flow rate with water for the lower flow rates to save power, and at the higher flow rates (4-6.5lpm), between 1-2lpm.

## 7.6 Thermal Characteristics

### 7.6.1 FC Operation

Tests were conducted to simulate the slurry operation with the fuel cell and how it would operate in a practical environment and with a 300lt thermal store.

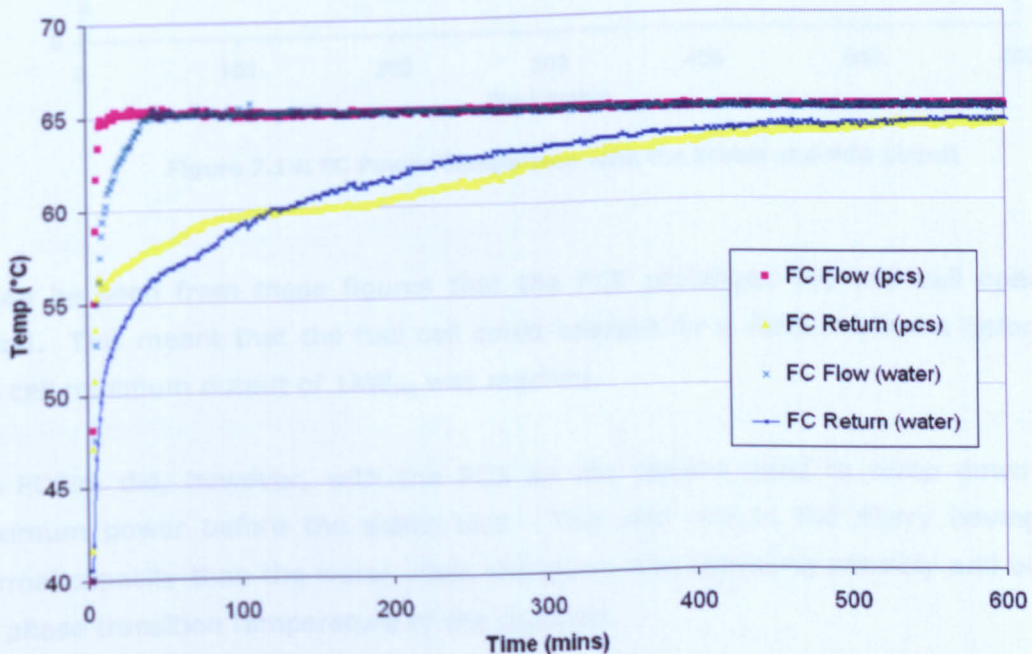


Figure 7.13: FC Simulator Flow and Return Temperatures with the Thermal Store

Figures 7.13 and 7.14 show the temperature and the power output of the fuel cell through a typical charge period. Figure 7.13 indicates the primary heating loop of the fuel cell and the relative flow and return temperatures when heating the thermal store. Two conditions are identified, the flow and return temperatures for the fuel cell loading when water was used as the heat transfer compared with the use of the PCS. The PCS was heated up more rapidly initially due to less sensible capacity over the larger  $\Delta T$ .

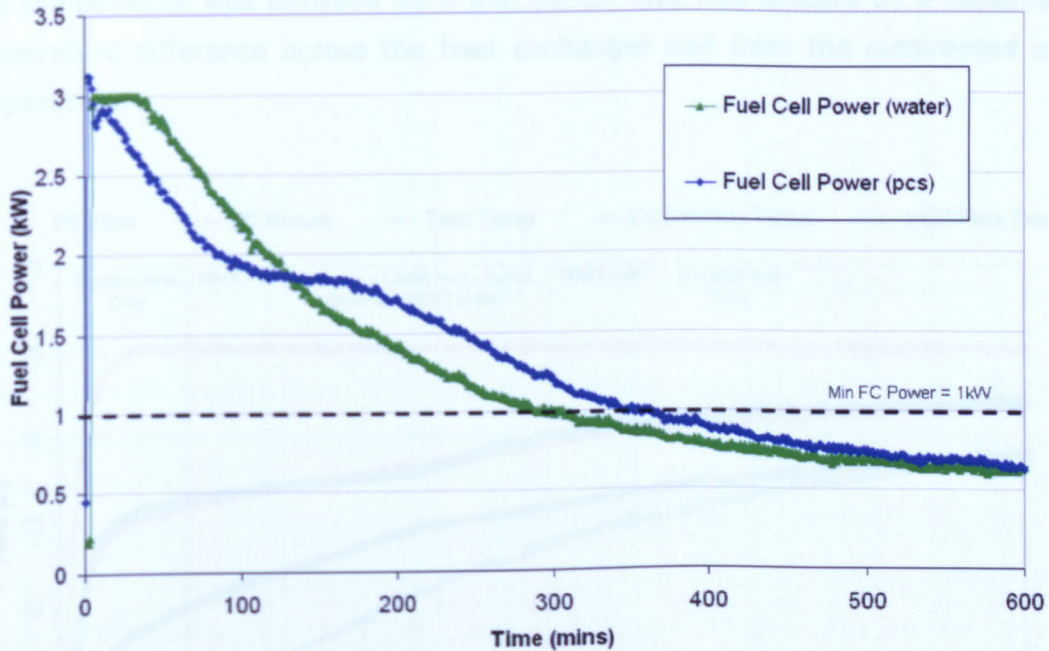


Figure 7.14: FC Power Comparison with the Water and PCS Circuit

It can be seen from these figures that the PCS prolonged the fuel cell operation period. This meant that the fuel cell could operate for a further 69mins before the fuel cell minimum output of  $1\text{kW}_{\text{TH}}$  was reached.

The FCSim did, however, with the PCS as the coolant need to ramp down from maximum power before the water test. This was due to the slurry having less thermal capacity than the water when the slurry was operating sensibly and outside the phase transition temperature of the capsules.

### 7.6.2 Tuning the Fuel Cell and Slurry

It was clear from the early tests with the fuel cell and thermal store that the current method of transferring the heat from the fuel cell to the thermal store was not maximising the latent capacity of the PCS. This was because the mean bulk temperature of the PCS was significantly below or above the peak phase change temperature of the PCS. Figure 7.15, demonstrates a typical loading profile of the thermal store and corresponding FCSim and PCS temperatures. The PCS temperature profile indicates that PCS was tuned to the system when the mean bulk fluid temperature was between 53°C and 58°C. This was evident by a reduction in temperature difference across the heat exchanger and from the suppressed outlet temperature.

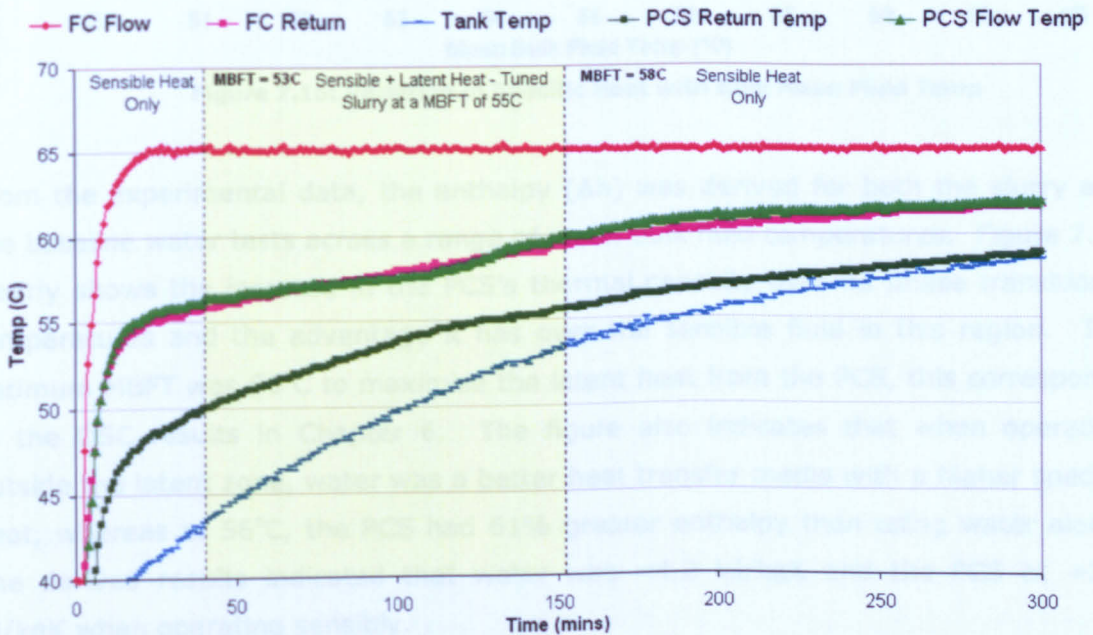


Figure 7.15: Variation in System Temperatures with the PCS

When the MBFT of the PCS increased above 58°C, it showed no latent heat of fusion. This can also be seen in figure 7.16, that shows the derived specific heat of the PCS in comparison with the tests with baseline water study.

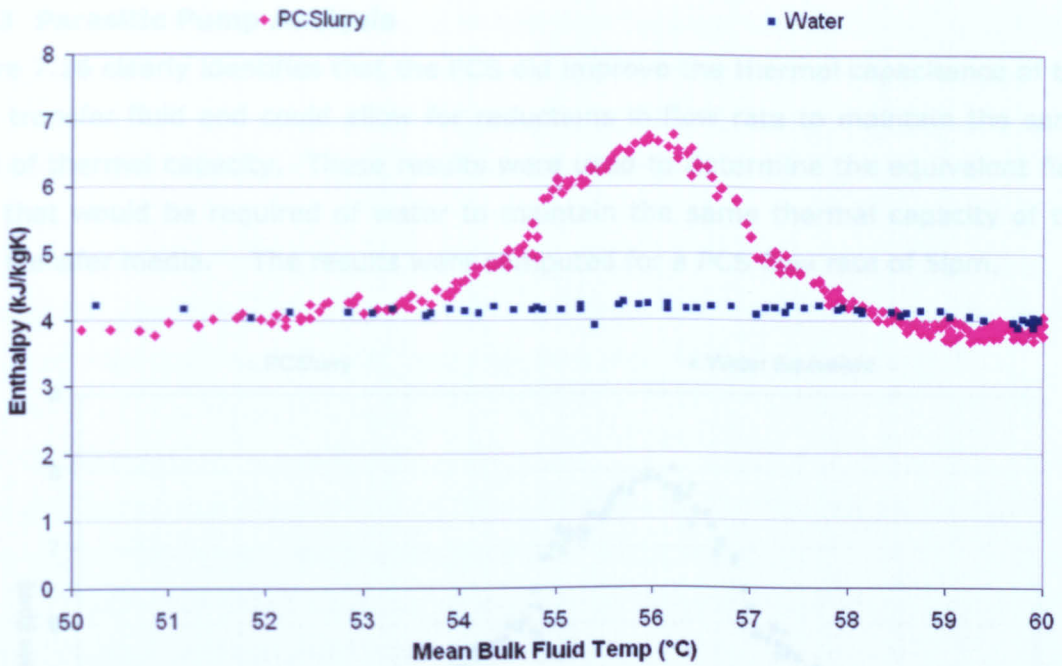


Figure 7.16: Variation in Specific Heat with Bulk Mean Fluid Temp

From the experimental data, the enthalpy ( $\Delta h$ ) was derived for both the slurry and the baseline water tests across a range of mean bulk fluid temperatures. Figure 7.16 clearly shows the increase in the PCS's thermal capacity over its phase transitional temperatures and the advantage it has over the sensible fluid in this region. The optimum MBFT was  $56^{\circ}\text{C}$  to maximise the latent heat from the PCS, this corresponds to the DSC results in Chapter 6. The figure also indicates that when operating outside the latent zone, water was a better heat transfer media with a higher specific heat, whereas at  $56^{\circ}\text{C}$ , the PCS had 61% greater enthalpy than using water alone. The derived results indicated that water was  $\sim 4.2$  kJ/kgK and the PCS at  $\sim 3.9$  kJ/kgK when operating sensibly.

For integration of the PCS into the real FCS, the BMFT across the heat exchanger that corresponded to the peak phase change temperature would need to be maintained. This could be done with a controlled variable pump, and combined with a control program that adjusts the flow rate dependent on the required heat transfer rate and inlet and outlet temperatures.

### 7.6.3 Parasitic Pump Analysis

Figure 7.16 clearly identifies that the PCS did improve the thermal capacitance of the heat transfer fluid and could allow for reductions in flow rate to maintain the same level of thermal capacity. These results were used to determine the equivalent flow rate that would be required of water to maintain the same thermal capacity of the heat transfer media. The results were computed for a PCS flow rate of 5lpm.

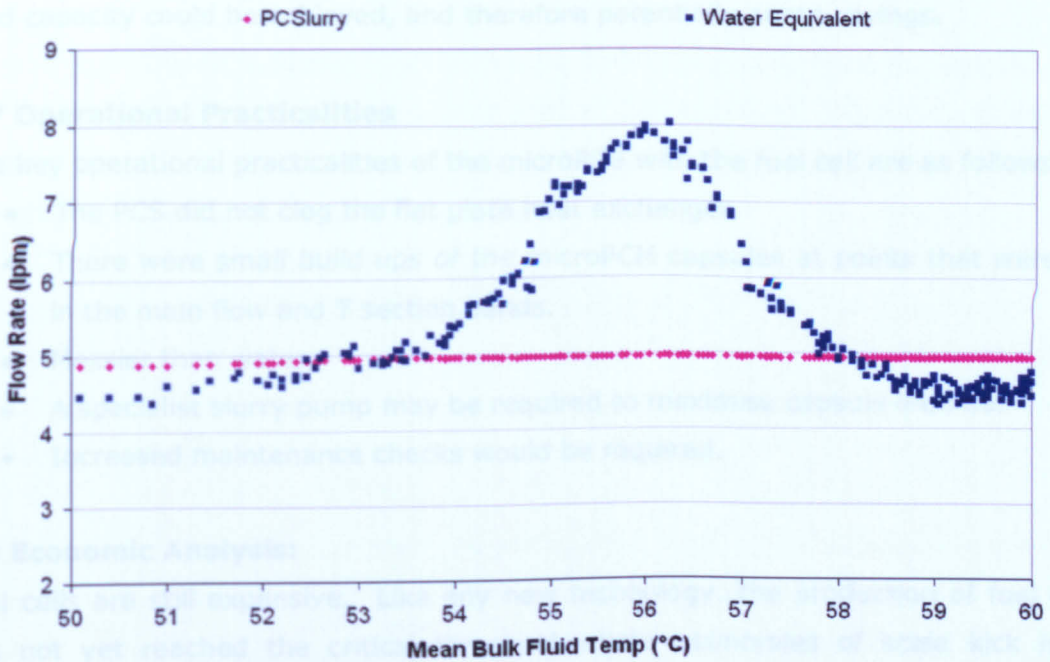


Figure 7.17: Equivalent Flow Rate Estimate

Figure 7.17, shows that when the PCS was operating at a MBFT of 56°C, the equivalent flow rate for water was at 8lpm – a 3lpm saving on pump power. The following table correlates the saving in flow rate with the equivalent pump power experiments in figure 7.12.

Mean Bulk Fluid Temp (°C)	Equivalent Water Flow Rate(lpm) to 5lpm PCS	Additional Flow Rate (lpm)	Pump Power Savings (W)
54	5.2	0.2	-8
55	7.0	2	-2
56	8	3	7
57	6.2	1.2	-5
<b>58</b>	5	0	-13

Table 7.1: Equivalent Flow Rate Estimate

The table shows that the difference in flow rate between the water and PCS was not great enough to overcome the increase in power consumption of the pressure drop from the slurry for most of the BMFT examined. The only exception was the optimum MBFT which had a marginal pump saving of 7W.

If the specific heat of the Octadecanol was increased to the same as the French M55 and/or the agglomeration problem with the French M55 was solved, greater thermal fluid capacity could be achieved, and therefore potentially pump savings.

### **7.7 Operational Practicalities**

The key operational practicalities of the microPCS with the fuel cell are as follows;

- The PCS did not clog the flat plate heat exchanger.
- There were small build ups of the microPCM capsules at points that were not in the main flow and T section bends.
- Messier than water.
- A specialist slurry pump may be required to maximise capsule lifetime.
- Increased maintenance checks would be required.

### **7.8 Economic Analysis:**

Fuel cells are still expensive. Like any new technology, the production of fuel cells has not yet reached the critical threshold where economies of scale kick in to significantly reduce the cost per manufactured unit. In comparison, however, the microPCMs developed in this investigation are currently relatively cost effective. Dependent on the costing of the PCM used for encapsulation, CISASC have confirmed that the price of the microPCM was ~£3 per Kg. In a fuel cell system containing 10lts of MicroPCM slurry at 30% concentration, the total additional cost would be just £9 compared to using water alone.

The additional cost of the slurry would be significantly offset with the use of smaller heat exchangers, which are relatively high cost components. Further analysis is required on the additional costings associated with the use of different types of pumping devices or components to prevent agglomeration.

This suggests that the small additional cost of the microPCM may be offset from the reduced costs of using smaller system components such as heat exchangers.

### **7.9 Concluding Remarks**

The present study investigated the performance of the fuel cell and phase change slurry. The fuel cell simulator was developed to mimic the fuel cell thermally and a 25% concentration of the Octadecanol PCM was successfully integrated.

The first experiments with the French M55 failed due to the high concentration, 40%, resulting in agglomeration and pipe blockage.

Results from the Octadecanol PCS indicated that the gain in thermal capacity with the PCS over using water was equal to that of the measured additional pump load from this slurry at 25%. An increase in the slurry thermal capacity in the lab, suggests that pump savings could be achieved.

The key points thermally from this study were; that the MBFT of the thermal fluid should be equal to that of the PCS peak phase change temperature. A thermal capacity from the Octadecanol PCS was 56% greater than water when operating in the tuned temperature band.

The key physical practicalities from the study were; That a compromise was required between PCS concentration, the relative pressure drop and the stability of the particles within the system. Particle agglomeration and capsule durability require further development for long term use in the fuel cell. The change of phase within the microcapsules causes differences in system pressure.

For the PCS to be commercially feasible with the Fuel Cell, it must be 100% reliable. It is competing against water, which is cheap, trustworthy and reliable. The PCS adds complexity to the system and the pump savings and thermal stability have to be significantly better. Currently, with the developed PCS, this was not the case, and would not aid the fuel cell system. These problems, however, could be overcome with further development of the microPCM and system components. The PCS does show potential to improve heat transfer and reduce the  $\Delta T$  across the fuel cell. The PCS could also reduce pumping loads and improve the overall system electrical efficiency and cost.

## **Chapter 8: Conclusions + Further Work**

### **8.0 Conclusions**

This thesis established that the fuel cell industry is currently “searching for methods of stabilising thermal conditions across the fuel cell” (Dr.Du, Plugpower, 2005). This was primarily to make water production within the stack more predictable and uniform. To this end; a functionally thermal fluid was developed to stabilise the temperature difference across the stack, and further, to reduce parasitic pumping loads to improve the overall electrical efficiency of the fuel cell system.

The feasibility of using a functionally thermal fluid within a fuel cell to enhance its performance was assessed. A fluid was developed that was specific to the fuel cell operating conditions, and over this temperature range, it had a greater enthalpy compared with that of water. Whilst thermally it was favourable, it still had some inherent challenges in its physical stability that must be overcome for it to be successfully integrated with the fuel cell. At this stage of its development, it proved less reliable than using water alone.

A series of studies were performed, including testing and analysis of the PEM fuel cell. An evaluation and literature study of functionally thermal fluids was undertaken, resulting in particular focus on microPCSs. These fluids could use the latent heat of fusion to store and release greater amounts of energy across a smaller temperature difference than other sensible fluids could.

In the limited time available, there was complete redesign and development of a new microPCM that was tuned to the fuel cell operating conditions. This development included material selection, encapsulation technology, material evaluation and finally system integration.

From the encapsulation development, two positive candidate microPCMs were selected to be experimentally evaluated in the fuel cell system. They displayed inherent strengths and weaknesses. One was stronger thermally, yet displayed weaker physical characteristics of separation and clogging (French composite), and the other, stronger physically, remaining colloidal and mixed, yet thermally weaker (Octadecanol).

A purpose built fuel cell test rig was constructed to experimentally evaluate the developed microPCMs. Agglomeration issues were experienced with the French composite at 40% concentration that resulted in the system clogging and becoming blocked. The Octadecanol slurry, however, at 25% concentration proved to operate well in the fuel cell test rig. Small pump savings of 7W were achieved compared with using water alone at the equivalent heat transfer at a higher flow rate. More significant savings could be achieved if the increase in pump load from the slurry was reduced. One suggestion for achieving this is to use a surfactant to reduce the viscosity of the slurry.

Whilst significant pump savings were not achieved compared with water at higher flow rates, the thermal capacity of the thermal fluid was increased and flow rates were reduced. The increase in thermal capacity of the PCS and associated pumping resistance was equal to the thermal capacitance of water with a comparable pump power at a greater flow rate.

This study suggested that pump savings could be achieved with further development of the microPCM slurry. The slurry has the potential to be improved with more development both thermally and physically. It also showed that the temperature difference across heat exchangers could be reduced with this type of functionally thermal fluid that incorporated the latent heat of fusion. This could potentially revolutionise the structure of the PEM fuel cell stack.

By studying and analysing the different aspects of the fuel cell and microPCM slurry, a better and deeper understanding of the operation and mechanics involved was gained. The main findings are translated in to the following conclusions and suggestions for further work.

Specifically, the following conclusions are presented:

- Fuel Cell experimentation identified a requirement for improved thermal stability across the stack and reduced parasitic pumping loads to improve the overall performance and electrical efficiency.
- The fuel cell stack indicated that isothermal conditions across the cells produced as a results of the PCS could have significant effects on their future design and performance.
- Thermal characterisation of microPCM slurries can be performed using Differential Scanning Calorimetry (DSC). DSC aided the determination of

the specific heat, latent heat of fusion, and melting and solidification temperature of the microPCMs developed and examined.

- The ESEM analysis visually tracked the phase transition of microPCM and identified a capsule volume increase of 5-15%.
- Heat transfer experimentation showed that the heat capacity enhancements of the PCS are considerable even at low mass fractions.
- Two promising PCMs were selected and developed as a potential PCS for use with the fuel cell.
- The thermally functional fluid could reduce the temperature difference across a heat exchanger and increase heat input.
- Reducing the effect of supercooling within the microPCM will reduce the melt range of the PCM.
- The implications of reducing the melt range of the microPCMs are; improved heat transfer by maintaining a greater temperature difference, stable tank temperature and therefore greater storage capacity.

### **8.1 Further Work:**

Further studies should focus on the following areas:

- Identification of microPCM capsule durability and ability to withstand harsh environments.
- Maintenance of neutral stability of the particles in the carrier fluid through the balance of material and liquid densities. This could be achieved using material such as silica to increase the density of the microcapsule and/or using a water glycol mix to increase the density of the carrier fluid.
- Identification of combinations of phase change materials and nucleating agents to maximise the thermal capacity and suppress the supercooling phenomenon.
- Identification and testing of heat exchanger systems that can enhance the microPCM heat transfer coefficient.
- Further evaluation of the potential and practicalities of using a microPCM with a fuel cell.
- Evaluation of the performance of microPCM slurries with other positive displacement and kinetic type pumps.
- Evaluation of component abrasion or wear from the use of particulate flow.

To further address the issue of temperature stability across the fuel cell stack, other techniques to achieve *isothermal conditions* could be pursued. This may include the use of alternative technologies such as heat pipes.

MicroPCM slurries and functionally thermal fluids have the potential to become *effective heat transfer fluids* in not only fuel cells, but in a wide variety of applications that require enhanced heat transfer *and have a small temperature difference*. Enhanced heat capacity of the microPCM slurries proves to be the best attribute as it can provide additional thermal capacity even at low mass fraction. Further research is needed, however, to be able to fully exploit its potential and to produce a reliable heat transfer fluid for the fuel cell.

## **References**

Abe, Y., Y. Takahashi, M. Sakamoto, K. Kanari, M. Kamimato, T. Ozawa, Charge and discharge characteristics of a direct contact latent thermal energy storage unit using form-stable high-density polyethylene, *J. Solar Energy Engng* 106 (1984) 465±474.

Abhat, A., Performance studies of a finned heat pipe latent heat thermal energy storage system. *Mankind's Future Source of Energy* , 1978, 1, 541-546.

Abhat, A., Low temperature latent heat thermal energy storage: Heat storage materials, *Solar Energy* , 1982, 30 (4), 313-332.

Abhat, A and Huy, T. Q, Heat and mass transfer considerations in a thermo-chemical energy storage system based on solid-gas reactions, *Solar Energy*, Volume 30, Issue 2, 1983, Pages 93-98.

Aboul-Enein, S., and Olofa, S, Thermophysical properties of heat-of-fusion storage materials for cooling applications, *Renewable Energy*, Volume 1, Issues 5-6, 1991, Pages 791-797.

Amplett, J.C., R.M. Baumert, R.F. Mann, B.A. Peppley, P.R. Raberge, and T.J. Harris. Performance modeling of the Ballard Mark IV solid polymer electrolyte fuel cell: I. Mechanical model development. *Journal of Electrochemical Society*, 1995. 142(1):1-15

Augood, P.C., M. Newborough, D.J. Highgate. Thermal behaviour of phase-change slurries incorporating hydrated hydrophilic polymeric particles. *Experimental Thermal and Fluid Science* 25 (2001) 457-468.

Ballard, 2005. Fuel cell technology 'roadmap', Available online at [http://www.ballard.com/be\\_informed/fuel\\_cell\\_technology/roadmap](http://www.ballard.com/be_informed/fuel_cell_technology/roadmap).

Banaszek. J., R. Domanski, M. Rebow, F. El-Sagier, Experimental study of solid-liquid phase change in a spiral thermal energy storage unit, Institute of Heat Engineering, Warsaw University of Technology, Warsaw, Poland. 1990.

Bellas. J, Chaer. I, and Tassou. S. A, Heat transfer and pressure drop of ice slurries in plate heat exchangers, *Applied Thermal Engineering*, Volume 22, Issue 7, May 2002, Pages 721-732.

Bernardi, D.M., and M.W Verbrugge. A mathematical model of the solid-polymer-electrolyte fuel cell. *Journal of Electrochemical Society*, 1992. 139(9):2477-2490.

Blawdziewicz, J. Structure and transport properties of colloidal suspensions in stationary shear flow. *CISM Courses and Lectures: Flow of Particles in Suspensions*, Italy: Springer Wien New York, 1996, 1-39.

Bo-Geng Li., et al., Micron-size uniform poly(methyl methacrylate) particles by dispersion polymerization in polar media. IV. Monomer partition and locus of polymerization, *Colloids and Surfaces A: Physicochemical and Engineering Aspects*, Volume 153, Issues 1-3, 15 August 1999, Pages 179-187.

Broka, K., and P. Ekdunge. Modelling the PEM fuel cell cathode. *Journal of Applied Electrochemistry*, 1997, 27(3):281-289.

Burns, P., Survey of thermal storage systems relevant to solar air heating: A review, *BHRA Project RP 21666* , 1981, 35.

Charunyakorn, P. Forced convection heat transfer in microencapsulated phase change material slurries: flow in circular ducts. *International Journal of Heat and Mass Transfer* , 1991, 34 (3), 819-833

Chen. K., Chen, M.M. An analytical and experimental investigation of the convective heat transfer of phase change suspension flows. *In proc. Of the International Symposium on Multiphase Flow (II)*, Zhejiang University Press, 1987, Vol. 2, pp. 496-501.

Chen, S.L and Chen, C.L. Effect of nucleation agents on freezing probability of supercooled water inside capsules. *HVAC&R Research*, Oct 1999, Vol. %, No. 4, pp. 339-351.

Choi, E. Cho, Y.I and Lorsch, H.G. Forced convection heat transfer with phase change material slurries: turbulent flow in a circular duct. *Int. J. Heat and Mass Transfer*, 1994, Vol. 37, no.2, pp. 207-2215.

Cibasc, M. Butters. *Internal Report*, CIBA Specialty Chemicals, (2005).

Colvin, D.P., J.C. Mulligan and Y.G. Bryant, Use of Two-Component Fluid of Microencapsulated PCM for Heat Transfer in Spacecraft Thermal Systems," with AIAA/ASME 6<sup>th</sup> Joint Thermophysics and Heat Transfer Conference, Colorado Springs, CO, AIAA Paper No. 94-2004, June 1994.

Colvin, D.P., J.C. Mulligan and Y.G. Bryant, Microencapsulated Phase-Change Material Suspensions for Heat Transfer in Spacecraft Thermal Systems. *Spacecraft and Rockets* Vol. 33, No.2, 1987.

Colvin, D.P., J.C. Mulligan, Y.G. Bryant, J.L. Duncan and B.T. Gravely. Microencapsulated PCM Slurries for Heat Transfer and Energy Storage in Spacecraft Systems. *Space Nuclear Power Systems*, 1989.

Colvin, D.P. and Mulligan, J.C. (1990) Method of using a PCM Slurry to Enhance Heat Transfer in Liquids, U.S. Patent 4911232.

Colvin, D.P., J.C. Mulligan, and Y.G. Bryant. (1993) Enhanced Heat Transport in Environmental Systems Using Microencapsulated Phase Change Materials. 22<sup>nd</sup> ~ Conference on Environmental Systems. SAE Paper 921244.

Daimler-Chrysler Multiphase Suspension Coolant (Pat; WO2004009728)

Danilatos, theory of the gaseous detector device in electron scanning electron microscope. *Advances in Electronics and Electron Physics*, 78:1-102 (1990)

Dittus. F and L. M. K. Boelter, *Univ. Calif. Publ. Eng.* 2, 443 (1930)

DomanÄski, R., M. Jaworski, M. Rebow, Thermal energy storage problems, Bulletin Institute Technical, Ciepłnej, Politechniki Warszawskiej 79 (1993) 231±255.

DTI, *UK Energy in brief 2000* (online), Available at <http://www.dti.gov.uk>, July 2003

Egolf, P. W., O. Sari, 2002. A Review from Physical Properties of Ice Slurries to Industrial Ice Slurry Applications. International Energy Agency, Annex 17, Advanced Thermal Energy Storage Techniques Through Application of Phase Change Materials and Chemical Reactions. Expert Meeting and Workshop, 2-5 April, Ljubljana, Slovenia.

Egolf, P.W., O. Sari, A. Kitanovski, D. Vuarnoz, 2003. Thermal Energy Storage with Phase Change Slurries. 9th International Conference on Thermal Energy Storage, Warsaw, Poland, September 1-4, 285-290.

Eikerling, M., Y.I. Kharkats, A.A Kornyshev. And Y.M Volfkovich. Phenomenological theory of electro-osmotic effect and water management in polymer electrolyte proton-conducting membranes. Journal of Electrochemical Society, 1998, 145(8): 2684-2699.

Ellis, 2002. 'Fuel Cells for Building Applications'. American Society of Heating, Refrigeration and Air-Conditioning Engineers, Inc.

EPS, *Plus-Ice Thermal Energy Storage Design Guide* , UK, 1996

FMG-400, User Guide for the FMG-400's Electromagnetic FLOWmeters (Flange type), [www.omega.com](http://www.omega.com).

Frisby, *Microencapsulated phase change materials* (online), Available at <http://www.frisby.com>, October 2002.

Fuller, T.F., and J Newman. Water and Thermal management in solid-polymer-electrolyte fuel cells. Journal of the Electrochemical Society, 1993, 140(5):1218-1225

Garg, H.P., S.C. Mullick, A.K. Bhargava, Solar thermal energy storage. Reidel, Dordrecht, 1985.

Gibbs B. and Hasnain S. DSC study of technical grade phase change heat storage materials for solar heating applications. *Proceedings of the 1995 ASME/JSME/JSEJ International Solar Energy Conference* , 1995, Part 2.

Goel, Manish. Laminar forced convection heat transfer in microencapsulated phase change material suspensions. *International Journal of Heat and Mass Transfer* , 1994, 37 (4), 593-604

Gschwander, S., P. Schossig and H.-M Henning. Micro-encapsulated paraffin in phase-change slurries. *Solar Energy Materials and Solar Cells*, 2004.

Gurau, V., H. Liu, and S.Kakac. Mathematical model for proton exchange membrane fuel cells. In *Proceedings of ASME Advanced Energy Systems Division*, 1998. Vol. 38, pp. 205-214.

Hale, D.V., Hoover, M.J., and O'Neil, M.J., "Phase Change Materials Handbook", NASA Contractor Report CR-61363, 1971.

Hao, Y. L., and Y.X. Tao. A numerical model for phase-change suspension flow in microchannels. *Numerical Heat Transfer, Part A*, 46:55-77, 2004.

Hard, K.D., S.Riffat and R.W. Wilson, (2004), *MicroPCM Slurry for a PEM Fuel Cell Thermal System*. 3<sup>rd</sup> International Conference on Sustainable Energy Technologies, Nottingham, UK

Hard, K.D., 2004. ISET Masters course laboratory worksheet. Nottingham, UK

Hariri, A.S. and Ward, I.C. A review of thermal storage systems used in building applications. *Building and Environment* , 1988, 2 (1), 1-11

Hawladar, M.N.A., M.S. Uddin, and M.M. Khin. Microencapsulation of Phase Change Materials. Paper #349. National University of Singapore.

Hayes, L.J., E.H. Wissler, D.P. Colvin. A Models for Encapsulated Phase Change Material in a Conductive Media.

M.Heuer, K.Leschonski, Results obtained with a New Instrument for the Measurement of Particle Size Distributions from Diffraction Patterns; Part. Characters. 2; 7-13 (1985)

Himran, S., A. Suwono, A. Mansoori, Characterisation of alkanes and paraffin waxes for application as phase change energy storage medium, *Energy Sources* 16 (1994) 117±128.

Hirschenhofer, J.H., Stauffer, D.B., Engleman, R.R., and Klett, M.G. 1998. *Fuel Cell Handbook* (4th ed.). U.S. Department of Energy, Office of Fossil Energy, Federal Energy Technology Center: Morgantown, VA

Humphries, W.R., and Griggs, E.I., "A Design Handbook for Phase Change Thermal Control and Energy Storage Devices", NASA Technical Paper 1074,

Inaba, H. New challenge in advanced thermal energy transportation using functionally thermal fluids. 2000 Editions scientifiques et medicales Elsevier SAS, 2000.

Inaba, H., C.Dai, A. Horibe. Natural convection heat transfer of microemulsion phase-change-material slurry in rectangular cavities heated from below and cooled from above. *International Journal of Heat and Mass Transfer* 46 (2003) 4427-4438.

Jahns, E. Microencapsulated Phase Change Material. BASF AG.

Kasza, E and Chen, M.M. Improvement of the performance of solar energy or waste heat utilisation systems by using phase change slurry as an enhanced heat transfer storage fluid. *Journal of Solar Energy Engineering* , 1985, 107, 229-236

Kim, J., S.M. Lee, S. Srinivasan, and C.E. Chamberlin. Modeling of proton-exchange membrane fuel-cell performance with an empirical-equation. *Journal of the Electrochemical Society*, 1995. 142(8):2670-2674

Lan, X-Z., Z-C. Tan, G-L. Zou, L-X. Sun, T. Zhang. Microencapsulation of n-Eicosane as Energy Storage Material. *Chinese Journal of Chemistry*, 2004, 22, 411-414.

Lamburg, 2003), Mathematical modelling and experimental investigation of melting and freezing processes in finned phase change material storage, PhD Thesis, University of Technology, Helsinki, Finland, 2003.

Larminie, *Fuel Cell Systems Explained*, Second Edition, James Larminie, August 4, 2000.

Lee, S.J., S. Mukerjee, J. Mc Breen, Y.W.Rho, Y.T.Kho, and T.H. Lee. Effects of Nafion impregnation on performances of PEMFC electrodes. *Electrochimica Acta*, 1998, 43(24):3693-3701.

Little, (2000) "Cost Analysis of Fuel Cell System for Transportation", Arthur D. Little, U.S. Department of Energy funded assessment. March 2000

Liu, K.V., U.S Choi and K.E. Kasza. Pressure drop and heat transfer characteristics of nearly neutrally buoyant particulate slurry for advanced energy transmission fluids. *ASME FED 75*, 107-113, 1988.

Mehalick, E.M. and Tweedie, A.T. *Two component thermal energy storage material program phase I final report* . 1979, (DOE EY-76-02-2845)

Miller, R.W. *Flow Measurement Engineering Handbook* . New York: McGraw-Hill Inc., 1989.

Mosdale, R., G. Gebel, and M. Pineri. Water profile determination in a running proton exchange membrane fuel cell using small-angle neutron scattering. *Journal of Membrane Science*, 1996, 118(2): 269-277

Mulligan, J.C., D.P. Colvin and Y.G. Bryant. Use of two-component fluids of microencapsulated phase-change materials for heat transfer in spacecraft thermal systems. The American Institute of Aeronautics and Astronautics. 1994.

Ogden, (1999) "Prospects for Building a Hydrogen Energy Infrastructure." Annual Review of Energy and Environment. Volume 24, pp 227-279. 1999.

Outlast, <http://www.outlast.com/flash.cfm>, 2005

Prater, K. The renaissance of the solid polymer fuel cell, Journal of Power Sources, Volume 29, Issues 1-2, January 1990, Pages 239-250.

Perry, H. Robert. *Perry's Chemical Engineers' Handbook* . USA: McGraw-Hill Inc, 1997.

Refocus, The international renewable energy magazine, Issue; April 2003.

Rifkin, The Hydrogen Economy, After Oil, Clean Energy From a Fuel-Cell-Driven Global Hydrogen Web, 2002.

Rogers, G.F. Mayhew Y,R. *Engineering Thermodynamics – Work & Heat Transfer: 4<sup>th</sup> Edition*, 1992.

Roy, S.K. An evaluation of phase change microcapsules for use in enhanced heat transfer fluids. *International Journal of Heat and Mass Transfer* , 1991, 18, 495-507

Roy, S.K. Laminar forced convection heat transfer with phase change material emulsions. *Int. Comm. Heat Mass Transfer*, 1997, 24 (5), 653-662

Roy, S.K. Avanic, B.L. Laminar forced convective heat transfer with phase change material emulsions. *Int. Comm. Heat Mass Transfer*, 1997, Vol.24. No.5, pp.653-662.

Roy, S.K. and Sengupta, S. An evaluation of phase change microcapsules for use in enhanced heat transfer fluids. *Int. Comm. Heat Transfer*, 1991, Vol. 18, pp.495-507.

Ryu, W. Hee., et al. Prevention of supercooling and stabilization of inorganic salt hydrates as latent heat storage materials. *Solar Energy Materials and Solar Cells*, 1992, 27 (2), 161-172

SBIR NASA, (1983) Small Business Innovation Research program, available at [http://nctn.hq.nasa.gov/innovation/Innovation\\_81/smsbir.html](http://nctn.hq.nasa.gov/innovation/Innovation_81/smsbir.html), 2004.

Singh, D., D.M. Lu, and N. Djilali. A two-dimensional analysis of mass transport in proton exchange membrane fuel cells. *International Journal of Engineering Science*, 1999. 37(4): 431-452.

Springer, T.E., T.A. Zawodzinski, and S. Gottesfield. Polymer electrolyte fuel cell model. *Journal of Electrochemical Society*, 1991, 138(8):2334-2342

Tahat, Babus'.Haq T., A. Callaghan, Thermal energy storage, *Build. Serv. Eng Res. Technol.*14 (1993) 1±11.

Vand, V. Theory of viscosity of concentrated suspensions. *Nature* , 1945, 155, 364-365

Verbrugge, M.W., and R.F Hill. Ion and solvent transport in ion-exchange membranes: I. A macrohomogenous mathematical model. *Journal of Electrochemical Society*, 1990, 137(3):886-892.

Verne, J., 1874, *The Mysterious Island* (Modern Library MM, April 27, 2004)

Yamagishi, Y. An evaluation of microencapsulated PCM for use in cold energy transportation medium. *Proc. IECEC* , Washington DC, 1996, pp. 2077

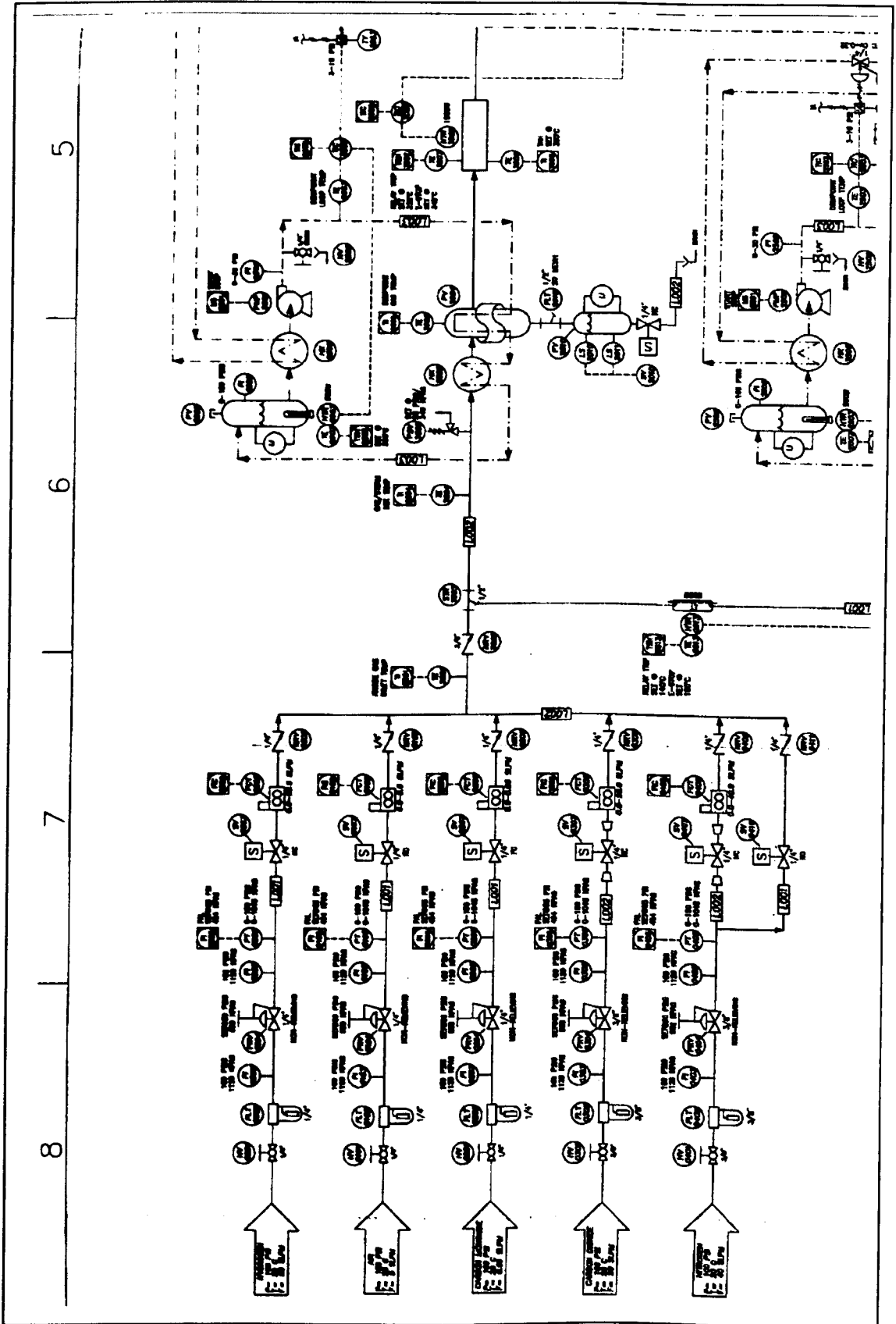
Yamagishi, Y., H. Takeuchi, A.T. Pyatenko and N. Kayukawa. Characteristics of Microencapsulated PCM Slurry as a Heat-Transfer Fluid. *AIChE Journal* 1999 V45 No.4 p696-707.

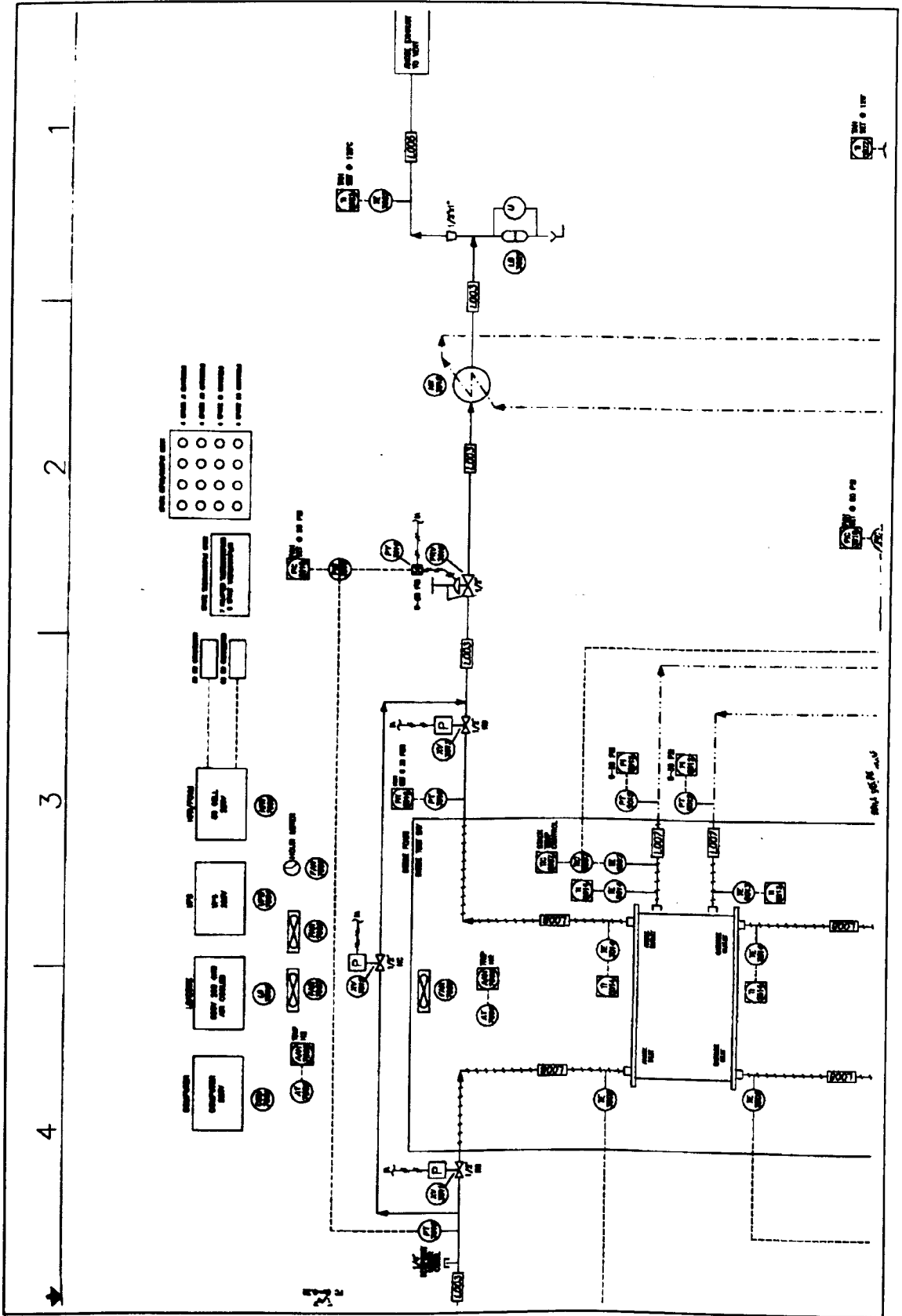
Yunus, A. and Michael A. Boles. *Thermodynamics: An engineering approach*. Singapore: McGraw-Hill Inc., 1989

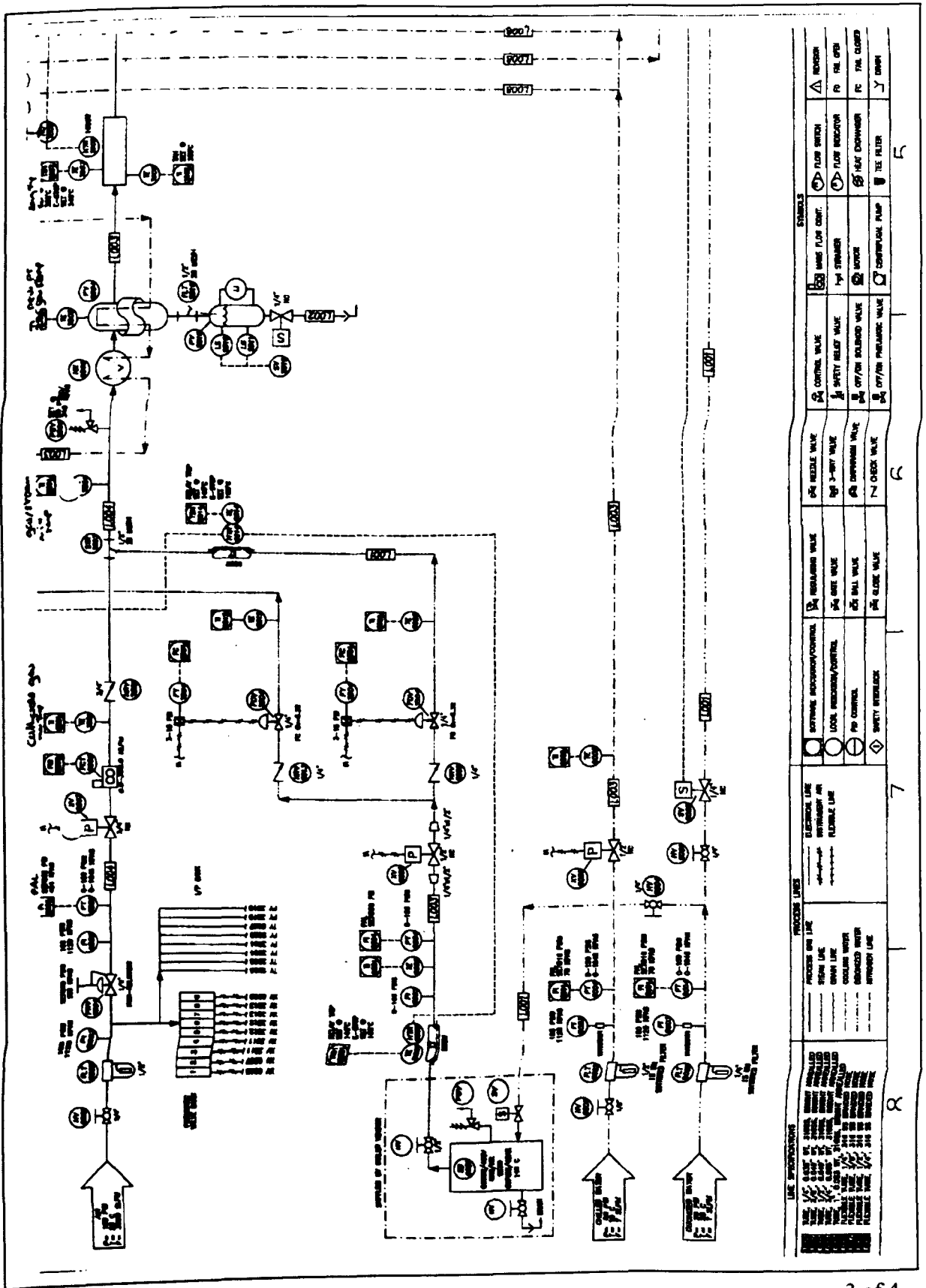
Yi, J.S., and Nguyen, T.V. An along-the-channel model for proton exchange membrane fuel cells. *Journal of the electrochemical Society*. 1998. 145(4):1149-1159

Zawodzinski, T.A., Springer, F. Urbine. 1993. Characterisation of polymer electrolytes for fuel-cell applications. *Solid State Ionics* 60(1-3): 199-211.

## **Appendix A**







LINE REPRESENTATION		PROCESS LINES		ELECTRICAL LINES		SYMBOLS	
10001	10002	10003	10004	10005	10006	10007	10008
10009	10010	10011	10012	10013	10014	10015	10016
10017	10018	10019	10020	10021	10022	10023	10024
10025	10026	10027	10028	10029	10030	10031	10032
10033	10034	10035	10036	10037	10038	10039	10040
10041	10042	10043	10044	10045	10046	10047	10048
10049	10050	10051	10052	10053	10054	10055	10056
10057	10058	10059	10060	10061	10062	10063	10064
10065	10066	10067	10068	10069	10070	10071	10072
10073	10074	10075	10076	10077	10078	10079	10080
10081	10082	10083	10084	10085	10086	10087	10088
10089	10090	10091	10092	10093	10094	10095	10096
10097	10098	10099	10100				



## A.2 PEM Fuel Cell Stack; Start-up, Operating and Shut-down

### 1 BEFORE STARTING-UP

Below is a list of things to consider before starting/fuelling the stack. The list should be adapted to the situation at hand, and irrelevant point should be removed.

- Connect all gas lines and cooling water circuit. Use a large piping diameter to avoid large pressure drops in the systems. At XXX the stack is usually placed in a horizontal position with a Z-flow geometry. That is, the inlets of gas and water are connected at the top cathode side (@ cell 70) and the outlets are connected at the bottom of the anode side (@ cell 1) The gas and cooling water is thus flowing co-current. The stack is designed to allow other flow configurations if needed.
- Connect load/inverter.
- Connect/mount Cell Voltage Monitoring system (CVM).
- Check safety system status.
- Start control/monitoring software/hardware.
- Check Inverter/load. Is it on. Is the communication ready?
- Check CVM. Is communication ready?
- Check N<sub>2</sub> supply. Is the pressure right?
- Check H<sub>2</sub> supply. Is the pressure right. Is the Reformer ready?
- Check Air supply. Is the pressure right. Is the compressor ready?
- Check cooling water level. Refill with deionised water if needed.
- Flush the anode gas line with low pressure N<sub>2</sub>, to remove traces of O<sub>2</sub> in the system. Is the N<sub>2</sub> flowing freely?
- Start cooling water flow. Does it flow? Can it be regulated? Is the cooling capacity ready?
- Start air flow at minimum flow. Does it flow? Can it be regulated.

When all systems are ready switch to H<sub>2</sub> gas.

- Set/keep Air flow at minimum flow
- Set H<sub>2</sub> flow to minimum flow. Does the stack voltage increase?
- Check CVM. Are the individual cell voltages correct? Is there a signal from all the cells?

The OCV (open circuit voltage) of each cell should be >0.85-0.90 V. If some cells have very low OCV's it might help to draw a small current (1-3 A) from the stack for a short while (a few seconds).

### 2 START-UP

A fuel cell stack is generally very robust in terms of varying operational parameters.

It should be noted that in order to protect the MEA's the pressure difference between anode and cathode gas should not exceed 0.5 bar. Also the voltage across any cell must never decrease below 0V.

Good stack performance is highly dependent on proper regulation and stability of temperatures and flows. Poor regulation may result in decreasing stack performance mostly caused by incomplete membrane humidification or flooding of flow channels. These effects can be reversed by proper adjustment of relevant parameters.

When using a humidifier utilising the stack exhaust humidity (like the humidifier) it should be noted that the humidifiers only resource of water is the water produced by the stack. Therefore if no current is drawn from the stack the gas flows should be minimised or stopped if possible.

## 2.1 Simple start-up procedure

For a system with the PEMFC70 2.00 S/N 001 fuel cell stack with the HUM 2.00 S/N 009 humidifier, the following procedure will work.

- Set cooling water flow to ~2.5 l/min
- Set cooling water inlet temperature to maximum 50-55°C
- Set air flow to 112 l/min ( $\lambda_{air} = 2.0$  @ 48 A for a 70 cell stack)
- Set H<sub>2</sub> flow to 35 l/min ( $\lambda_{H_2} = 1.5$  @ 48 A for a 70 cell stack)
- Set current load to  $I = 48$  A.

No significant back pressure should be applied (>300mbar) on any of the gas systems.

Wait for the stack and humidifier to heat up.

Depending on the thermal insulation and length of the gas and water lines the system should have reached thermal equilibrium after approximately 20 min.

The cooling water temperature difference should now be 10-15K.

## 2.2 Operating hints.

The fuel cell stack can be used without having reached thermal equilibrium.

Due to the nature of the humidifiers the stack should always be operated with a cooling water inlet temperature that ensures a good humidification of the inlet air (humidifier outlet temperature). This parameter is highly temperature and current dependent. A 10-15K difference between cooling water inlet and outlet is recommended.

If the current load is below 20 A, the gas flow at  $\lambda_{air} = 2.0$  is becoming too low to effectively remove liquid water drops from the flow channels. Some cells might show unstable behaviour and fluctuate down to very low voltages (<100mV). This can be solved by increasing the air flow from  $\lambda_{air} = 2.0$  to 2.5 or even 3.0 for a short while or permanently depending on the situation.

## 3 SHUT-DOWN

- Remove the current load
- Remove back-pressure if used.
- Reduce air and H<sub>2</sub> flows to minimum flows.
- Switch from H<sub>2</sub> to N<sub>2</sub> and flush the anode system until the H<sub>2</sub> has been removed.
- Shut down all gas and water flows.
- Shut down electronics and external units if necessary.

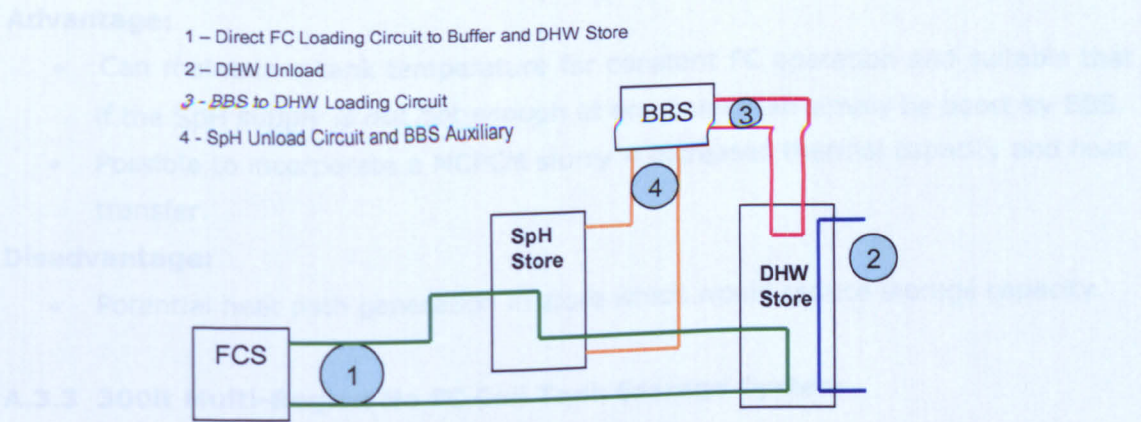
### A.3 Further Fuel Cell TES System Developments to Consider

The following systems are developments of the original storage system designs in the search for optimum storage performance. They are concepts that may provide as alternative and effective solutions or have reduced associated cost, number of connections and volume. The aim of further concept design is to identify areas where the current system performs well and areas that do not perform on par, and hence eradicated or improved.

#### A.3.1 600lt Direct FCS Buffer Storage System - Concept Development

##### Concept - Buffer System Development

Figure 6.0: 600ltr Direct FC Buffer Store System Diagram Concept 2



##### Advantage:

- Single Fuel Cell Heating loop that is separate from SpH and DHW supply, therefore can eliminate the additional Hex and pump requirement
- Double coil approach allows for a better distribution of heat between the two store with a significantly reduced FCS return temperature
- Store temperatures have less influence on each other when compared to other designs under loading and unloading conditions, therefore may provide more consistent outlet temps

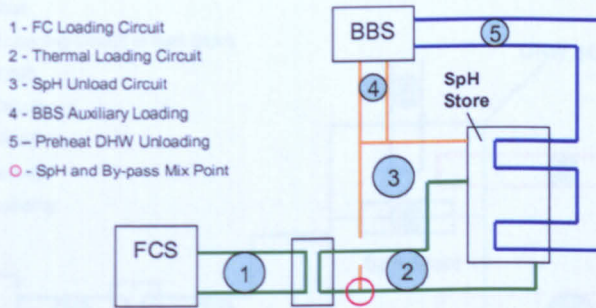
##### Disadvantage:

- Two storage tanks are required
- Cannot significantly charge DHW when SpH is at low temp (dependent on positioning height of coil in SpH store)

### A.3.2 300lt SpH Buffer, DHW Preheat Tank Storage System

#### Concept - 300lt SpH Buffer, DHW Preheat Tank Storage

Figure 6.1: 300ltr SpH Buffer, DHW Preheat Store System Diagram



#### Advantage:

- Can maintain a tank temperature for constant FC operation and suitable that if the SpH supply is not hot enough at one point, can simply be boost by BBS.
- Possible to incorporate a MCPCM slurry = increased thermal capacity and heat transfer.

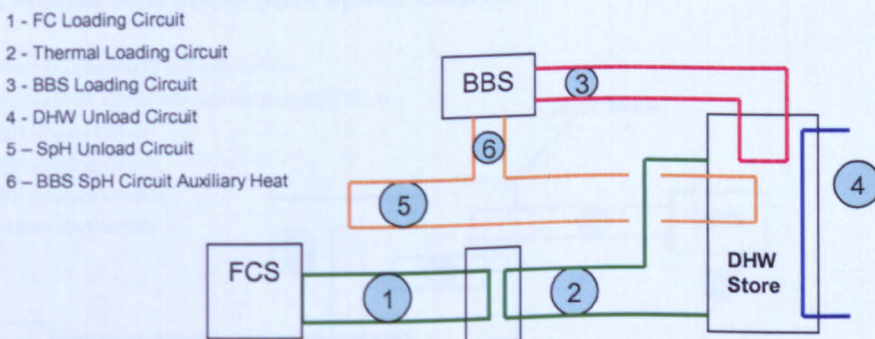
#### Disadvantage:

- Potential heat path generation in store which would reduce storage capacity.

### A.3.3 300lt Multi-Region No FC Coil Tank Storage System

#### Concept 3 - 300lt Multi-Region No FC Coil Tank

Figure 6.2: 300ltr Multi Region Store System Diagram



#### Advantage:

- Can take the coldest part of the store easier and reduced pump size.

#### Disadvantage:

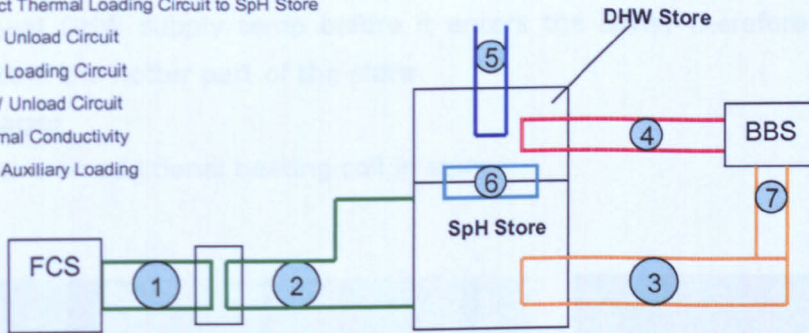
- Requires the Hex and pump of circuit 2. Difficult to maintain stratification in the store

### A.3.4 No FC Coil 1000lt Combi Store System

#### Concept - No FC Coil 1000lt Combi

Figure 6.3: No FC Coil Combi Store System Diagram

- 1 - FC Loading Circuit
- 2 - Direct Thermal Loading Circuit to SpH Store
- 3 - SpH Unload Circuit
- 4 - BBS Loading Circuit
- 5 - DHW Unload Circuit
- 6 - Internal Conductivity
- 7 - BBS Auxiliary Loading



#### Advantages

- Reduced FC loading circuit pumping power. Can more effectively use the cold region of the SpH store.

#### Disadvantages

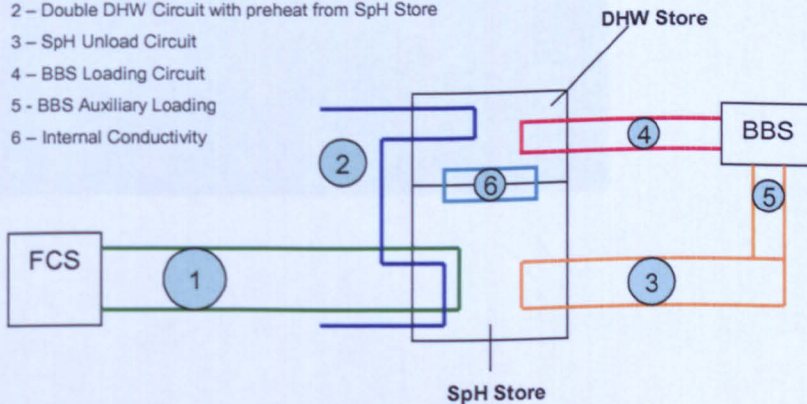
- No isolation from the FCS circuit can be obtained, requiring the separate FC circuit with the pump and Hex.
- May reduce stratification within the store and produce heat flow paths.

### A.3.5 Preheat DHW Coil in SpH Store of Combi Tank

#### Concept - Preheat DHW Combi

Figure 6.5: Preheat DHW Combi Store System Diagram

- 1 - Direct FC Loading Circuit with no Hex
- 2 - Double DHW Circuit with preheat from SpH Store
- 3 - SpH Unload Circuit
- 4 - BBS Loading Circuit
- 5 - BBS Auxiliary Loading
- 6 - Internal Conductivity



Nb. There is just a coil in the SpH store not the DHW the DHW store

**Advantage:**

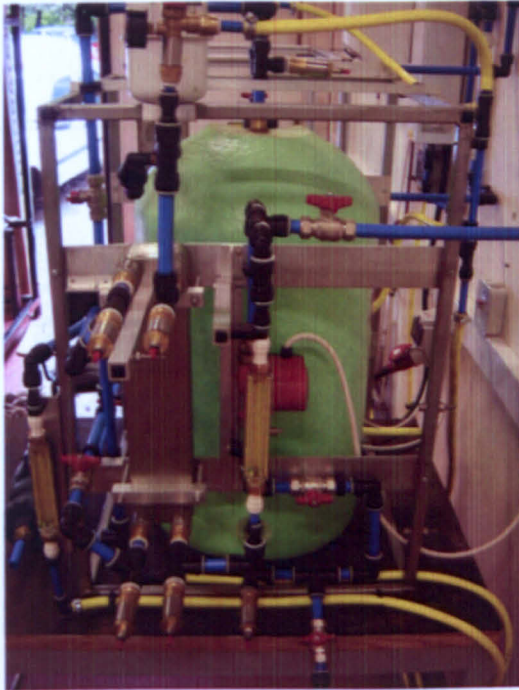
- No additional pumping requirement
- Improve cooling (reduce temperature) around the FC loading coil in the SpH store
- Preheat DHW supply temp before it enters the DHW, therefore less cooling effect in the hotter part of the store.

**Disadvantage:**

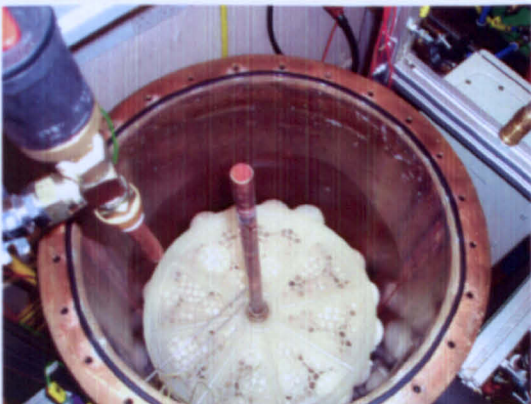
- Require an additional heating coil in store



**PCM Storage Tank –  
In collaboration with Heatrai  
Sadia and EPS.**



**Domestic Thermal Demand Profile Test Rig**



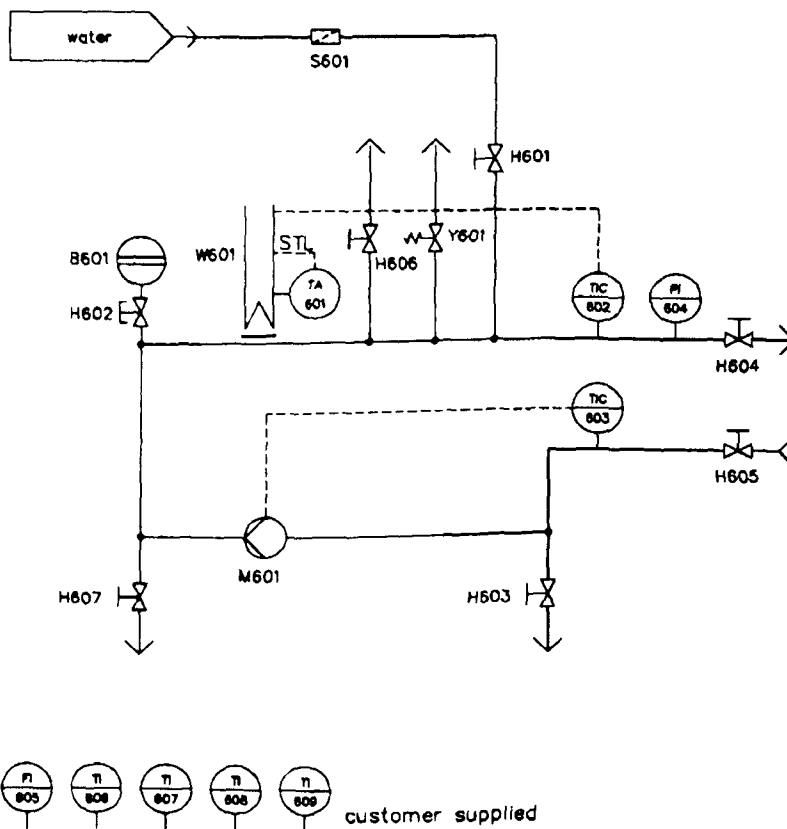
**Prototype 300lt Thermal store and PCM test Rig**

## Appendix B

C No	IUPAC Systematic	Common	MW	Melt	Boil	Density	LHF J/g	J/L	Aldrich £/kg	LH Cost £/kg	K → kJ/mol →		
											dC	BT	MW
											298	15	284.5
											23	52.72408	120.476
<b>Alkanes</b>													
C10	Decane	Decane	142.3	-30	174		n/a						
C12	Dodecane	Dodecane	170.3	-10	216		n/a						
C14	Tetradecane	Tetradecane	198.4	8	250		227						
C16	Hexadecane	Cetane	226.4	18	281		228						
C18	Octadecane	Octadecane	254.5	29	317	0.777	242	188	£15	£18			
C20	Eicosane	Eicosane	282.6	37	343		244						
C22	Docosane	Docosane	310.8	44	369		253						
C24	Tetracosane	Tetracosane	338.7	51	387		242						
C26	Hexacosane	Hexacosane	366.7	57	n/a		162						
<b>Aliphatic alcohols</b>													
C12	Dodecanol	Lauryl alcohol	186.3	24	261		n/a					Sublimes?	
C14	Tetradecanol	Myristyl alcohol	214.4	38	289		230						
C16	Hexadecanol	Cetyl alcohol	242.4	49	340		143						
C18	Octadecanol	Stearyl alcohol	270.5	58	n/a		n/a					Sublimes?	
<b>Diaols - triols etc</b>													
C4	1,4-Butanediol	Butylene glycol	90.1	27	230	1.02	211	215	£13	£16		Water soluble - yes	
C6	1,6-Hexanediol	Hexamethylene glycol	118.2	42	250		216					Water soluble?	
C8	1,8-Octanediol	Octamethylene glycol	146.2	60	n/a		247					Water soluble?	
<b>Aliphatic carboxylic acids - Saturated</b>													
C6	Hexanoic acid	Caproic acid	116.2	-4	204		n/a						
C8	Octanoic acid	Caprylic acid	144.2	16	237		141						
C10	Decanoic acid	Capric acid	172.3	32	257	0.893	163	145	£14	£12			
C12	Dodecanoic acid	Lauroic acid	200.3	44	265		185						
C14	Tetradecanoic acid	Myristic acid	228.4	54	n/a		189		£16	£12			
C16	Hexadecanoic acid	Palmitic acid	256.4	62	339		214						
C18	Octadecanoic acid	Stearic acid	284.5	70	360		225	0	£12	£10			
C20	Eicosanoic acid	Arachidic acid	312.5	75	n/a		n/a						
C4	1,4-Butanedioic acid	Succinic acid	118.1	188	n/a		278						
C6	1,6-Hexanedioic acid	Adipic acid	146.1	162	n/a		259						
C8	1,8-Octanedioic acid	Suberic acid	174.2	141	n/a		165						
C10	1,10-Decanedioic acid	Sebacic acid	202.3	131	n/a		201						
C12	1,12-Dodecanedioic acid	Unknown	230.3	130	n/a		220						
<b>Aliphatic polycyclic acids - Unsaturated</b>													
C18	Octadecanoic acid	Oleic acid	282.5	16	n/a		142						
<b>Aliphatic carboxylic acid esters</b>													
C13	Methyl dodecanoate	Methyl laurate	214.3	5	n/a		n/a						
C15	Methyl tetradecanoate	Methyl myristate	242.4	17	323		207						
C17	Methyl hexadecanoate	Methyl palmitate	270.5	29	n/a		56						
C19	Methyl octadecanoate	Methyl stearate	298.5	38	n/a		216						
C21	Methyl eicosanoate	Methyl arachidate	326.5	46	n/a		228						
C23	Methyl docosanoate	Methyl behenate	354.6	52	n/a		232						
C24	Methyl tetracosanoate	Methyl lignocerate	382.7	n/a	n/a		n/a						
C18	Ethyl hexadecanoate	Ethyl palmitate	284.5	23	n/a		53						
C20	Ethyl octadecanoate	Ethyl stearate	312.5	34	n/a		n/a						
<b>Aliphatic carboxylic acids</b>													



## Appendix C



c o n f i d e n t i a l

company name FuelCon AG Steinfeldstr. 3 39179 Magdeburg-Barleben Germany			(allowance)	(surface)	scale material semifinished part	(weight)	
			Date	Name	(appellation)		
			design	06.10.04	R&I		
			trim				
			signed	06.10.04	(drawing number)		
			checked	06.10.04	4200083-010001-01-01		
			customer			file name	page
						<b>FuelCon</b>	1
01	initial	06.10.04				Lue	4200083-010001-01
stat.	changing	Date	Name			A4	